Fabrication and Characterisation of a Novel Blue Organic Light-Emitting Diode (OLED) —

Structure: Glass/Indium-Tin Oxide/Poly(N-vinylcarbazole) doped with Dye *p*-Bis(*o*-methylstyryl)benzene/Aluminium

by

Jens Ramsbrock
Diplom-Geophysiker

A thesis submitted to the Faculty of Engineering at Napier University in Edinburgh for the degree of Doctor of Philosophy

January 2000

Contents

Acknowledgements

I wish to thank:

Isocom Components Ltd in co-operation with Simpson Research Ltd., the industrial partners and sponsors for this very interesting modern research project.

Napier University, Edinburgh, for having provided facilities and supervision as well as for having paid a grant for four years as a starting point towards covering my living expenses.

Prof. J. Hajto (Director of Studies) and Dr. A. Werninck, the team of my supervisors, for having given constructive supervision and support for theory and experiment.

Dr. Z. He, Napier University, for having given help with Photoluminescence and Electroluminescence measurements.

Dr. K. Turvey , Napier University, for very stimulating discussions about the time resolved Photoluminescence and also the Electroluminescence experimental results.

Prof. H. Milburn, Napier University, for a few supportive discussions.

The technicians at Napier University, for having given support with the experimental equipment and materials supply.

The librarians at Napier University, in particular Mr M. Jones, for their excellent support in finding the scientific information I needed.

Dr. D. Näther, Edinburgh Instruments Ltd., for having given up several weekends by helping with Photoluminescence measurements.

Bank of Scotland for having given me an interest free overdraft.

Declaration

I certify that I, the undersigned, am the author of this thesis, that I have consulted the cited references, that the work in this thesis was done by me, and that this work has not been previously accepted for a higher degree.

Jens Ramsbrock

Certification

I, Prof. Janos Hajto of the School of Engineering at Napier University in Edinburgh, hereby certify that Mr. Jens Ramsbrock has spent four years of research under my supervision[1] and that he has fulfilled the conditions of the ordinance of Napier University so that he is qualified to submit the following thesis in application for the degree of Doctor of Philosophy.

Prof. Janos Hajto

[1] Of which the first three years were carried out in the department of Applied Chemical and Physical Sciences.

Some Fundamental Physical Constants

Quantity	Symbol	Value
Avogadro constant	N_A	$6.0221367(36)\times10^{23}$ mol^{-1}
Electrical field constant	ε_0	8.854187×10^{-12} [F/m]
Electron rest mass	m_0	0.91095×10^{-30} [kg]
Elementary (electron) charge	q	1.60218×10^{-19} [C]
Planck's constant	h	$6.6260755(40)\times10^{-34}$ Js
Speed of light in vacuum	c	299792458 m/s
Zero of the Celsius scale	-	273.15 K

Recommended by the CODATA Task Group on fundamental constants, taken from 'Quantities, Units and Symbols in Physical Chemistry', by I. Mills, T. Cvitas, N. Kallay, K. Homann and K. Kuchitsu, Blackwell Scientific Publications, Oxford, 1988.

List of Abbreviations

AFM	atomic force microscope
a.c.	alternating current
a.u.	arbitrary units
Bis-MSB	*p*-Bis(2-methylstyryl)benzene
cts	number of counts of photodetector for light intensity measuremets [no unit]
d.c.	direct current
EL	electroluminescence
FLA900	Analysis Toolkit for time-resolved spectroscopy, Edinburgh Instruments
FS900	FS900 Spectrofluorimeter System, Edinburgh Instruments
HOMO	highest occupied molecular orbital
ITO	indium tin oxide
LED	light-emitting diode
LUMO	lowest unoccupied molecular orbital
OLED	organic light-emitting diode
PELS	Perkin Elmer Luminescence Spectrometer LS 50B
PL	photoluminescence
PVK	Poly(N-vinylcarbazole)
Q-scope	AFM from Quesant Instrument Corporation
rpm	rounds per minute
SCL	space charge limited

List of non-locally used Symbols

$E\,(e)$	energy [J]
J	current density [A/m^2]
λ	wavelength [m]
ε_s	dielectric constant [-]
ν	frequency [1/s]
q	[C]

List of Figures

List of Tables

1. Abstract

A novel thin film organic light-emitting diode (OLED) of the layer structure glass/indium tin oxide (ITO)/blue light-emitting laser dye embedded in an electrically conducting transparent polymer matrix/aluminium (Al) was fabricated.

The surface profile and texture of the ITO and the dye doped polymer films, the photoluminescence (PL) properties of the polymer-dye films as well as the electroluminescence (EL) properties under d.c. and unipolar pulsed operation of the OLED were characterised.

Thin films of about 100 nm thickness consisting of poly(*N*-vinylcarbazole) (PVK) as an electrically conducting transparent polymer matrix doped with the blue emitting (maximum emission between 395 nm and 430 nm in chloroform) laser dye *p*-Bis(*o*-methylstyryl)benzene (Bis-MSB) on top of an ITO coated glass substrate were fabricated. Steady-state as well as time-resolved photoluminescence spectra of the compounds used and of the PVK films doped with different Bis-MSB concentrations were measured.

The PL light intensity vs. dye doping concentration dependence showed a maximum at a dye doping concentration of about 10 wt%. The half-intensity decay time vs. dye doping concentration relationship revealed a rapid decrease in the decay time from 3.6 ns (6.0×10^{-5} wt% Bis-MSB) to values of around 1 ns at about 2 wt% Bis-MSB dye doping concentration. A decrease in PL emission light intensity occurs at an average dye molecule distance of around 16 Å and a decrease in decay time occurs at a distance of about 28 Å due to concentration quenching. The PL decay data could be fitted with an equation for a non-exponential decay which involves a single recombination path.

The EL of OLEDs based on a glass/ITO/PVK+Bis-MSB/Al structure was characterised using a constant as well as a rectangular unipolar pulsed applied voltage (d.c. and unipolar pulsed mode of operation). Under d.c operation, electroluminescence spectra, the current-voltage (I-V) relationship and electroluminescent light intensity - voltage (L-V) characteristics as well as the device operational lifetime were measured; under unipolar pulsed operation the device response time to the applied field and EL light intensities as a function of the pulse frequency.

The EL spectra showed only a small shift of the EL intensity maxima of about 10 nm compared to the PL peak intensities which suggests that the principal process leading to EL

is not affected significantly by the applied high electric field. The current-voltage (I-V) and EL light intensity characteristics show a diode like behaviour with a turn-on voltage between 22 V and 33 V for light generation. A power law with exponents of about 2.5 to 5 in the voltage region of light emission for current density - voltage (J-V) characteristics was found suggesting the presence of space charge limited current. The barrier height for carrier injection could be estimated as 0.07 eV. The EL light intensity closely follows a linear dependence on the current through the device. The effects of dye doping concentration, emission layer thickness and sample area were investigated. A rapid decrease to about one third of the initial EL light intensity after about 3 hours operation of the device in air without encapsulation was observed. A fast EL device response time of about 0.75 μs was obtained. The frequency dependence of EL was measured and an asymmetric peak found at frequencies of around 260 kHz to 310 kHz at a constant applied voltage. From this pulsed operation response, the mobility of charge carriers was estimated as 6×10^{-7} cm^2 V^{-1} sec^{-1}.

2. Introduction

2.1. Aim of Research and Structure of Dissertation

The task of this work was to fabricate and subsequently characterise a novel thin film Organic blue Light-Emitting Diode (OLED) for display applications using a readily available transparent polymer and a laser dye having in mind a cost effective mass production process.

The main advantages of this approach are that one can combine the processing benefits of the polymer used as a matrix with the high quantum efficiency for light generation of the molecular dye and that a large variety of cheap commercially readily available materials can be used.

The historic background and motivation for this research project is highlighted in the following subchapter. As a first step towards the aim, PVK polymer films embedded with the laser dye Bis-MSB were coated onto an electrically conducting transparent material, ITO glass (chapter 4) and their surface topography and thickness characterised, chapter 5.1. The photoluminescence properties of the fabricated films were studied by experiments and the results presented and discussed in chapter 5.2. In a second step, aluminium was deposited onto the polymer-dye films (chapter 4) to give an OLED. Electroluminescent properties of these OLEDs were characterised under d.c. and unipolar pulsed operation and the results discussed in chapters 5.3 and 5.4 respective.

Essentials of the theory of Photophysics and Photochemistry are given in chapter 3 also including topics needed to understand the operation of an OLED. Concluding remarks (chapter 6) and suggestions for future work (chapter 7) round off this dissertation.

2.2. Electroluminescence and Review of Previous Work

The history of screen technology goes back for over 100 years now. It started in 1897 with the invention of the cathode ray tube to demonstrate alternating current by Karl Ferdinand Braun (BOWONDER, 1994). The operation principle of this kind of screen is based on the horizontal and vertical deflection of an electron beam in a vacuum which generates a light dot on a screen coated with a luminescent phosphor. Different colours are generated by superposition of emissions of phosphors in the basic colours red, green and blue. The de-

velopment of cathode ray tubes can be regarded as complete. They can be produced cheaply and find wide spread applications as computer and television screens.

However, for mobile applications, for instance as displays in portable computers or video cameras or in vehicles, the relatively high weight, the large volume and the high power consumption for the generation of the not convenient high electron acceleration voltage are significant disadvantages. Lighter and flatter displays with lower power consumption have in these areas already replaced the cathode ray tube. To achieve colour or brightness, light is either modulated by liquid crystals or alternatively luminescent inorganic or organic materials are excited by projected electrons, photons or injected charge carriers.

Electroluminescence under d.c. operatiton

Generation of light in Carborundum (SiC) was discovered by H. J. Round in 1907 (ROUND). An electrical field applied to a device containing this material leads to an injection of charge carriers and, because of their recombination, to the emission of light. This behaviour, called electroluminescence (EL), has been observed in the following decades in a number of inorganic and organic materials.

Electroluminescence at low voltages can be achieved in inorganic III-V and II-VI semiconductors[2]. A forward bias is applied to a p-n junction. Minority charge carriers get through the boundary area into the semiconductor doped of opposite polarity and recombine thereby emitting light. The structure of a red light-emitting diode (LED) is schematically given in figure Fig. 2.1. Onto a GaP-substrate, a $GaAs_{1-x}P_x$-adjustment layer ($0<x<0.4$) and a n-doped $GaAs_{0.6}P_{0.4}$-emission layer are grown. By Zn-diffusion a p-n junction is realised. After first demonstrations of a red LED by HOLONYAK and BEVAQUA in 1962 the efficiency of the LED could be improved by nitrogen doping. The emitted light can actually be increased by addition of a transparent substrate such as GaP and also by fitting the diode into a curved plastic body in order to avoid total reflection (SZE, 1981:693f).

[2] For most II-VI semiconductors both p and also n-type forms cannot be prepared.

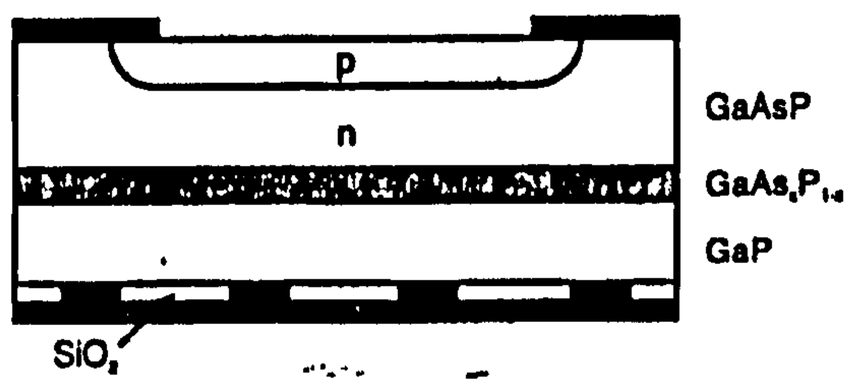

Fig. 2.1: Structure of a red emitting light-emitting diode made of GaAsP (AMMERMANN, 1997:3)

Efficient emission in the yellow and green spectral region has been achieved by electron transition across the indirect gap[3] in the semiconductors GaP and $GaAs_{1-x}P_x$ (orange: x=0.65; yellow: x=0.85; green: x=1.0) and also by the implementation of nitrogen as an isoelectronic defect. In the p-doped part of the material an electron is captured at such a defect. It is removed from the conduction band and then excitonically bound to a hole of the valence band. The recombination of the electron-hole-pair leads, with a high probability, to a radiative transition and to the emission of a photon with an energy slightly below the energy of the indirect transition.

Radiative efficiency of such inorganic LEDs can be increased by using direct connecting[4] semiconductors which were grown, lattice-adjusted, onto the GaAs- or GaP-substrates. Emission in the red range of the spectrum was achieved in the 80's (MOON, 1995) and in the yellow and orange region at the beginning of the 90's using $Al_xGa_yIn_{1-x-y}P$ material systems, (HÖFLER, 1996). Efficient blue and green LEDs have only been available since 1994 (NAKAMURA, 1994). Whilst up to that time indirect luminescence in SiC had been used, LEDs made of direct band gap blue semiconductors, such as AlGaInN, achieved light intensities and efficiencies comparable to red LEDs (ZOLINA, 1996).

Even though inorganic LEDs were widely used as individual components their integration into displays causes significant difficulties. Because of the lattice-adjusted growing process on monocrystalline semiconducting substrates only very small areas can be monolithically integrated at low costs. Individual LEDs have to be positioned and contacted electrically with quite some effort for large displays. Very large displays with several meters in the diagonal and of low pixel size have been produced from 3.05 million LEDs (METZGER, 1995).

[3] An indirect optical transition involves both a photon and a phonon.
[4] A direct optical transition exclusively involves a photon.

In organic compounds electroluminescence was first discovered by POPE, KALLMANN and MAGNATE in anthracene crystals in the blue spectral area from about 420 nm to 440 nm (POPE, 1963). By using liquid contacts, a hole current is injected into the crystal and reaches the opposite electrode from which, at sufficient field strength, electrons are emitted which recombine with holes. The excited molecules fall by recombination back into the ground state, emitting photons after a few nanoseconds for spin-allowed and after a few milliseconds for spin-forbidden transitions. HELFRICH and SCHNEIDER (1965) could inject electrons as well as holes with the help of liquid contacts into a 5 mm thick anthracene crystal and significantly increase the current flow and light intensity. The current density shows, in this case, a quadratic dependence of the applied voltage which is characteristic for space charge limited current transport in materials with low mobility and intrinsic carrier density. The light intensity is almost a linear function of the current, except for low currents where radiationless recombination seems to take place.

In the following years various metal contacts onto anthracene have been investigated (DRESNER, 1969), the sample thickness has been reduced to a few micrometers (KAO, 1981:554) and anthracene has been doped with tetracene (SCHWOB, 1971). Significant problems, however, have still been caused by the high operating voltages of over 100V, the low quality of the evaporated thin films and the inefficient electron injection into anthracene. Only TANG and VanSLYKE in 1987 using a two layer structure of novel organic semiconductors and magnesium contacts achieved operating voltages below 10 V and quantum efficiencies (see chapter 3.2.2) above 1%. The structure of such an organic light-emitting diode (OLED) and the materials used are shown in Fig. 2.2.

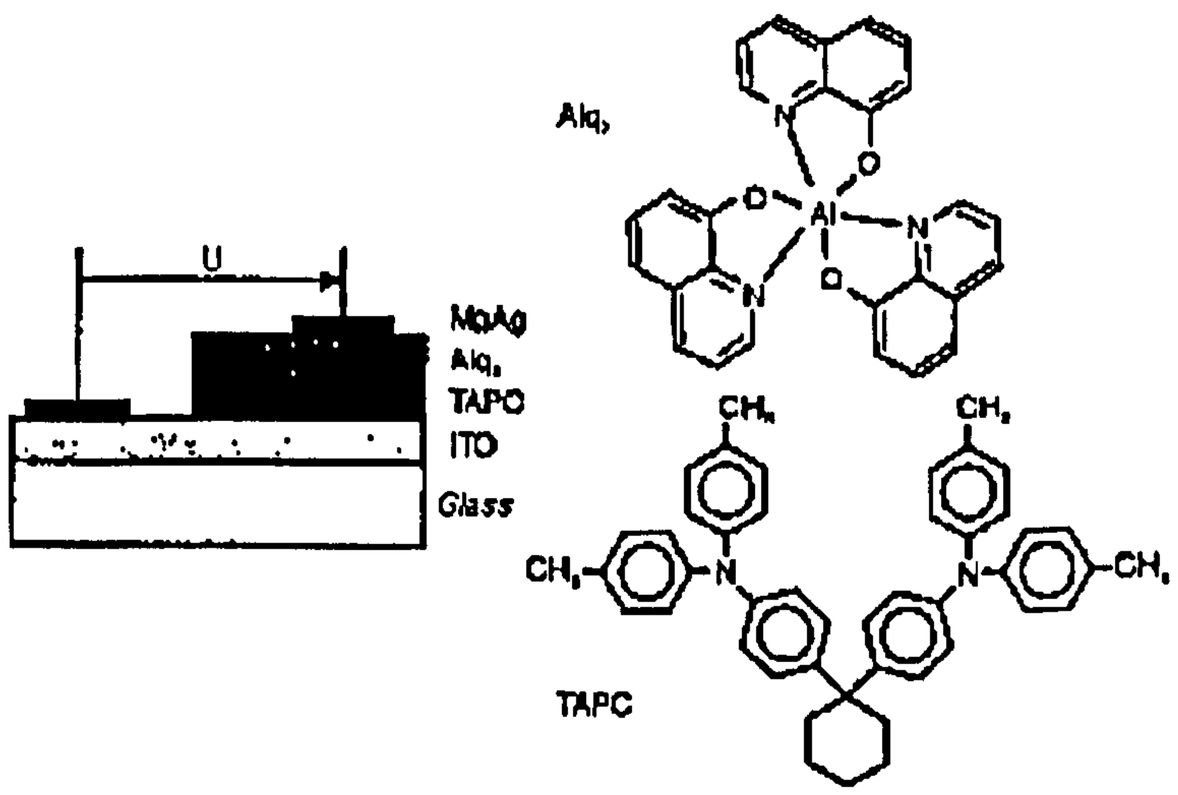

Fig. 2.2: Structure and materials of an organic light-emitting diode (TANG, 1987).

Two layers, 20 nm to 100 nm thickness each, consisting of the aromatic diamine-derivat TAPC and the fluorescent metal-chelate-complex Alq_3 are deposited in a vacuum onto a cleaned indium tin oxide glass substrate. A metal with a low work function, for example magnesium, and a protecting metal layer of silver are deposited on top of the structure as a contact. The TAPC layer allows selective transport of holes from the ITO electrode into the Alq_3 layer where they recombine with electrons injected from the Mg-contact. Most recombination occurs close to the organic boundary area. During the relaxation of the excited Alq_3 molecules to the ground state, light in the green range of the visible spectrum is emitted. Electroluminescence in these structures can be achieved throughout the whole visible spectrum by use of suitable dye molecules which are either deposited as a pure molecular layer or molecularly doped into a matrix.

BURROUGHES demonstrated in 1990 that OLEDs could also be fabricated consisting of long conjugated polymer chains, for example Poly(p-phenylenvinylene). In this case a precursor is spincoated onto an ITO-glass substrate and subsequently polymerised by UV radiation or thermally. The emission wavelength can be tuned by the selection of different chain forming prepolymers.

For the deposition of organic layers, in contrast to inorganic semiconductors, no external voltage need to be applied to the substrate for layer formation as the organic molecules are connected to each other only by weak Van-der-Waals interactions instead of covalent bonding by electron pair formation for the elementary semiconductors. Therefore it can be expected that large area electroluminescence displays can be produced relatively cheaply.

The best OLED performance (HEEGER, 1998:674) is obtained from alkoxy derivatives of PPV. These polymer LEDs turn on below 2V (d.c.) and reach 100 cd/m^2 (the brightness of a colour TV) around 2 V and reach 4000 cd/m^2 for voltages $V < 4V$ (the brightness of a fluorescent lamp) and over 10000 cd/m^2 for voltages $V > 5V$. The external quantum efficiency (photons generated per electrons injected) of these polymer LEDs has been improved to greater than 2% with excellent reproducibility and the luminous efficiency is 1.5-1.8 cd/A, values which are competitive with existing display technologies.

The most advanced polymer LEDs have 'luminous efficiencies' (light power emitted in lumens per electrical power input) that rival those of traditional incandescent filament lamps, which are generally less than 20 lumens/W (FRIEND, 1999).

The operating life, the time needed for light emission to degrade to half the initial value at constant current, has been a question of concern. Operational lifetimes in the order of at least 10000 hours are required for most commercial applications. Recent progress at UNIAX (Santa Barbara, USA) has demonstrated that high performance polymer LEDs can be fabricated with long operating life. At 400-500 cd/m^2 initial brightness, room temperature operating lifetimes of several thousand hours have been obtained. The extrapolated lifetime at 100 cd/m^2 is in excess of 10000 hours. Accelerated life-time studies carried out at 85 °C (initial brightness of 100 cd/m^2) indicate in excess of 400 h to half brightness, indicative of more than 20000 hours at room temperature (independent measurements give an acceleration factor of approximately 100 between 85 °C and room temperature operation).

Electroluminescence under a.c. operation

Alternating-current (a.c.) electroluminescent devices trace their origin back to 1936 when DESTRIAU discovered electroluminescence (EL) in Cu-doped ZnS phosphors. By doping devices with manganese and rare earth elements as well as with new phosphors, e.g. SrS or (Sr, Ca)Ga_2S_4, light intensity and lifetime have been increased significantly. Electrons accelerated in these devices by high electrical fields caused the doped materials or chromophors to emit light by impact ionisation. Difficulties in the fabrication of displays are caused by lack of efficient blue emitting materials and the required high voltages of over 150 V.

Although there was a large research effort in the 1950s on a.c. powder EL devices, such devices never achieved practical application. The existing a.c. thin film electroluminescent devices (MULLER and MACH, 1993: 113, 229, respective) based on, for example, Mn-doped ZnS have considerable drawbacks, e.g. high fabrication cost and high operating voltages.

However, due to the asymmetry of the device configuration, efficient charge injection generally occurs only in one direction (forward d.c. bias). Under reverse bias, most of the devices either degrade quickly or show very poor performance.

A possible way to overcome these problems was demonstrated by KASIM and ELSENBAUMER (1997). Sulfonium-salt PPV and xanthate PPV ITO/polymer/metal devices emitted light under a.c. or forward/reverse bias when ITO substrates were annealed

in air at 110 °C before polymer film casting. However, devices made on non-heat treated ITO substrate showed light emission with lower EL onset electric fields, higher brightness, and higher quantum efficiencies compared to the ones prepared on heat treated ITO substrates.

Recently also the fabrication of symmetrically configured alternating-current light-emitting (SCALE) devices based on conjugated polymers has been reported (WANG, 1996). The SCALE devices consist of an active electroluminescent layer sandwiched between two redox polymer layers which are able to accept both electrons and holes[5]. This structure is sandwiched between two conducting electrodes, one of which is (semi)transparent. This configuration enables the SCALE devices to work under both forward and reverse d.c. bias as well as in a.c. modes.

[5] The term redox comes from *red*uction and *ox*idation. A reduction involves gaining of electrons and an oxidation freeing of electrons. In a redox reaction both reactions take place together.

3. Elements of Photophysics and Photochemistry and Theory of Organic Light-Emitting Diodes

Selected elements of Photophysics and Photochemistry with particular relevance to OLEDs are outlined at the beginning of this chapter. In addition there are topics covered which lead to the theoretical understanding of OLEDs including a discussion of most common electrically conducting polymers. The last sub chapter is about OLEDs as a whole.

3.1. Electronic Structure of Molecules

Each electron in an isolated atom is under the influence of the nuclear charge and the charges of all other electrons present. Within atoms coming together forming molecules, a rearrangement of electrons occurs such that electrons of one atom are influenced by the nucleus of the other atom (i.e. electrons are shared or transferred). If this rearrangement produces an energetically stable condition then bond formation can occur. There are two main theories which attempt to explain the arrangement of electrons in molecules - valence bond theory (VBT) and molecular orbital theory (MOT) (HARRISON, 1996:19). VBT considers atoms in molecules to behave like isolated atoms except that one or more electrons - the valence electrons - from the outer shell of one atom reside in the outer shell of the second atom. Thus a simple diatiomic molecule is visualised as two isolated atoms, in close proximity to each other, in which valence electrons of one atom spend part of the time in the outermost shell of the second atom. This theory can account well for the structure and magnetic properties of metal complexes. VBT presents a simple picture of electrons in molecules. MOT is believed to describe more precisely the interaction of atoms forming molecules and the distribution of electrons within them.

Whereas VBT considers electron orbitals of isolated atoms to be conserved in molecules, MOT starts by assuming that a new set of orbitals (molecular orbitals) is created when atoms interact during bond formation. MOT treats the electron distribution in molecules in a similar way to that in which atomic theory treats electrons in atoms. Initially the locations of atomic nuclei are specified. Orbitals are then defined around the nuclei. These molecular orbitals define the region in space around the molecule as a whole where there is a high probability of locating a particular bonding electron. Molecular orbitals are therefore not localised around a single nucleus but extend over part or all of the molecule. The shapes of molecular orbitals are difficult to calculate but a simple approach has been adopted in order to visualise their appearance. The assumption is that molecular orbitals

resemble the shape of the atomic orbitals from which they were derived; from the known shape of atomic orbitals the approximate shape of molecular orbitals can be deduced. This method is known as linear combination (addition and subtraction) of atomic orbitals. For any particular pair of atomic orbitals which interact during bond formation, one molecular orbital arises from the addition of parts of the atomic orbitals that overlap and one molecular orbital arises due to subtraction of atomic orbitals.

3.1.1. The σ Bond in Diatomic Molecules

Such principles are illustrated in Fig. 3.1, where two atomic s orbitals interact producing a pair of molecular orbitals. The 'bonding' orbital results from the addition of s atomic orbitals in the region of space between the two nuclei. The resulting molecular orbital is of lower energy than either of the two parent atomic orbitals. The 'antibonding' molecular orbital, which is of greater energy than the parent atomic orbitals, results from subtraction of parts of the atomic orbitals that overlap but does not include the region of space between the nuclei. The bonding molecular orbital can be understood more clearly if it is considered to contain electrons which reside in the region between two nuclei and have an energetically favourable interaction with both nuclei. In antibonding molecular orbitals, electrons are influenced by only a single nucleus and will therefore have a less energetically favourable state.

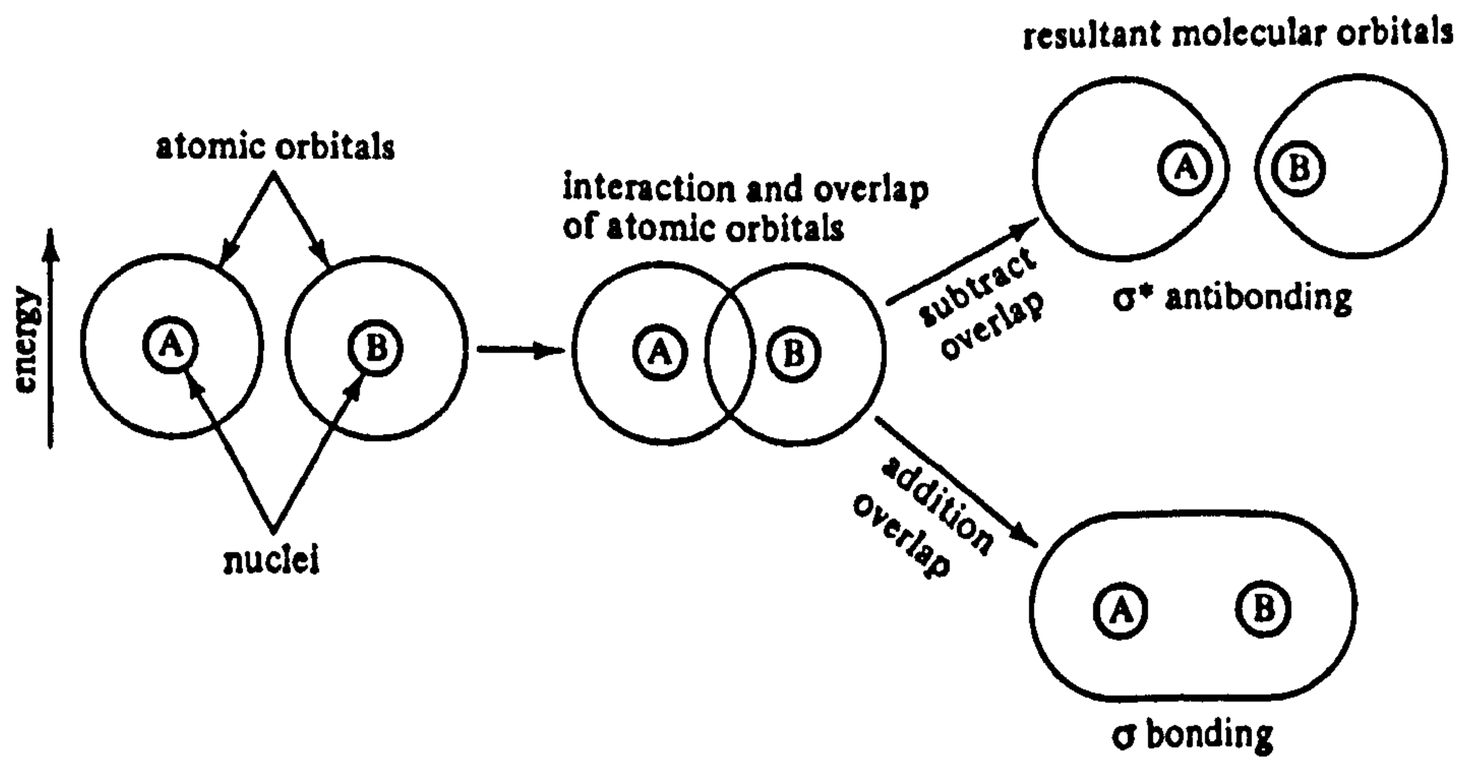

Fig. 3.1: Interaction of s atomic orbitals producing a pair of molecular orbitals (HARRISON, 1996:20).

In summary, each pair of atomic orbitals on interacting gives rise to two molecular orbitals, one bonding orbital of lower energy than either parent atomic orbital, and one antibonding orbital of higher energy than either parent atomic orbital.

Combination of s atomic orbitals gives rise to σ and σ* molecular orbitals (antibonding orbitals are signified by an asterisk).

To illustrate how molecular orbitals are used to rationalise the stability of formation of certain molecules from individual atoms, consider as an example the molecular orbital diagram of the hydrogen molecule (Fig. 3.2). The single electron in each hydrogen atom is accommodated in a 1s atomic orbital. Since the electrons now occupy lower energy levels than they did in isolated hydrogen atoms, the hydrogen molecule is more stable than the isolated hydrogen atoms. The difference in energy, ΔE (Δe in the diagram), between atomic orbitals and bonding molecular orbitals is a consequence of the extent of overlap between atomic orbitals in the molecule forming the molecular orbitals. Large overlap produces a large ΔE and hence a strong chemical bond. With little atomic orbital overlap the converse is true and a weak bond is formed between component atoms within the molecule.

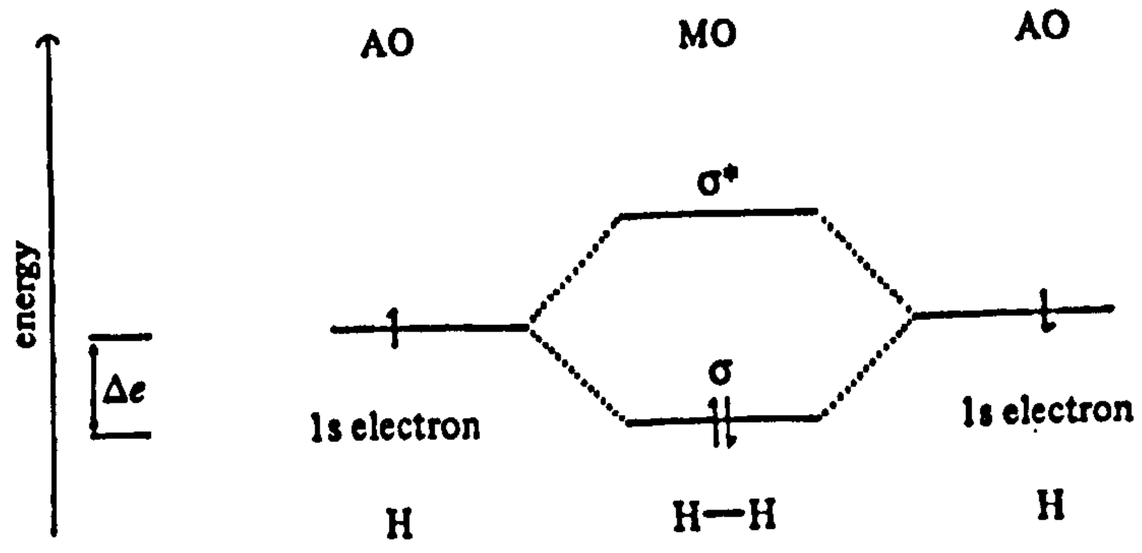

Fig. 3.2: Energy diagram for the formation of molecular orbitals in the hydrogen molecule (HARRISON, 1996:22).

3.1.2. The π Bond in Diatomic Molecules

p atomic orbitals can interact in two ways depending on the spatial distribution of the orbitals. If the interacting atomic orbitals lie around the same axis, as is the case for p_x-p_x interactions, then a σ molecular orbital develops (Fig. 3.3). σ molecular orbitals formed from p orbitals develop in a similar way to those of σ formed from s orbitals, as the electron density is concentrated along the axis of the two nuclei. There is some difference in spatial arrangement of the molecular orbitals since the parent p atomic orbital's geometry differs from that of s atomic orbitals.

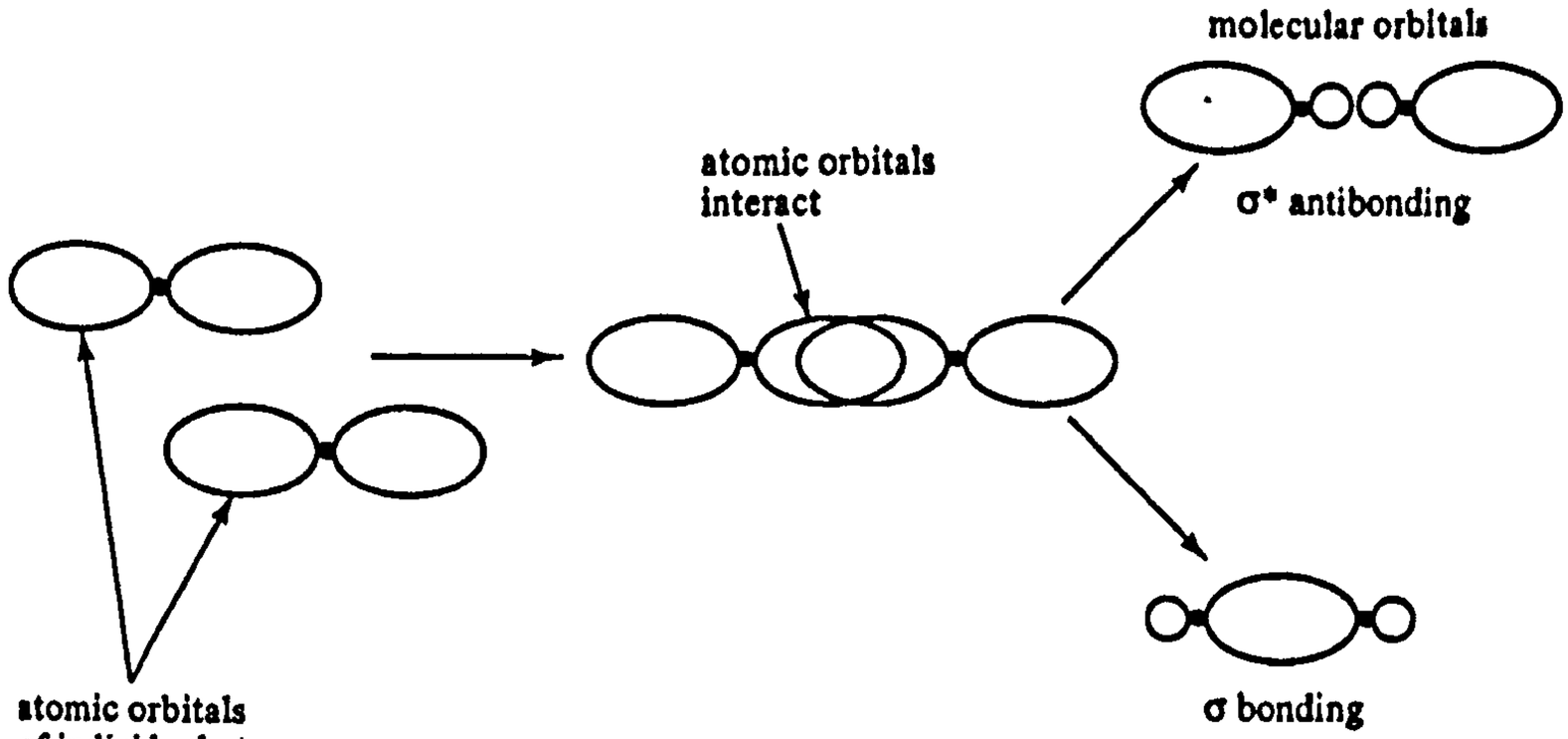

Fig. 3.3: Interaction of p atomic orbitals, which lie along the same axis, giving rise to a pair of σ molecule orbitals (HARRISON, 1996:21).

A second type of interaction occurs when two atoms share two or three pairs of electrons from π orbitals. As shown in Fig. 3.4, the additional bonds can form when spatial geometries of two interacting atomic orbitals have a parallel orientation to each other, i.e. p_y-p_y or p_z-p_z, interactions. The orbital addition product, termed a π molecular orbital, consists of a plane passing through both nuclei along which the electron probability distribution is zero, i.e. the likelihood of finding an electron is negligible. Electrons in π molecular orbitals reside only above and below the bond axis. Two atoms may share all three pairs of p orbitals giving rise to one σ and two π bonds. As indicated here, multiple bonds may be formed between two atoms.

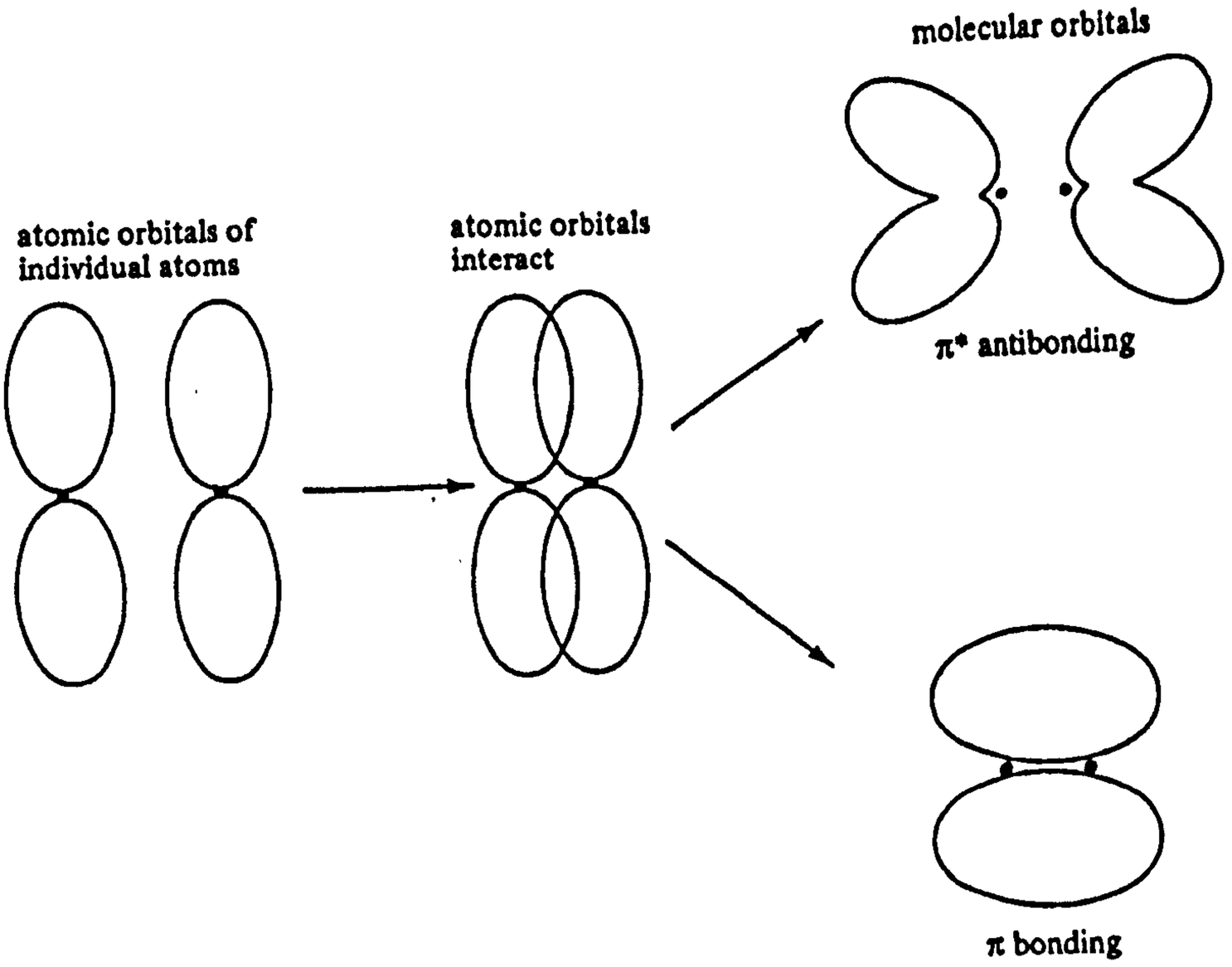

Fig. 3.4: Interaction of p atomic orbitals, of two atoms having parallel orientation to each other, giving rise to a pair of π molecular orbitals (HARRISON, 1996:22).

As an example for a σ and π bonded diatomic molecule the energy diagram of Nitrogen, N_2, is given in Fig. 3.5. The electron occupancy is also included in the diagram. Each arrow represents an electron, the direction of the arrow indicates either 'spin up' or 'spin down'. In the classical description of atomic structure a point charge moving in a Coulomb field gives rise to a magnetic moment which, in the presence of a magnetic field, may take up one of two orientations (GILBERT, 1991:6).

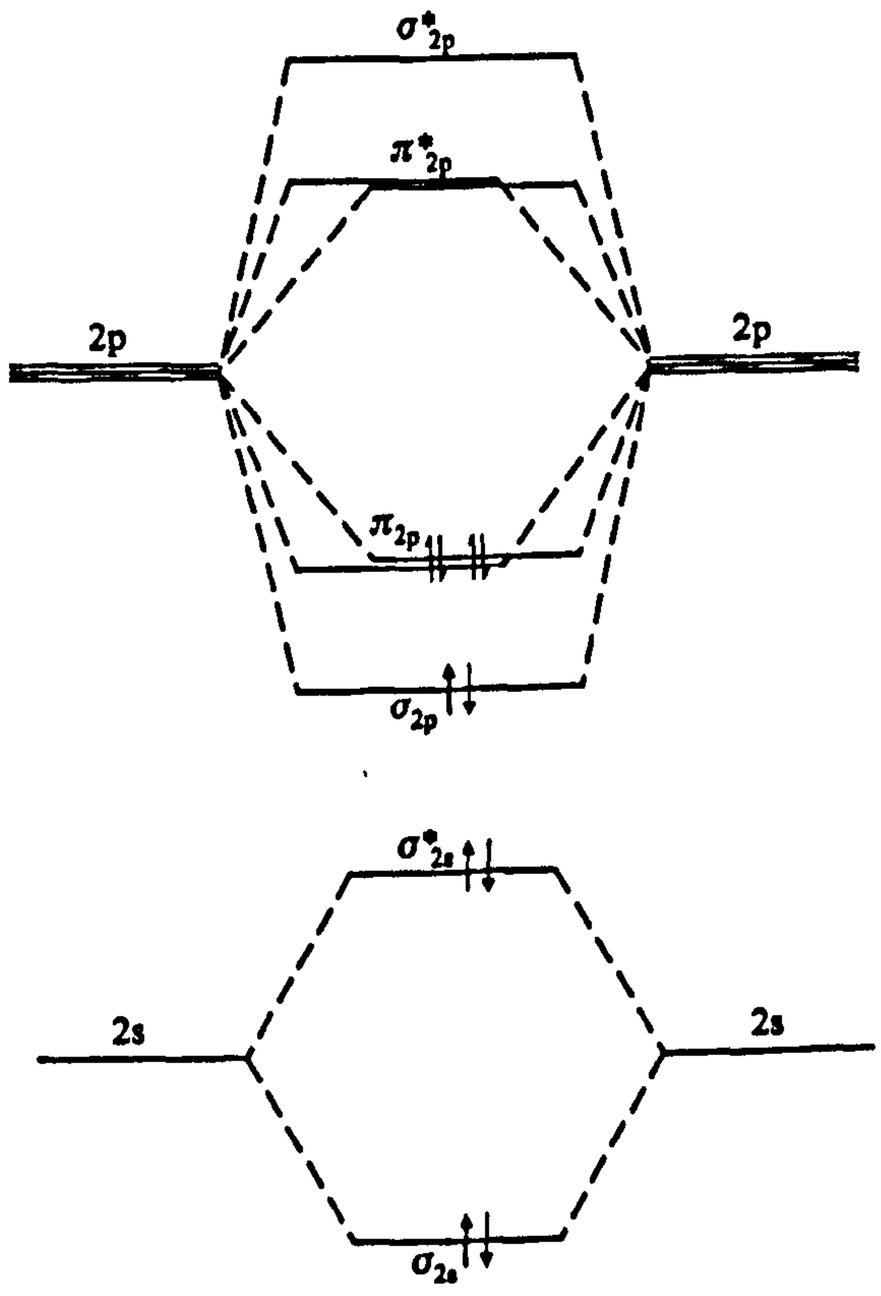

Fig. 3.5: Representation of the energies of the bonding and antibonding orbitals formed from the interaction of two atoms of second row elements. The occupancy of these reflects the structure of N_2 (LOAGAN, 1998:42).

An electronic state with all electrons spin-paired, which is the case for the ground electronic states of most organic molecules, is referred to as a singlet state (GILBERT, 1991:6). The combination of ground state and singlet state is abbreviated by the symbol S_0. If one molecular electron is promoted into the first excited state (see next sub-chapter) and the excitation does not involve a change in the electron spin, this singlet state is abbreviated by the symbol S_1. If there exists some means of changing the spin of the excited electron so that it becomes aligned parallel to the one 'left behind', this excited

state generated is termed a triplet state[6]. The first excited triplet state is abbreviated by the symbol T_1.

It is usual to present these different spin states on a simplified molecular energy level diagram to which the appropriate labels are attached. An example of such a state diagram is illustrated in Fig. 3.6 for a generalised unsaturated[7] hydrocarbon.

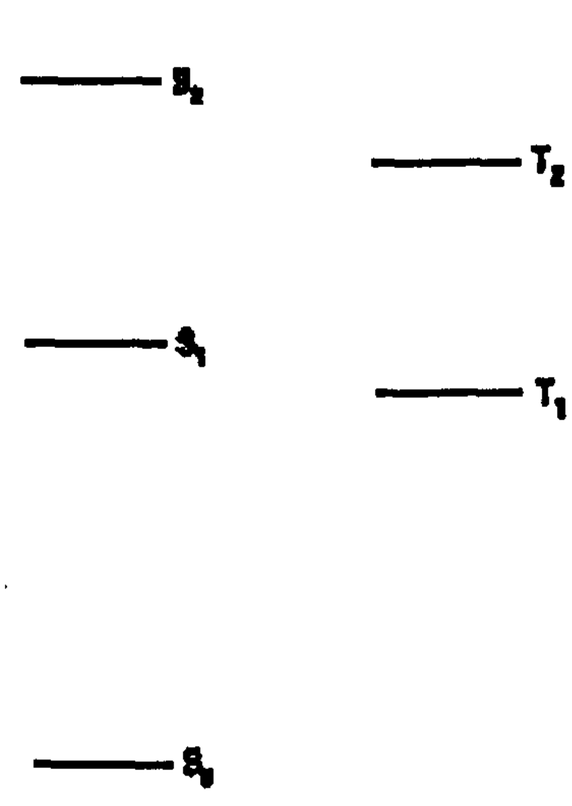

Fig. 3.6: Generalised electron energy state diagram (the energy increases with increasing position on the y-axis). Each state is indicated by the (relative) energy of the lowest vibrational level (GILBERT, 1991:7).

In Fig. 3.6, it is shown that the T_1 state has an energy lower than that of the excited S_1 state; this lowering of the T_1 state is due to spin correlation[8]. Usually, excitation to the first excited state is the most favourable process and the most readily observed in an absorption spectrum (see chapter 3.2).

3.1.3. Delocalised Molecular Orbitals

The molecule which, most of all, exemplifies the role of delocalised molecular orbitals is benzene, C_6H_6. The best representation of the structure is given in Fig. 3.7.

---

[6] In a magnetic field, each such state is found to split up into three sub-states of slightly different energies (RENDELL, 1987:39).

7 An unsaturated hydrocarbon is one which allows double and triple bonds between carbon atoms or ring structures. This means it has less hydrogen atoms then could be held by the number of carbon atoms present. A saturated hydrocarbon has the general formula C_nH_{2n+2}.

[8] The energies of triplet states are usually lower than those of the corresponding singlet states (GILBERT, 1991:43). Triplet states have lower energies by virtue of the fact that the repulsion between two electrons occupying different orbitals is minimised if their spins are opposed. This is called *Hund's rule* of maximum multiplicity.

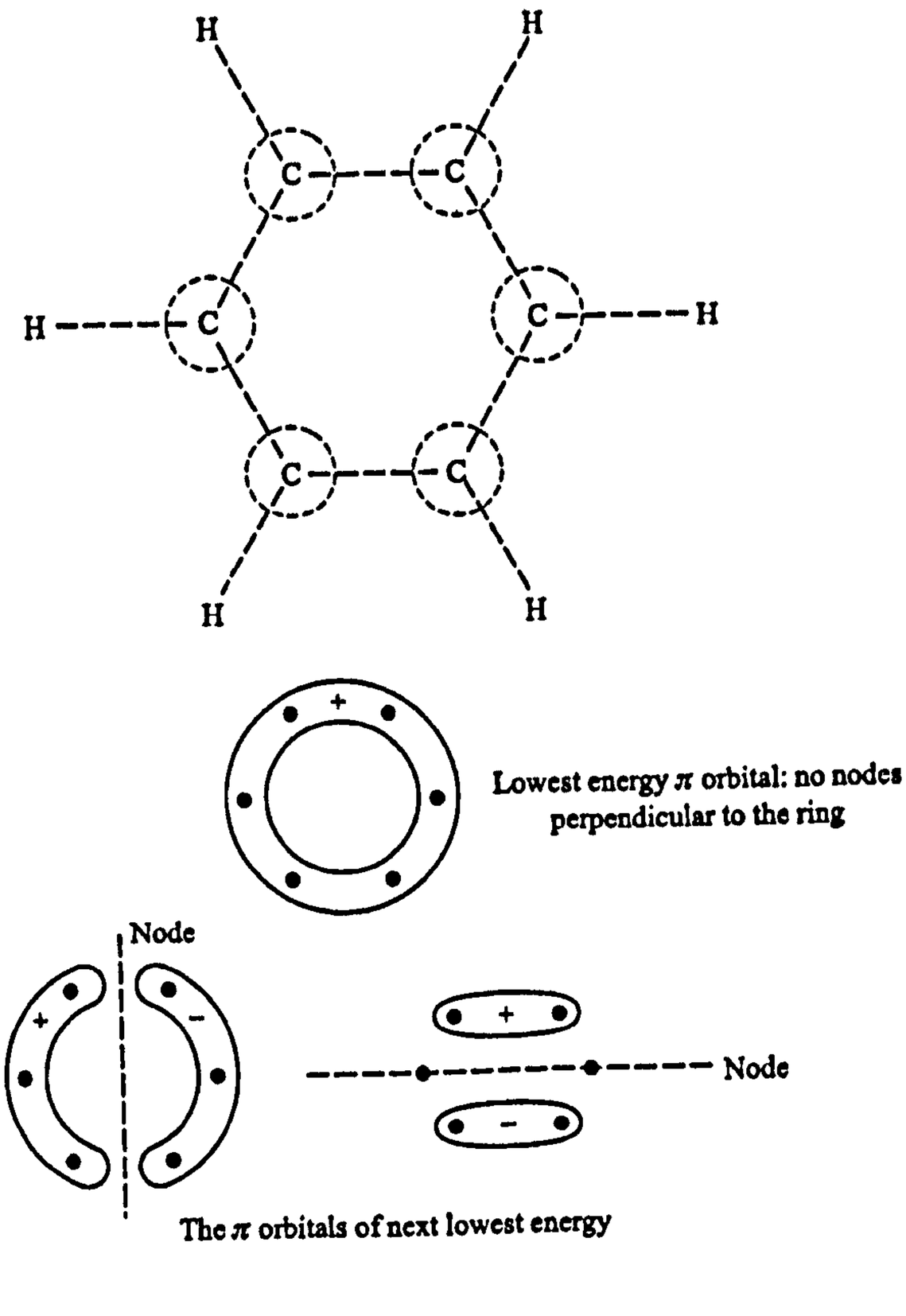

Fig. 3.7: Illustration of the localised σ bonds and delocalised π orbitals in benzene (LOAGAN, 1998:52).

This makes clear that, while benzene is an 'unsaturated' hydrocarbon, the bonding in it is quite different from that in an alkene[9]. The symbol is also suggestive of the ease with which, in a molecule containing a benzene ring, electrical effects are conveyed from one end to the other.

3.2. Luminescence Mechanisms

When a molecule absorbs a photon of u.v. radiation, it undergoes a transition to an excited electronic state and one of its electrons is promoted to an orbital of higher energy (RENDELL, 1987:4). The process of absorption in the context of fluorescence spectroscopy is conventionally called excitation. The transition is classified by reference to the orbitals concerned.

[9] An alkene is an hydrocarbon containing a carbon-carbon double bond in the chain.

The Energy of the photon involved in a transition between two energy states equals the energy difference of the two states according to Planck's law,

$$\Delta E = h\,\nu \qquad \text{Eq. 3.1}$$

with h as Planck's constant.

An electronically excited molecule that does not undergo some kind of chemical reaction (see chapter 3.2.1) cannot persist in an excited state indefinitely, since it represents a situation unstable with respect to the ground state (GILBERT, 1991:8). Electron de-excitation must somehow occur, the excess energy being released as thermal or radiation energy. Transitions involving the de-excitation of electronically excited states that do not involve the emission of radiation are called non-radiative transitions.

Transitions that give rise to the emission of radiation are called radiative transitions. Due to the operation of various physical processes (see GILBERT, 1991 chapter 4), the energy of the emitted radiation is usually lower (longer wavelength) than that used to create the excited state. The emitted radiation is called fluorescence if it originates in the de-excitation of an excited state that has the same spin orientations as the ground state. Since all closed-shell molecules have singlet ground states, fluorescence is most frequently observed from S_1 states; the emission is called phosphorescence if it originates in the de-excitation of an excited state of spin orientations different from that of the ground state (for example, $T_1 \rightarrow S_0$).

The diagram given in Fig. 3.8 indicates all possible transitions that may occur between the different energy levels, it is called a *Jablonski diagram*. Transitions that involve electromagnetic radiation (both absorption and emission) are indicated as straight arrows and non-radiative transitions as wiggly arrows. To illustrate the possibility of generating vibrationally excited electronic states the vibrational levels associated with each electronic energy level are also drawn in Fig. 3.8. Radiative transitions are 'vertical' transitions and involve a change in the total energy of the molecule only due to the absorption and emission of a photon. Non-radiative transitions are (nearly) 'horizontal' transitions and involve conversion from one state to another at (nearly) constant energy. Conversion between states of the same spin orientations is called *internal conversion* (IC) and for states of different spin orientations the term *intersystem crossing* (ISC) is used. Intersystem crossing in this diagram from S_1 to T_1 leaves the molecule with some excess vibrational

energy above the lowest (vibrationless) T_1 level. In the solution phase this excess energy for instance is rapidly removed by collisions with solvent molecules, a process sometimes referred to as *vibrational relaxation* (VR). Other selected non-radiative processes are discussed in chapter 3.3.

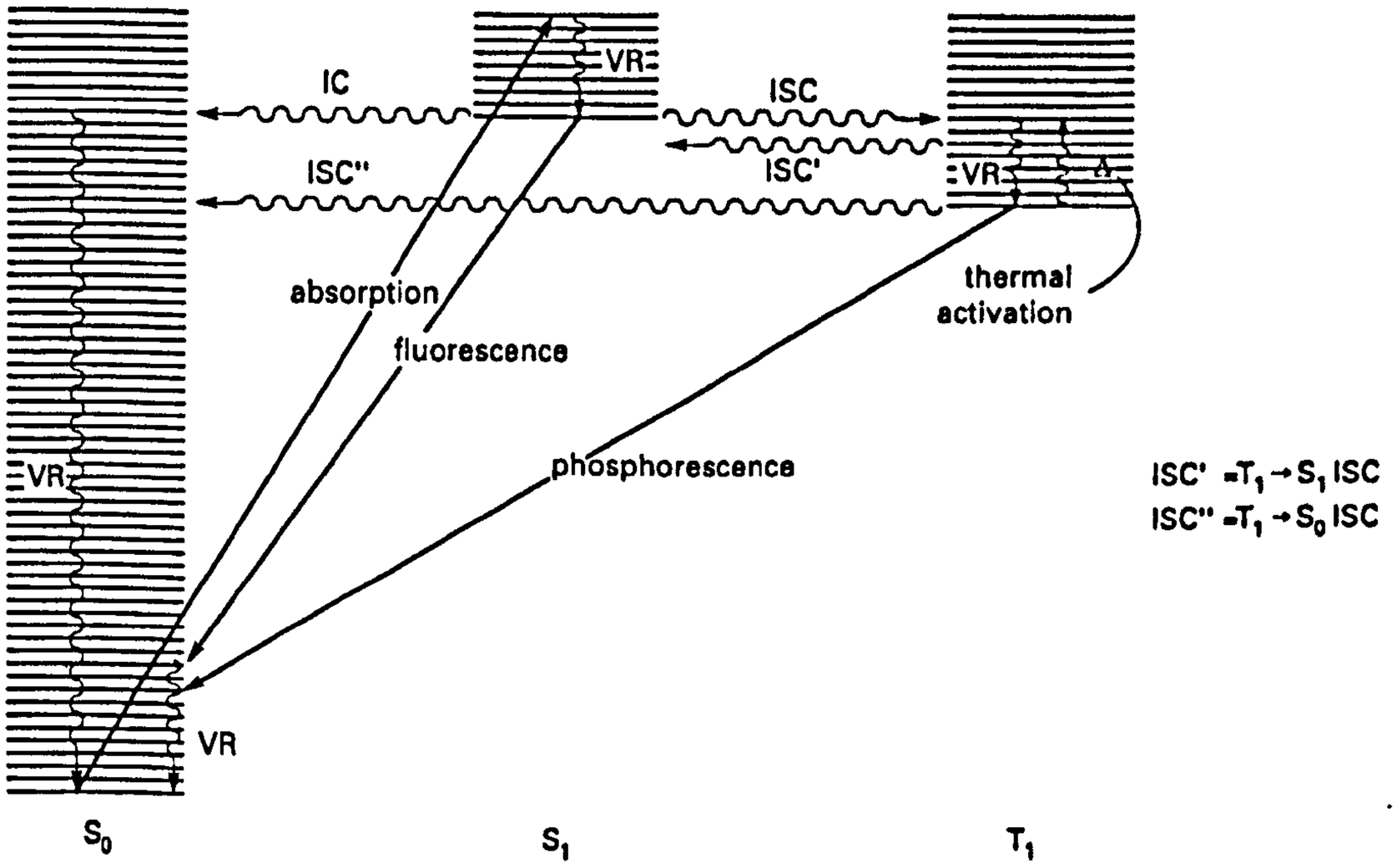

Fig. 3.8: *Jablonski diagram*[10] The y-axis represents the energy level. The S_1 and T_1 state are displayed besides the S_0 state simply for reasons of presentational clarity. (GILBERT, 1991:9).

3.2.1. Mirror Symmetry

Fig. 3.9 shows schematically the different possible transitions for absorption and emission of a molecule and their resulting spectra. Transition intensities are determined by the probability of individual transitions (AMMERMANN, 1997:14). The 0-0 transition (v''=0 in the ground state to v'=0 in the excited state) is, in this particular example, the most intense, although the possibility of excitation to v'= 1, 2, 3, etc. being more intense exists. In solution, any vibrational excitation is rapidly lost through collisions with solvent molecules and emission therefore occurs from the v'=0 level of the excited electronic state. For the reverse emission process the emission intensity is greatest for the 0-0 transition but there will also be the possibility of emission from v'=0 down to v''= 1, 2, 3, etc. being more intense. Whereas excitation to the v'=1, 2, 3 etc. levels in absorption costs more energy (requiring shorter wavelength radiation) than excitation to v'=0, de-excitation to v''=1, 2, 3 etc. is accompanied by the emission of radiation of lower energy (longer wavelengths) than that of the 0-0 emissive transition. If the relative vibrational level spacings are similar in

[10] In reality the vibrational energy levels are not evenly spaced due to anharmonicity of vibration.

both states, the emission spectrum will appear as a mirror image of the absorption spectrum, as shown in Fig. 3.9 (c). The reason for the small difference in the wavelength of the 0-0 absorption and emission transitions, called *Stokes' shift* in general between maximum absorption and emission, is related to the properties of the solvent molecules and their slightly different interactions with the two electronic states involved.

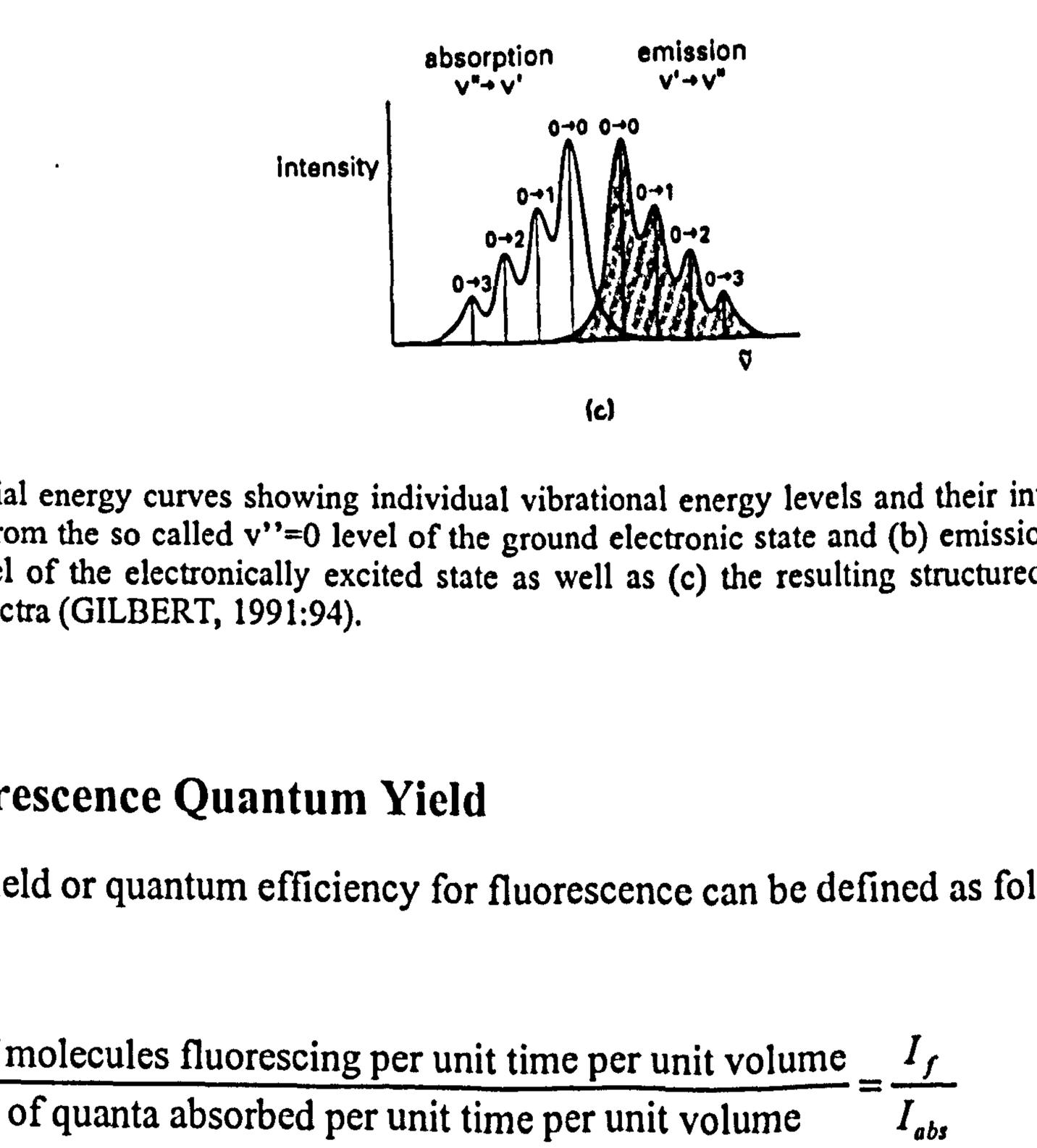

Fig. 3.9: Potential energy curves showing individual vibrational energy levels and their involvement in (a) absorption from the so called v''=0 level of the ground electronic state and (b) emission from the v'=0 labelled level of the electronically excited state as well as (c) the resulting structured absorption and emission spectra (GILBERT, 1991:94).

3.2.2. Fluorescence Quantum Yield

A quantum yield or quantum efficiency for fluorescence can be defined as follows:

$$\Phi_f = \frac{\text{No. of molecules fluorescing per unit time per unit volume}}{\text{No. of quanta absorbed per unit time per unit volume}} = \frac{I_f}{I_{abs}} \qquad \text{Eq. 3.2}$$

Where I_f is the intensity of fluorescence and I_{abs} is the intensity of absorbed radiation (as distinct from I_0, the incident intensity, since not all photons incident on the sample are ab-

sorbed by it) the number of photons absorbed or emitted are related to the intensities (GILBERT, 1991:101)[11].

3.2.3. Radiative Lifetimes

Two models for radiative decay, exponential and also a non-exponential, are described in this sub chapter.

3.2.3.1. Exponential Decay

The radiative process in isolation can be imagined as a situation where a concentration of electronically excited molecules, [M*], has been formed which decays to zero as a function of time due to the spontaneous emission of radiation:

$$M^* \rightarrow M + h\,\nu' \qquad \text{Eq. 3.3}$$

where $h\nu'$ is a lower energy photon compared to the one initially absorbed by the ground state molecule. Spontaneous emission is a random process, in the same sense that radioactive decay is random. Such random processes follow first-order kinetics:

$$-\frac{d}{dt}[M^*] = k_r^0[M^*], \qquad \text{Eq. 3.4}$$

i.e. the rate of removal of M* is linearly dependent on [M*]. The rate coefficient k_r^0 characterises the rate of the spontaneous emission process and is determined by the nature and properties of the emitting state. The superscript r (for radiative) may be replaced by f (fluorescence) or p (phosphorescence) whenever appropriate. Integration of the given equation yields

$$[M^*] = [M^*]_0 e^{-k_r^0 t} \qquad \text{Eq. 3.5}$$

and hence the concentration of M* decays exponentially to zero from some initial concentration $[M^*]_0$ at t=0. In photochemistry the rate of an emission process is characterised by the lifetime. The so-called 'natural' lifetime, τ_r^0, of a radiative process is defined as the reciprocal of the radiative rate coefficient.

[11] For the experimental measurement of quantum yields see GILBERT, 1991, p. 117 f..

$$\tau_r^0 = \frac{1}{k_r^0} \qquad \text{Eq. 3.6}$$

It can readily be deduced from Eq. 3.6 that in a time $t = \tau_r^0$, the concentration of excited molecules falls to 1/e of its initial value and therefore τ_r^0 is sometimes referred to as the 1/e lifetime. Since k_r^0 has the units of a first-order rate coefficient [s^{-1}], the lifetime has units of [s].

3.2.3.2.Non-Exponential Decay

A set of ground states is initially fully occupied before any excitation is applied. Electrons are activated from the ground states to a set of excited states. During luminescent decay, electrons fall from the excited states to the ground states. The concentration of occupied and also non-occupied ground states per unit volume is defined as *n(t)*. Therefore, it follows for the decay rate, $\frac{d\,n(t)}{dt}$,

$$\frac{d\,n(t)}{dt} \propto \text{(conc. of occupied excited states) x (conc. of non - occupied ground states)}.$$

In other words

$$\frac{d\,n(t)}{dt} = -r\left[n(t)\right]^2 \qquad \text{Eq. 3.7}$$

where *r* is a recombination coefficient. Eq. 3.7 transformed leads to

$$\frac{1}{\left[n(t)\right]^2} d\,n(t) = -r\,dt \qquad \text{Eq. 3.8}$$

Integration of Eq. 3.8 gives:

$$-\frac{1}{n(t)} = -r\,t + C \qquad \text{Eq. 3.9}$$

where C is a constant of integration. With $n(0) \equiv n_0$ follows $C = -\frac{1}{n_0}$.

Eq. 3.9 can now be written in the form:

$$\frac{1}{n(t)} = \frac{1}{n_0} + r\,t$$

so

$$n(t) = \frac{n_0}{1 + n_0\, r\, t}.$$

As $n_0\, r$ obviously has the dimensions [time^{-1}] it can be denoted by $1/\tau$ with τ as a decay time constant. It follows

$$n(t) = \frac{n_0}{1 + \frac{t}{\tau}} \qquad \text{Eq. 3.10}$$

The light intensity, L_int(t), is proportional to $\frac{d\,n(t)}{dt}$ which can also be written as

$$L\_\mathrm{int}(t) = -k\frac{d\,n(t)}{dt} = \frac{n_0 k}{(1 + \frac{t}{\tau})^2}\frac{1}{\tau}$$

with k>0 as a constant. Denoting $\frac{n_0 k}{\tau}$ as L_int_0, the emission at zero time, gives:

$$L\_\mathrm{int}(t) = \frac{L\_\mathrm{int}_0}{(1 + \frac{t}{\tau})^2} \qquad \text{Eq. 3.11}$$

According to Eq. 3.11, assuming there is only one decay route involved, a plot of $\sqrt{\frac{L\_\mathrm{int}_0}{L\_\mathrm{int}(t)}}$ against the decay time t gives a straight line with a gradient of $1/\tau$.

3.2.4. Measured Lifetimes

Experiments can be performed in which a large initial concentration of electronically excited molecules is produced by a short and intense burst of radiation (GILBERT, 1991:99). Observation of the emitted radiation as a function of time allows us to quantify the rate of decay of emission and hence the rate of decay of the excited molecule concentration. However, under these circumstances, the measured rate coefficient, k_r, cannot be identified as k_r^0 since additional processes may contribute to the decay of the excited molecule concentration, including non-radiative processes.

3.3. Selected Photochemical Reactions

In the following section selected 'quenching mechanisms' and photochemical reactions which compete with the radiative emission of an excited molecule are outlined.

Quenching involves the removal of the energy from an excited molecule by another molecule , usually as the result of a collision (RENDELL, 1987:123). This can be important in an analysis since the fluorescence of the analyte might be quenched by the molecules of some compound present in the sample - an example of a 'matrix effect'.

In the presence of a reactive molecule, usually called a quencher, Q, a new reaction channel is possible which competes with emission (GILBERT, 1991:9). Because some of the excited molecules will interact or react with Q, not all are able to emit radiation and, consequently, the intensity of emission is reduced by an amount that will be proportional to the concentration of Q. In addition, the extra reactive channel introduced by the presence of Q increases the rate of decay of the excited molecule M^*.

3.3.1. Excimers

A complex containing two molecules of the same kind, one in its (first) electronically excited state and the other in the ground state has been given the name 'excimer', since it is a di*mer* which is stable only in an electronically *exci*ted state (GILBERT, 1991:145). Its formation is represented as follows:

$$M^* + M \rightarrow (MM)^* \qquad \text{Eq. 3.12}$$

The excimer is an electronically excited entity that may be formed in a concentrated solution containing excited organic molecules. It has its own electronic and geometrical structure, bound vibrational and rotational energy levels, and its own characteristic reactivity. Since it is electronically excited, it will undergo all of the processes which were described in the previous chapter, including fluorescence (singlet eximers), phosphorescence (triplet excimers) and a variety of non-radiative processes. There is, however, an important distinction between radiative processes undergone by an excimer compared to the excited monomer: the absence of a bound ground state means that emission must lead to dissociation of the complex, e. g.

$$(MM)^* \rightarrow M + M + h\,\nu_{excimer} \qquad \text{Eq. 3.13}$$

where $h\,\nu_{excimer}$ gives the energy of the excimer emission. The vibrationless level of the bound excimer has an energy substantially below the separated components M* + M (the difference is the binding energy). Thus, emission of light from the lowest level of the excimer involves a transition to the lower repulsive potential energy surface with a considerably smaller energy difference compared to that for emission from the M* monomer. It can therefore be expected that the excimer emission will always involve the release of photons of lower frequencies (longer wavelengths) compared to monomer emission. The excimer emission is structureless because the overlapping orbitals now include a multitude of levels associated with the low-frequency vibrations of the excimer. These many levels overlap and it becomes impossible to discern any vibronic structure in the emission spectrum. Since the concentration of the M* monomer is reduced by excimer formation, the emission intensity from free M* will be reduced. Hence excimer formation represents a form of emission quenching. The extent of quenching is directly related to the concentration of the monomer in its ground state, and so the term 'concentration quenching' is sometimes used to describe this phenomenon[12].

3.3.2. Exciplexes

In a nonpolar solvent, the process of exciplex (*excited complex*) formation can be thought of in much the same way as above for excimers (GILBERT, 1991:157). No bound ground-state exists in most cases, although there are some combinations of aromatic hydrocarbon

[12] It must be differentiated between 'concentration quenching', which involves excimer formation, and 'impurity quenching', where the quenching results because of the presence of an impurity in the sample whose concentration increases in proportion to the concentration of ground state molecules (GILBERT, 1991:147).

molecules where such ground-state complexes, called electron donor-acceptor (EDA) complexes, are possible. However, the formation of a complex becomes possible if one of the components is electronically excited, in exact analogy to excimer formation. The process may be written as

$$M^* + Q \rightarrow (MQ)^* \qquad \text{Eq. 3.14}$$

where M* indicates the electronically excited monomer and Q indicates what is, in effect, a quencher.

There are significant differences between the two types of complex (excimer and exciplex), however. For example, the exciplex emission is very sensitive to the solvent polarity in contrast to excimer emission. The exciplex emission maxima and intensities are sensitive to the reduction-oxidation properties of components. These facts suggest that an element of electron transfer is involved in the process of exciplex formation.

3.3.3. Electronic Energy Transfer

An important overall mechanism which is responsible for the quenching of molecular emission involves the transfer of excitation energy to the quencher in a bimolecular process which may be written

$$M^* + Q \rightarrow M + Q^* \qquad \text{Eq. 3.15}$$

(GILBERT, 1991:168). This is also referred to as a 'photosensitization' reaction; Q becoming 'sensitised' to a wavelength of radiation absorbed not by Q but by M.

In this reaction, excitation energy provided initially to M via the absorption of a photon appears in Q with a subsequent reduction in the concentration of excited M molecules and hence a reduction in the total emission from M*. For this kind of reaction to occur, the energy level of Q* must be lower than (or, at the very most, equal to) that of M*.

A number of different energy transfer processes might be distinguished:

1. *Radiative Energy Transfer*, in which the emission from M* is reabsorbed by Q:

$$M^* \rightarrow M + h\nu' \quad \text{and} \quad Q + h\nu' \rightarrow Q^* \qquad \text{Eq. 3.16}$$

This process is sometimes referred to as 'trivial' and it simply requires that the emission spectrum of M* and the absorption spectrum of Q overlap. Obviously, such a mechanism does not require that M* and Q share the same solvent cage.

2. *Non-radiative Energy Transfer* requires the presence of a specific interaction between M* and Q. Two types of interaction may be identified which are termed Coulombic and electron-exchange energy transfer.

Coulombic energy transfer is dominated by long-range dipole-dipole interactions which cause perturbations of the electronic structures of the energy donor and acceptor. These perturbations are transmitted by the electromagnetic fields of the M* and Q molecules, in which the dipole oscillation of M* induces a corresponding oscillation in Q. These process may take place at large intermolecular separations (up to the order of 100Å). In this mode of energy transfer electrons which are resident on M* remain on the de-excited M.

In contrast, electron-exchange energy transfer requires much closer contact between M* and Q[13] since it involves an electron transfer mechanism in which the electron from the excited state of M* transfers into the lowest unoccupied molecular orbital (LUMO) of Q with a simultaneous transfer of an electron from the highest occupied molecular orbital (HOMO) of Q into the corresponding orbital on M. This process can be thought of as involving the simultaneous transfer of both the excited electron and the vacancy created by excitation from M* to Q (see Fig. 3.10). This kind of energy transfer mechanism requires that M* and Q be sufficiently close together to allow overlap of the electron orbitals involved.

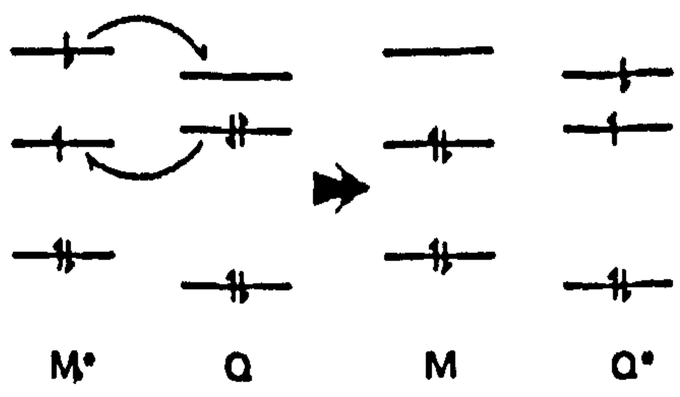

Fig. 3.10: Energy level diagram showing electron transfer steps in electron-exchange energy transfer (GILBERT, 1991:169).

[13] The excited state M* is both a better electron donor and acceptor.

Non-radiative energy transfer processes may thus take place over relatively large distances (anything from 20 to 100 Å) or much shorter 'encounter' distances (6-20 Å) depending upon the type of energy transfer mechanism involved.

3.3.4. Photodecomposition

A typical C-C σ-bond energy is 350 kJ mol^{-1} (GILBERT, 1991:5) [14]. The corresponding energy of each bond is 3.63 eV, i.e. the energy carried by a photon which has 343 nm as its associated wavelength. It follows that u.v. radiation might therefore lead to breaking of a bond, a process called photodecomposition. Photodecomposition can be regarded as an alternative fate of molecules in the excited state (RENDELL, 1987:128).

A decrease in the photo-emission intensity would be observed if the fluorescent species decomposed into non-fluorescent products. An increase in the intensity would be observed if the fluorescent species decomposed to give products which were more fluorescent than the original species under the same conditions of excitation and observation. Another possibility is that some other component present in the sample such as a fluorimetric reagent (which is always in excess over the analyte) may decompose to give fluorescent products. Other effects may arise from the destruction or formation of quenching agents in the sample through photodecomposition.

3.3.5. Photochemical Formation of Compounds

Photochemistry offers the possibility of initiating chemical processes that appear to have no analogue in thermal chemistry (GILBERT, 1991:3). The introduction of initiating electromagnetic radiation into the scheme effectively 'changes the rules' (excited states in general have a different electronic structure compared to the ground state and exhibit therefore different chemical properties) and opens up a whole new set of possibilities. The formation of cyclobutene from Buta-1,3-diene by absorption of u.v. light serves as one example.

3.4. Experimental Study of Radiative Transitions

In the following section the instrumentation required for fluorescence measurements is explained including a measurement procedure for steady-state fluorescence spectroscopy.

[14] $\Delta E = N_A h\nu$ and $\nu = c/\lambda$.

3.4.1. Steady-State Fluorescence Spectroscopy

Instrumentation

In a commercial fluorescence spectrometer, a near-continuum source of u.v.-visible radiation (for example, a xenon or mercury arc lamp) is passed through a monochromator to select an excitation wavelength (GILBERT, 1991:109). A sample - if liquid is usually contained in a 1 cm^2 section Pyrex or quartz cuvette - absorbs the exciting radiation and emits fluorescence[15]. Radiation that is emitted at right angles to the excitation beam is focused on to the entrance slit of a second monochromator which disperses the emitted radiation and a selected wavelength is transmitted to a detector (usually a photomultiplier), see Fig. 3.11. The fluorescence is monitored at right angles to the optical axis of the incident exciting radiation in order to reduce the amount of interference from scattered exciting light. (This is the most common system used.)

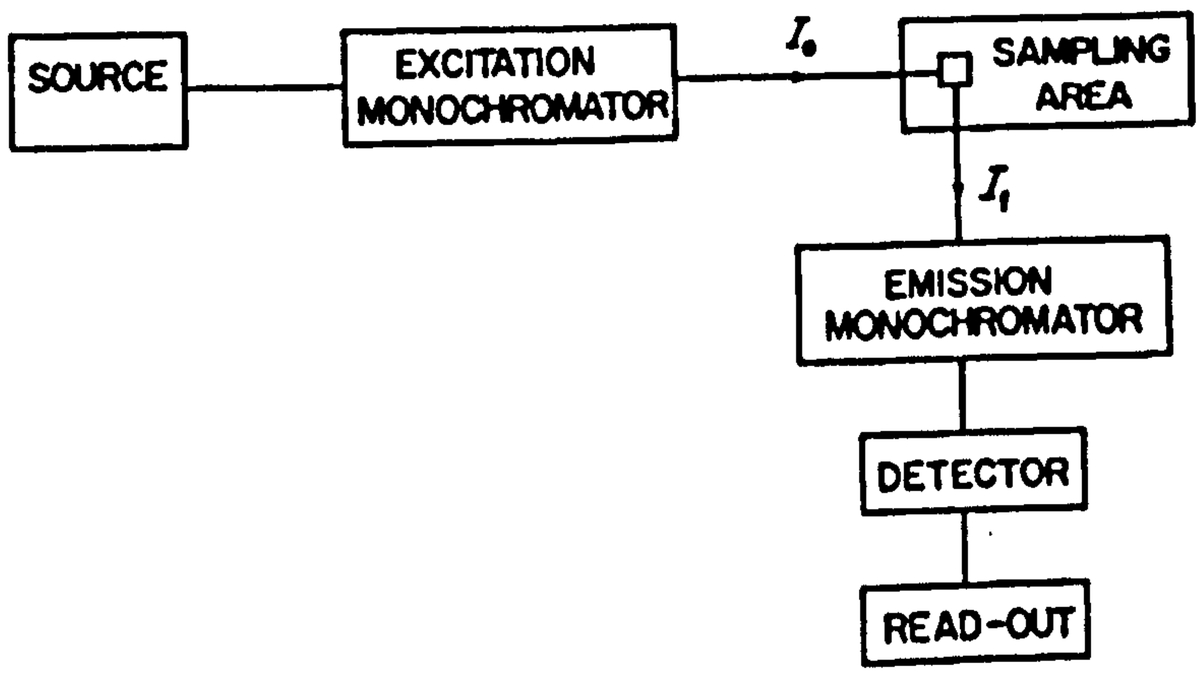

Fig. 3.11: Layout of a typical fluorescence spectrometer (RENDELL, 1987:60)

Measurement procedure

The use of two monochromators means that two kinds of spectra may be measured:

(i) A fluorescence '<u>emission spectrum</u>' is measured by setting the first (excitation) monochromator to a wavelength known to be absorbed by the sample. The second (emission) monochromator is then scanned over the wavelength region of the emission, and the dispersed fluorescence spectrum is recorded.

(ii) A fluorescence '<u>excitation spectrum</u>' is measured by setting the second monochromator to a wavelength known to be emitted by the sample. This wavelength will usually be at, or close to, the emission maximum. The first monochromator is then scanned to discover the

[15] Instruments to measure phosphorescence are specified differently.

range of wavelengths at which this sample absorbs and which gives rise to emission at the selected wavelength[16].

3.4.2. Time-Correlated Single Photon Counting

A powerful time-resolved technique is known as time-correlated single photon counting. Single photon counting is a flash technique in the sense that the excitation is provided by a pulsed flashlamp or laser. A typical single photon counting apparatus is illustrated schematically in Fig. 3.12.

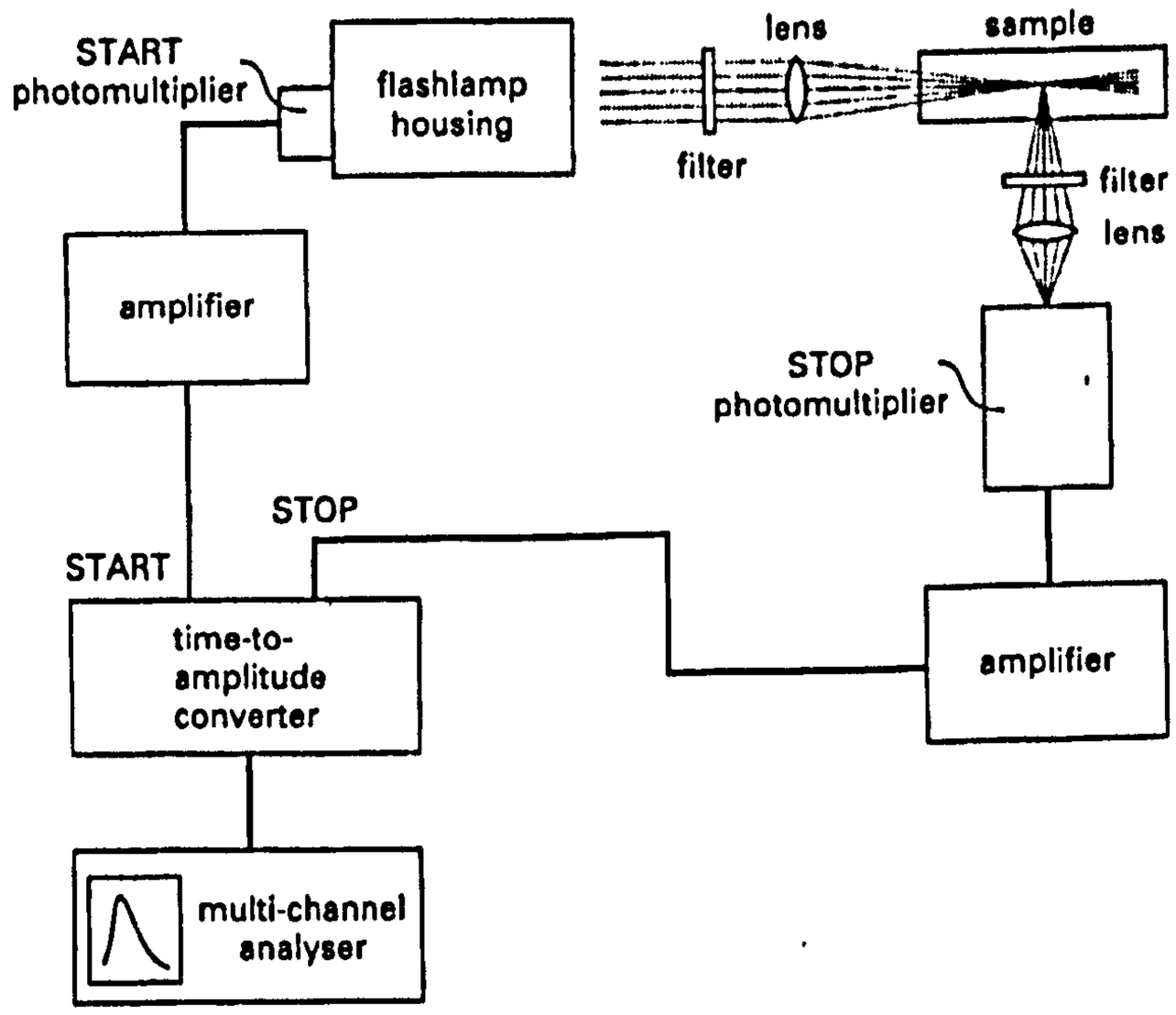

Fig. 3.12: Simplified schematic diagram of a time-correlated single photon counting apparatus (GILBERT, 1991:116).

It consists of two light detectors (in this case photomultipliers). The first, called in Fig. 3.12 the START photomultiplier, is attached to the back of the housing which contains the excitation light source, usually a small pulsed discharge lamp. The START photomultiplier produces a signal when it detects a pulse of light from the lamp and triggers an electronic device called a time-to-amplitude converter. The time-to-amplitude converter initiates a voltage ramp which increases steadily from zero at a rate set by the experimenter. Emission from the sample is detected at right angles to the excitation light path by an extremely sensitive STOP photomultiplier, capable of responding to the detection of a single photon. The STOP photomultiplier sends a signal to the time-to-amplitude converter which halts any further increase in the voltage ramp. Hence the time difference between excitation of the

[16] The fluorescence excitation spectrum provides information that is complementary to, but not necessarily equivalent to, the absorption spectrum of the sample (GILBERT, 1991:110).

sample and detection of an emission photon is converted into a voltage. If no photon arrives before the voltage ramp has increased to its maximum value, the electronics are simply reset and the cycle begins again. The time-to-amplitude converter is usually connected to a multichannel analyser which breaks the voltage range into a sequence of 500 or 1000 channels, each channel keeping a count of the number of times a specific voltage level is obtained. The cycle is repeated thousands to millions of times per second.

After a relatively short period, which depends on factors like the flashlamp pulse repetition rate and the emission quantum yield, a complete spectrum of voltages (amplitudes) and hence time differences is produced in the memory of the multichannel analyser. The probability that an emission photon will be detected within a given narrow time interval, corresponding to a single channel of the multichannel analyser, decreases exponentially with the increasing time interval. Basically, the intensity of emitted light is simply a measure of the probability of observing a photon to be emitted within a specific time interval. Thus, the spectrum of amplitudes in the memory of the multichannel analyser is a direct measure of the time history of the emitted light intensity and corresponds to the emission decay profile.

The decay profile generated by a single photon counting apparatus represents an enormous average of many absorption-emission 'events'. Even with a 1% detection efficiency, a decay profile accumulated in something like 15 min with a pulse repetition frequency of 100 kHz represents an average of nearly a million such events. These decay profiles can give very precise estimates of radiative lifetimes, and the single photon counting technique is perhaps the only one in which the lifetimes of two (or more) emitting states can be reliably separated by computer analysis of the corresponding multi-exponential decays. Because of the tremendous averaging advantage, deconvolution procedures can be used routinely, allowing nanosecond lifetimes to be measured despite that fact that the excitation pulse profile might possess widths of the order of a few nanoseconds. The disadvantage of low detection efficiency (which is usually necessary to prevent more emission photons arriving at the detector whilst the electronics are 'processing' the first) is offset by the use of high repetition rates.

3.5. Electrically Conducting Polymers

3.5.1. Introduction

Conducting materials are regarded as having conductivity values in the range of 10 to 10^6 S cm^{-1}. Traditional conductors include for instance metals and graphite. Semiconductors have conductivity values ranging from 10^{-9} to 10 S cm^{-1} and include materials such as silicon and germanium while insulators such as glass and indeed the common traditional bulk polymers have conductivities ranging from 10^{-16} to 10^{-10} S cm^{-1}.

The conductivity of electrically conducting polymers, which are π-bonded or conjugated polymers, i.e. polymers having an alternation of single and double bonds at least in the backbone, spans a very wide range ($<10^{-12}$ to $\approx 10^5$ S cm^{-1}) depending on doping.

The superiority of organic conductive materials resides in their tremendous architectural flexibility, inexpensiveness and ease of processing and fabrication (NALWA, 1997:xi). However, conjugated polymers in general tend to have one main drawback: they are often not stable to moisture, air or oxygen and may therefore require encapsulation in use.

Conductivity depends on the presence of a charged and mobile entity which is most commonly an electron or hole or it can be an ion. These charge carriers can be introduced into polymers of appropriate type. For electron/hole conduction, highly conjugated polymers are doped with charge transfer compounds while for ionic conduction, saturated flexible polymers are doped with ionic compounds. Because ionic conduction is not relevant for LED applications only polymeric electron/hole conduction is briefly reviewed in the following subchapter. Practical fabrication techniques with examples are then discussed and this chapter is rounded off by a brief discussion of the most common classes of electrically conducting polymers.

3.5.2. Polymeric Electron/Hole Conduction

Two equivalent pictures of polymeric electron/hole conduction are given in the following two subchapters.

Though as outlined below the mechanism for charge transport in these materials is not the same as in more traditional inorganic semiconductors, device engineering can take advantage of many lessons previously learned by classic semiconductors. For example the use of heterostructures, commonplace in III-V technology, can also be applied to polymer devices for improved carrier confinement, or for varying offsets with respect to injection electrodes.

Since conduction necessitates the movement of charge from one chain to another, it is natural that the ultimate conductivity is a function of how aligned the chains are within a sample (GALVIN, 1997). This means that the conductivity is dependent on how the polymer was synthesised and whether the sample was stretched to align chains. These differences are reflected in the spread of conductivity reported for a given polymer.

3.5.2.1.Polarons, Bipolarons and Solitons

The chain relaxation or deformation that results from adding electrons or holes to a chain produces a variety of charged entities , polarons, bipolarons and solitons, each with its own characteristic transport properties.

When an electron is added to a perfect chain, within fractions of a picosecond it causes the chain to deform, creating a characteristic pattern of bond deformation about 20 sites long (NALWA, 1997:3). The electron plus the deformation pattern constitute a polaron. In the case of trans-Polyacetylene (t-PA) the deformation causes the difference between single and double bonds to decrease gradually, but not vanish, in the progression from either end of the polaron to its centre. For most more complex polymers the deformation is better described as a tendency for the interchange of single and double bonds. Along with the chain deformation there is a change in the energy level structure. A level is pulled out of the valence band into the gap with its two electrons and a level is pulled out of the conduction band. To form an electron polaron, P^-, an electron taken from a donor, or a result of photoexcitation, is added to the upper conduction level. To form a hole polaron, P^+, an electron from the lower polaron valence level leaves, going into an acceptor or into a hole created by photoexcitation. Having one half filled level, the polaron has spin ½. The energy interval between a polaron level and the nearest band edge depends, as does the band gap, on the chain length, or more accurately, conjugation length. For typical conjugation lengths, say 40 Å, the polaron level is a few tenths of an electron volt from the band edge.

A bipolaron is formed by the union of two polarons of like sign. The bipolaron also has two levels in the forbidden gap. For a negative bipolaron, BP^{2-}, they are each occupied by two electrons, while for a positive bipolaron, BP^{2+}, they are both empty, i.e. occupied by two holes. The bipolaron has no spin. Because of the repulsion of the two like charges the stability of an isolated bipolaron has been questioned. Bipolarons that result from doping and are therefore close to the charged donors or acceptors that produce them are undoubtedly stable.

The soliton is an excitation that occurs only in conjugated polymers. For the following discussion a t-PA chain with double bonds sloping downward in going from left to right, as in Fig. 3.13, is denoted as type A, one with the double bonds sloping the other way, type B. A type A region next to a type B region may occur on the same t-PA chain. Characteristically, there is a region between them, approximately 14 sites long, in which the transition takes place. In this region the double bond to single bond difference reduces progressively, vanishing at the centre, i.e. at the centre the bonds are of equal length. The domain wall between the different directions of the double bonds, i.e. between regions A and B, is called a soliton. Although as described so far the soliton is neutral, S^0, it is characterised by a bound electron whose wave-function is spread over the region in which the delocalisation is varying. In a simple picture, where Coulomb forces between electrons are neglected, this bond electron, being neither bonding or antibonding, occupies a level at the centre of the gap. The neutral soliton therefore has spin ½. A second electron may occupy this level, resulting in a negatively charged soliton, S^-, which has no spin. Alternatively, the electron may leave this level, resulting in a positively charged soliton, S^+, with no spin.

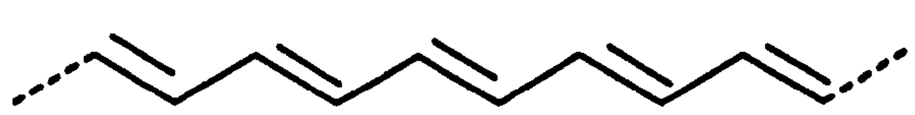

Fig. 3.13: Structure of trans-Polyacetylene (t-PA)

A polaron, bipolaron or soliton can travel along a chain as an entity, the atoms in its path changing their positions so that the deformation travels with the electron or hole. Except for the highly conducting metallic-like state these are the entities through which charge transport is accomplished in conducting polymers.

Because it is a topological defect, the soliton has some special properties that polarons and bipolarons do not possess. There is a difference between a soliton that connects a type A region on the left and B on the right and a soliton that connects B on the left and A on the right. To distinguish between them it is customary to call one, say the one with A on the left, a soliton, S, and the one with B on the left an anti-soliton, $\overline{S}$. It is apparent that on a chain with more than two solitons, S and $\overline{S}$ must alternate. A single soliton cannot hop between chains because it would require all the bonds to one side or the other to change. Solitons cannot go through each other, a feature that is possible for polarons.

So far it has been assumed that the properties of the particles are determined by a single chain, i.e. that interchain interactions have no effect. This assumption has been questioned,

particularly for the case of polarons. VOGL and CAMPBELL in 1990, from their local density functional calculations for polyacetylene, concluded that the effect of interchain interactions was sufficient in that case to destabilise the polaron, and thus make the electron into a conduction band electron of the kind usually found in three-dimensional semiconductors. These calculations were done for an infinite lattice of perfect polyacetylene. It was pointed out, however, that the many defects and short conjugation lengths in these materials would tend to stabilise the polaron (MIZES, 1993).

For a more detailed picture of polarons, bipolarons and solitons the reader is referred to review articles by CONWELL in 1987, HEEGER et al. in 1988, and CONWELL and MIZES (1992:583-625).

3.5.2.2.Delocalised π-Electron Systems

An equivalent picture of the electrical conduction mechanism to the one given above is to look at the molecular orbitals of conjugated polymers. These polymers possess a delocalised π-electron system along the polymer backbone. That system confers semiconducting properties to the polymer and gives it the ability to support positive and negative charge carriers with high mobilities along the polymer chain.

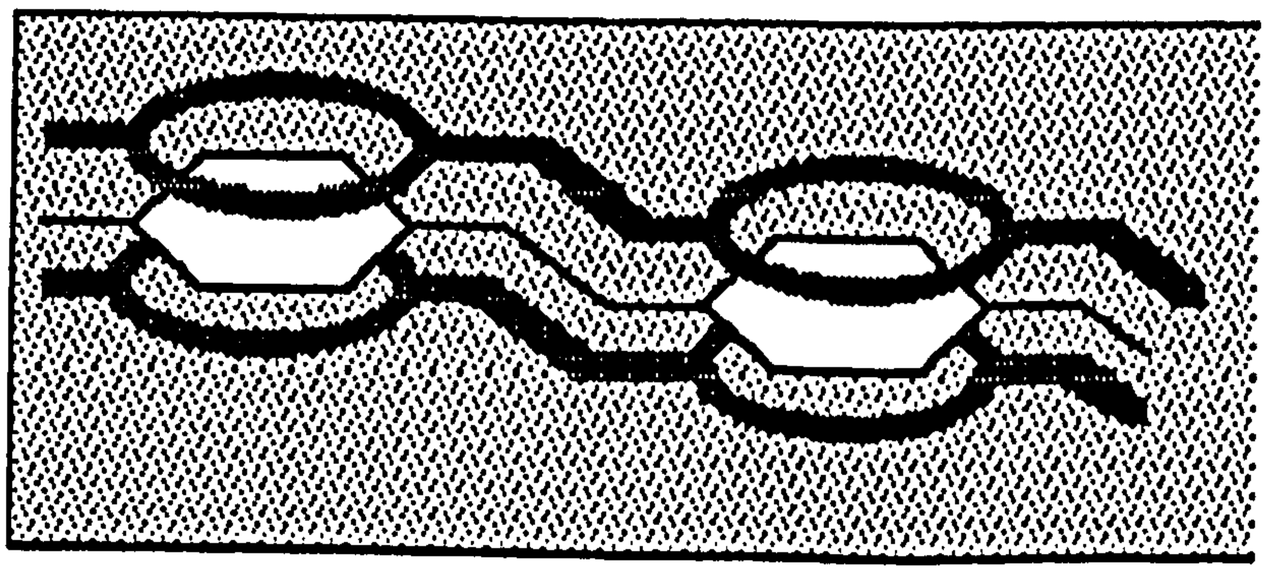

Fig. 3.14: Overlap of p_z orbitals which leads to the formation of a delocalised π-electron cloud above and below a conjugated polymer chain (CAMBRIDGE DISPLAY TECHNOLOGY LTD., homepage).

The semiconductor properties of these materials arise from the overlap of p_z orbitals that originate from the double or triple bonds, see Fig. 3.14. If the overlap is over several sites, the formation of a well delocalised π valence and π^* conduction band occurs, with a defined band gap.

3.5.3. Most Common Classes of Electrically Conducting Polymers

The most common classes of electrically conducting polymers are briefly outlined below with some fabrication routes given or quoted (GALVIN, 1997). A mixing across these classifications can also be found.

The tractability of conducting polymers may be improved by:

1) blending and forming dispersions or composites;
2) forming copolymers, graft of block;
3) utilising precursor polymers in processing followed by formation of the conducting polymer in situ;
4) using unusual solvents such as iodine to give soluble conducting polymers.

Examples for these techniques can be found in the following literature: For (2): YASSER, 1987; for (3): BRADLEY, 1992 and GUSTAFSSON, 1992; for (4): GALVIN, 1982.

Polyacetylene (PA)

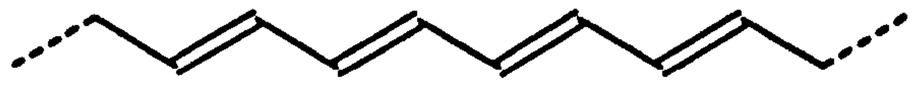

Fig. 3.15: Structure of Polyacetylenes

Films of this material (see Fig. 3.15), probably the most studied of all conjugated polymers, are commonly made by:

1) the Shirakawa method (IRO, 1974);
2) using tractable[17] precursor polymers (EDWARDS, 1984; MARTINS, 1993);
3) direct synthesis using new catalysts (GINSBERG, 1990:65).

Spin coated films aligned by stretching during polymer formation are the most common morphological form. The doping of these films can be p-type using Br_2, I_2, AsF_5, $HClO_4$ or H_2SO_4 or it can be n-type using sodium naphthalide in Tetrahydrofuran (THF) or via the electrolysis of LiI in THF with the polyacetylene film as the cathode. P-type doping is more common than n-type.

Polyacetylene films are unstable to air or moisture and a number of methods have been adopted to deal with this. Encapsulation using glass or polyparaphenylene, barrier resins

[17] A tractable precursor material can be moulded or shaped easily without fracturing, i.e. is plastic and not brittle.

and sacrificial layers have all been tried. Antioxidants such as hindered amines, phenols and nitrones have also all been tried. The dopant counterion has an effect on stability. Encapsulation is the most widely adopted technique but the general instability of polyacetylene has led to an increasing interest in other conjugated polymers. Its conductivity is reported to be in the order of 10^2 to 10^5 (stretched) S cm^{-1} (GALVIN, 1997).

Polyparaphenylene (PPP)

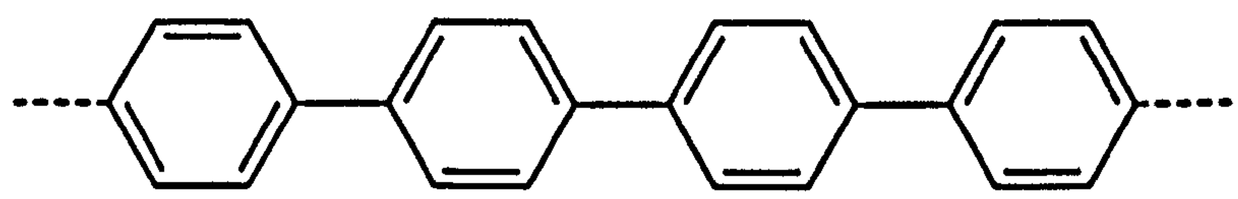

Fig. 3.16: Structure of Polyparaphenylene

This material, see Fig. 3.16, is prepared from benzene using either $AlCl_3$ and $CuCl_2$ at 35 °C or bacteria. The polymer formed is then doped by potassium naphthalide in THF for 100 hours inducing a change in conductivity from 10^{-14} S cm^{-1} to 7.2 S cm^{-1}. Films of this material are stable in air to 450 °C and to 550 °C in an inert atmosphere, hence their use as encapsulators. Recently, water soluble derivatives, Fig. 3.17, have been made (WALLOW, 1991:7411; CHATVURVEDI, 1993:2607; RAU, 1993:2607; CHILD, 1994:1975;). These have the advantage of allowing processing without the problem of environmental pollution from organic solvents.

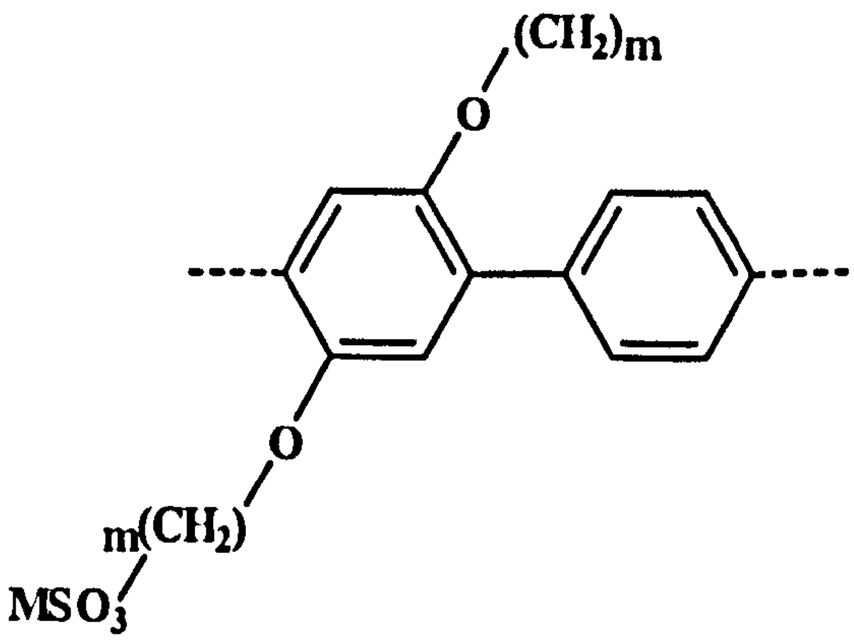

Fig. 3.17: Structure of water-soluble derivatives of Polyparapheynylene

Polypyrrole

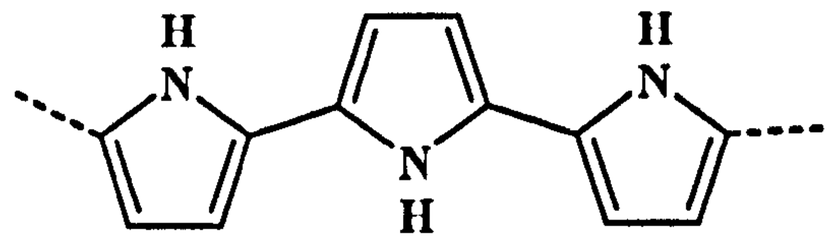

Fig. 3.18: Structure of Polypyrrole

Polypyrrole, Fig. 3.18, is commonly prepared by the electropolymerisation of pyrrole in a mixture of tetrethylammonium tetrafluoroborate in acetonitrile. A blue-black conducting polymer forms directly at the anode.

Conductivity can be as high as 10 to 10^3 (stretched) S cm^{-1} (GALVIN, 1997) and the film is stable up to 250°C in air. In general, there are four pyrrole rings to one positive charge with counterions such as perchlorate and p-tosyl sulphonate. Electropolymerisation of this type has yielded conducting polymer based azulene, benzene, bithiophene, carbazole, fluorene, furan, indole, pyrene and thiophene. There are a considerable number of derivatives of polypyrrole that have been produced including some which are water-soluble as the example shown in Fig. 3.19.

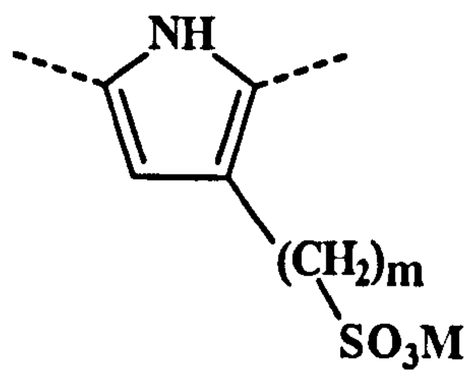

Fig. 3.19: Structure of water-soluble derivative of Polypyrrole

Polythiophenes

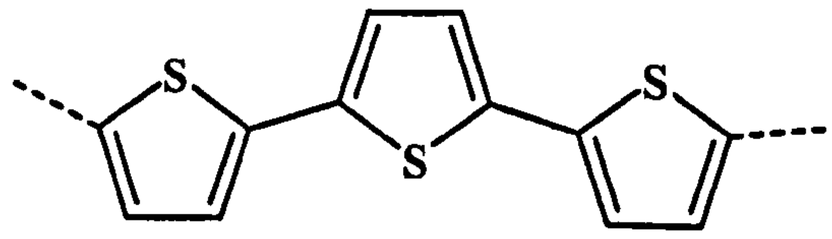

Fig. 3.20: Structure of Polythiophene

Conducting polythiophenes, Fig. 3.20, can be directly prepared by electrochemical means both anodic and cathodic (RONCALI, 1992). A cathodic film occurs during electroreduction of (2-bromo-5-thienyl)triphenylnickel bromide in acetone to give 100 nm thin neutral films (ZOTTI, 1984). Anodic films involve using noble metal

electrodes in anhydrous aprotic solvents. Up to 1997, the best conductivity result reported for a polythiophene film is 10^2 to 10^4 S cm^{-1} (GALVIN, 1997). A number direct chemical synthesis can also be performed, e.g. Grignard reaction[18] on 2,5 dihalothiophenes to give conductive films of 14 S cm^{-1} (KOBAYASHI, 1984).

A very large number of polythiophene derivatives has been made involving mono-, di-and trisubstituted rings and fused rings (RONCALI, 1992). More recent work with polythiophenes has involved degrees of functionalisation via soluble self-doping derivatives (PATIL, 1987; IKENOUE, 1988; NGUYEN, 1995) or improving thermal stability with retention of conductivity by limited ring substitution (ANDERSON, 1993; PEI, 1993; INGANAS, 1994). Stability and processibility of polythiophenes has also been attempted by producing composites. A number of these are also described by RONCALI in 1992.

Polyaniline

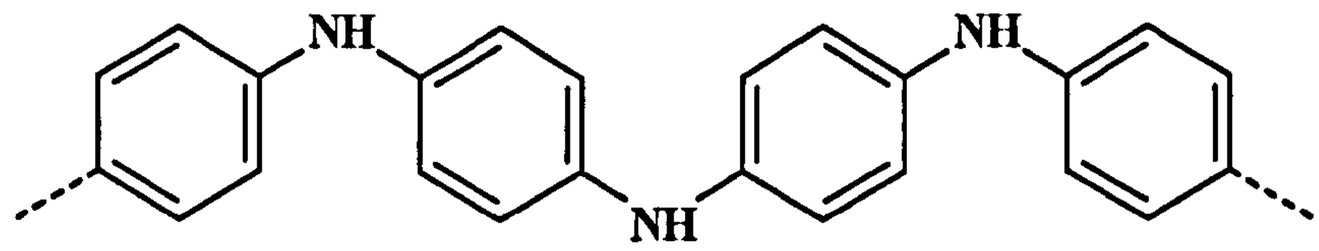

Fig. 3.21: Structure of Polyaniline

Another conjugated polymer, polyaniline (Fig. 3.21), can be prepared by electrochemical oxidation (MORITA, 1995) and thus has the advantage of relatively easy preparation. There are further advantages that such a monomer is inexpensive and readily available. The polymerisation is of high yield and the conducting polymer is stable (HEEGER, AJ, 1995). The doping of polyaniline can be oxidative using electrochemical means or suitable chemical oxidants or it can be protonic using strong acids (RAY, 1988).

Processing of the polymer can involve solvents such as N-methylpyrrolidone (ANGELOPOULOS, 1988), pyrrolidine, tripropylamine (HAN, 1991) or sulphuric acid (ANDREATTA, 1988) which cosolubilize other polymers though conductivity in such cases may be reduced. Functionalised protonic acids can be used to dope the polymer yielding complexes soluble in weakly polar organic solvents, e.g. dodecylbenzenesulphonic acid (CAO, 1992). Conductivity in this case has been reported to be between 10 to 150 (heated) S cm^{-1} (GALVIN, 1997).

---

[18] *Grignard reaction*: Magnesium in dry ether or furan forms R-Mg-OX which is a good reagent for a wide range of synthesis involving R-X → R-Y with X as a halogen and Y for example as CO_2H.

In a similar manner as for other cases, polyaniline can be functionalised to be water soluble (NGUYEN, 1995).

Polyarylene Vinylenes

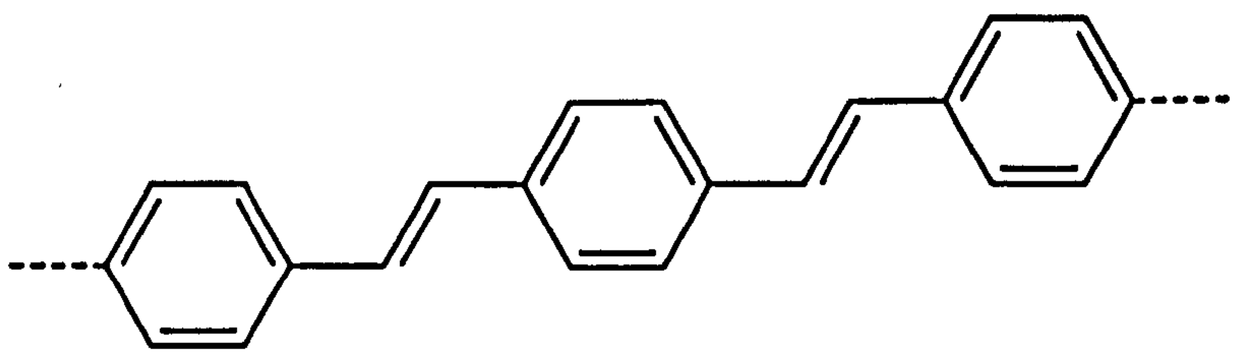

Fig. 3.22: Structure of Polyarylenevinylene

The traditional synthetic methods used to produce polyarylene vinylenes, see Fig. 3.22, are:

1) Polycondensation of aldehydes using the Witting and Knoevenagle-Doebner reactions[19];
2) 2-fold XY elimination in

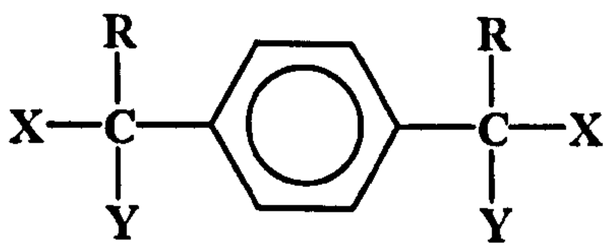

;

3) Step growth and elimination/polymerisation/elimination

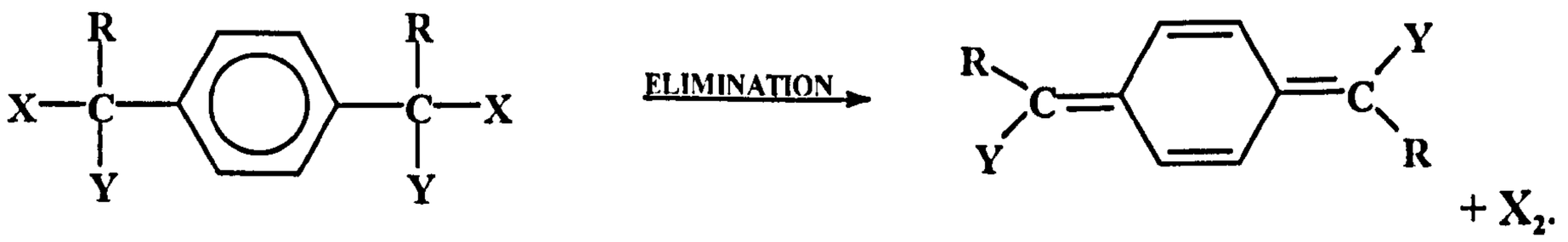

Addition polymerisation then follows and further elimination yields the desired polymer.

A wide variety of polyarylene vinylenes were synthesised by HÖRHOLD and co-workers in 1982; the simplest structure, Poly(phenylenevinylene) (PPV), is shown in Fig. 3.23. Its conductivity in the order of 10^3 S cm^{-1} (GALVIN, 1997).

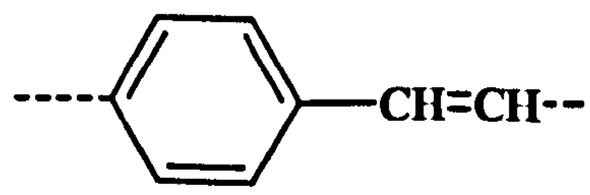

Fig. 3.23: Structure of Poly(phenylenevinylene)

[19] The *Wittig and Knoevenagle-Doebner reactions* involve the transformation of the group C=O to C=C.

Apart from being conducting on doping, many polyarylene vinylenes are electroluminescent leading to further revival of interest in them. Much of the published work on OLEDs of CAMBRIDGE DISPLAY TECHNOLOGY, see for instance FRIEND (1999), involves the synthesis of a wide range of this type of compound.

3.6. Charge Injection

3.6.1. Introduction

In this section a short description of some models for the processes of charge carrier injection in classical semiconductors is given. These models provide a starting point for understanding the processes in conjugated polymers. In contrast to classical semiconductors the charge carrier mobilities in polymer films are very low, hence, space charge effects are likely to be important in determining the electrical characteristics of polymer devices. One must therefore distinguish between injection effects and bulk effects such as the build-up of space charge (GREENHAM, 1995).

Charge injection from metallic contacts into solids, and in particular into semiconductors has been extensively studied (RHODERICK, 1988). To understand the injection process, it is first necessary to examine the detailed nature of the interface and to identify any barriers formed. The current flowing in a device is frequently limited by these barriers at the contacts rather than by the properties of the bulk of the solid. The two principal mechanisms for injection of charge are thermionic emission and quantum mechanical tunneling. These processes are described in section 3.6.3 and chapter 3.6.4, respectively. Metal-Semiconductor and Metal-Insulator contacts are described in the next sub-chapter.

In the given summary the contacts between metal and semiconductor have been assumed to be ideal, and the surface structure of the semiconductor has been assumed to be identical with the bulk structure. For a real contact the possibility of defect states has to be taken into account. If the charge contained in these states is sufficient to cause the band-bending necessary to equalise the Fermi levels of metal and semiconductor, then the barrier to injection will be determined solely by the surface states, independent of the work function of the metal. The injection characteristics can also be radically altered by the existence of an interfacial barrier which can be created due to chemical reactions during the formation process of the layers.

Further, all the injection models presented were developed for conventional three-dimensionally bonded semiconductors. In conjugated polymers the situation is considerably more complicated due to structural relaxation and polaron formation.

3.6.2. Metal-Semiconductor and Metal-Insulator Contacts

When a metal and another solid are brought into intimate contact, their Fermi levels (i.e. the energy level up to which most electrons are located at a given temperature or, more accurately, the energy for which the expected occupancy of a state is 0.5) must be equal at the interface in order to achieve thermodynamic equilibrium. Since the work function of the metal (equivalent to its Fermi level) and the Fermi level of the semiconductor (as measured from the vacuum level) are not necessarily equal, in general this requires a transfer of charge between the metal and the solid.

The situation for a contact between a metal and a lightly-doped n-type semiconductor where the work function of the metal, ϕ_m, is larger than the Fermi energy of the semiconductor, ϕ_s, is shown in Fig. 3.24. Negative charge from the semiconductor conduction band is transferred to the metal contact, leaving behind a positive space charge in the semiconductor due to the ionised dopants. This space charge zone is called *depletion region*, and its width, *W*, is approximated by

$$W = \sqrt{\frac{2(\phi_m - X)\,\varepsilon_s}{N_D\, q^2}} \qquad \text{Eq. 3.17}$$

where N_D is the dopant concentration, X is the electron affinity of the semiconductor, and ε_s is its permittivity (GREENHAM, 1995).

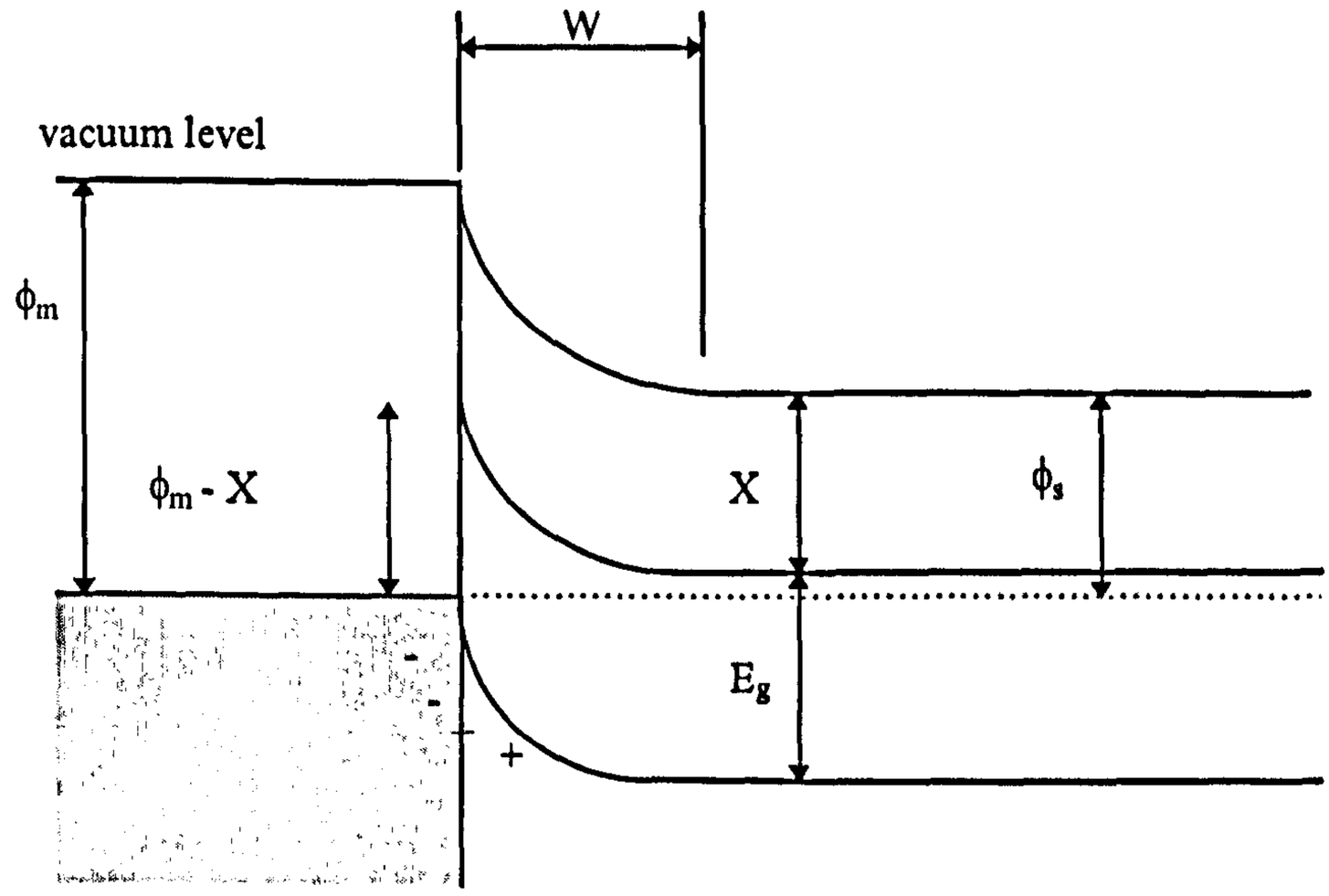

Fig. 3.24: Blocking contact between a metal and a n-type semiconductor

The term W represents the distance over which the bands are bent. This barrier to electron injection at the metal-semiconductor interface is called *Schottky barrier*. The difference between the work function of the metal and the electron affinity of the semiconductor, $\phi_m - X$, gives the height of the barrier. This type of contact is known as a blocking contact.

For an applied bias, V, across the junction (with the metal negative) the depletion region becomes

$$W = \sqrt{\frac{2(\phi_m - X + qV)\,\varepsilon_s}{N_D\, q^2}} \qquad \text{Eq. 3.18}$$

If the Fermi energy of the semiconductor is larger than the work function of the metal then electrons are transferred from the metal into the semiconductor in order to achieve thermodynamic equilibrium. This case is shown in Fig. 3.25.

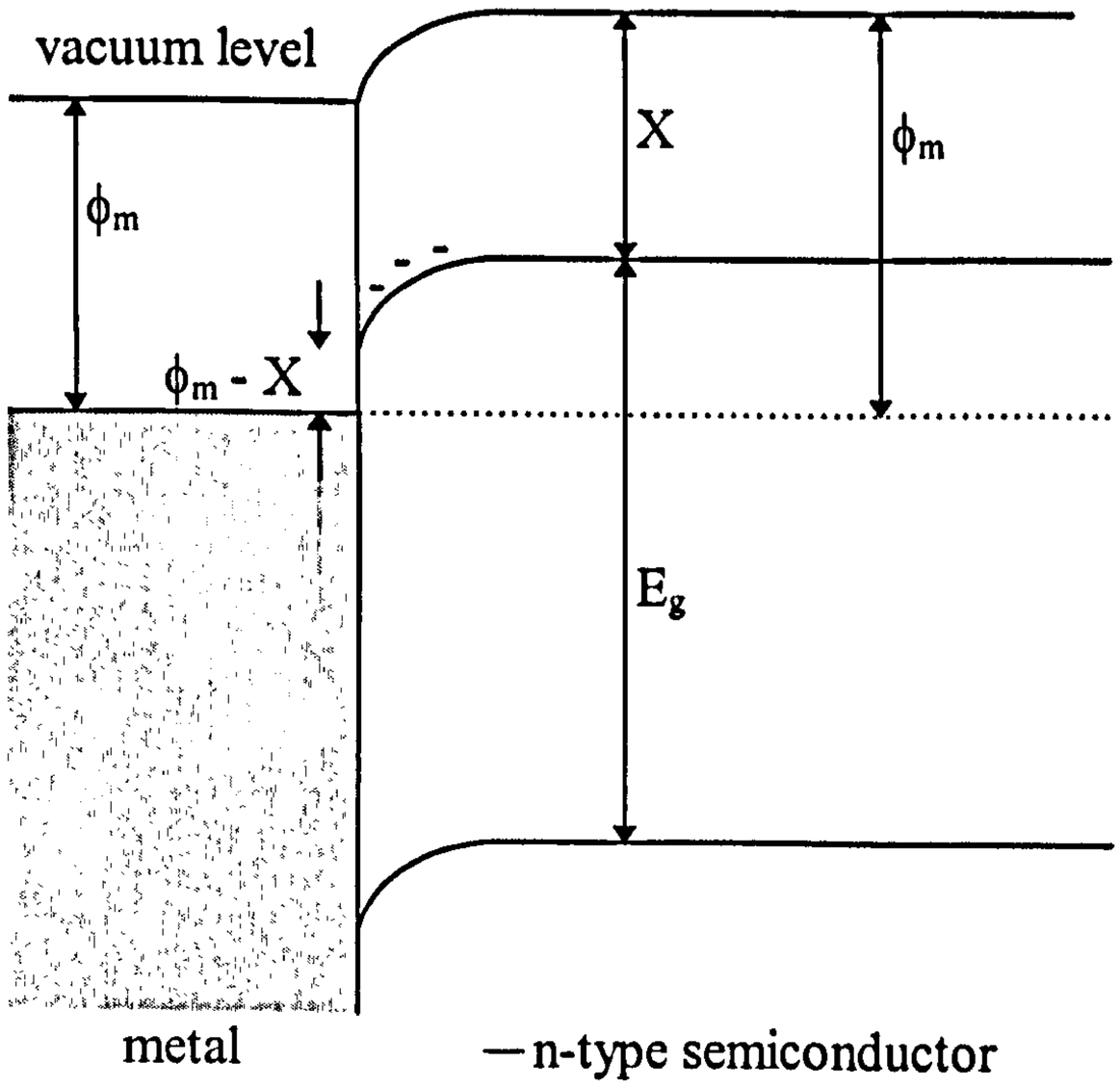

Fig. 3.25: Ohmic contact between a metal and a n-type semiconductor

Since there are now free electrons in the semiconductor conduction band at the contact, the current flow at low biases is no longer limited by the barrier to injection, and the contact is known as ohmic.

Under bias, as can be seen in Fig. 3.26, electrons are released from the point where $dV/dx = 0$ with zero kinetic energy. This point is known as the virtual cathode and with increasing applied bias it moves towards the contact until that point and the contact coincide. Then the current is only limited by the barrier at the electrode.

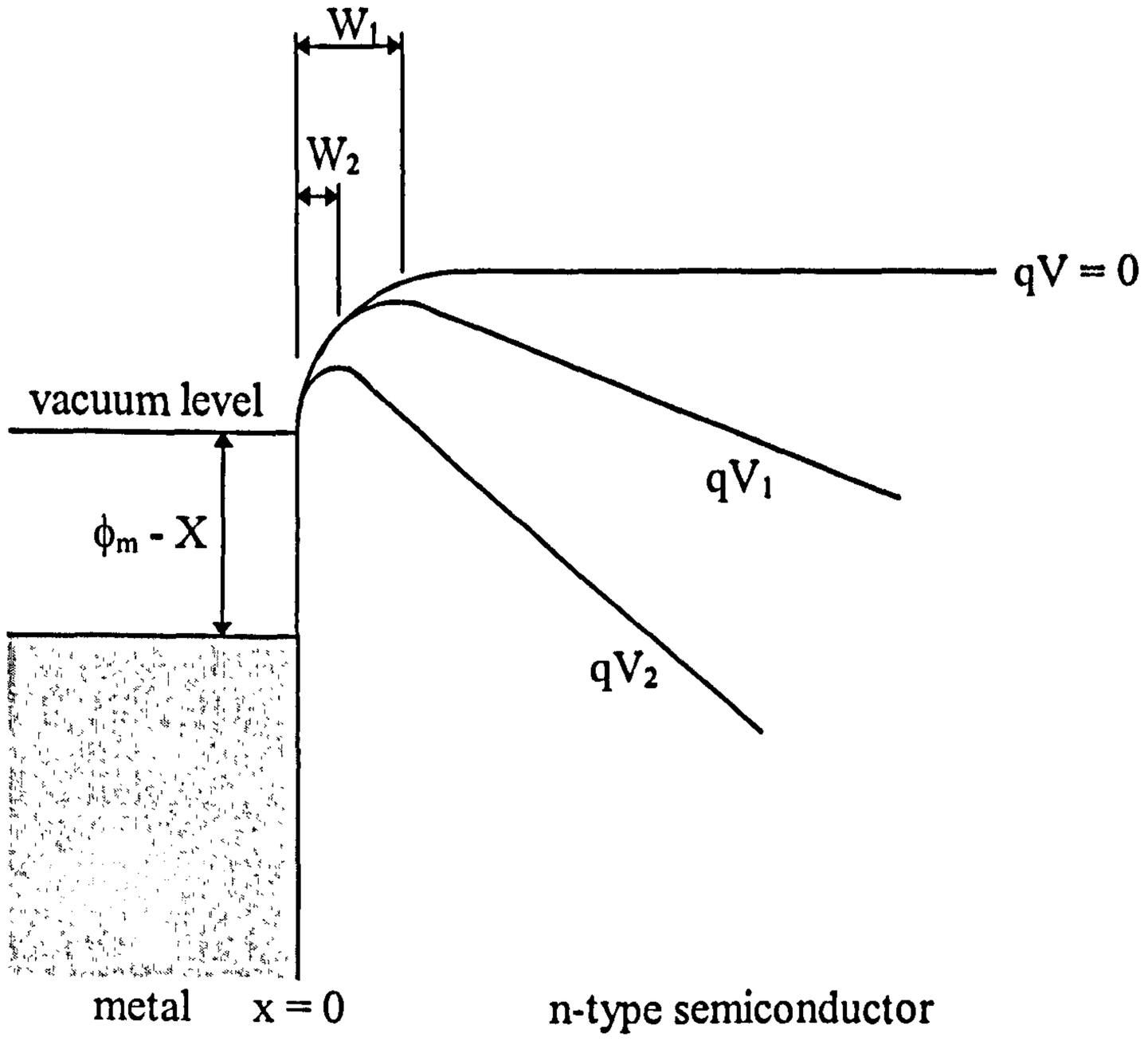

Fig. 3.26: Ohmic contact under applied bias showing the change in *W* with bias voltage

The density of traps (i.e. sites with lower potential energy for the charge carriers) inside the semiconductor determines the band-bending. For a density N_t of shallow traps at an energy E_t below the conduction band, the width of the depletion band, W, is approximately given by

$$W = \frac{\pi}{2}\sqrt{\frac{2kT\varepsilon_s}{q^2 N_t}}\exp\left(\frac{\frac{E_g}{2} - E_t}{2kT}\right) \qquad \text{Eq. 3.19}$$

where k is Boltzmann's constant and T is the absolute temperature.

In order to model the operation of a polymer EL device, it is clearly important to determine the thickness W of the depletion regions relative to the thickness of the device. If W is much greater than the thickness of the device, then the semiconductor cannot support sufficient charge carriers to achieve significant band-bending in equilibrium, and the bands are effectively flat.

3.6.3. Thermionic Emission

For thermionic emission over a triangular barrier of height ϕ_b from a metal into a high-mobility semiconductor, the current density is given by

$$J = \frac{4\pi q k^2 m^*}{h^3} T^2 \exp(-\phi_b / kT) = A_1^* T^2 \exp(-\phi_b / kT) \qquad \text{Eq. 3.20}$$

where A_1^* is known as the effective Richardson constant and m^* is the effective electron mass (SZE, 1981:256).

An applied field, F, causes a lowering of the barrier which is usually referred as image-force lowering (see Fig. 3.27). If an electron is placed at a distance x from a metal surface, a positive charge is induced on the surface of the metal. The effect of this charge is the same as that of an "image charge" placed at a distance x behind the surface. The forces between these charges build up a potential given by

$$V = \frac{q^2}{16\pi\varepsilon_s x} \qquad \text{Eq. 3.21}$$

When the effect of the applied field is superposed on the image force, a field-depended lowering of the barrier, $\Delta\phi$, is obtained, given by

$$\Delta\phi = \sqrt{\frac{q^3 F}{4\pi\varepsilon_s}} \qquad \text{Eq. 3.22}$$

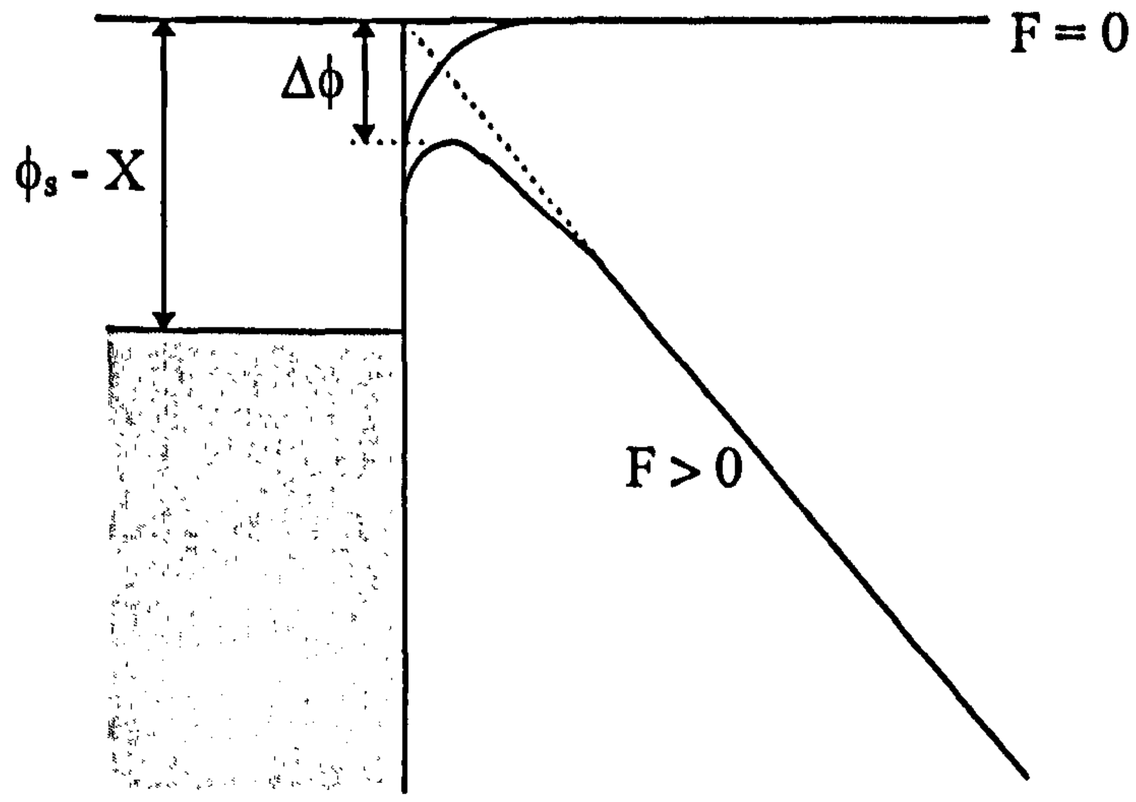

Fig. 3.27: Image-force lowering of barrier height (GREENHAM, 1995)

For a Schottky barrier under a bias V, the lowering of the barrier is denoted as

$$\Delta\phi = \left[\frac{q^6(qV-\phi_b)N_D}{2(8\pi)^2\varepsilon_s^{\,3}}\right]^{1/4}. \qquad \text{Eq. 3.23}$$

In a semiconductor with a low mobility (e.g. a conjugated polymer) it is necessary to take into account the diffusion of charge carriers within the barrier region back towards the contact. The analysis is complicated and depends on the type of barrier assumed. The effective Richardson constant A_1^* is now replaced by A_2^*, which depends on field F, temperature T and mobility μ (GREENHAM, 1995). In the high-field limit, the case for an intrinsic semiconductor gives

$$\frac{A_2^*}{A_1^*} = \mu(2m^*)^{1/2}\left[4\varepsilon_s\left(\frac{F}{q}\right)^3\right]^{1/4}\exp(-\phi_b/kT) \qquad \text{Eq. 3.24}$$

For a Schottky barrier in the low-mobility limit and also at high field, the relationship between A_2^* and A_1^* is given by

$$\frac{A_2^*}{A_1^*} = \frac{\left(\frac{2\pi m^*}{kT}\right)^{1/2}}{\int_{x_m}^{W} \frac{q}{\mu\, kT} \exp\left(-\frac{\phi_b - \Psi}{kT}\right) dx} \qquad \text{Eq. 3.25}$$

where x_m is the position of the maximum barrier height (taking into account image-force lowering) as shown in Fig. 3.28. Under non-equilibrium conditions such as the injection of charge carriers, the carrier populations no longer follow the usual Boltzmann relations. It is useful to replace the Fermi energy by quasi-Fermi energies for electrons and holes so that the modified Boltzmann relations still apply. In Eq. 3.25, Ψ represents the energy difference between the quasi-Fermi energy for electrons and the conduction band of the semiconductor.

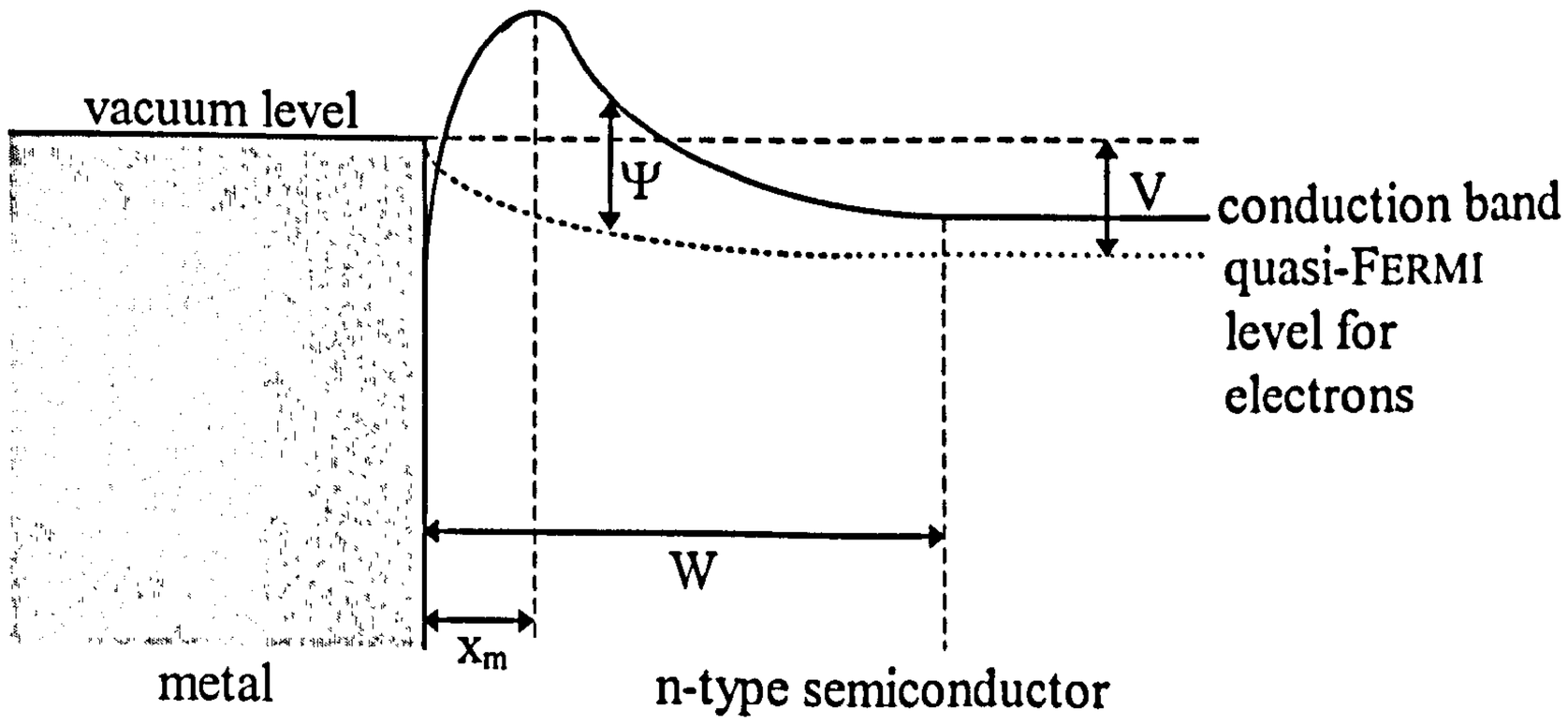

Fig. 3.28: Schottky barrier between a metal and an n-type semiconductor, including image-force effects and quasi-Fermi energy for electrons (GREENHAM, 1995).

3.6.4. Quantum Mechanical Tunnelling

For large barriers at high fields or at sufficiently low temperatures, emission due to quantum mechanical tunnelling through the barrier, also known as field emission, can become an important charge carrier injection process (KAO, 1981). The rate of tunnelling through a triangular barrier of height ϕ_b at a low temperature T and applied field F is given by

$$J = \frac{A_1^* T^2}{\phi_b}\left(\frac{qF}{\alpha kT}\right)^2 \exp\left[-\frac{2\alpha\phi_b^{3/2}}{3qF}\right] \qquad \text{Eq. 3.26}$$

where

$$\alpha = \frac{4\pi\left(2m^*\right)^{1/2}}{h} \qquad \text{Eq. 3.27}$$

To extract the barrier height from Eq. 3.26 tunnel currents can be analysed in the following way: $\ln\left(J/F^2\right)$ is plotted against $1/F$ which gives a straight line, of which the gradient can be used to obtain the barrier height.

For a Schottky barrier, the tunnelling rate is given by

$$J = A_1^* T^2 \left(\frac{E_{00}}{kT}\right)^2 \frac{\left(\phi_b + qV\right)}{\phi_b} \exp\left[-\frac{2\phi_b^{3/2}}{3E_{00}\left(\phi_b + qV\right)^{1/2}}\right] \qquad \text{Eq. 3.28}$$

where

$$E_{00} = \frac{2q}{\alpha}\left(\frac{N_D}{2\varepsilon_s}\right)^{1/2} \qquad \text{Eq. 3.29}$$

with N_D as the dopant concentration of the semiconductor. Looking at Eq. 3.28 we can see that the tunnelling current is nearly insensitive to temperature, but strongly dependent on the applied field. The tunnelling rate also depends strongly on the width of the barrier, thus thermal excitation can significantly increase the tunnelling current.

3.7. Current Transport

3.7.1. Single-Carrier Currents

The transport of electrons in a trap-free semiconductor is described by the mobility, μ_0, which is the average drift speed of an electron per unit applied field. The drift current is given by

$$J_\mu = n_f q \mu_0 F \qquad \text{Eq. 3.30}$$

where n_f is the number density of free charge carriers at an applied field F (GREENHAM, 1995).

In a semiconductor with significant trapped charge that does not contribute to the carrier transport, the total number density of charge, n, is the sum of the free and trapped parts, n_f and n_t, such that

$$n = n_f + n_t \qquad \text{Eq. 3.31}$$

It is useful to define an effective mobility

$$\mu_{eff} = \mu_0 \frac{n_f}{n_f + n_t} \qquad \text{Eq. 3.32}$$

With this definition the drift current becomes

$$J_\mu = n \mu_{eff} F \qquad \text{Eq. 3.33}$$

In conventional three-dimensionally bonded semiconductors, mobilities at room-temperature are high, typically 10^2 to 10^4 cm^2 V^{-1} s^{-1}, and are limited by scattering from impurities, phonons, etc.. In molecular crystals the mobility is limited by hopping of the charge between conjugated units, and mobilities are typically in the range of 10^{-2} to 10^1 cm^2 V^{-1} s^{-1}. For conjugated polymers, hole mobilities have been found to be typically less than 10^{-4} cm^2 V^{-1} s^{-1}, which is attributed to larger hopping distances, increased disorder and also to the effect of traps. Electron mobilities have proved difficult to measure by time-of-flight techniques and are estimated to be at least two orders of magnitude lower than hole mobilities (OBRZUT, 1989). This difference is often referred to the trapping of electrons at defect sites due to impurities such as oxygen (MARKS, 1993).

Two theories have been put forward for the field and temperature dependence of hopping mobilities in disordered materials consisting of charge-transporting molecules dispersed in

an inert polymer matrix. One is based on the assumption that structural relaxation in the excited state is important, the polaron-model (see chapter 3.5) and the other is based on the assumption that disorder is the dominant effect (BÄSSLER, 1984). The models predict different temperature and field dependencies. The polaron-model gives

$$\ln \mu \propto -(T_0/T) \text{ at constant field} \qquad \text{Eq. 3.34}$$

and

$$\ln \mu \propto F^{-1} \sinh(aF) \text{ at constant temperature} \qquad \text{Eq. 3.35}$$

whereas the disorder model gives the temperature proportionality at constant field,

$$\ln \mu \propto -(T_0/T)^2 \text{ at constant field} \qquad \text{Eq. 3.36}$$

but

$$\ln \mu \propto F^{1/2} \text{ at constant temperature.} \qquad \text{Eq. 3.37}$$

In practice, neither theory can adequately explain all experimental data. It is difficult to measure over a sufficient range of temperatures to be able to distinguish between the T^{-1} and T^{-2} temperature dependencies without causing a morphological change that affects the results.

Transport in conjugated polymers is highly dispersive, meaning that the broadening of the leading edge of the transient photoconductivity signal measured in time-of-flight experiments is larger than that predicted by the *Einstein* relation

$$qD = kT\mu \qquad \text{Eq. 3.38}$$

where D is the diffusion coefficient for charge carriers.

For the injection of a single-carrier type into a semiconductor, provided that the contact is able to supply sufficient current, the total current will be limited by the build-up of a space charge within the semiconductor. The results presented next are derived for electrons, identical results apply for holes. For a trap free material, neglecting diffusion currents, and when the equilibrium charge density is negligible in comparison to the injected charge density, the space-charge-limited (SCL) current is given by

$$J_{SCL} = \frac{9}{8}\varepsilon_s \mu \frac{V^2}{d^3}, \qquad \text{Eq. 3.39}$$

where V is the applied voltage and d is the sample thickness. At low voltages where the equilibrium charge density, n_0, is larger than the injected charge density, and the ohmic current

$$J_\Omega = qn_0\mu \frac{V}{d} \qquad \text{Eq. 3.40}$$

is predominant over the SCL current.

For a sample with traps at a single level, μ is replaced by μ_{eff},(see Eq. 3.32) and the SCL current is then given by

$$J_{SCL} = \frac{9}{8}\varepsilon_s \mu_{eff} \frac{V^2}{d^3}. \qquad \text{Eq. 3.41}$$

If the injected charge density is high enough that the quasi-Fermi energy moves above the trapping level, then the traps become completely filled. In this case, known as the trap-filled limit, the density of charge in traps becomes negligible compared to the injected charge, and the current reverts to the trap-free value. For sufficiently deep traps, the current can change directly from the ohmic regime to the trap-filled regime as the voltage is increased (see Fig. 3.29.)

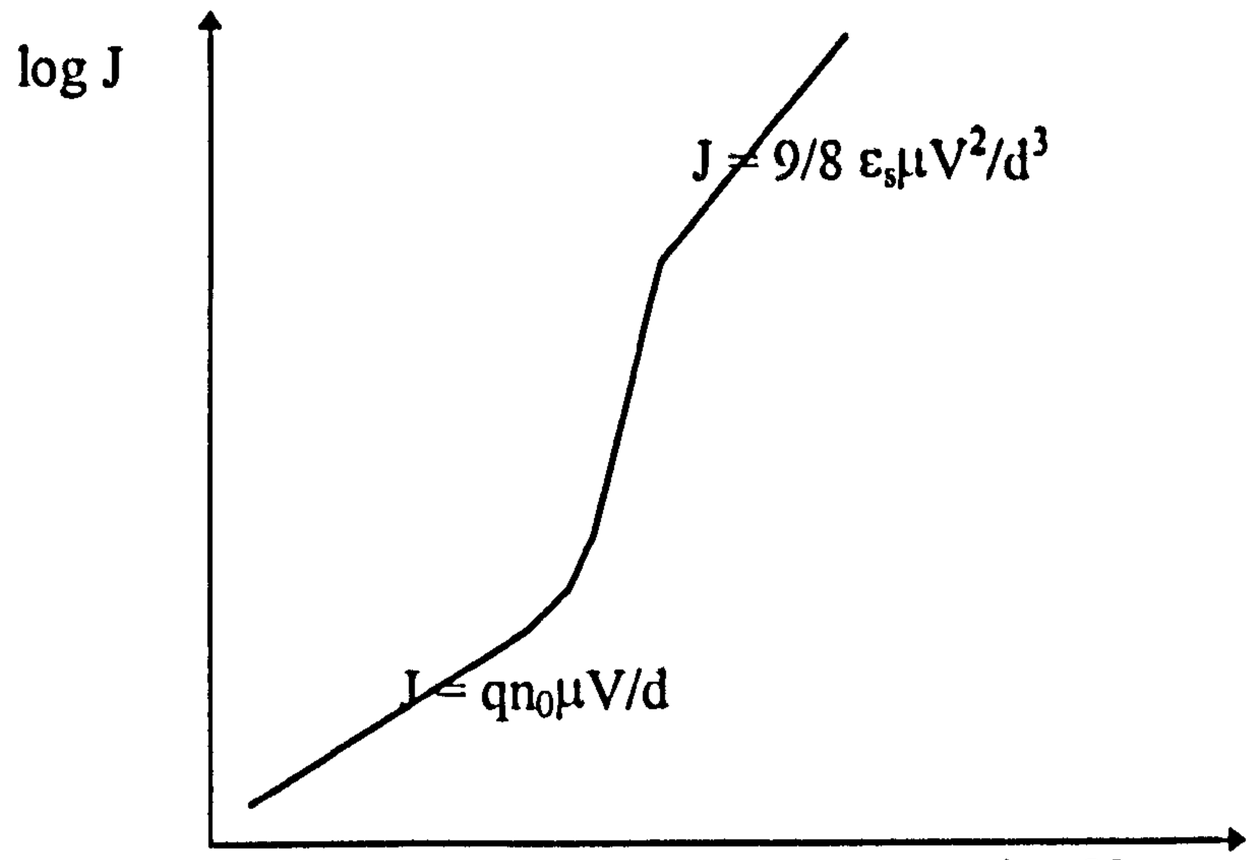

Fig. 3.29: Current density, *J*, versus voltage, V, for single carrier injection

The SCL current is the maximum current that can be passed under any circumstances. In conjugated polymers, where mobilities are low, space charges effects are likely to be important. In a polymer LED, it is important to find out whether the current is limited largely by the injection process, by space charge processes, or by a combination of the two (GREENHAM, 1995).

3.7.2. Electron-Hole Capture

In an electroluminescent device, carriers of opposite sign are injected from either side of the semiconductor. For the calculation of space charge effects, the total charge from both electrons and holes has to be considered, and therefore the situation becomes considerably more complicated than the single-carrier case.

The capture of electrons and holes to form bound, neutral excited states (excitons in the case of conjugated polymers) is a prerequisite for the emission of light in a polymer LED and can cause a profound effect on the current-voltage characteristics of a two-carrier device due to the removal of mobile charged carriers. A simple capture argument states that a bound excited state will form when an electron and a hole approach within a distance r_c, such that the Coulombic binding energy is greater than the thermal energy, kT, giving

$$r_c = \frac{q^2}{4\pi\varepsilon_s kT}. \qquad \text{Eq. 3.42}$$

(For $\varepsilon_r = 4\,\varepsilon_0$ and $T = 300$ K a value of $r_c = 14$ nm is obtained.) This argument is clearly an oversimplification because it neglects both the anisotropy of the polymer film and the effect of the external field.

For electrons and holes, number densities n and p, approaching each other with average speed v, it is useful to define a circular recombination cross section, σ_r, such that the generation rate for excitons per unit volume, G_E, is given by

$$G_E = npv\sigma_r \qquad \text{Eq. 3.43}$$

For conventional semiconductors, v is usually taken to be the average relative thermal velocity and is therefore independent of the applied field. However, in conjugated polymers, where the transport is largely due to hopping and the mean free path of a charge carrier is small, this picture may not be appropriate (GREENHAM, 1995). The relevant speed in the limit where thermally induced hopping is very much less likely than field-induced hopping is the relative drift velocity. Writing the electron and hole drift speeds in terms of their mobilities, μ_e and μ_h, gives

$$G_E = npF(\mu_e + \mu_h)\sigma_r . \qquad \text{Eq. 3.44}$$

3.7.3. A.C. conductivity in amorphous semiconductors

There are three mechanisms of charge transport that can contribute to direct current in amorphous semiconductors. They can all contribute also to the a.c. conductivity, as follows (MOTT and DAVIS, 1971: 211ff):

1) Transport by carriers excited to extended states[20], i.e. they can move freely, near the energies of the conduction and valence bands. For these the dependence of the conductivity vs. frequency, $\sigma(\omega)$, is given by

$$\sigma(\omega) = \frac{\sigma(0)}{1 + \omega^2 \tau^2}, \qquad \text{Eq. 3.45}$$

with τ as the time of relaxation.

[20] In an extended state electrons can move freely.

The relaxation time will however be very small, $\tau \approx 10^{-15}$s, and a decrease in $\sigma(\omega)$, is not expected until a frequency of about 10^{15} Hz is reached. This corresponds to an energy quantum lying above the fundamental optical absorption edge in most materials of interest. Therefore, in the electrical range of frequencies, up to about 10^{7} Hz, no frequency dependence of the conductivity due to carriers in extended states is expected.

2) Transport by carriers excited into localised states[21] at the edges of the valence or conduction band. Transport here is by hopping[22] and therefore the conductivity is expected to increase with the frequency according to

$$\sigma(\omega) \propto \omega \left(\ln \left(\frac{\nu_{Phonon}}{\omega} \right) \right)^{4} \qquad \text{Eq. 3.46}$$

with ν_{Phonon} as the phonon vibration frequency.

For $\omega << \nu_{Phonon}$, $\sigma(\omega)$ is approximately proportional to $\omega^{0.8}$. The temperature, T, dependence of this component of the a.c. conductivity should be the same as that for the part of d.c. conductivity involving excitation to the band edge , i.e. for the valence band it should increase as exp $(-(E_{Fermi}-E_B)/kT)$, with E_{Fermi} as the Fermi level and E_B as the energy level of the localised state at the band edge of the valance band (see MOTT and DAVIS, 1971:197ff).

3) Hopping transport by carriers with energies near the Fermi level (provided the density of states for the Fermi level is finite). This again should increase with frequency in the same manner as for process (2). However, the exponential dependence on the temperature will be absent, and $\sigma(\omega)$ should be proportional to T if kT is small compared to the width of the occupied part of the defect band; and independent of T otherwise.

Experimentally the mechanism giving the highest conductivity at a particular temperature would be observed.

---

[21] In a localised state electrons cannot move.

[22] Hopping describes a process where an electron hops between pairs of localised states absorbing or emitting a phonon each time.

3.8. Organic Light-Emitting Diodes

3.8.1. Structure and Principal of Operation

Modern standard electroluminescent[23] devices consist, in the simple case, of a semi-transparent indium-tin oxide (ITO) bottom electrode for hole injection, a light-emissive polymer layer and a metal top electrode for electron injection, often aluminium (Al). After injection of holes and electrons from the positive and negative electrodes, respectively, these charge carriers capture one another within the light-emissive polymer layer and form excitons, either singlets or triplets, see chapter 3.1. Of these, the singlet excitons may decay radiatively, giving out light which is observed through one of the electrodes which has to be at least semi-transparent. Triplet excitons, usually, tend not to decay radiatively.

A schematic energy-level diagram for an ITO/PPV/Al LED is given in Fig. 3.30, showing the ionization potential (I_P)[24] and electron affinity (E_A)[25] of PPV, the work functions of ITO and Al (Φ_{ITO} and Φ_{Al}), and the barriers to injection of electrons and holes (ΔE_e and ΔE_h).

Electrons and holes under applied bias are injected into the LUMO and HOMO band of the polymer, respective. Exciton formation of an electron and hole pair may take place within the polymer, indicated by a dotted line in Fig. 3.30. The excition may recombine in a radiative way, i.e. the device is emitting light.

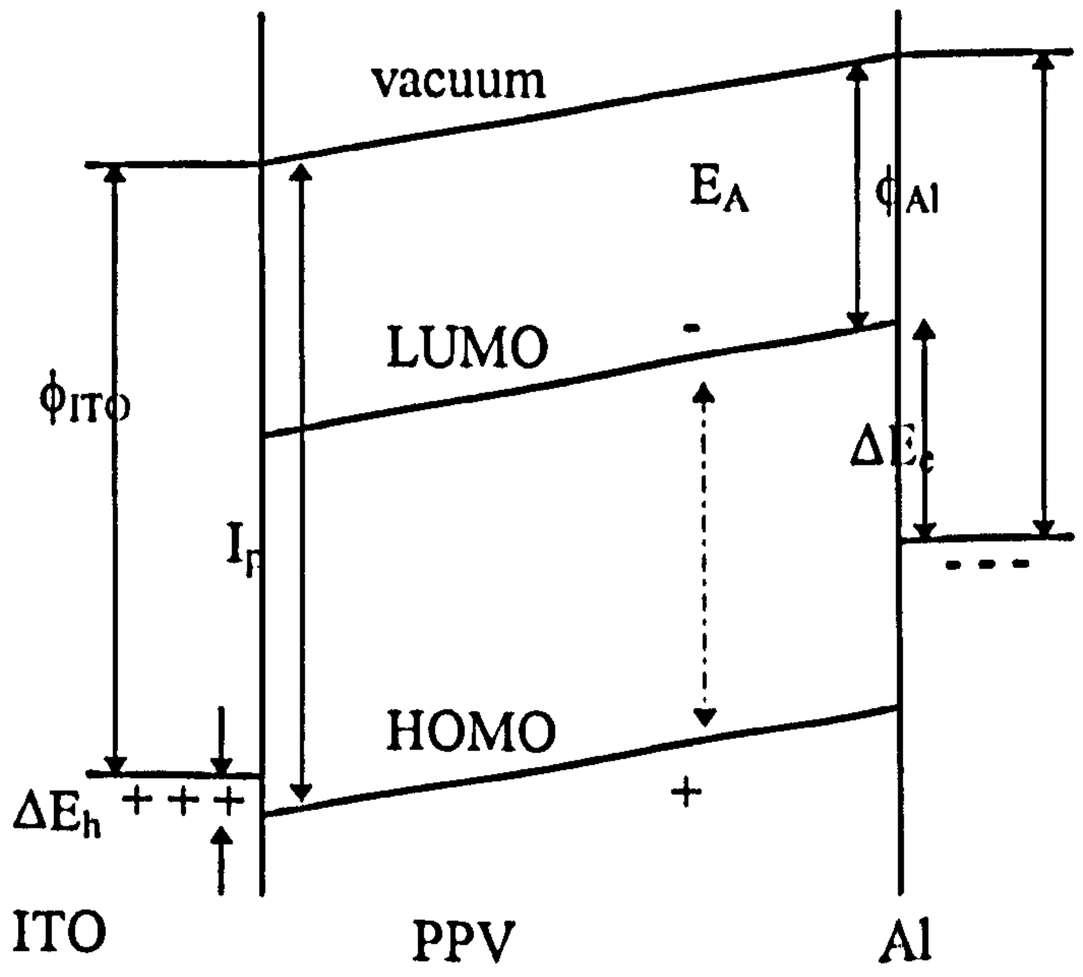

[23] Electroluminescence (EL) is the process of light emission from a material after injection of electrical charge carriers.
[24] The energy between the HOMO level and the vacuum level is called ionization potential.
[25] The energy between the LUMO level and the vacuum level is called electron affinity.

Fig. 3.30: Schematic energy-level diagram for an ITO/PPV/Al LED (GREENHAM, 1995)

The internal quantum efficiency, η_{int}, defined as the ratio of the number of photons produced within the device to the number of electrons flowing in the external circuit, is given by

$$\eta_{int} = \gamma r_{st} \eta_{st}, \qquad \text{Eq. 3.47}$$

where γ is the ratio of the number of exciton formation events within the device to the number of electrons flowing in the external circuit, r_{st} is the fraction of excitons formed as singlets and η_{st} is the efficiency of the radiative decay of these singlet excitons.

To achieve efficient luminescence, it is necessary to have efficient charge carrier injection, good balancing of electron and hole currents, efficient capture of the charge carriers within the emissive layer and efficient radiative decay of singlet excitons and finally efficient outcoupling of the generated photons.

3.8.2. Choice of Colour

In common polymer LEDs the colour of emission is fixed and determined by the band gap of the polymer or dye molecule. For example, the substitution of electron-donating groups at phenyl rings leads to absorption and emission at lower energies, thus the emission colour is shifted towards red. Blue-shifted emission, for instance, can be obtained from PPV by introducing non-conjugated units into the backbone to reduce the average conjugation length, which leads to a larger band gap between π and π^* orbitals.

The colour selection for systems consisting of dye-doped polymer films with conjugated sidegroups is even simpler: The dye acts as centre for the radiative decay of the generated excitons, therefore it is their band gap which determines the colour of emission.

A major problem in obtaining EL from materials with high energy gap, i.e. light emission in the blue spectral region, is that the barrier to electron injection, hole injection, or both is inevitably larger than in materials with lower energy gaps, imagine a larger distance between HOMO and LUMO band in Fig. 3.30. This makes the problem of balancing electron and hole injection even more difficult, and tends to lead to devices with high driving voltages and low efficiencies.

3.8.3. Single Layer Devices

Single layer devices show inherent drawbacks (AMMERMAN, 1997: 41):

1) Organic materials very rarely have equally good electron and hole transport capabilities. The effective mobility of electrons or holes can be reduced by traps. In a material with a low hole mobility for instance, the effective mobility of electrons can be reduced by deliberately introduced traps to equalise the mobilities. However, the disadvantage of this approach is that higher electrical fields, i.e. higher operational voltages, are required.
2) In a single layer device there is less opportunity to select electrode materials for electron and hole injection. Often injection limited EL cannot be avoided as it is difficult to balance positively and negatively space charged areas in the organic layer. As a consequence the recombinations take place near one electrode which reduces the quantum efficiency (chapter 3.2.2) due to quenching.
3) The thickness of the device is quite restricted. If the recombination zone is in the middle of the light emissive layer its thickness should be at least twice the mean exciton diffusion length. Because of the low mobilities of the charge carriers relatively high thicknesses may be needed. Therefore the required high electrical fields are often close to the breakthrough voltage. The emitted light intensity is approximately proportional to the current density. The generated heat is proportional to the electrical power, i.e. the product of injected current and applied voltage. For the same current density at higher film thicknesses there are higher applied voltages required according to the power law given in Eq. 3.41 which then might lead to the thermal destruction of the device.
4) The selection of the emission colour is limited. The material with the desired wavelength also needs to fulfil the criteria for the charge transport properties. Often then a high quantum efficiency cannot be achieved. Appropriate dye doping can provide more options, however, the dye molecules themselves may act as additional traps for charge carriers.

More choices for the selection of organic materials and contacts are generally given by using multilayer structures.

4. Device Fabrication

After an overview the materials used are listed and the spin coating thin film deposition technique as well as the vacuum deposition technique applied for this work to fabricate an OLED are explained.

4.1. Overview

A photograph of a typical fabricated device is given in Fig. 4.1. The eccentric aluminium dot serves as the anode being directly deposited onto the ITO layer after wiping off the polymer-dye film underneath, the dots in the regular array were directly deposited onto the polymer-dye film serving as Cathodes. All these dots are connected via a very thin gold wire to the more easily accessible larger contacts at the left and right hand side of the ceramic sample holder. The carrier glass substrate was glued onto that holder.

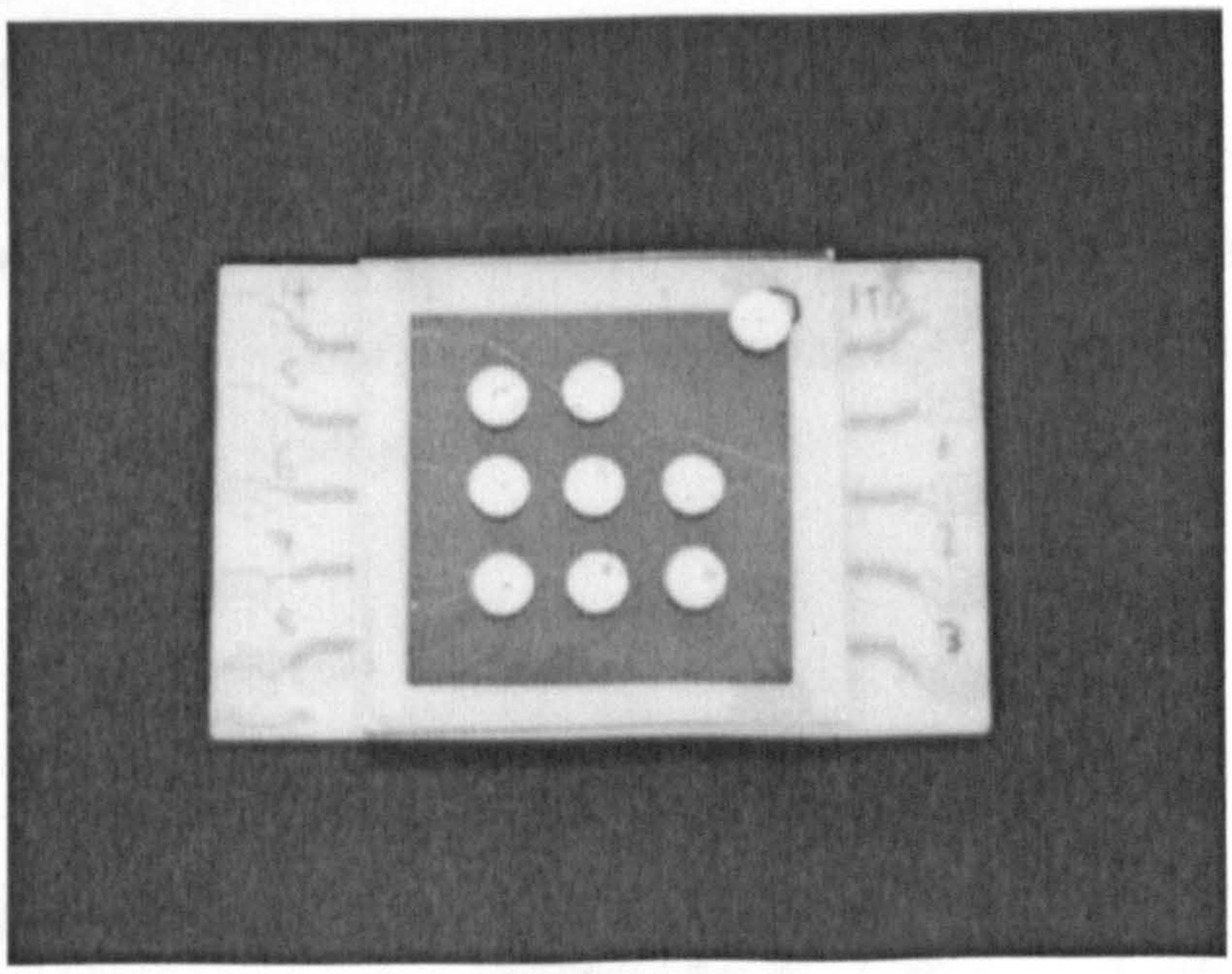

Fig. 4.1: Photograph of a typical device (not connected)

The device can be seen in operation in Fig. 4.2.

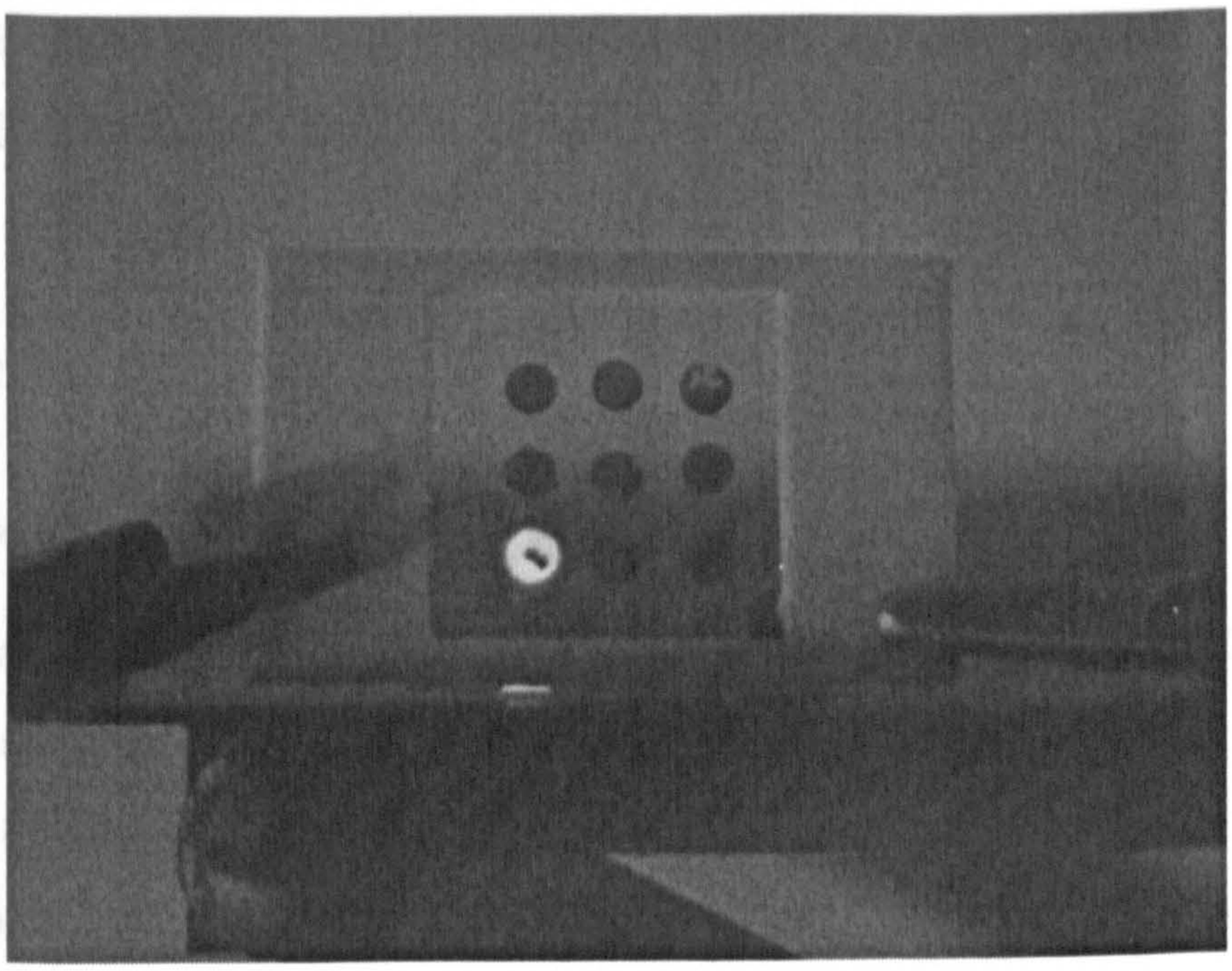

Fig. 4.2: Photograph of a typical device under operation (the bottom left pixel shows EL and includes also some defective area)

The thin film light-emitting diode to be investigated in this work is a so called single layer device consisting of a transparent bottom electrode on a glass substrate, a light producing dye doped polymer layer and a top electrode, see Fig. 4.3. Indium-Tin Oxide is used for the bottom electrode, the laser dye *p*-Bis(*o*-methylstyryl)benzene (Bis-MSB) embedded in a polymer matrix of poly(*N*-vinylcarbazole) (PVK) for the light producing layer, and aluminium (Al) is used for the top electrode.

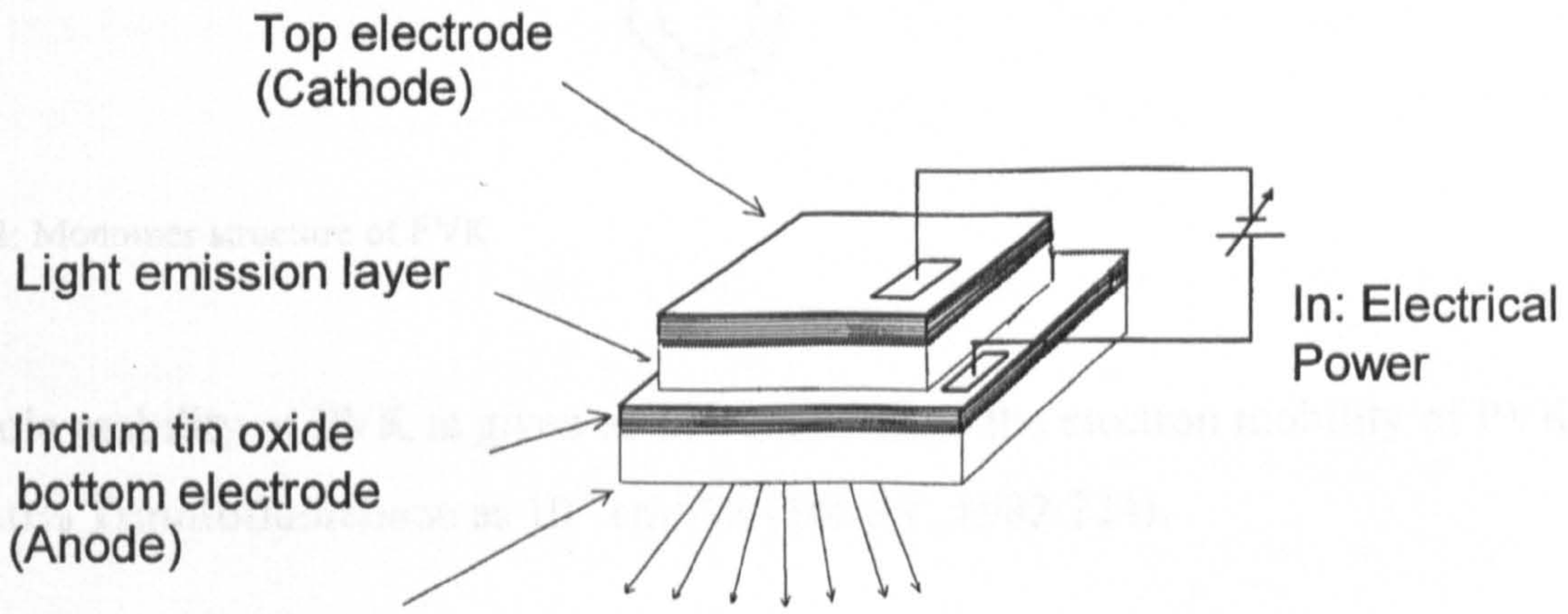

Fig. 4.3: Schematic sketch of a single layer thin film light-emitting diode

In order to prepare the devices the ITO glass had been dry cleaned thoroughly with a sterile paper towel devoid of lint. Afterwards the dye polymer solvent solution, see chapter 4.2, was spin coated onto the ITO glass substrate to obtain a thin dye doped polymer film. And

then the aluminium contacts had been vacuum deposited, see chapter 4.3, on top of the polymer-dye film.

4.2. Materials

4.2.1. The Polymer: Poly(*N*-vinylcarbazole)

Poly(*N*-vinylcarbazole) (PVK) (secondary standard from Sigma-Aldrich Company Ltd., Dorset, UK) is a non-conjugated polymer, see Fig. 4.4 for its monomer structure. It is commercially available as a colourless granulate and possesses a carbazole group on each repeat unit which has a widely delocalised π electron system. The latter accounts for the semiconducting properties of the polymer. The energy gap between π and π* orbitals lies in the region of about 3.5 eV and it shows blue electroluminescence (KIDO, 1993). Its ionisation potential, I_P, has been measured as 5.8 eV, and the electron affinity, E_a, as 2.3 eV (KIDO, 1995).

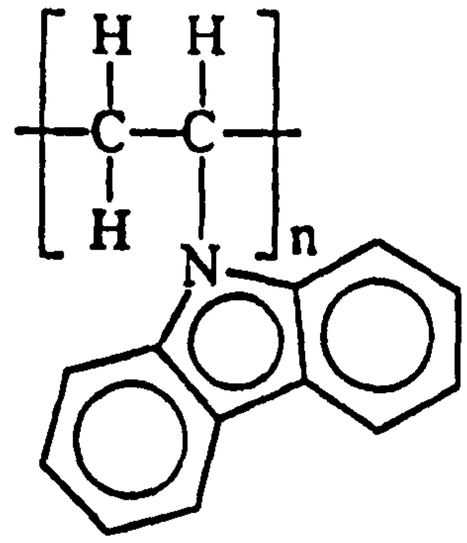

Fig. 4.4: Monomer structure of PVK

The hole mobility of PVK is given as 10^{-6} cm²/Vs and the electron mobility of PVK doped with 10% Trinitrofluorenone as 10^{-9} cm²/Vs (MORT, 1982:224).

4.2.2. The Solvent: Chloroform

Chloroform (99.8%, spectrophotometric grade, water content < 0.03%) from Sigma-Aldrich Company Ltd., Dorset, U.K was used.

At room temperature chloroform (trichloromethane) is a colourless non-flammable liquid. Its fusion point is -63.5 °C and the boiling point is 61-62 °C. Besides PVK and Bis-MSB it

dissolves resins, fats, waxes, rubber etc. It is also a powerful anaesthetic. The chloroform used in this work was purchased from Sigma-Aldrich with a purity of 99.9% (HPLC grade).

4.2.3. The Dye: *p*-Bis(2-methylstyryl)benzene

P-Bis(2-methylstyryl)benzene (Bis-MSB) (99% from Sigma-Aldrich Company Ltd., Dorset, U.K), see Fig. 4.5 for its monomer structure, is a blue laser dye with maximum fluorescence emission wavelengths in the region of blue visible light, see chapter 5.2.1. Its absorption peak measured in toluene lies at around 350 nm. The empirical formula is $C_{24}H_{22}$ and the molecular weight 310.44.

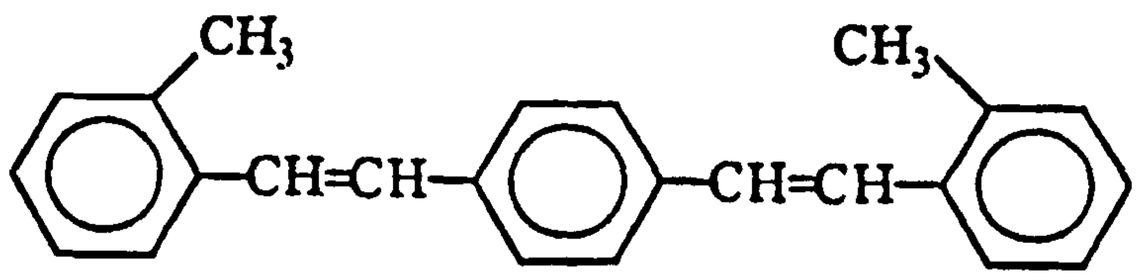

Fig. 4.5: Molecular structure of Bis-MSB

4.2.4. The Electrodes: Aluminium and Indium-Tin Oxide

Aluminium (purity:99.99% from Sigma-Aldrich Company Ltd., Dorset, U.K) has a high work function with a value of 4.3 eV (MAL'TSEV, 1995). After formation of an oxide layer it is not very reactive, which makes it attractive for commercial applications.

The Indium-Tin Oxide (ITO), work function depending on preparation but up to 4.8 eV (FRIEND, 1999), coated glass had been purchased from Balzers Ltd., Milton Keynes, UK. Indium-tin oxide has a high conductivity and can be deposited as a very thin transparent film on a glass substrate. The ITO deposited glass slides used in this work have a sheet resistance of 20 ohm sq^{-1} and a thickness of about 100 nm.

4.3. Preparation Techniques

4.3.1. Spin Coating

4.3.1.1.The Spin Coating Process

For the spin coating process a fixed amount of polymer solution is dispensed onto a carrier substrate which consists in this work of a piece of ITO coated glass. The carrier substrate is then rotationally accelerated up to a pre-set speed until a thin film is formed, see Fig. 4.6.

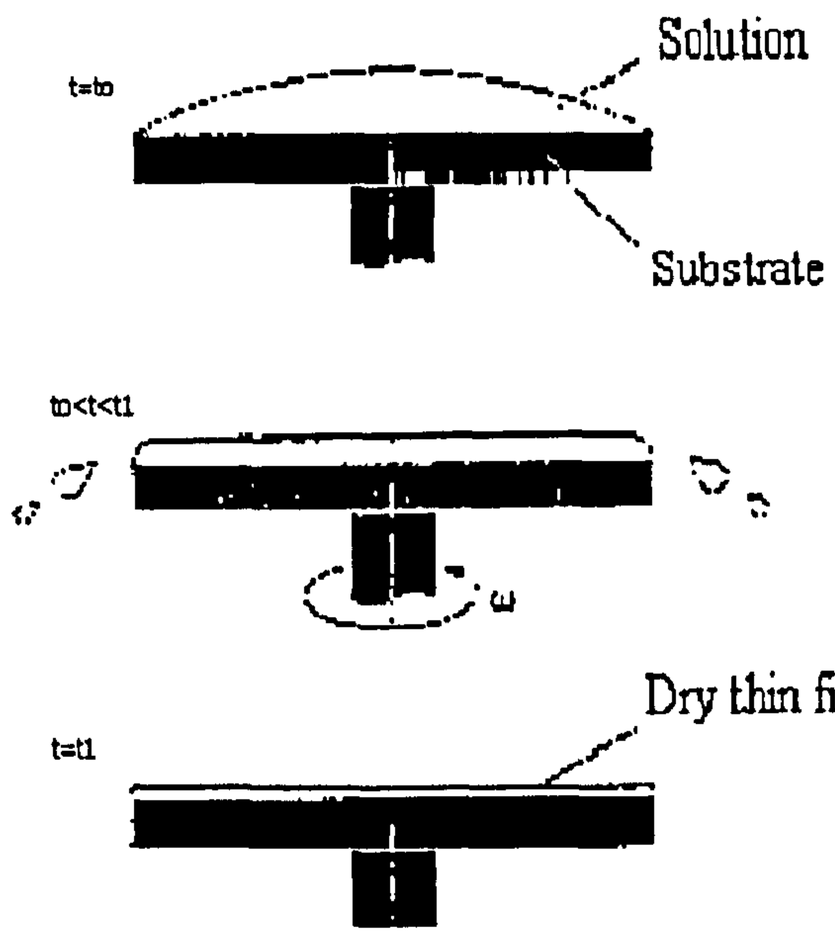

Fig. 4.6: Spin coating process (BROSIUS, 1990:142)

Several authors derived and numerically validated physical-mathematical models for the detailed description of the quite complex Physics and Chemistry involved in the spin coating process (BROSIUS, 1990; FLACK, 1984). In general the descriptions are based on the conservation of mass and momentum, the solvent evaporation, the viscosity dependence of the solvent concentration, empirical relations for viscosity and diffusion coefficients along with rheological substance properties. For instance the flow of the liquid is governed by a balance between centrifugal driving force and viscous resisting force. Because a polymeric solution normally consists of large molecules SHIMOJI (1987 and 1989) treats it as a Non-Newtonian fluid[26]. BORNSIDE (1989) also takes thermal energy effects into account. All relations lead to a system of coupled partial differential equations in connection with start and boundary conditions which have to be solved.

[26] The viscosity of a Non-Newtonian fluid depends not only on temperature and pressure but also on the rate of shear (DUGDALE, 1983; WILKINSON, 1960).

Summarising the above quoted literature five main results are presented in this work:

1) As can be seen from inspection of Fig. 4.7, calculation shows that most of the thickness loss is due, in the early stage of the process, to convective motion of the solution and, in the later stage of the process, the evaporation of the solvent. The initial rise in convective loss is due to (uncontrolled) angular acceleration of the spinner.

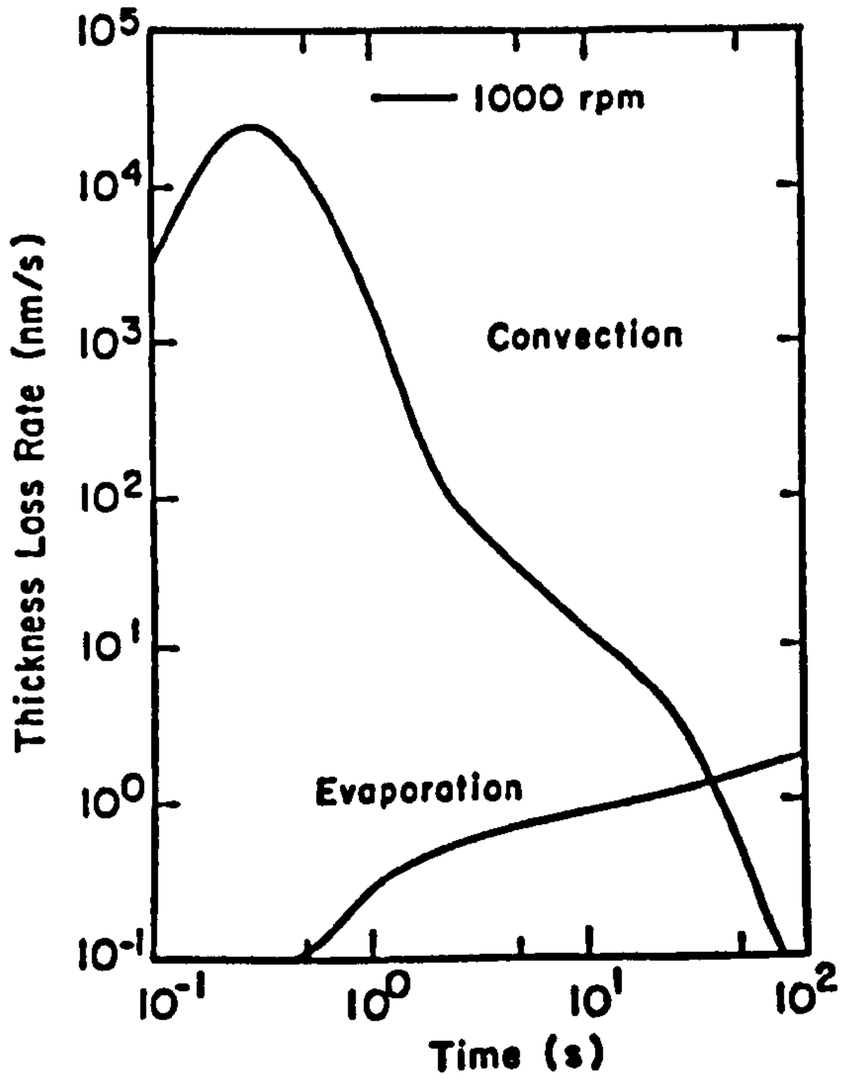

Fig. 4.7: Calculated thickness loss attributed to convective motion and solvent evaporation for a process involving a 6% Poly(methyl methacrylate) Chlorobenzene solution spun at 1000 rpm (FLACK, 1983:1204).

2) The initial amount of solution dispersed on the substrate has a negligible effect on the final film thickness.

3) A solution with high polymer concentration, i.e. with high viscosity, leads to a large dry film thickness. Fig. 4.8 illustrates the dependence of the dry film thickness on solvent mass fraction and spin speed.

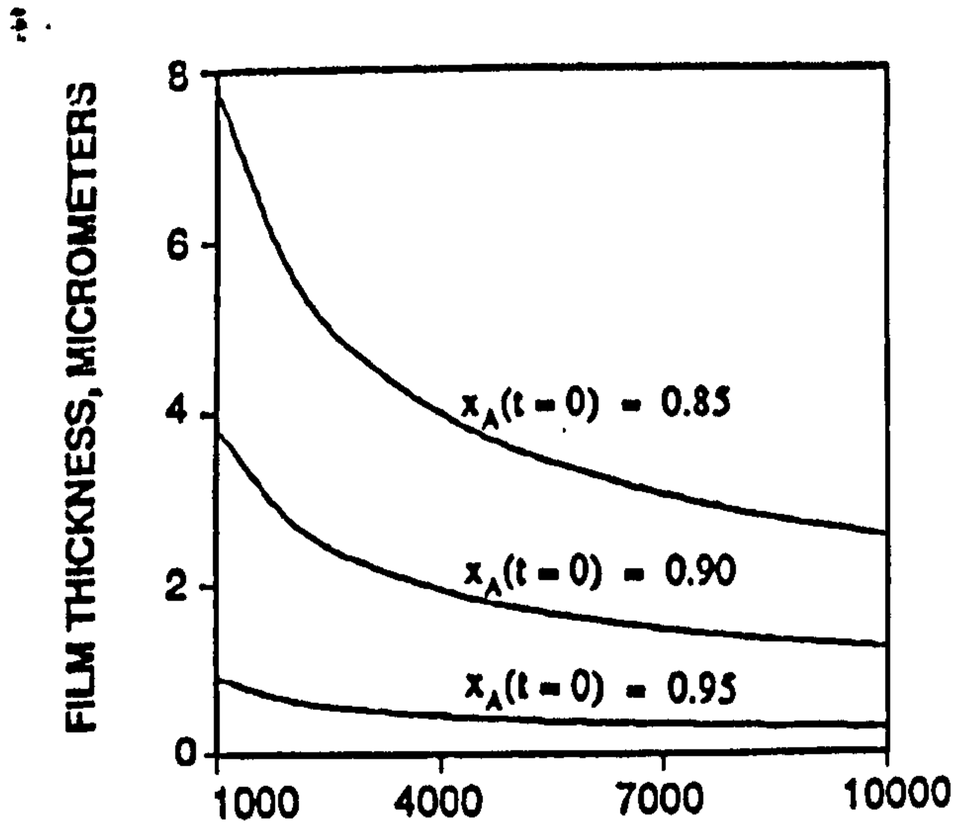

Fig. 4.8: Dry film thickness as a function of spin speed at initial solvent mass fractions, x_A, of 0.85, 0.90, 0.95. (The initial film thickness is 0.1 mm, and the concentration of solvent in the bulk of the overlying gas is zero.) (BORNSIDE, 1989:5189)

4) The time allowed for acceleration to the final spin speed influences the final film thickness and its radial uniformity. The plots in Fig. 4.9 show film thickness versus distance from the centre of the disk with time for 1-, 10-, 20-s acceleration periods to reach a final spin speed of 1000 rpm as a parameter. It is evident that the length of the acceleration period strongly influences the initial portion of the thickness-time history but not the final thickness of the film. In the given example - with no materials specified - a 1-s acceleration period produces a much more uniform film than acceleration periods of 10 or 20s.

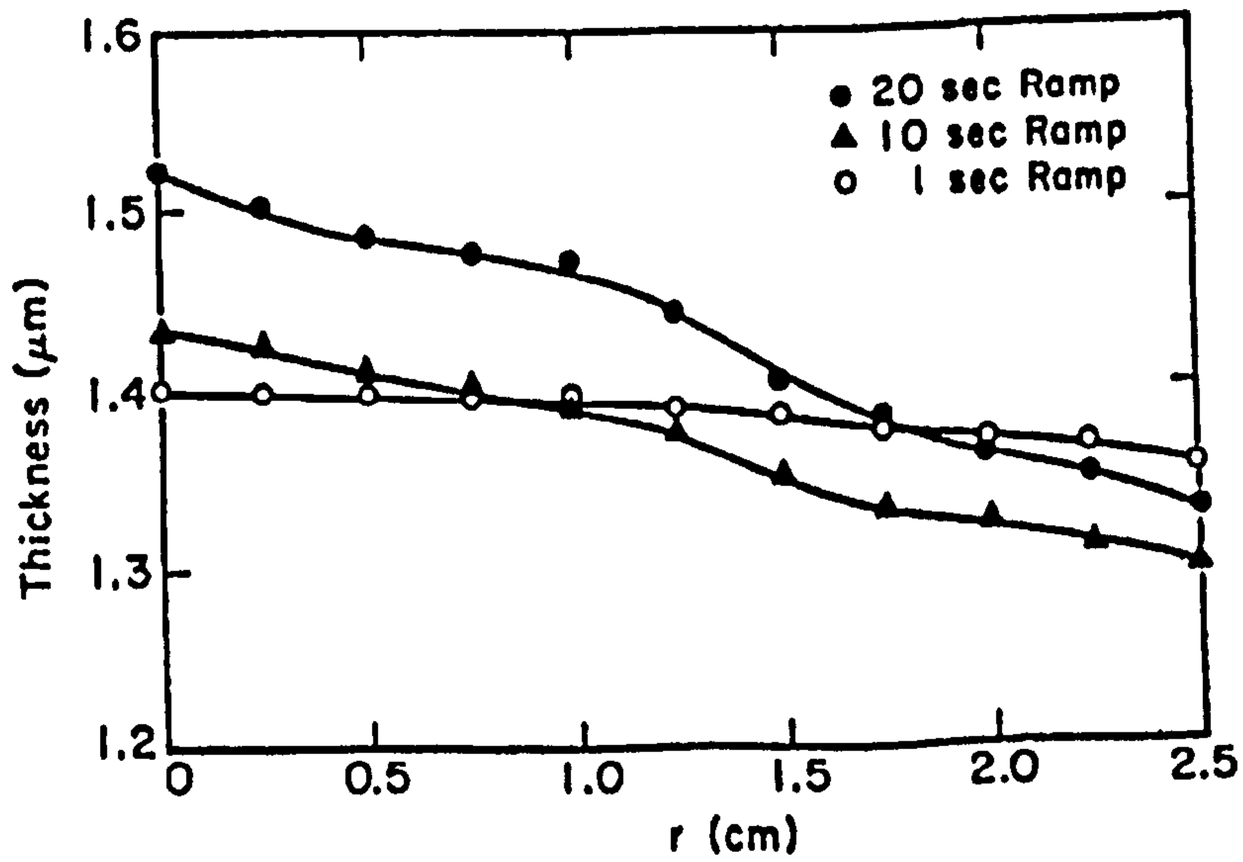

Fig. 4.9: Experimental film thickness profiles (materials not specified). (FLACK, 1984:1205)

5) When the rate of convective outflow during the spin coating process has fallen to approximately the rate of evaporation, the solution viscosity increases dramatically. At the surface a region of extremely low solvent concentration, a 'solid skin', then forms which retards further solvent evaporation. If the mass transfer from the centre to the edges is taking place too quickly or the solvent diffusion is too slow, or both, skin formation can occur before the convective flow ceases. Then the flow beneath the surface stretches the skin and can damage it, e.g. the skin could crack radially.

4.3.1.2.Applied Settings

As no calibration data for the used materials was accessible in published literature experiments have been carried out by systematic variation of the parameters involved in order to achieve a polymer film thickness of about 100 nm. For this thickness it was anticipated that no problems with pinholes should occur.

Solutions containing 0.03 g PVK polymer doped with up to 20 wt% of the dye Bis-MSB dissolved overnight in 1.8 ml of Chloroform and spun for 20s at 2000 rpm showed the desired result, see chapter 5.1.1.4. The spin coater used in these experiments, Headway Research EC 101, did not allow control over acceleration rates.

4.3.2. Vacuum Deposition

An Edwards Vacuum System Auto 306 was used for the deposition of the aluminium electrodes. The objects to which these electrodes are to deposited onto, in this work the polymer-dye thin films on the carrier substrate, are placed in sample holders which are fixed to a rotating plate in order to achieve high uniformity of the deposited layer. The material used for the deposition is put into a small metal boat or has been wound around a metal coil. This allows a high current to pass through the system. The sample chamber is evacuated to a pressure below 1.33×10^{-4} Pa and the material to be deposited is electrically heated and evaporated. When the evaporated material cools down, it condenses onto the surface of the samples. The current flow through the system which determines the deposition rate was controlled manually in such a way that the aluminium constantly glows dull red. In order to get aluminium dots deposited on the films the polymer-dye films were covered with masks. A schematic sketch of a vacuum deposition device is given in Fig. 4.10.

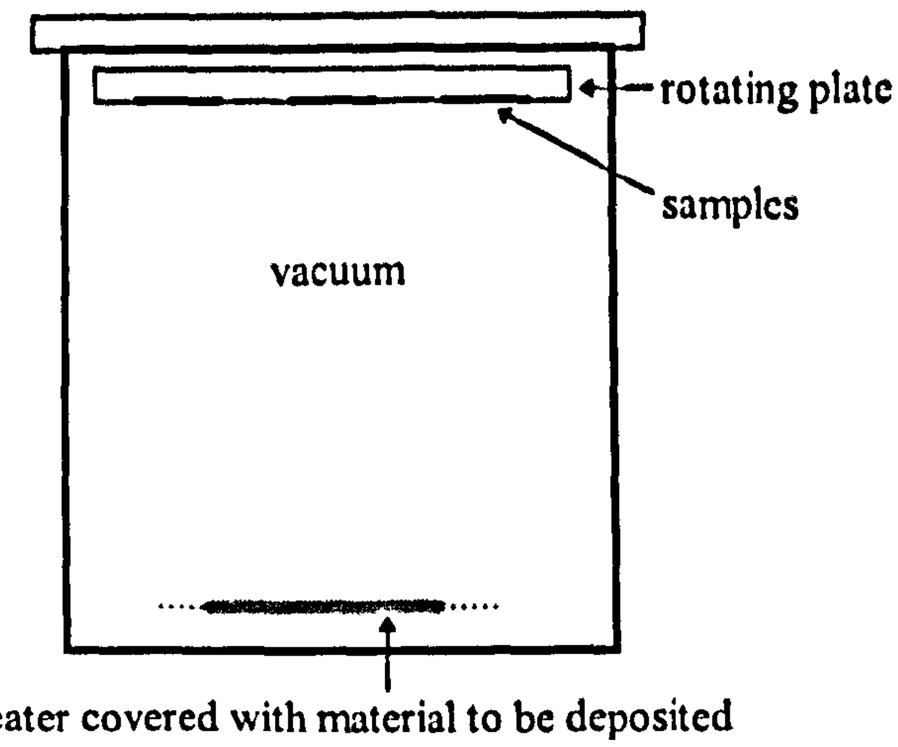

Fig. 4.10: Schematic sketch of a vacuum deposition device

5. Device Characterisation with Discussion

The results of using both a mechanical stylus surface profiler and an atomic force microscope to determine the surface characterisation of ITO glass purchased and PVK thin films coated onto it are presented at the beginning of this chapter. Steady-state and time-resolved photoluminescence measurements of the materials used and of PVK films containing Bis-MSB are then given. This is followed by electroluminescence characterisations of complete OLED devices under d.c. and unipolar pulsed mode of operation.

5.1. Surface Characterisation

The surface textures of the ITO glass used and its coating with a thin PVK film were measured with a Mechanical Stylus Surface Profiler and an Atomic Force Microscope.

5.1.1. Mechanical Stylus Surface Characterisation

5.1.1.1.Instrumentation

A Mechanical Stylus Surface Profiler of the type Dektak V 200-Si and Dektak 8000, Veeco Surface Metrology, was used.

5.1.1.2.Indium Tin Oxide Surface Profile and Texture

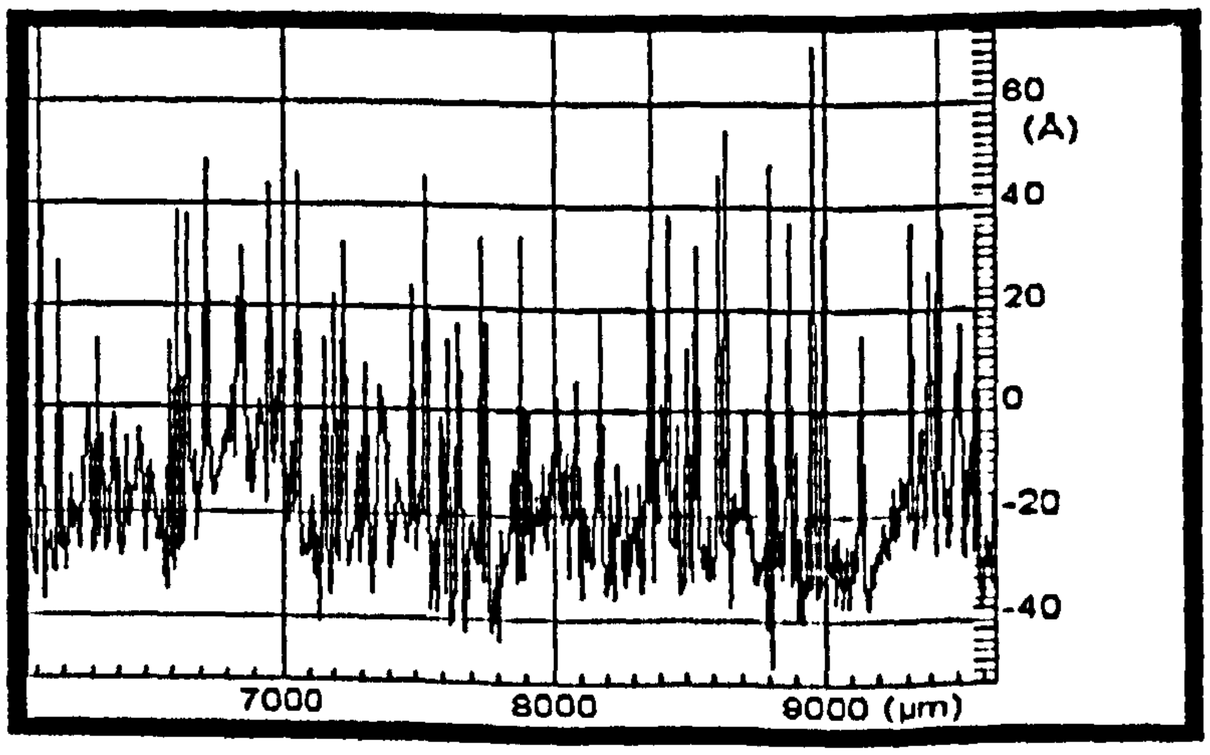

Fig. 5.1: Profile of ITO coated glass (Dektak V 200-Si)

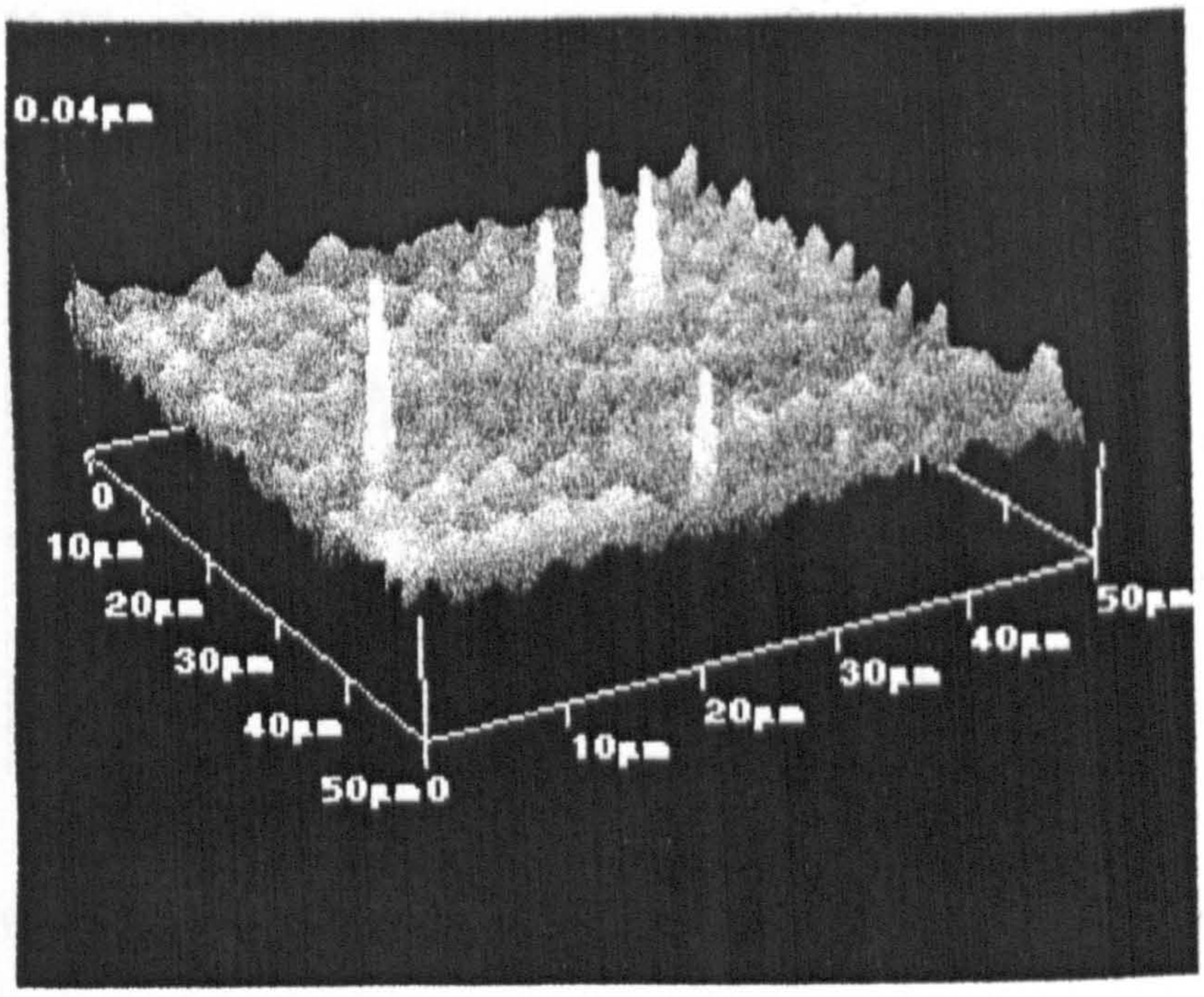

Fig. 5.2: Texture of ITO coated glass (Dektak V 200-Si)

The ITO surface profile (Fig. 5.1) and texture (Fig. 5.2) show an arithmetic average roughness[27], R_a, of 1.5 nm (15 Å) with a maximum peak to valley roughness, R_t, of 19.7 nm (197 Å).

These high values caused problems later on for the fabrication of OLED devices as different electrical field strengths resulted from different local film thicknesses and it is suspected that short circuits occurred more often in the surroundings of these conducting tips due to field enhancement effects. See also the chapter concluding remarks in this context.

[27] R_a is the arithmetic average deviation from the mean line within the assessment length (L):

$$R_a = \frac{1}{L}\int_{x=0}^{x=L}|y|dx\ .$$

5.1.1.3.Thin PVK Film Surface Profile

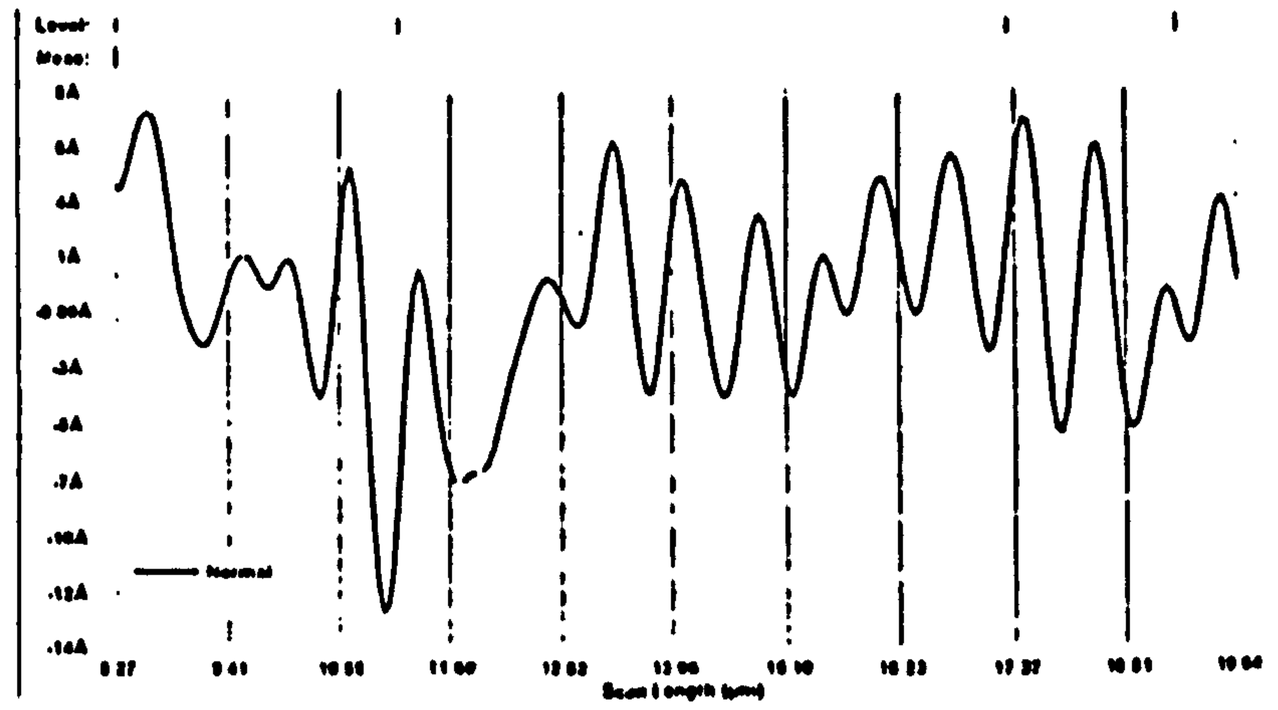

Fig. 5.3: Surface profile of PVK thin film coated ITO glass (Dektak 8000)

A maximum peak to valley roughness, R_t, of 2.1 nm (21 Å) was obtained for the PVK surface profile, see Fig. 5.3. This means the spikes of the ITO layer had been smoothed out by the PVK film deposited resulting in a locally varying PVK film thickness.

5.1.1.4.PVK thin film thickness

A part of the PVK thin film coating of the ITO glass was wiped off using a cloth lubricated with the solvent Chloroform. Subsequently the surface profile along the border of the coated and uncoated ITO glass was measured (see Fig. 5.4) and the average height difference in the shaded regions calculated.

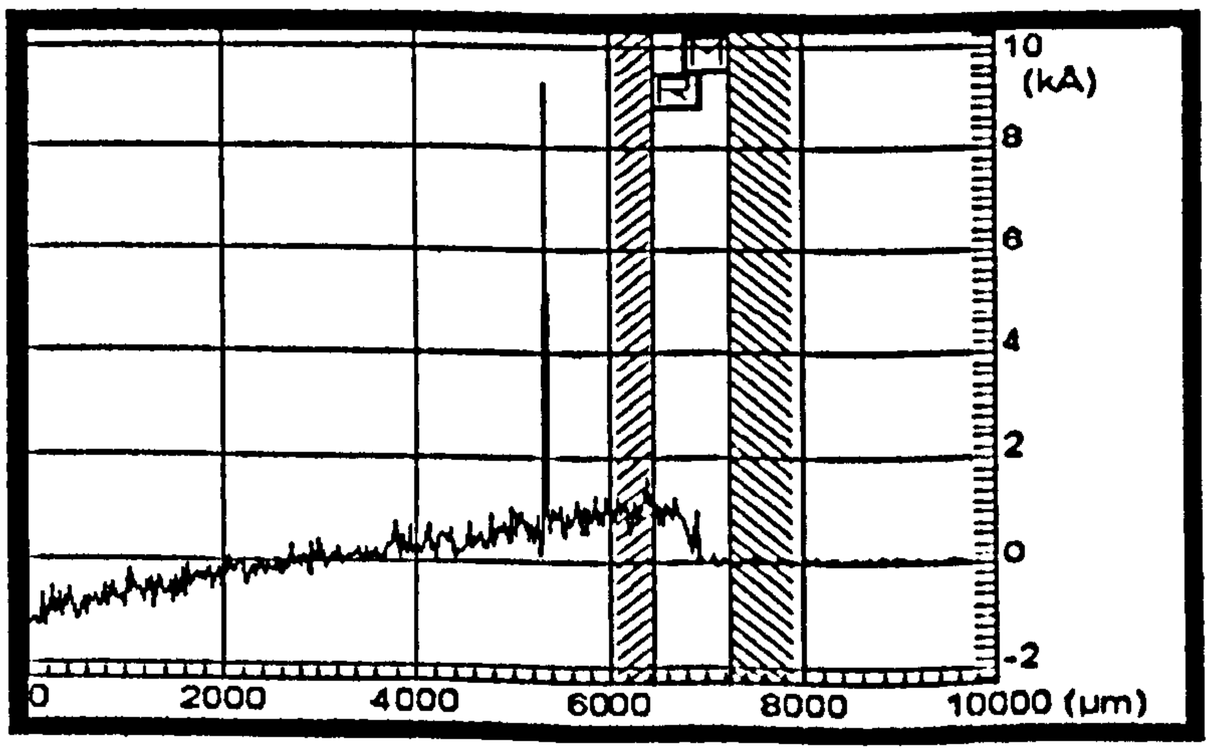

Fig. 5.4: Step height between uncoated and PVK thin film coated ITO glass (Dektak V 200-Si)

An average PVK film thickness of about 105 nm (1050 Å) was obtained in several measurements using the parameters in chapter 4.3 described for the film preparation.

The film thickness envisaged (see chapter 4.3.1.2) of about 100 nm (1000 Å) was successfully fabricated.

5.1.2. Atomic Force Microscopy (AFM) Surface Characterisation

5.1.2.1.Instrumentation

A Q-scope 250[28] AFM from Quesant Instrument Corporation on a stone base had been used.

5.1.2.2.Indium Tin Oxide Surface Texture

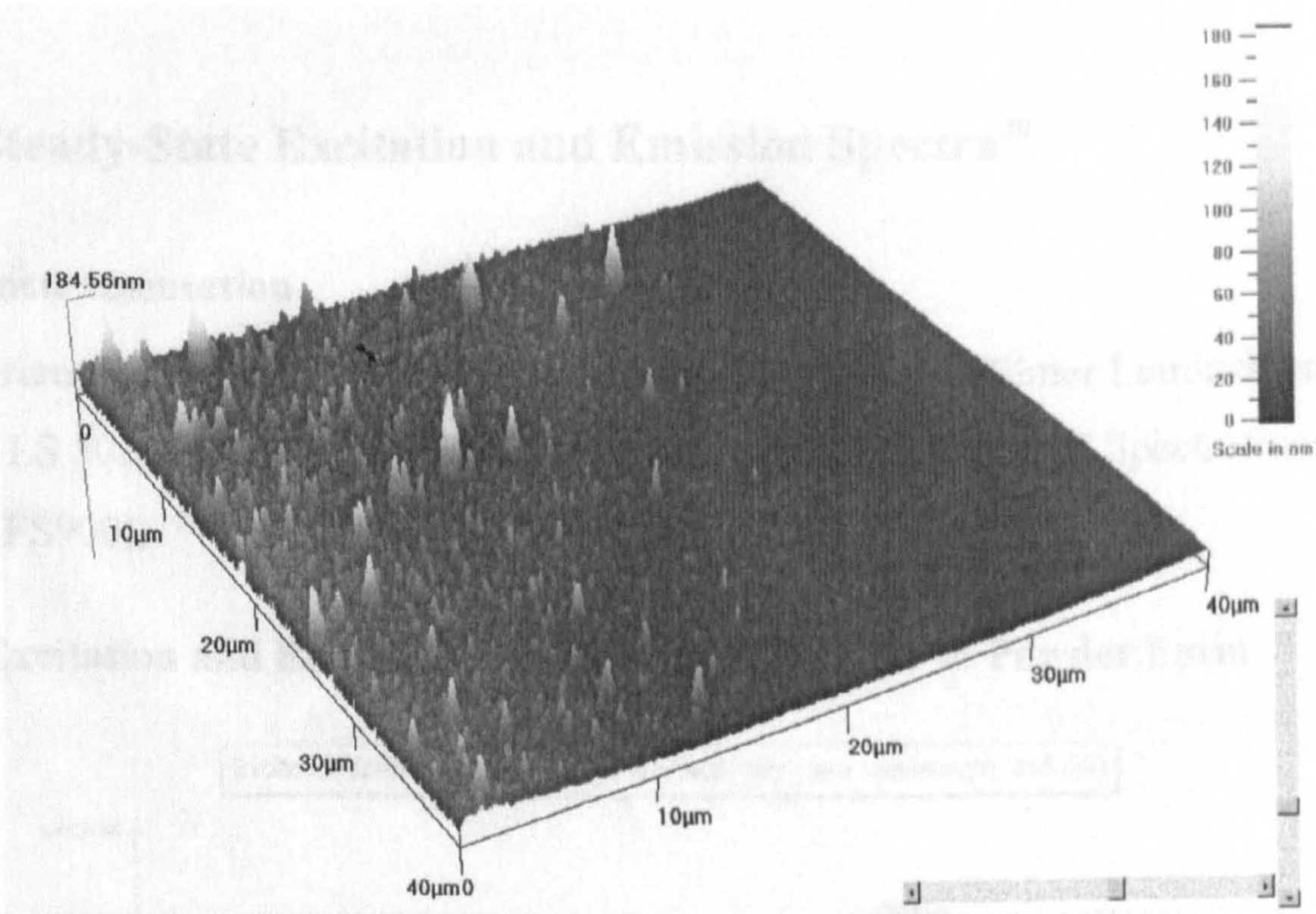

Fig. 5.5: Texture of ITO surface (Q-scope 250)

The ITO topography, Fig. 5.5, looks realistic[29] but the scaling is surprising. Even up to 10-times higher spikes compared to those obtained with the mechanical stylus surface profiler, 180 nm (1800 Å) and 19 nm (190 Å) respectively, were obtained.

Assuming that the purchased ITO glass is of similar surface quality for all sheets this substantial difference cannot be explained. If the AFM results should represent the true picture, the high failure rate of the devices fabricated having used the untreated purchased ITO glass can be explained.

---

[28] Scanning head: solid state laser; Probe tips: silicon nitride Q-lever; X-Y range: up to 40x40 micrometer; Z-range: up to 9.0 microns; Scan rate: up to 20Hz; Scan resolution: 100-600 points per horizontal line; Scan direction: 0-355 degrees; control: 120Mhz Pentium PC.

[29] Dust for instance is not that spiky in its appearance.

5.2. Photoluminescence Characterisations

Steady-state excitation and emission spectra of the materials used (for the dye as a powder and in chloroform solution), of the undoped and, in different concentrations, dye doped thin polymer films were obtained at room temperature and at 77.4 K.

Time-resolved photoluminescence spectra were taken from the dye as a powder and in chloroform solution and also from the undoped and, in different concentrations, doped polymer thin film.

5.2.1. Steady-State Excitation and Emission Spectra[30]

5.2.1.1.Instrumentation

Two instruments had been used: At Napier University a Perkin Elmer Luminescence Spectrometer LS 50B (PELS) and at Edinburgh Instruments Ltd. a FS 900 Spectrofluorimeter System (FS900).

5.2.1.2.Excitation and Emission Spectra of Dye Bis-MSB in Powder Form

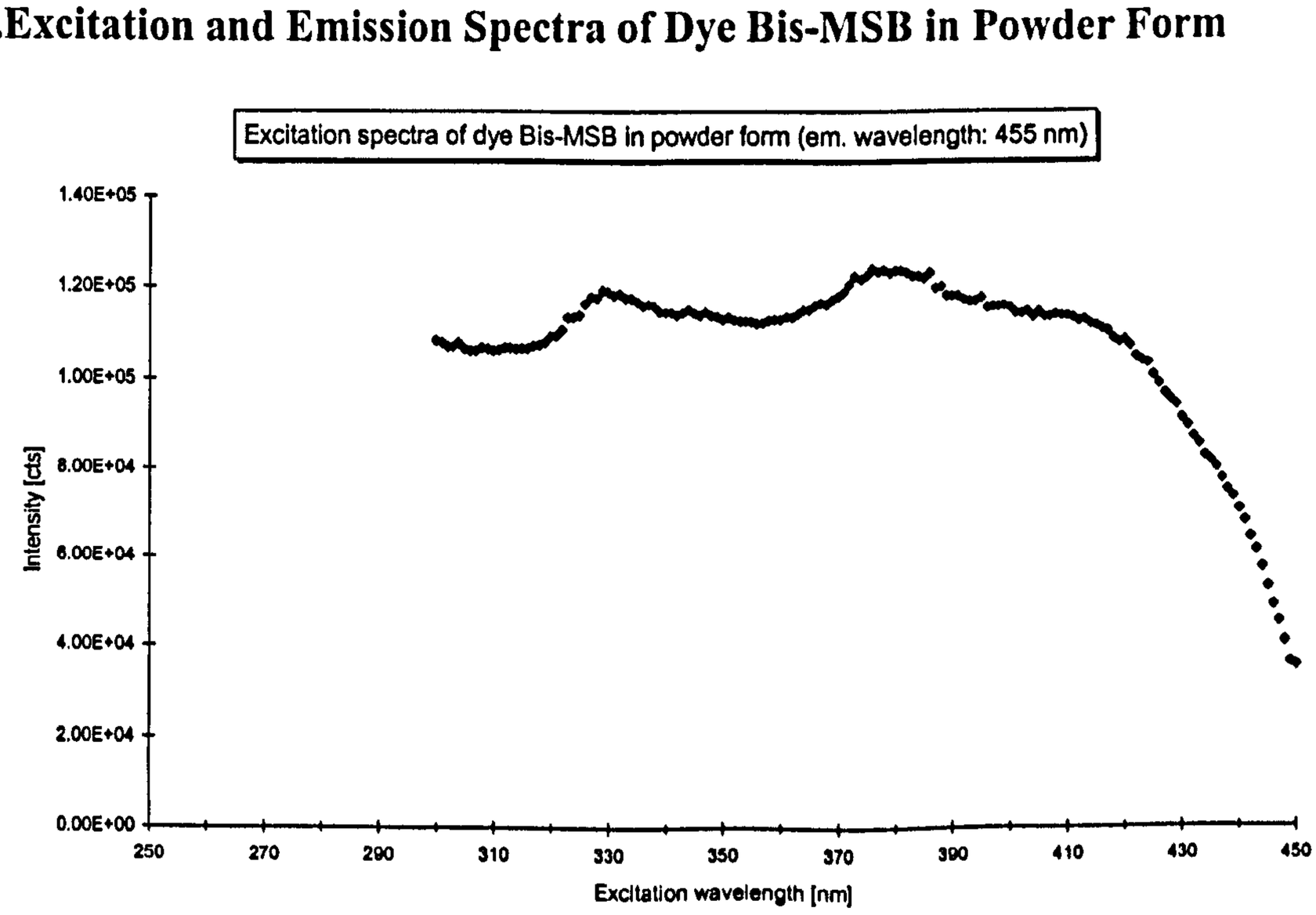

Fig. 5.6: Excitation spectrum of dye Bis-MSB in powder form (FS900)

[30] The wavelengths in the spectra presented are accurate within 1 nm. They are probably more accurate than this but the detection of superior accuracy relies on the preparation of rigorously prepared standards. The time required to prepare such standards is longer than can be justified in achieving the objectives of this project.

The excitation spectrum, Fig. 5.6, can basically be regarded as a plateau from 300 to about 410 nm with a corresponding light intensity of around 1.13E+05 cts. Two small peaks (330 nm; 1.18E+05 cts and 378 nm; 1.23E+05 cts) can be identified.

This very broad absorption spectrum indicates two possible explanations: First that this system has a wide band of energy levels with small energetic differences available for absorption, second the absorption is superimposed by scattering due to the random distribution of the dye particles - which is more likely.

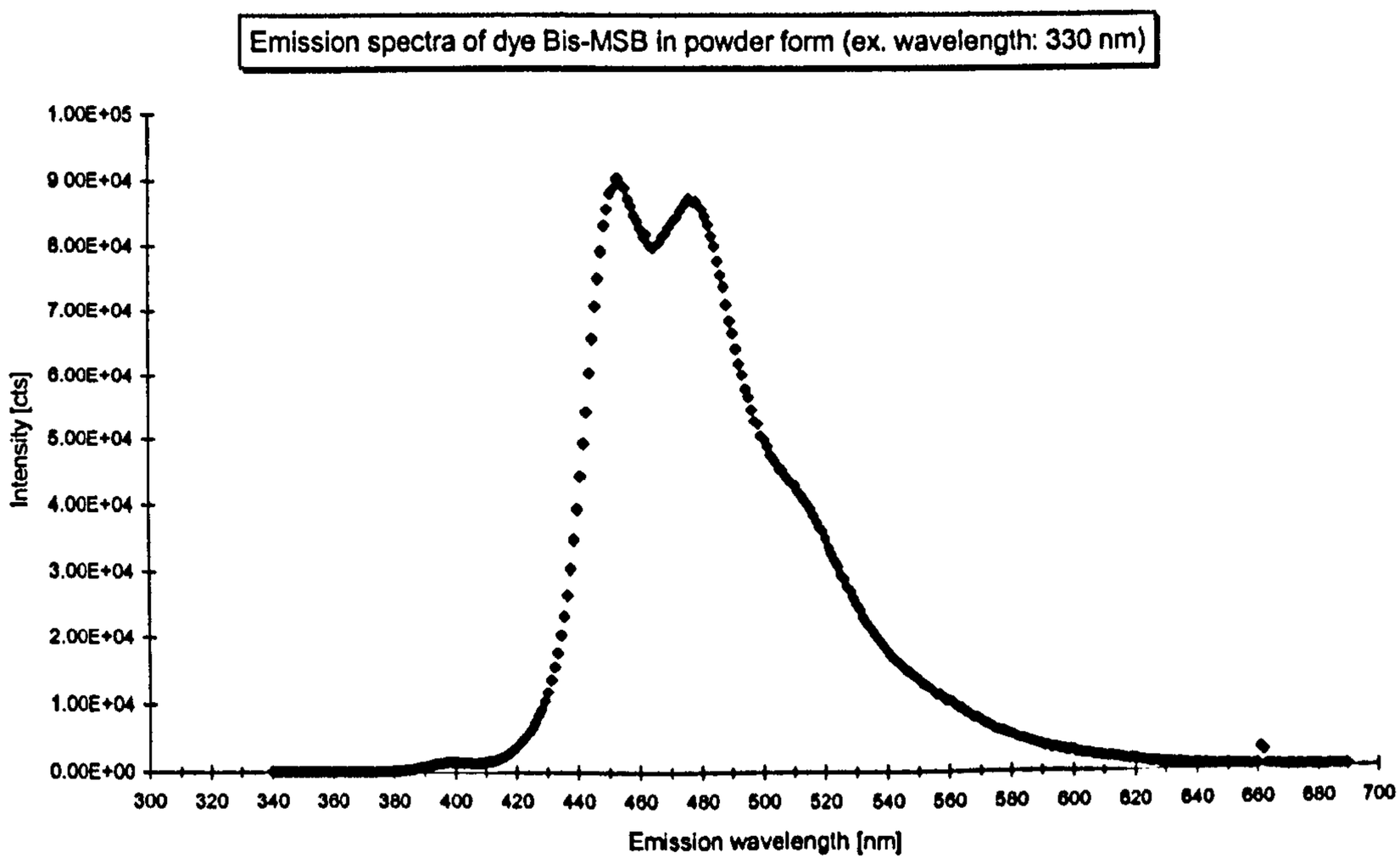

Fig. 5.7: Emission spectrum of dye Bis-MSB in powder form (FS900)

The emission spectrum, Fig. 5.7, shows a clear double peak with the two maxima at 453 nm (9.0 E+4 cts) and at 478 nm (8.7 E+4 cts). There can also be recognised a hint of a shoulder at 400 nm and 515 nm.

The sharply rising intense 452 nm peak probably represents the S_1 (v'=0) to S_0 (v''=0) transition. The subsequent peak and shoulder may represent the S_1 (v'=0) to S_0 (v''=1) transition.

5.2.1.3.Excitation and Emission Spectra of Dye Bis-MSB in Chloroform Solution

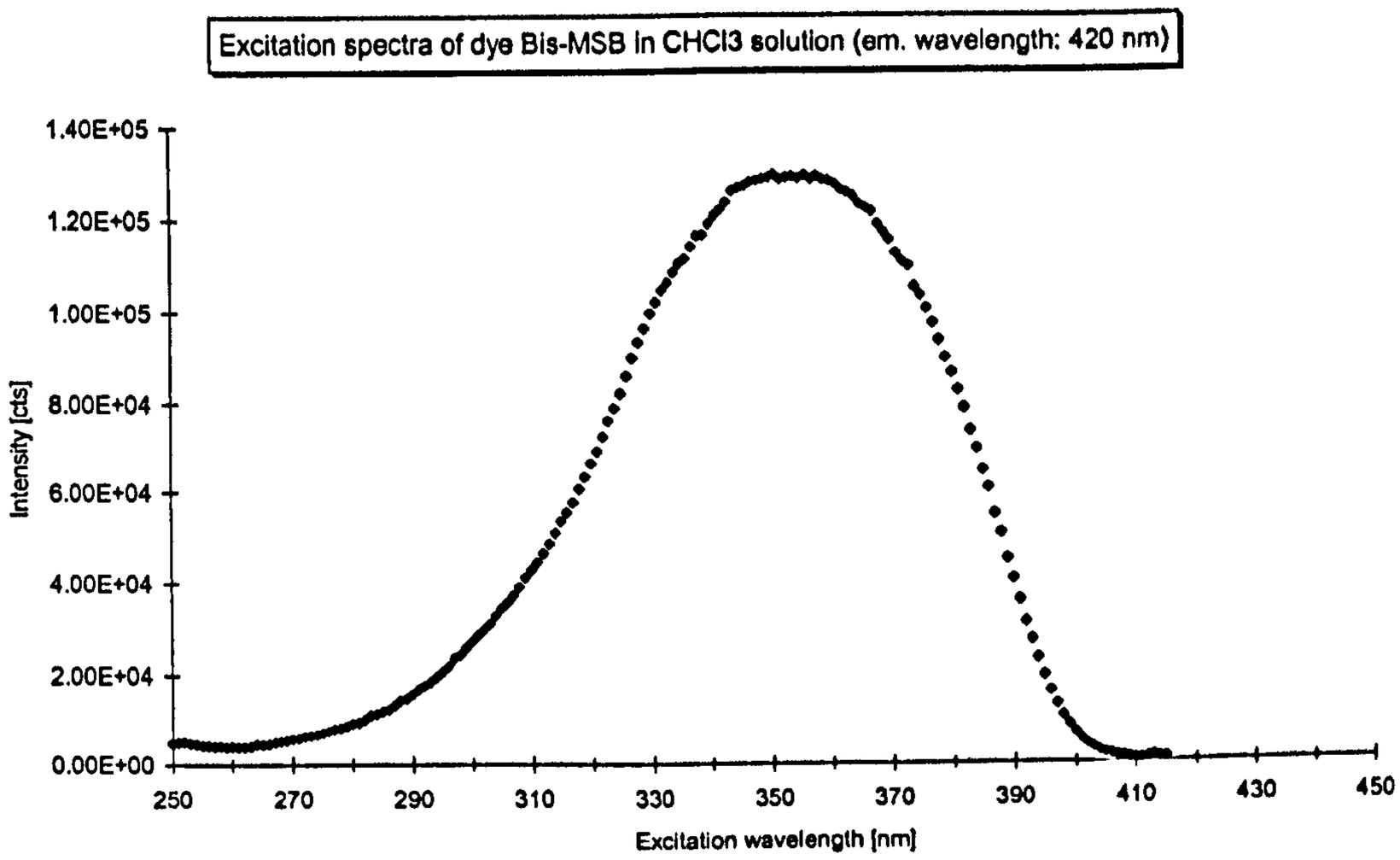

Fig. 5.8: Excitation spectrum of dye Bis-MSB in Chloroform solution (FS900)

The excitation spectrum, Fig. 5.8, shows a broad peak with its maximum at 353 nm (1.29E+5 cts) and a full width at half maximum of 65 nm.

Here an energy band gap associated with an excitation wavelength of about 350 nm for Bis-MSB is revealed as the solvent significantly reduces the scattering.

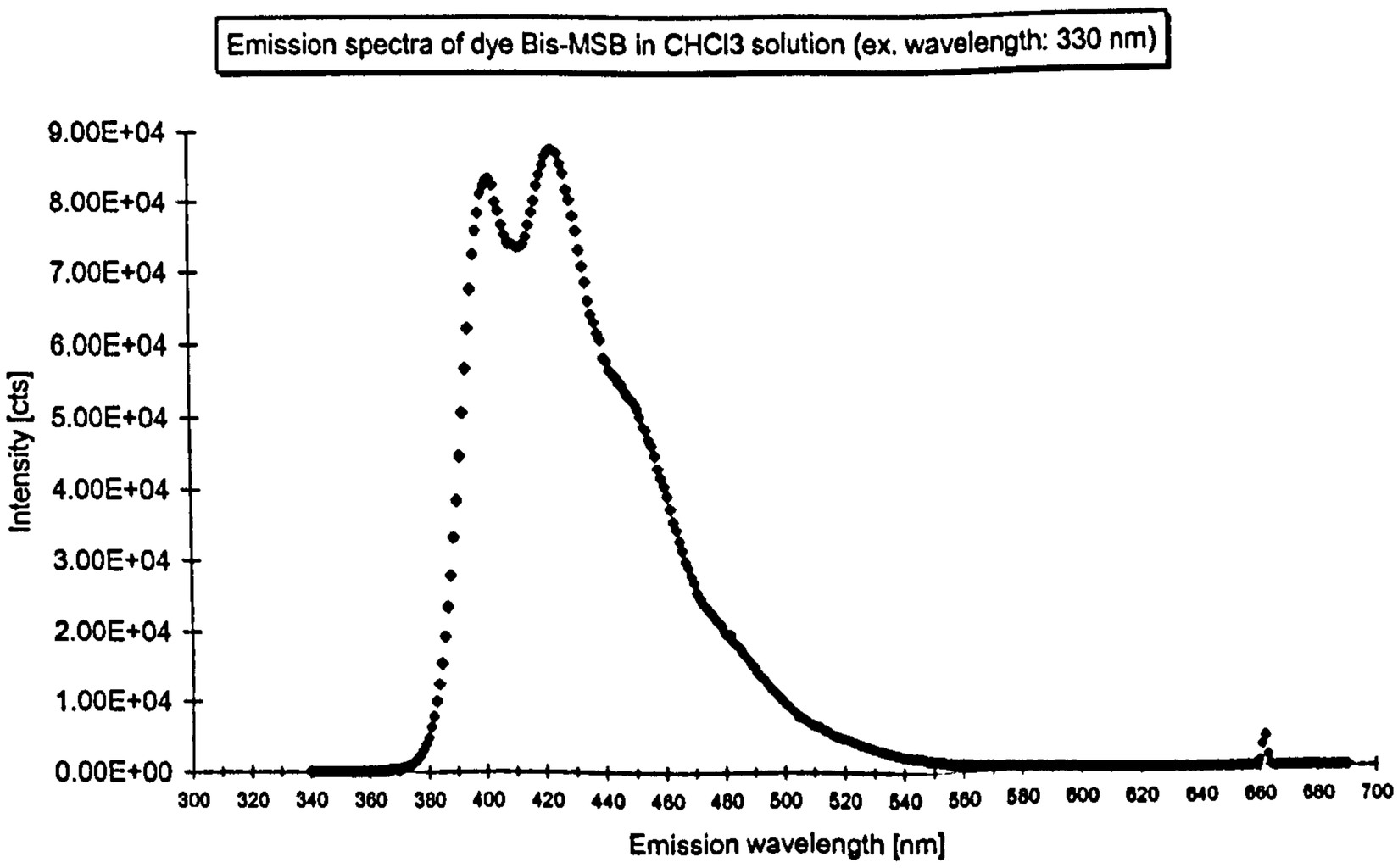

Fig. 5.9: Emission spectrum of dye Bis-MSB in Chloroform solution (FS900)

The emission spectrum, Fig. 5.9, consists of a clear double peak with its maxima at 400 nm (8.3E+4 cts) and at 423 nm (8.8E+4 cts) as well as s shoulder showing up at around 450 nm and about 5.0E+4 cts.

The shift towards lower wavelengths of about 50 nm and the change of the relative intensity of the maxima of this spectrum compared to the emission spectrum of Bis-MSB in powder form can be explained as a matrix effect.

5.2.1.4.Excitation and Emission Spectra of an Undoped PVK Film

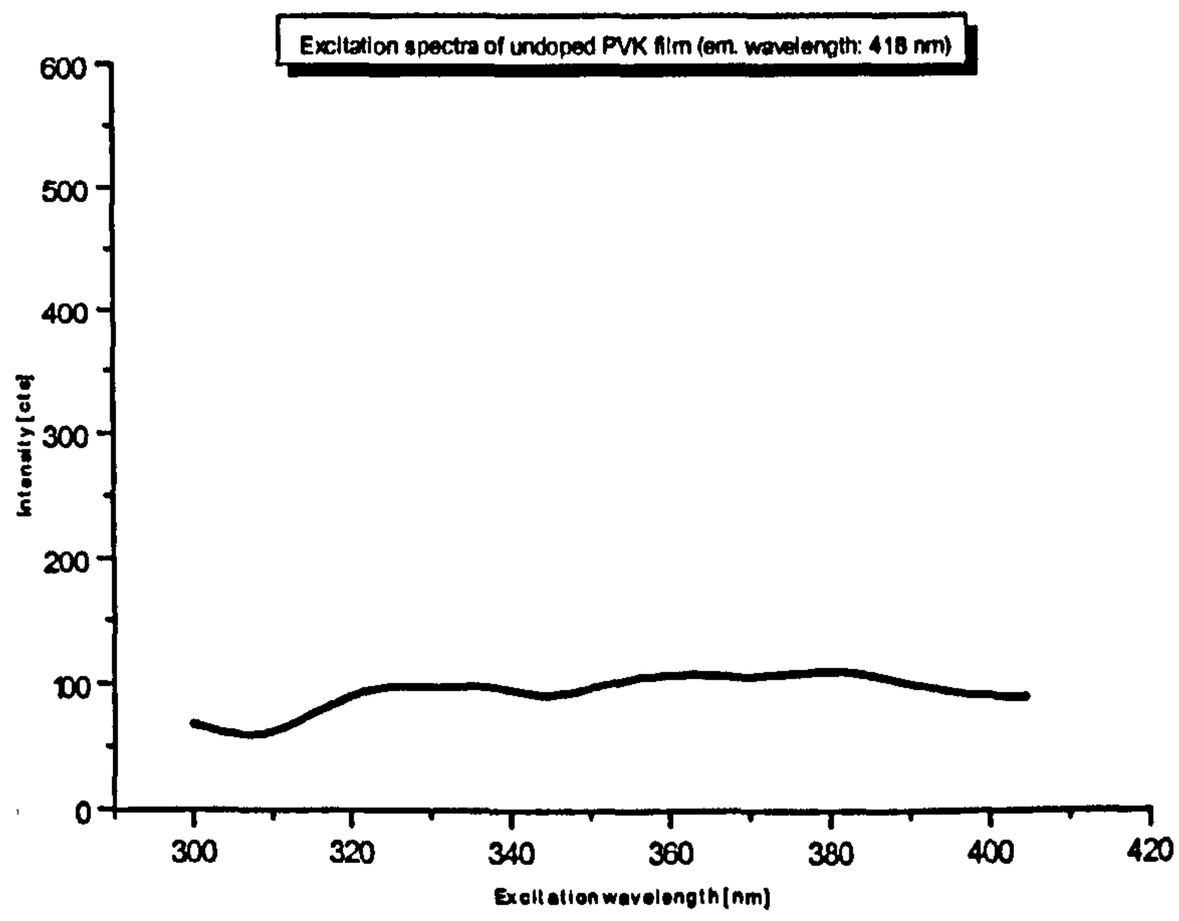

Fig. 5.10: Excitation spectrum of undoped PVK film (PELS)

The excitation spectrum of the undoped PVK film, Fig. 5.10, consists of an almost even plateau within the measured region from 300 to 405 nm at an light intensity level of about 100 cts.

The uniform low level absorbency indicates the presence of many quantum levels close to each other with relatively small band gaps.

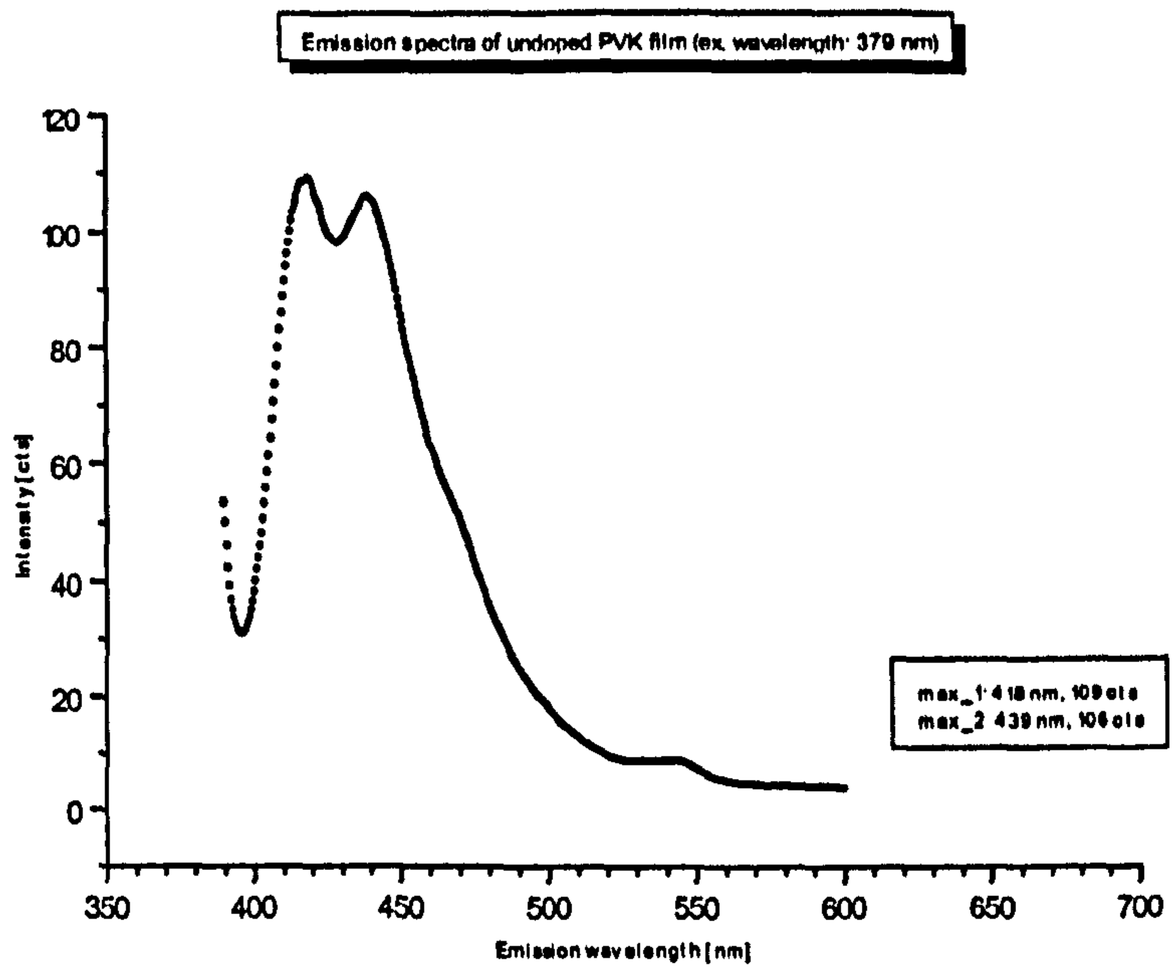

Fig. 5.11: Emission spectrum of undoped PVK film (PELS)

The emission spectrum, Fig. 5.11, shows a clear but low intensity double peak with the maxima at 418 nm (109 cts) and 440 nm (104 cts). Further, the hint of another emission band is visible at around 540 nm.

The spectra of pure PVK and Bis-MSB in solution are similar in appearance and in their emission wavelength region which might be due to the fact that they both contain benzene rings. The light emission intensity from PVK is very much less than that of Bis-MSB. Therefore the effects of Bis-MSB are reliably studied.

5.2.1.5.Emission Spectra of an Undoped PVK Film on ITO Glass in Different Positions

Nine measurements were taken in equidistant positions in the middle of the substrate with a distance between successive positions of about 0.2 mm. The measurement positions were counted from the left to the right edge of the PVK coated ITO square sized glass substrate (edge length: 20 mm).

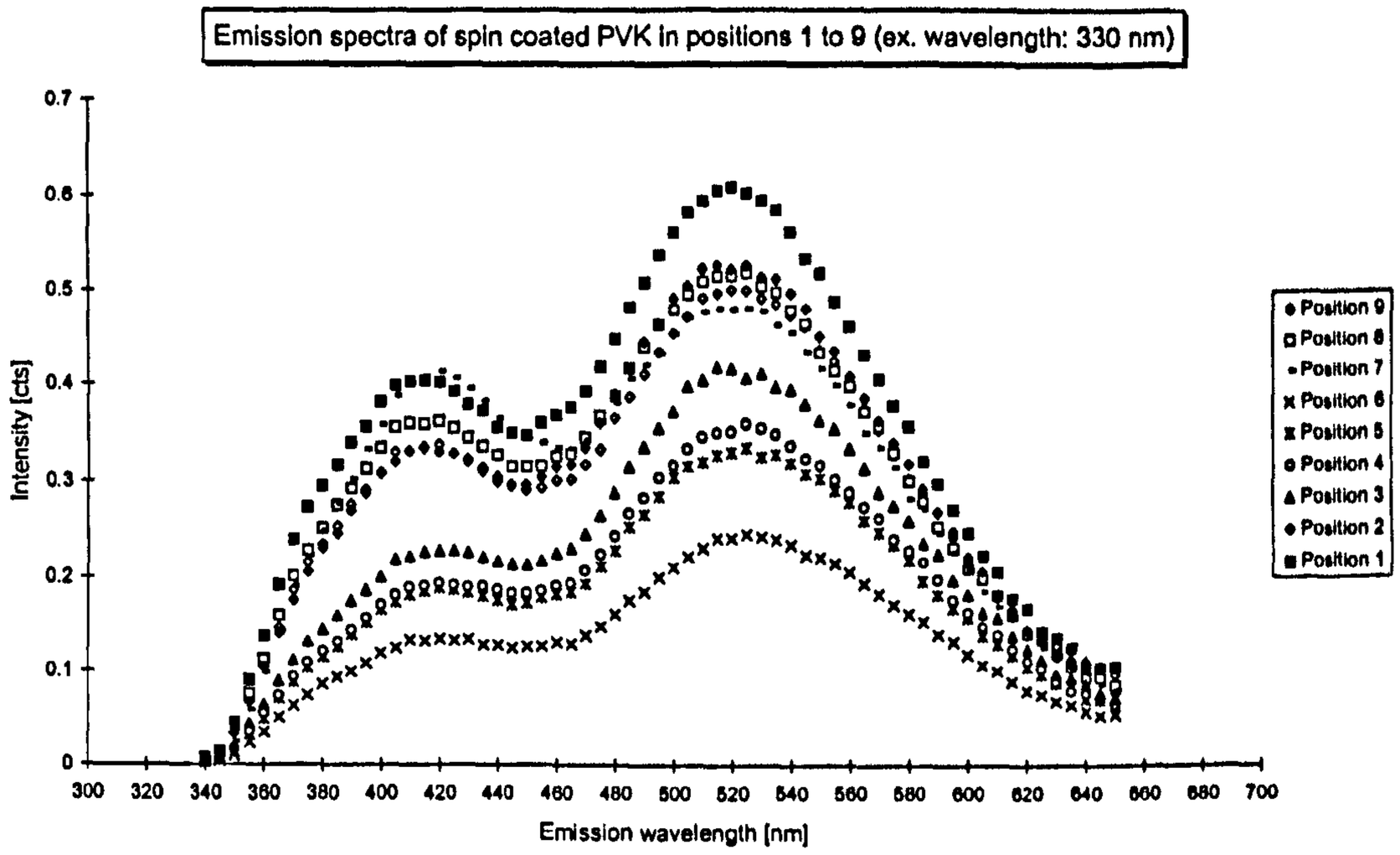

Fig. 5.12: Emission spectra of undoped PVK film on ITO glass in different positions (FS900)

In almost all emission spectra, Fig. 5.12, two peaks at around 415 nm and 520 nm can clearly be identified. The two peak intensities vary around 50% compared to their mean values. The largest intensities were obtained in the positions 1&2 and 8&9 which lie close to the edges of the sample.

All curves show a similar shape therefore the intensity variations can be explained by different film thicknesses. The higher intensities at the edges of the sample with a lower film thickness can be explained by the fact that there less absorption of the emitted light occurs, i.e. more light is emitted. The first peak is relatively flat which means that it might consist of the PVK double peak seen previously which cannot be resolved in this measurement. The second peak lies roughly in a wavelength region where a shoulder is visible in the previous pure PVK spectrum which might well be due to higher energetic excitation in this experiment.

5.2.1.6.Excitation and Emission Spectra of PVK Films Doped with Dye Bis-MSB in Different Concentrations

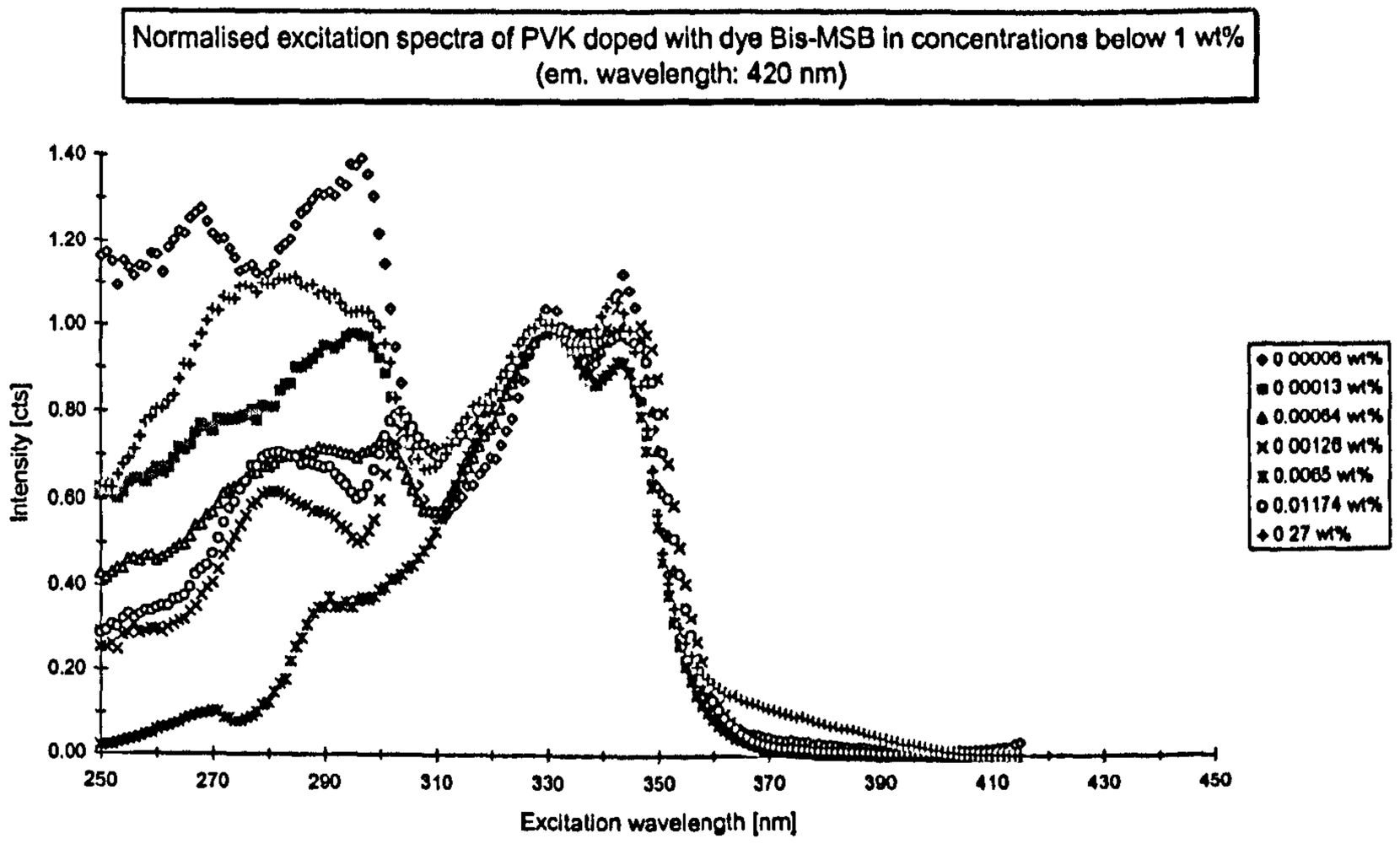

Fig. 5.13: Normalised excitation spectra of PVK doped with dye Bis-MSB in concentrations below 1wt % (FS900)

The intensities of the excitation spectra for Bis-MSM concentrations below 1 wt%, Fig. 5.13, were normalised to 1 Count at the excitation wavelength of 330 nm (noticeable peak), a position of a common peak. A further peak for all concentrations can clearly be identified at 344 nm (normalised intensities 0.9 cts to 1.12 cts). The intensities in general decrease towards lower wavelengths without any further regular pattern despite the fact that the spectra of all concentrations except 0.0065 wt% show a local minimum intensity (0.54 cts to 0.71 cts) at around 310 nm.

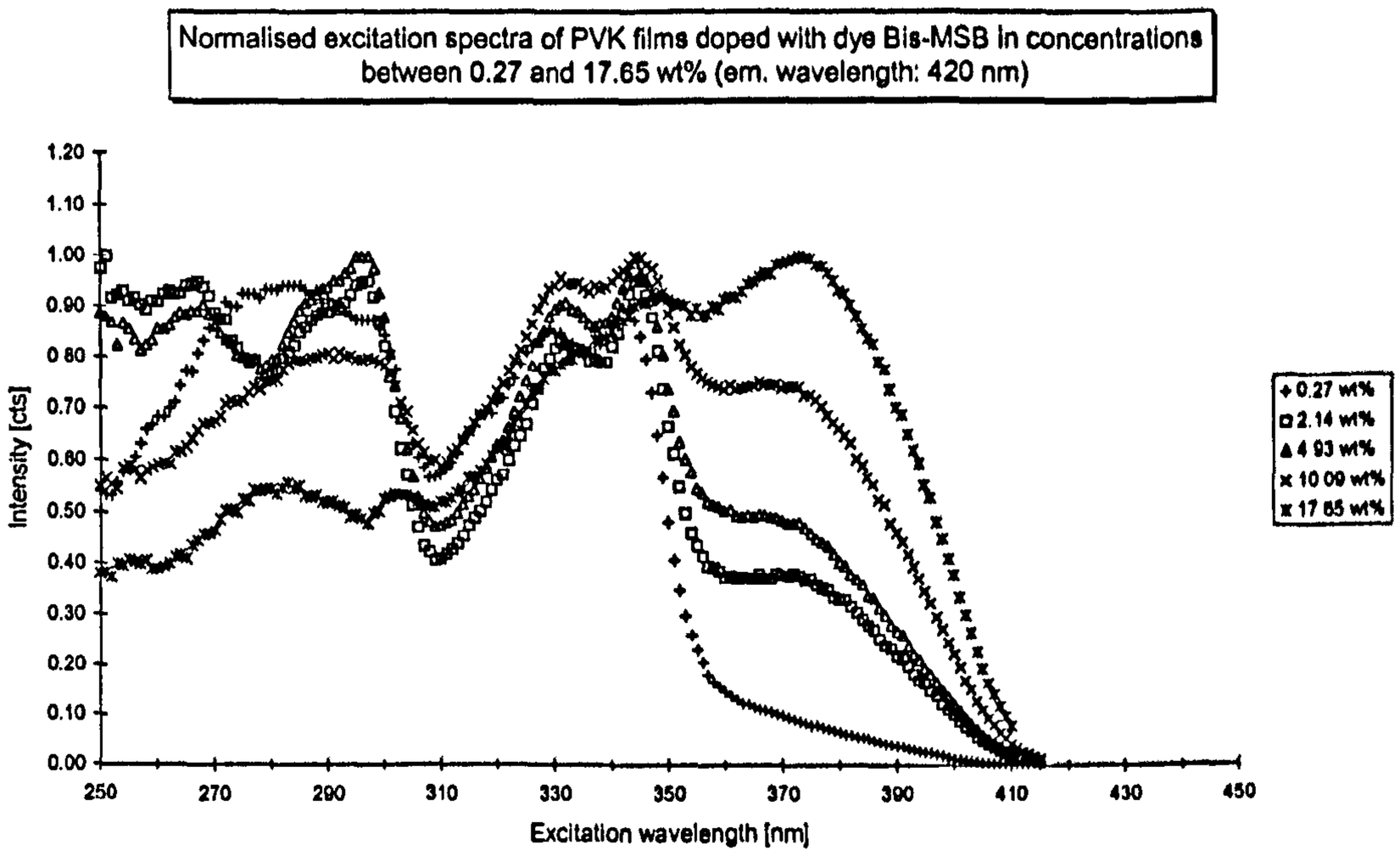

Fig. 5.14: Normalised excitation spectra of PVK doped with dye Bis-MSB in concentrations between 0.27 and 17.65 wt % (FS900)

The above presented excitation spectra were normalised to 1 Count at an excitation wavelength of 344 nm (second noticeable peak) except the spectra of the concentration of 17.65 wt% for reasons of presentational clarity which had been corrected to 0.9 cts at that wavelength. The spectrum of 17.65 wt% dye concentration has another peak at 372 nm (corrected intensity: 1 count). The spectra of the concentrations 10.09, 4.93 and 2.14 wt% show a plateau in the region between approx. 358 to 372 nm (norm. intensities: 0.73 cts; 0.48 cts and 0.38 cts respectively); the spectra of concentration 0.27 wt% decreases rapidly. As in the case of low concentrations a second peak, 330 nm (normalised intensities: 0.80 to 0.95), and local minimum at 310 nm (norm. intensities: 0.53 to 0.70 cts) can be identified except for the spectra of 17.65 wt% dye concentration. Further the two spectra of the concentrations 2.14 and 4.93 wt% show a peak at 296 nm (norm. intensity: 0.95 cts and1 count respectively).

The after excitation emitted light intensities at the two peaks at about 330 nm and 344 nm[31] remain relatively constant whereas a further peak at around 370 nm is gradually build up starting with a dye concentrations of 2.14 wt%. This suggests that the first two peaks are due to absorption by PVK and the latter is due to absorption by the dye Bis-MSB or a newly formed complex. A common dip at around 310 nm and the variable nature of the spectra at wavelength less than 300nm are difficult to interpret in the scope of this work.

[31] The intensities at the chosen wavelength showed little variations before the normalisation.

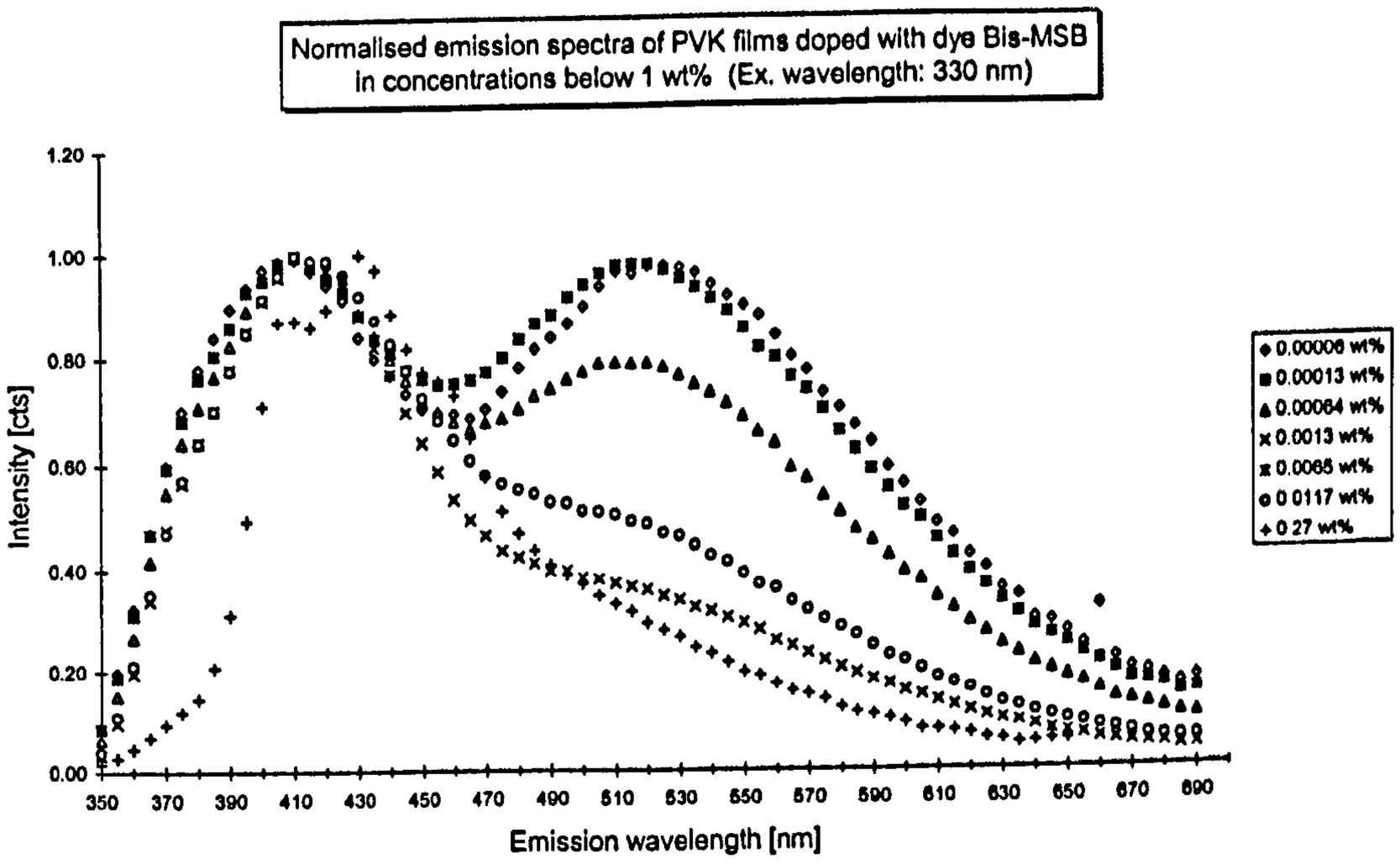

Fig. 5.15: Emission spectra of PVK films doped with dye Bis-MSB in concentrations below 1 wt% (FS900)

The above emission spectra, Fig. 5.15, normalised for clarity to the common peak at 410 nm (intensity set equal to 1 count) with exception of the spectrum of 0.27 wt% dye concentration which is normalised for the peak at 430 nm instead of the one at 410 nm. The spectra for the dye concentrations 0.00064, 0.00013 and 0.00006 wt% show a second peak at 512 nm (0.78 cts), 517 nm (0.98 cts) and 522 nm (0.98). The remaining three concentrations show a shoulder in this region or at least a hint of a shoulder (0.27 wt% concentration).

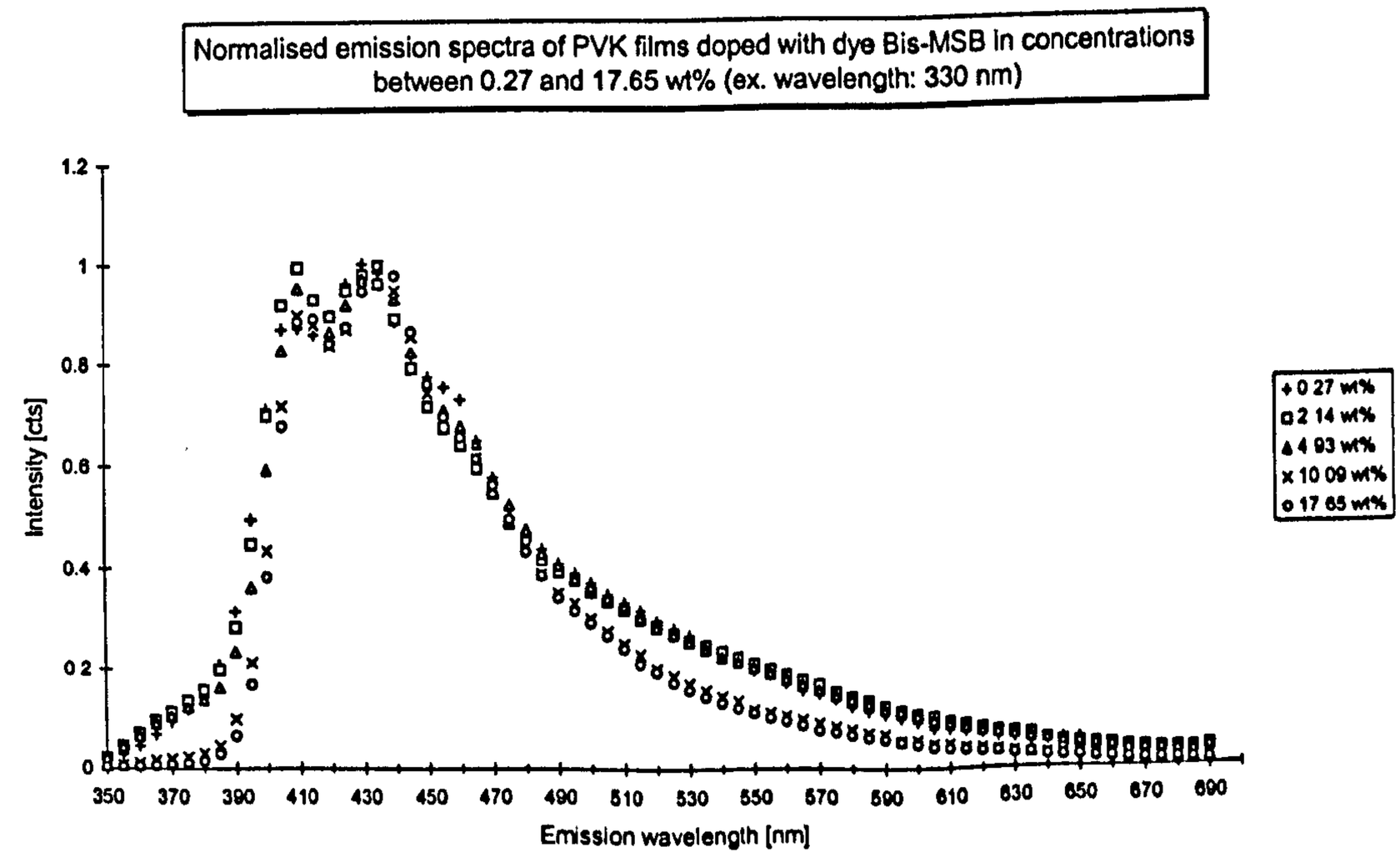

Fig. 5.16: Emission spectra of PVK films doped with dye Bis-MSB in concentrations between 0.27 and 17.65 wt% (FS900)

All the emission spectra in Fig. 5.16 show a clearly identifiable double peak. The first at around 410 nm with intensities of 0.88 to 1 count(s) after normalisation of the peak intensity for the emission wavelength of 430 nm to 1 count. There can also be a shoulder identified at around 460 nm.

With the increasing amount of added Bis-MSB the peak around 520 nm is more and more suppressed and can therefore be identified as having been caused by the low intensity emission from PVK. Furthermore, the initially single emission peak at around 410 nm is split up into a double peak which is also sharpened by an increasing amount of added dye and becomes very similar in shape to the spectrum of Bis-MSB in Chloroform (see Fig. 5.9). which shows that the emission is due to a transition within Bis-MSB.

5.2.1.7.Integrated Peak Intensity of the Emission Spectra of PVK Films Doped with Dye Bis-MSB in Different Concentrations

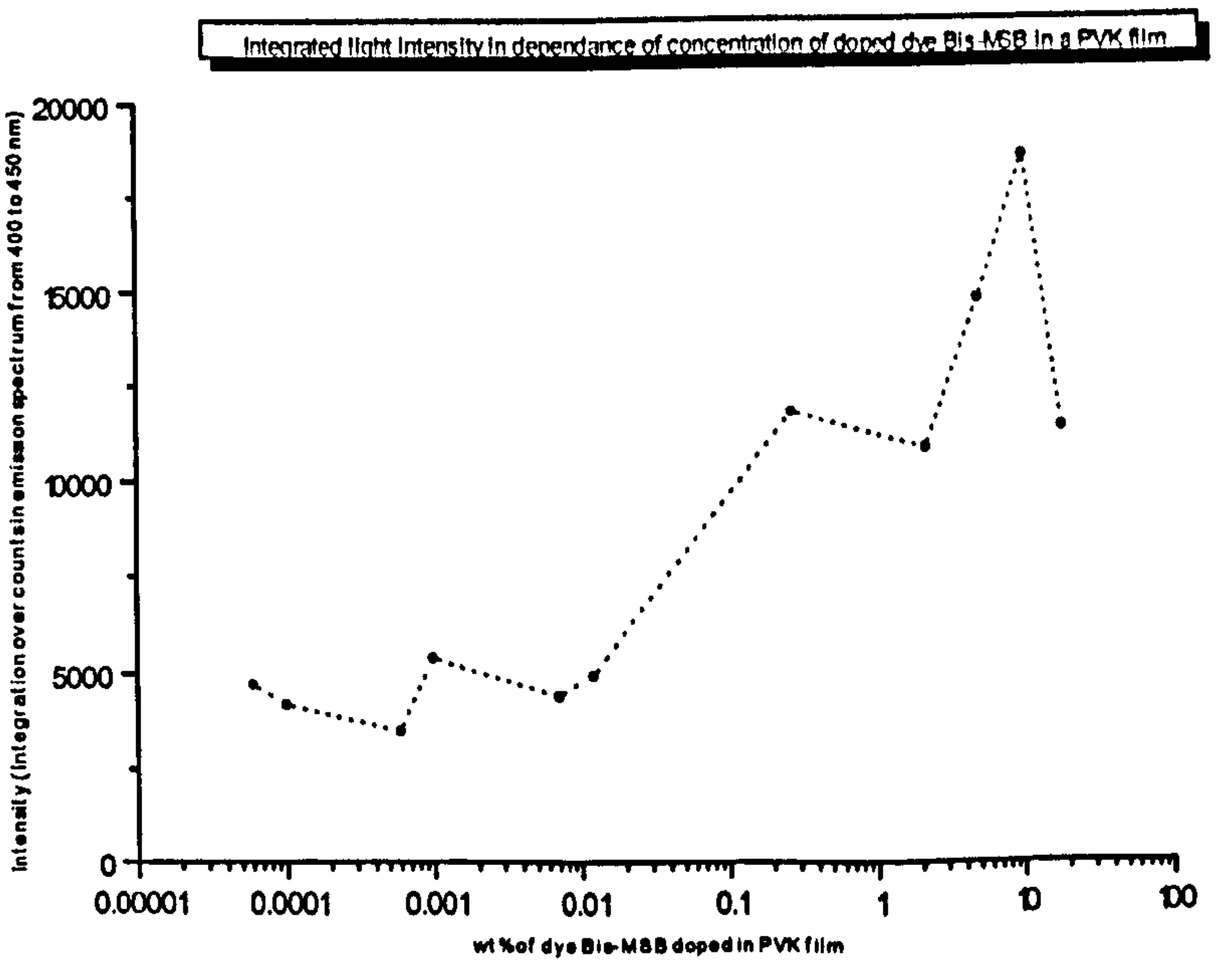

Fig. 5.17: Integrated light intensity vs. concentration of doped dye Bis-MSB in a PVK film (FS900) (Measurement error: ±100 cts)

The integrated intensity, shown in Fig. 5.17, can roughly be regarded as constant up to doping concentrations of about 0.01 wt% of the dye (approx. 4000 cts). After that there is a steep intensity increase to a maximum at around 10 wt% doping concentration (18400 cts) with also an indication of a rapid decrease[32].

[32] Obviously, further measurements of samples with dye concentrations above 10wt% dye concentration would be desirable. However, such measurements had not been carried out as the drop in PL intensity had been expected already at much lower dye doping concentrations.

The data suggests that quenching becomes effective at dye concentrations of above 10 wt% dye content which relates to an average distance of the centre of the dye molecules in a PVK host matrix of about 16 Å (see Appendix B)[33]. The occurrence of quenching within that distance range can theoretically be expected (see chapter. 3.3).

5.2.1.8.Emission Spectra of PVK Film Doped with 4.93 wt% of Dye Bis-MSB Measured at 77.4 K

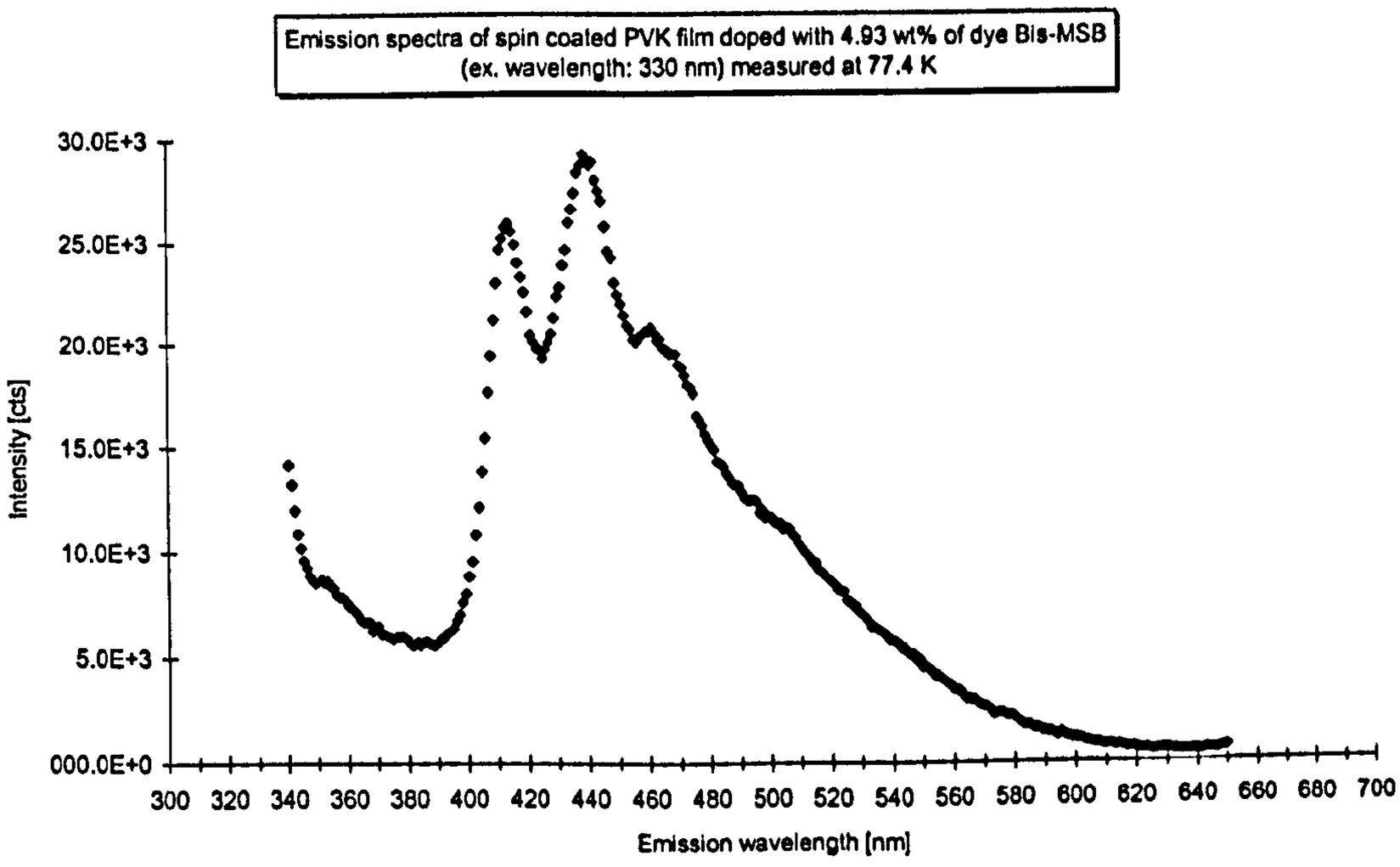

Fig. 5.18: Emission spectrum of dye Bis-MSB doped PVK film measured at 77.4 K (FS900)

The spectrum in Fig. 5.18 taken at 77.4 K shows two significant relatively sharp peaks at 412 nm (26.0E+3 cts) and at 439 nm (29.2E+3 cts). A third peak can also be identified at 461 nm (21E+3 cts) and a shoulder at around 510 nm (12.5E+3 cts) as well as the possible hint of a further shoulder at 575 nm.

A comparison between the emission spectrum at 77.4 K with one taken at room temperature (see for instance Fig. 5.16) does not reveal any new peaks if the faint shoulder at 575 nm is neglected, that means the emissions are caused by the same transitions.

[33] The fact that the formula in Appendix B is only valid for a very small amount of dye molecules compared to the matrix had knowingly been ignored for this rough estimation.

5.2.2. Time-Resolved Photoluminescence Spectra

Graphs of spectra measured (labelled as 'sample') and fitted data are presented. The curve fitting procedure, fitted parameters and the identified mean half-intensity decay times are also presented and discussed at the end of this chapter.

For these measurements an excitation wavelength of 330 nm and emission wavelength of 430 nm was chosen.

5.2.2.1.Instrumentation

All measurements were carried out with an 'Analysis Toolkit for Time-Resolved Spectroscopy', FLA 900, from Edinburgh Instruments Ltd..

5.2.2.2.Time Dependence of the Photoluminescence Intensity of Dye Bis-MSB in Powder Form

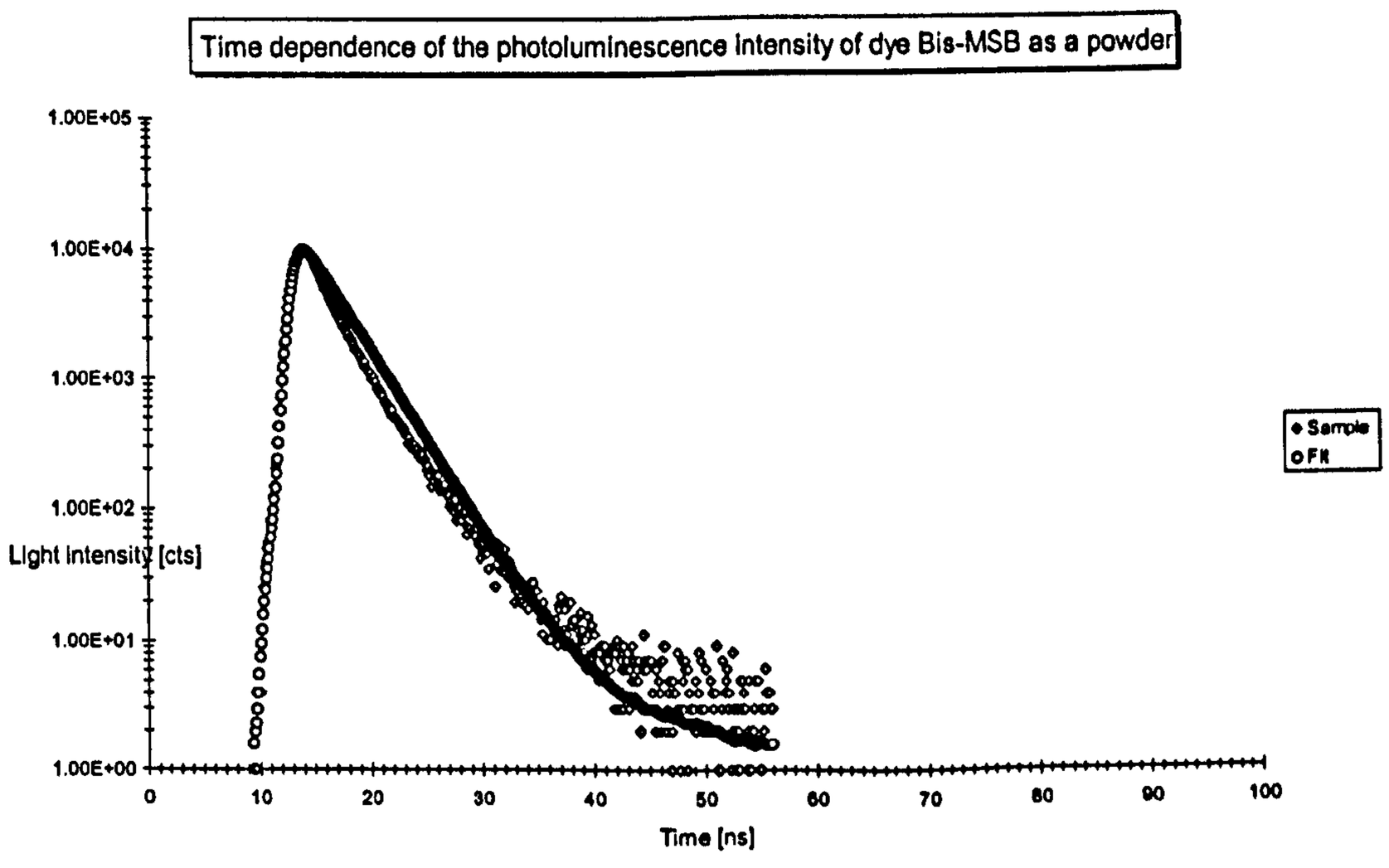

Fig. 5.19: Time dependence of the photoluminescence intensity of dye Bis-MSB in powder form

5.2.2.3.Time Dependence of the Photoluminescence Intensity of Dye Bis-MSB in Chloroform Solution

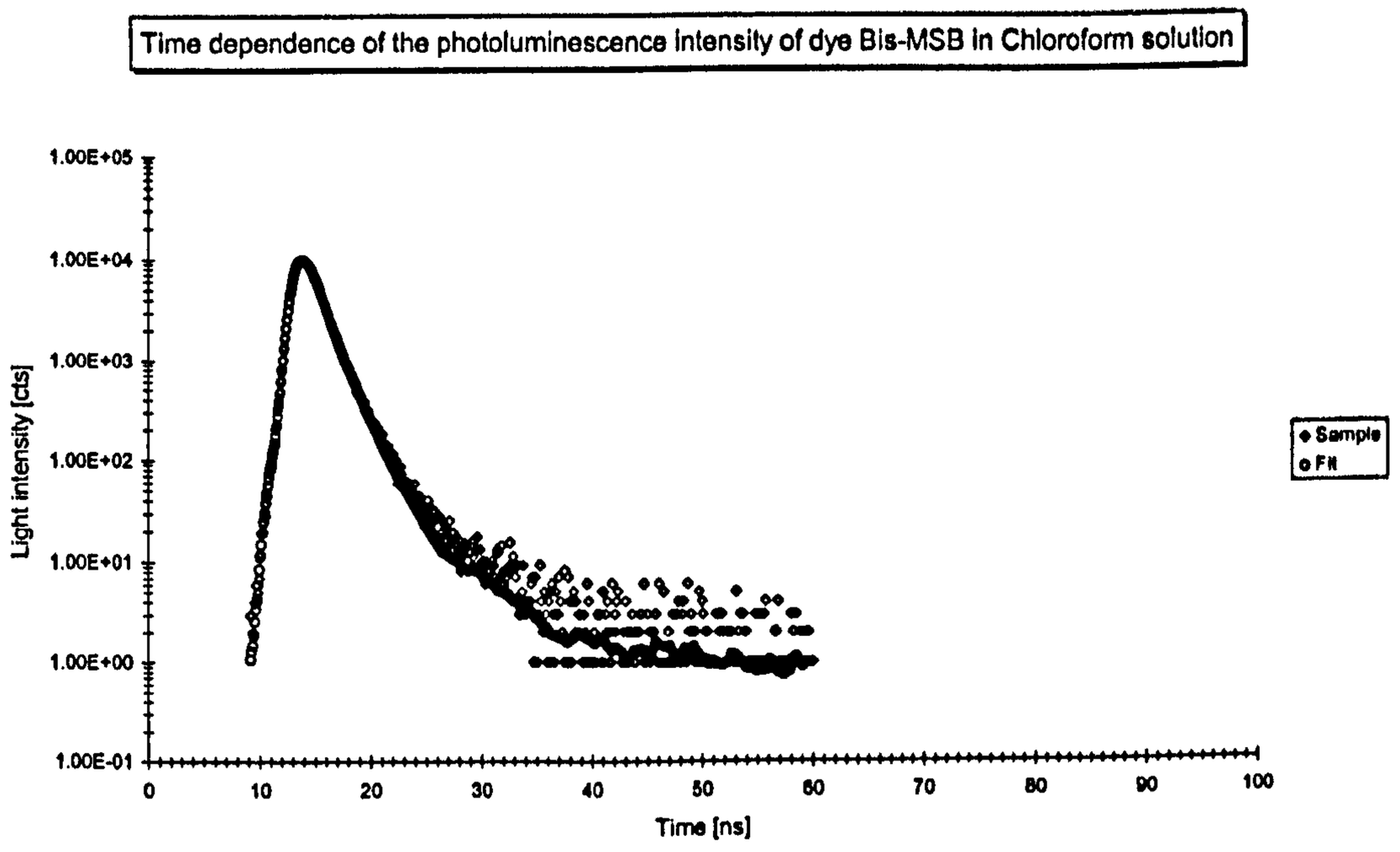

Fig. 5.20: Time dependence of the photoluminescence intensity of dye Bis-MSB in Chloroform solution

5.2.2.4.Time Dependence of the Photoluminescence Intensity of an Undoped PVK Film

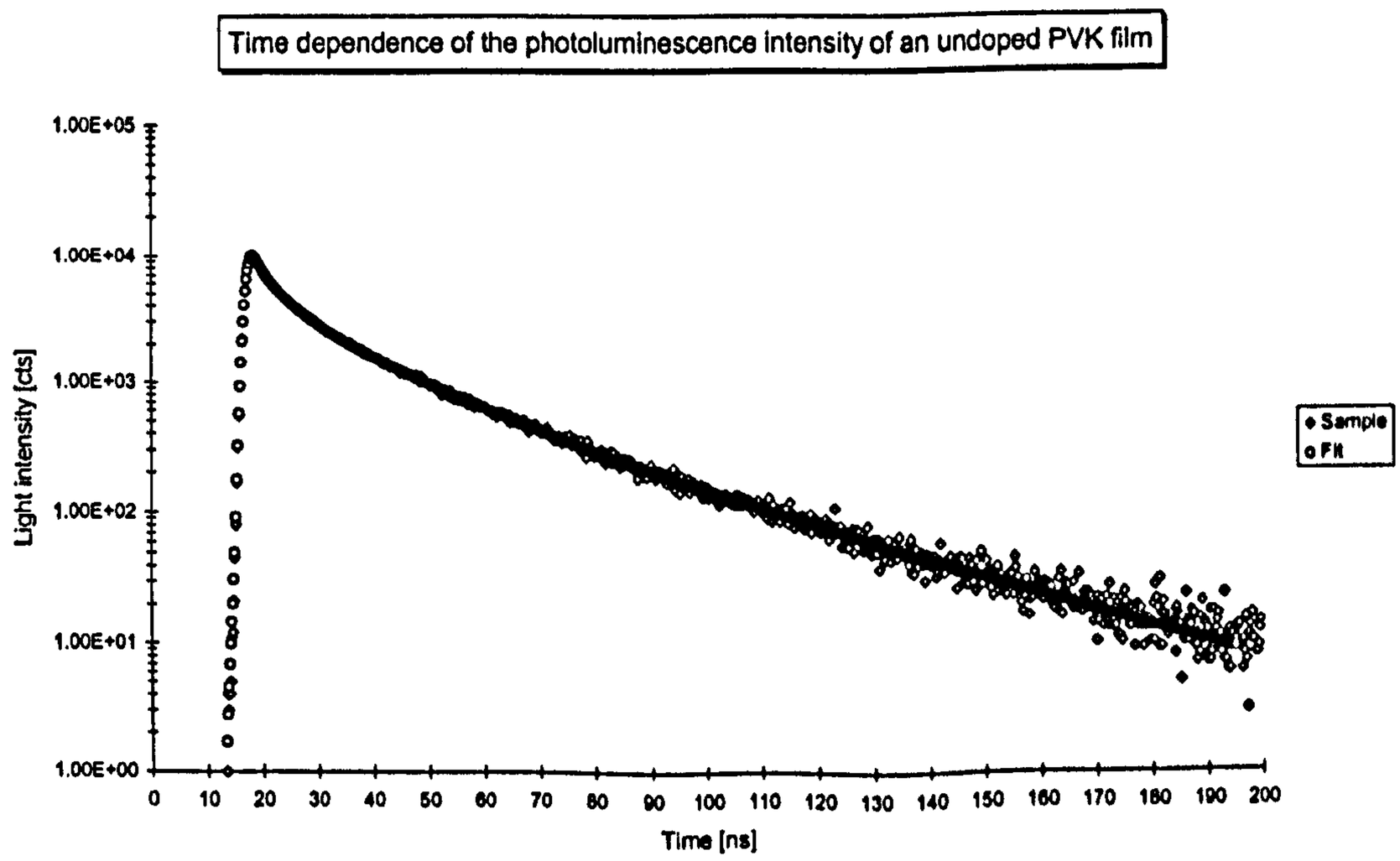

Fig. 5.21: Time dependence of the photoluminescence intensity of an undoped PVK film

5.2.2.5.Time Dependence of the Photoluminescence of PVK Doped with Dye Bis-MSB in Different Concentrations

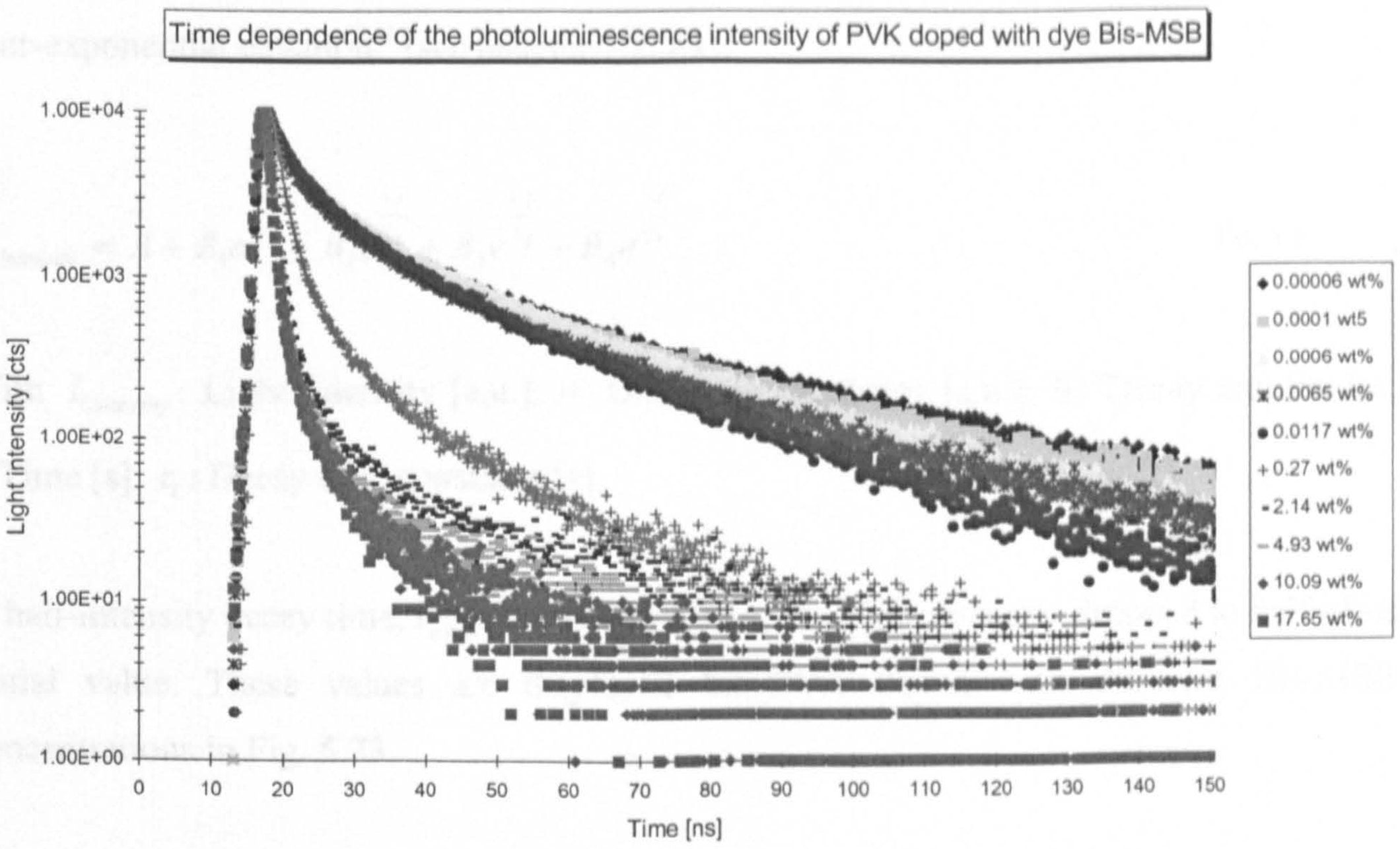

Fig. 5.22: Time dependence of the photoluminescence intensity of PVK films doped with dye Bis-MSB in 10 different concentrations

5.2.2.6. Exponential Decay Curve Fitting and Half-Intensity Decay Times

The measured decay curves, Fig. 5.19 to Fig. 5.22, were fitted according to the following four-exponential equation[34] (see chapter 3.2.3.1):

$$L_{Intensity} = A + B_1 e^{\frac{-t}{\tau_1}} + B_2 e^{\frac{-t}{\tau_2}} + B_3 e^{\frac{-t}{\tau_3}} + B_4 e^{\frac{-t}{\tau_4}} \qquad \text{Eq. 5.1}$$

With $L_{Intensity}$: Light intensity [a.u.]; A: Displacement factor [a.u.]; B_i: Decay amplitudes; t: Time [s]; τ_i: Decay time constants [s].

A half-intensity decay time, $t_{1/2}$ [s], was taken when the light intensity dropped to half of its initial value. These values are displayed for PVK doped with different Bis-MSB concentrations in Fig. 5.23.

The results of the curve fitting together with the half-intensity decay times are given in Table 5.1:

[34] Attempted fits using single-, double- and triple-exponential equations did not give satisfying results for PVK and Bis-MSB doped PVK.

	Decay time constants and half-intensity decay time[ns]					Decay amplitudes [a.u.]				Relative fluorescence intensity $I_{FL,\,rel.\,i} \equiv B_i\tau_i/(B_1\tau_1+B_2\tau_2+B_3\tau_3+B_4\tau_4)$ (individually rounded [%])				Shift	Fit quality
Sample	τ_1	τ_2	τ_3	τ_4	$t_{1/2}$	B_1	B_2	B_3	B_4	$I_{FL,\,rel.,\,1}$	$I_{FL,\,rel.,\,2}$	$I_{FL,\,rel.,\,3}$	$I_{FL,\,rel.,\,4}$	A	χ^2
5.2.2.2	2.58	4.65	-	-	2.7	0.083	0.011	-	-	80.5	19.5	-	-	0.337	1.28
5.2.2.3	4.44	1.22	-	-	1.6	0.0005	0.1452	-	-	1.3	98.7	-	-	0.224	1.12
5.2.2.4	0.70	3.85	34.33	14.31	5	0.096	0.051	0.014	0.036	5.3	15.8	38.0	41.0	0.012	1.01
5.2.2.5															
6.0E-5	13.90	0.72	3.61	45.10	3.6	0.029	0.147	0.056	0.011	33.6	8.7	16.7	41.0	0.108	0.96
0.0001	5.13	0.99	45.58	16.80	3.4	0.050	0.131	0.008	0.024	21.7	11.0	32.8	34.5	0.158	1.06
0.0006	95.10	4.38	36.95	14.31	4	0.116	0.048	0.011	0.032	9.3	17.5	35.2	38.1	0.062	1.09
0.0065	5.15	1.07	16.23	42.44	3.2	0.048	0.139	0.0241	0.007	23.2	13.9	36.7	26.2	0.430	0.99
0.0117	5.41	1.28	16.70	34.95	3.6	0.053	0.100	0.027	0.006	26.6	11.8	42.0	19.6	0.096	1.02
0.27	0.84	2.08	7.47	26.71	1.7	0.198	0.052	0.009	0.002	42.9	27.8	18.2	11.0	-0.415	1.090
2.14	0.59	12.15	41.10	2.75	1.2	0.391	0.001	0.0005	0.008	81.8	4.0	6.6	7.7	0.042	1.10
4.93	3.18	0.49	114.5	22.26	1.1	0.006	0.466	5.0 E-5	0.0006	6.9	86.3	2.0	4.8	-0.410	1.03
10.09	14.30	0.51	85.49	2.75	1.1	0.0007	0.447	3.0 E-5	0.007	4.1	88.1	0.9	6.9	0.166	1.10
17.65	10.40	0.43	50.90	2.73	0.9	0.0008	0.516	6.0 E-5	0.004	3.4	90.5	1.3	4.8	0.057	0.94

Table 5.1: Fitted parameters and half-intensity decay times for time resolved emission spectra of Bis-MSB as a powder (Sample: 5.2.2.2), Bis-MSB in Chloroform solution (Sample: 5.2.2.3), undoped PVK (Sample: 5.2.2.4) and PVK doped with Bis-MSB in 10 different concentrations [wt%] (Sample: 5.2.2.5). (Standard deviations of the fitted parameters are listed in Appendix C.)

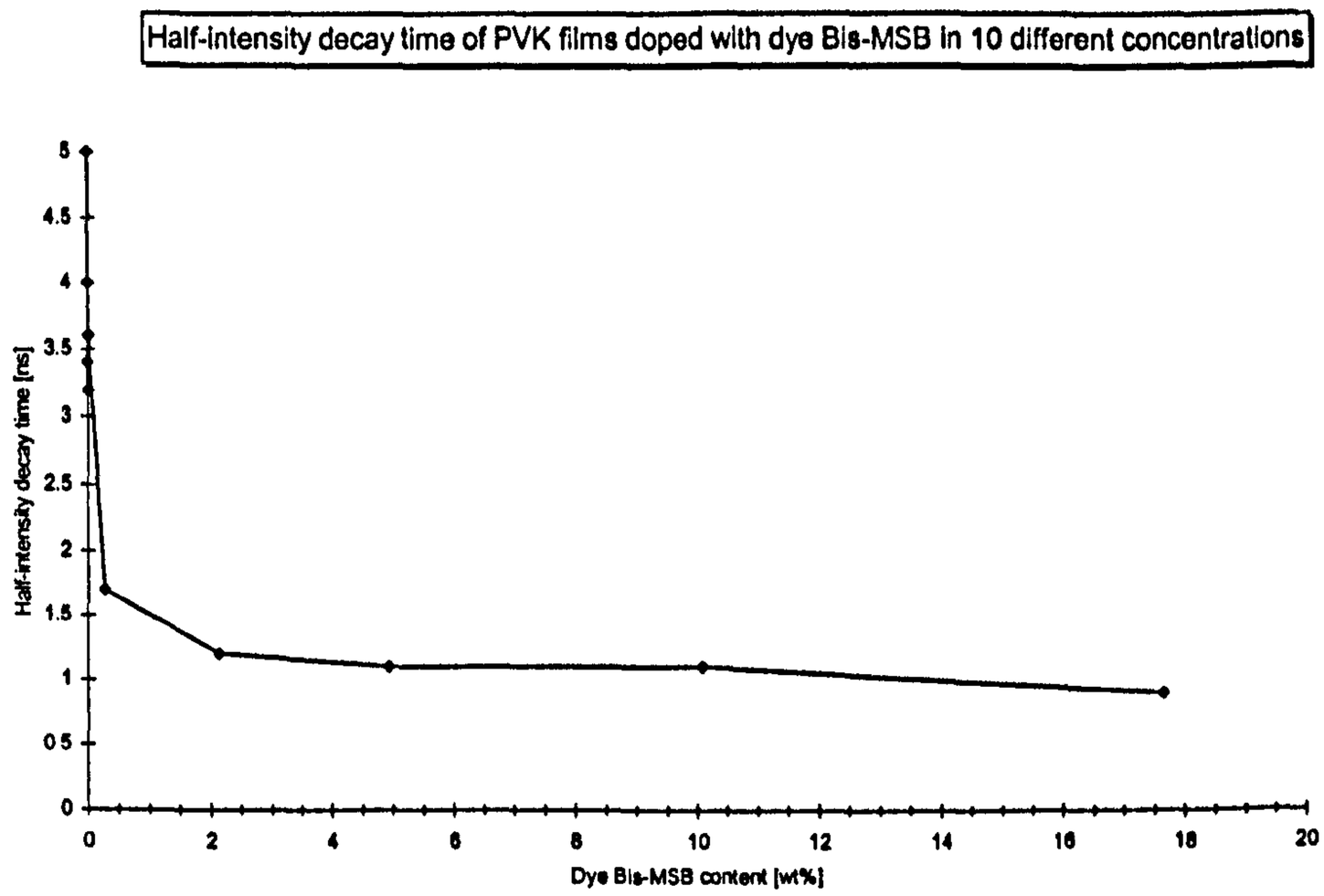

Fig. 5.23: Half-intensity decay time of PVK films doped with dye Bis-MSB in 10 different concentrations

The higher value of $t_{1/2}$ for Bis-MSB in form of a powder (2.7 ns) compared to $t_{1/2}$ for Bis-MSB in Chloroform (1.6 ns) is due to the diffusion processes within the solvent which enables interactions for the excited molecules.

In general, the rapid decrease of $t_{1/2}$ with the increase of the Bis-MSB concentration in the PVK thin film host matrix from 3.6 ns to about 1 ns from approximately 2 wt% dye concentration onwards, i.e. an average dye molecule centre distance of 28 Å (see Appendix B), can be explained by concentration quenching, see chapter 3.3.

5.2.2.7.Non-Exponential Decay Analysis

The PL light intensity vs. time data for very low, medium and high dye doping concentrations are displayed as $\sqrt{\frac{L\_\mathrm{int}_0}{L\_\mathrm{int}(t)}}$ vs. time according to Eq. 3.11.

Analysis for 0.00006 wt% dye Bis-MSB in PVK

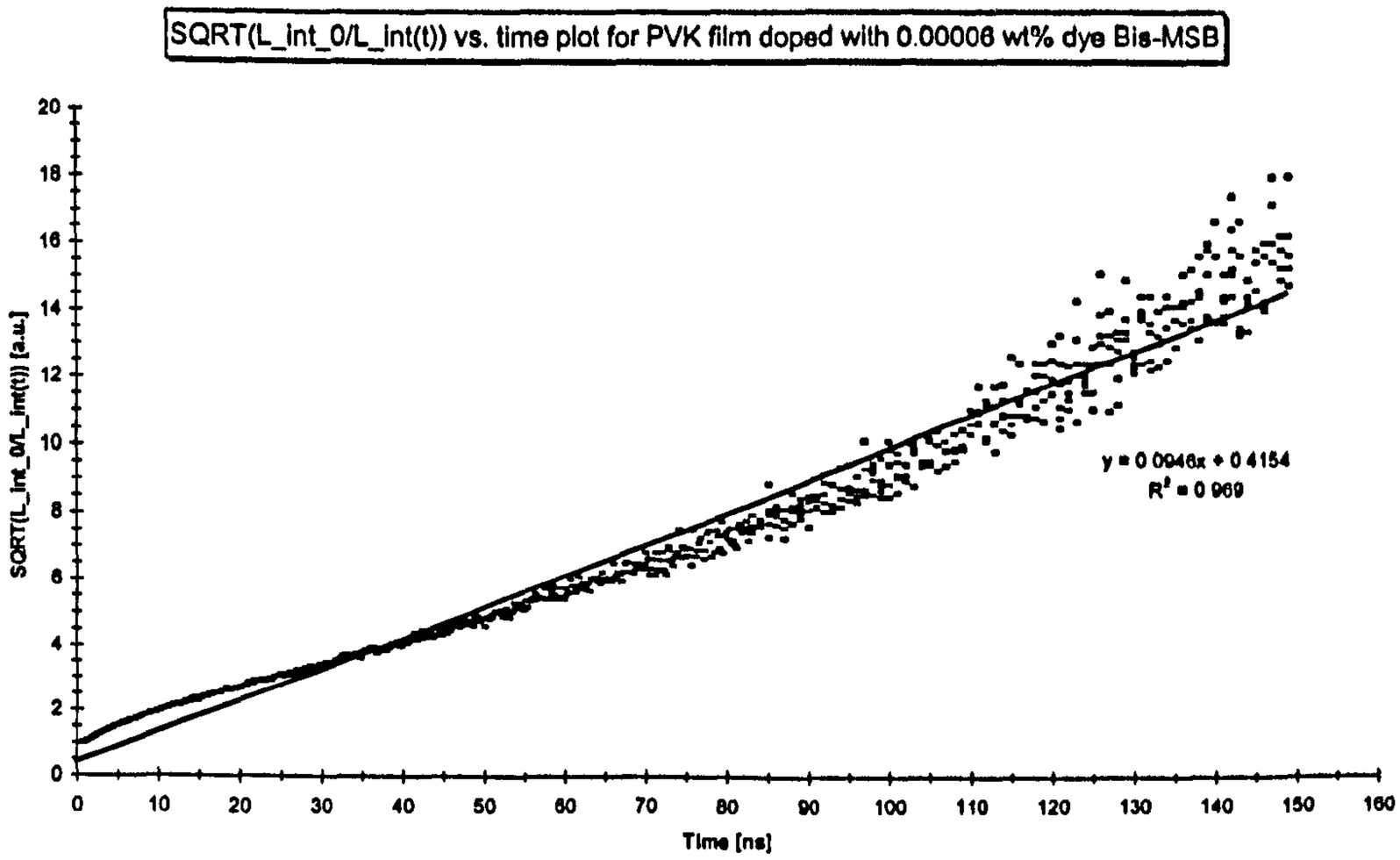

Fig. 5.24: SQRT(L_int_0/L_int(t)) vs. t plot for PVK film doped with 0.00006 wt% dye Bis-MSB

The PL light intensity vs. decay time for a PVK film containing 0.00006 wt % dye Bis-MSB displayed according to Eq. 3.11, Fig. 5.24, can well be fitted by a linear function (R^2=0.969); the increasing deviation of the fitted line from about 110 ns onwards (i.e. of more than 10 units on the y-axis) can be neglected as the light intensity after that time has already decreased to less than 1% of its initial value. The reciprocal value of the slope (0.0946 ns^{-1}) gives a decay constant of τ=10.6 ns.

Analysis for 0.27 wt% dye Bis-MSB in PVK

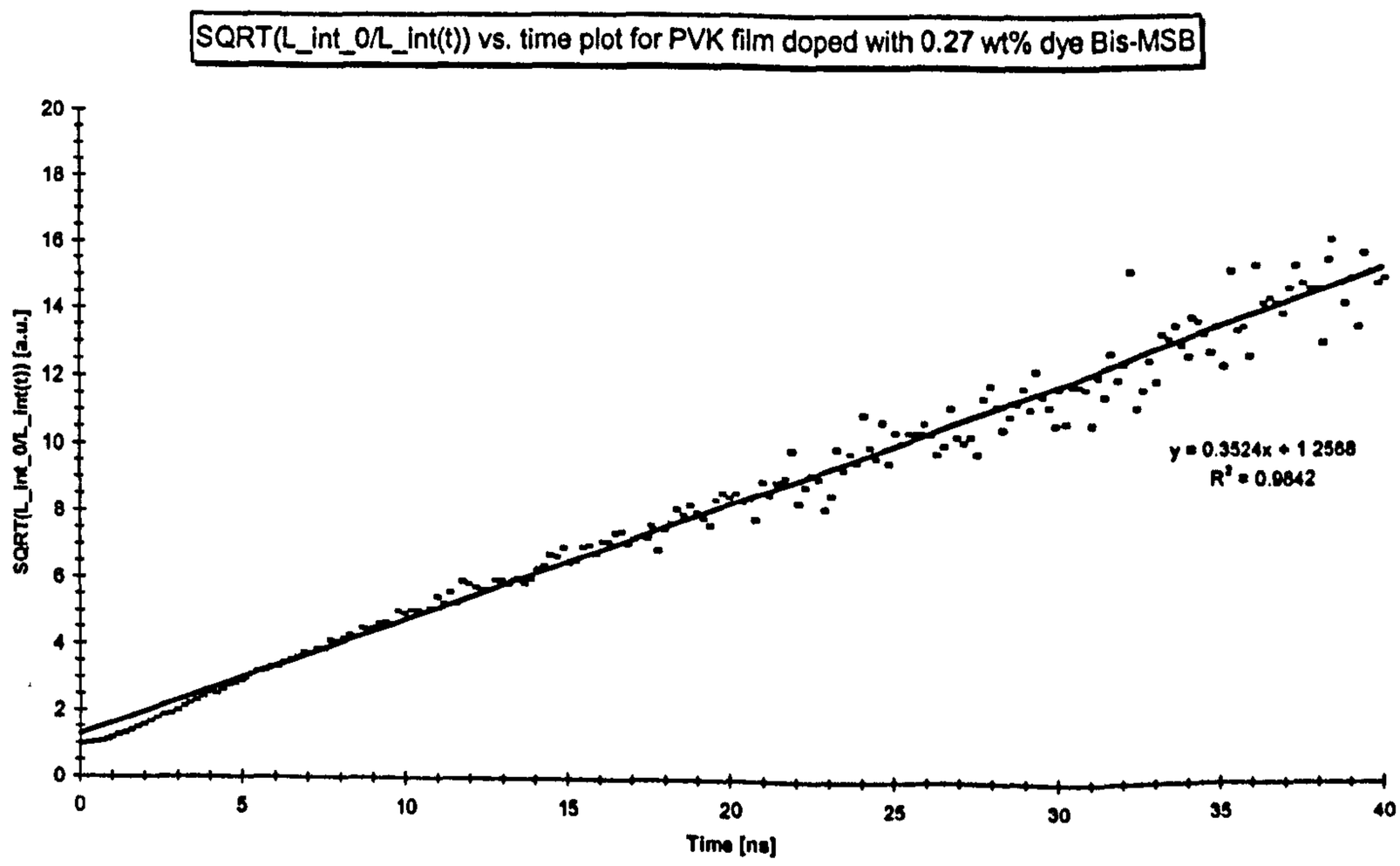

Fig. 5.25: SQRT(L_int_0/L_int(t)) vs. t plot for PVK film doped with 0.27 wt% dye Bis-MSB

The inverted value of the slope (0.3534 ns^{-1}) of the PL light intensity vs. decay time for a PVK film containing 0.27 wt % dye Bis-MSB displayed according to Eq. 3.11, leads to a decay constant of τ=2.8 ns, Fig. 5.25. As R^2=0.9842 the fit describes the correlation very well.

Analysis for 17.65 wt% dye Bis-MSB in PVK

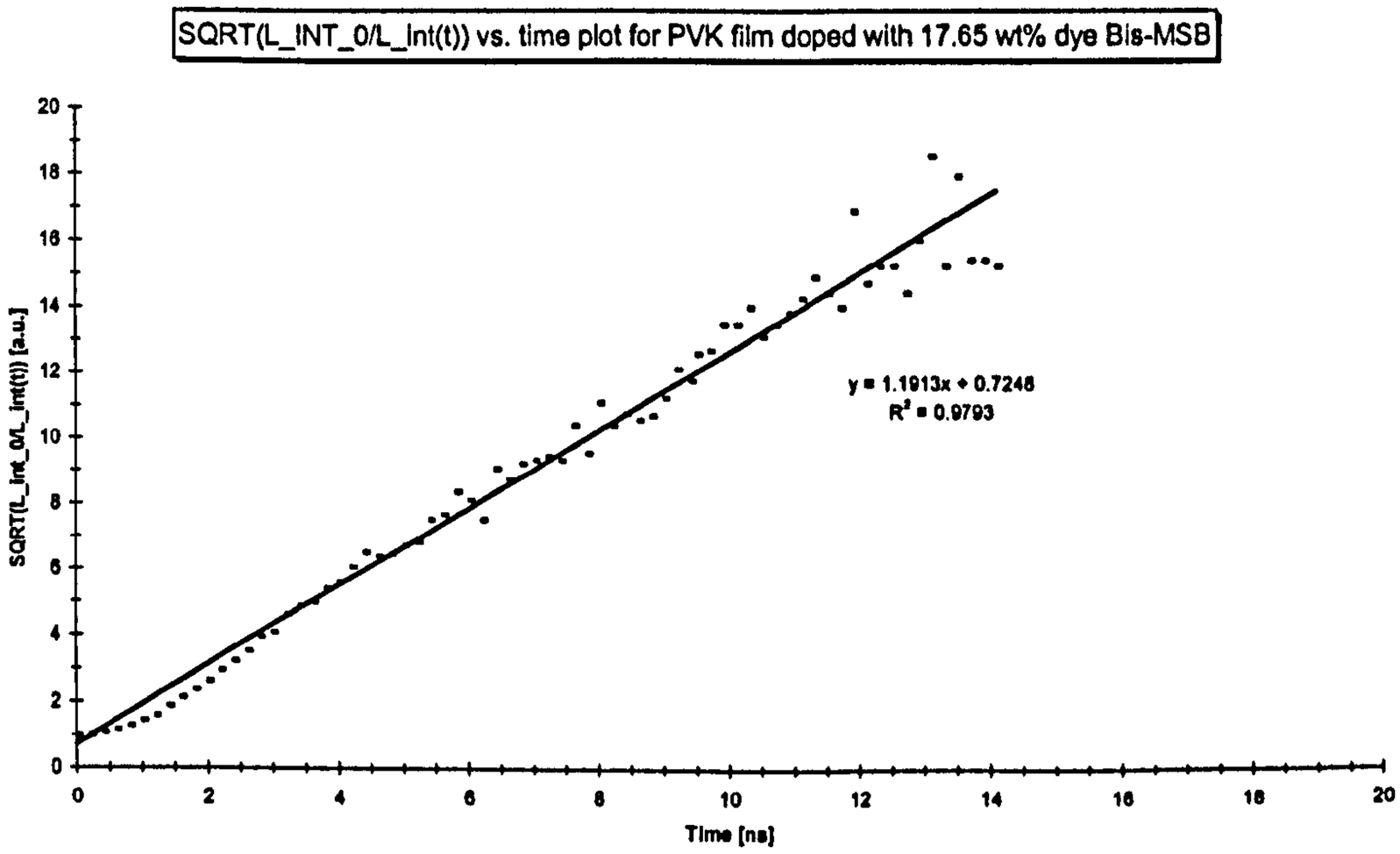

Fig. 5.26: SQRT(L_int_0/L_int(t)) vs. t plot for PVK film doped with 17.65 wt% dye Bis-MSB

Fitting the PL light intensity vs. decay time data for a PVK film containing 17.65 wt % dye Bis-MSB displayed according to Eq. 3.11, Fig. 5.26, gives a well secured (R^2=0.9793) decay constant of τ=0.8 ns.

Discussion of non-exponential decay

These three selected fits indicate that all data can well be described by Eq. 3.11. The decrease of the decay constant with increasing dye doping concentration is due to concentration quenching, see chapter 3.3.

Discussion of both exponential and non-exponential PL decay

The PL light intensity decay of Bis-MSB embedded in PVK vs. time could be fitted by using a four-exponential function as well as by using a non-exponential underlying decay process. As it is much easier to fit any given set of data by having 9 variables, like in the case of the four-exponential decay, and there is also from the photoluminescence

measurements (see Fig. 5.18) only weak evidence for four energy levels being present in the system it can be assumed that a non-exponential decay is the underlying process.

5.3. D.C. Driven Electroluminescence Characterisation

5.3.1. Electroluminescence Spectra

5.3.1.1.Instrumentation and measurement procedure

A Keithley 236 Source Measure Unit (accuracy: ± 10 nA) together with a Bentham M 300 BA Monochromator (accuracy: ± 10^{-4} a.u.) was used.

A constant voltage of about 2 volts above the turn-on voltage was applied to the sample whilst the emitted light intensity over a wavelength range of 350 nm to 500 nm was measured.

5.3.1.2. Electroluminescence spectra of Bis-MSB doped PVK film EL devices with 1.03 wt % and 4.96 wt % doping concentration

Two electroluminescence spectra of the fabricated devices doped with 1.03 wt % dye concentration and one doped with 4.96 wt % dye concentration were obtained at different wavelength scan rates, Fig. 5.27 to Fig. 5.29.

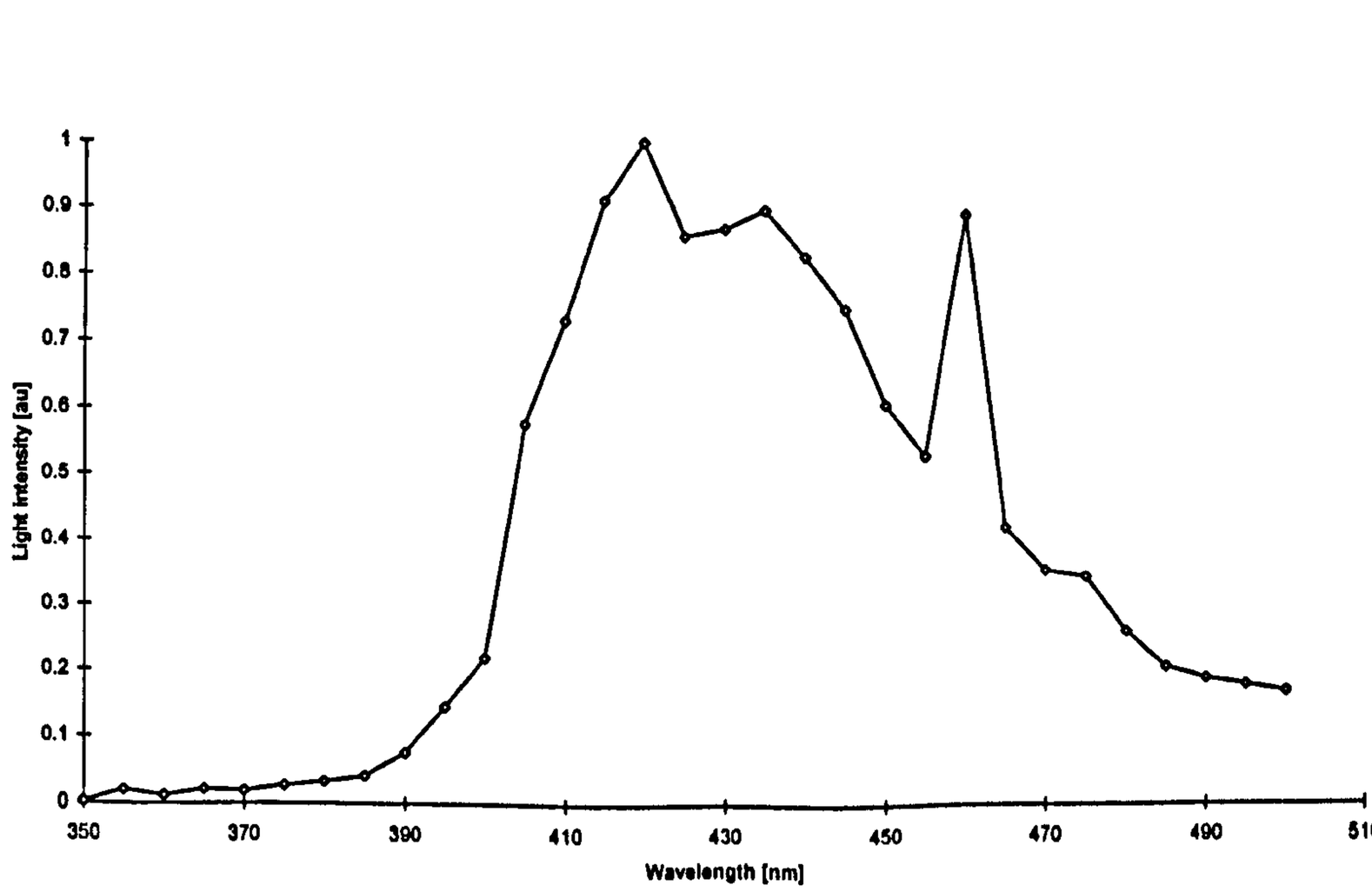

Fig. 5.27 Electroluminescence spectrum of ITO/Bis-MSB and PVK/Al OLED (Bis-MSB concentration: 1.03 wt %; scan rate: 5 nm/step)

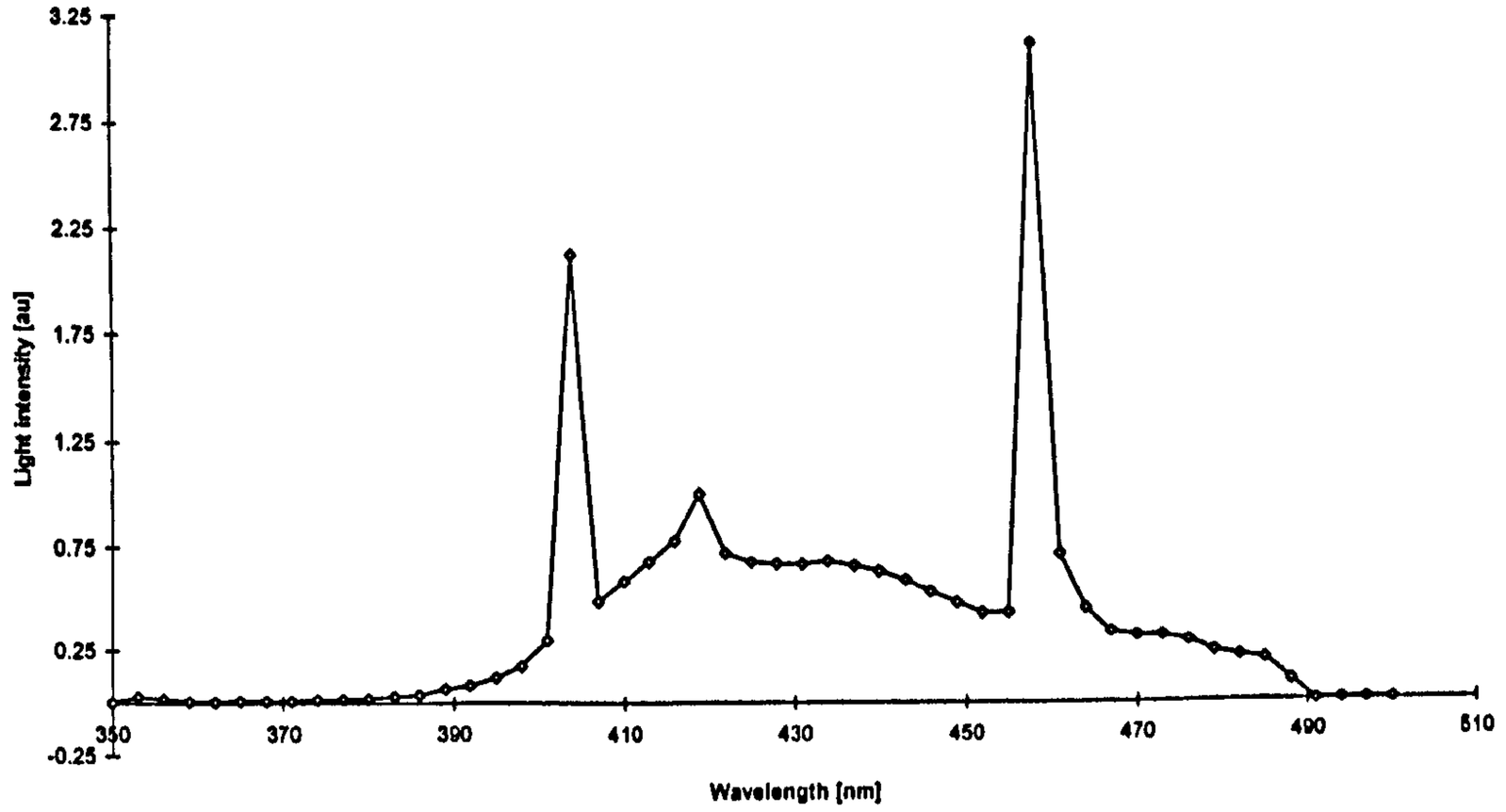

Fig. 5.28: Electroluminescence spectrum of ITO/Bis-MSB and PVK/Al OLED (Bis-MSB concentration: 1.03 wt %; scan rate: 3 nm/step)

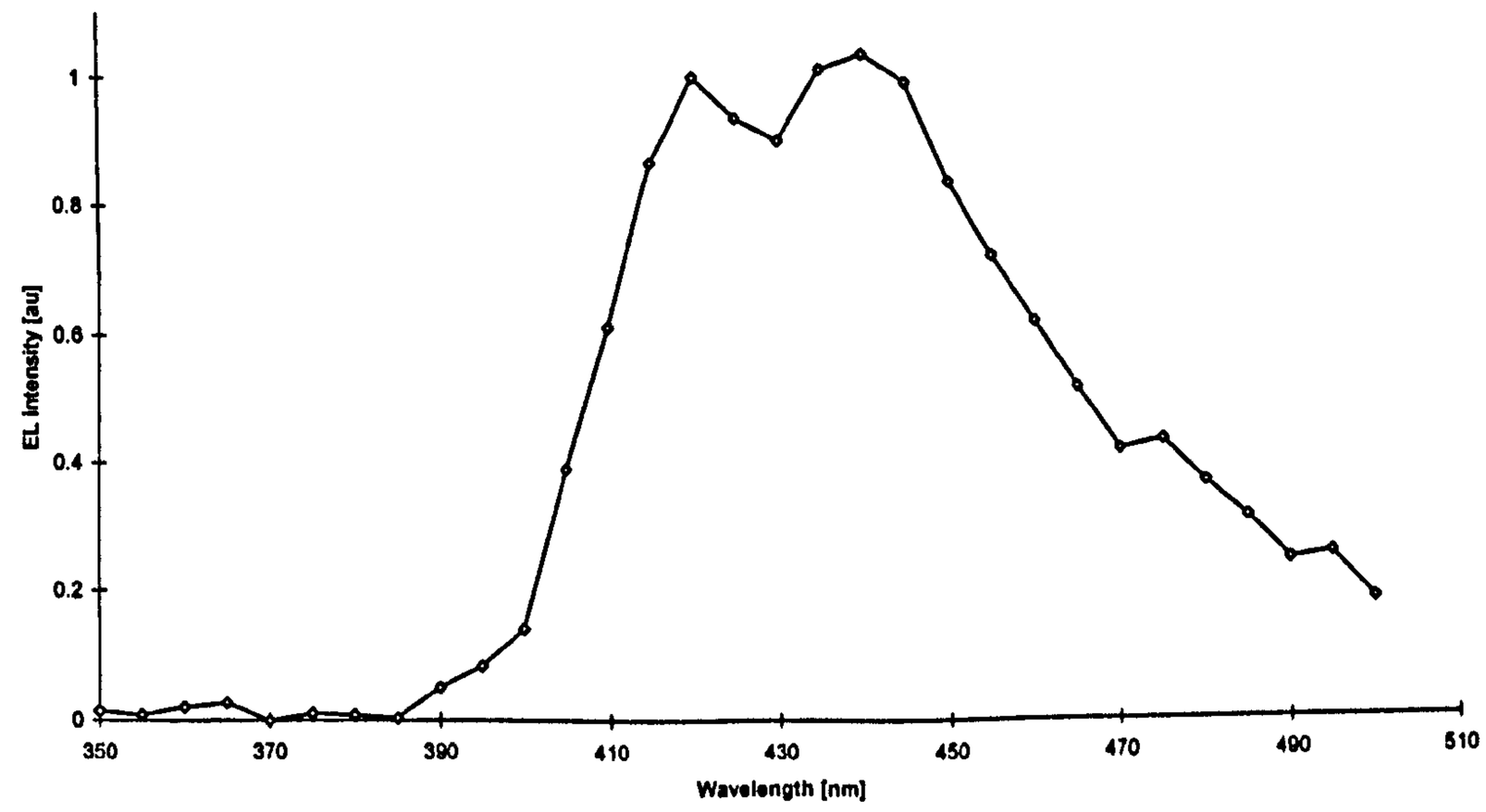

Fig. 5.29: Electroluminescence spectrum of ITO/Bis-MSB and PVK/Al OLED (Bis-MSB concentration: 4.96 wt %; scan rate: 5 nm/step)

The samples from which Fig. 5.27 to Fig. 5.29 were obtained were not encapsulated (see chapter 7) and operated in air and were therefore not very stable. Only these three presented spectra could be measured out of the whole range of samples with different dye concentrations. A rapid decline of the resulting current was observed and also of the light intensity, since the emitted light intensity is approximately proportional to the current (see chapter 5.3.2.4). Dark spots on top of the aluminium electrodes indicated a corrosion reaction.

The contribution of sparks to the light output is clearly visible in these spectra as additional peaks at about 405 nm and 460 nm. The relative height of the superposed peaks compared to the electroluminescence emission is higher when a lower scan rate (longer measurement time) had been applied.

A double peak in the electroluminescence spectrum can be observed at around 420 nm and 435/440 nm. A small shift of the EL intensity maxima towards higher wavelengths by about 10 nm compared to the PL peak intensities (see Fig. 5.16) was found. This suggests that the excitons responsible for the light emission are slightly affected by the large applied electric field (HE, 1997).

Due to the severe problems outlined above with the sample fabrication an EL light intensity vs. Bis-MSB doping concentration plot could not be obtained.

5.3.2. Current-Voltage (I-V), EL Light Intensity-Voltage (L-V), Current Density-Voltage (J-V) and EL Light Intensity-Current (L-I) Characterisation

Four samples (No. 1 - 4) with different dye concentration, emission layer thickness and/or active sample area were presented. All measurements were carried out on ITO/PVK+Bis-MSB/Al devices. A discussion of the data obtained for all four samples follows after the data description of sample 4.

5.3.2.1.Sample 1: Dye concentration: 3.7 %; emission-layer thickness[35]: 35 nm; active area: 0.071 cm^2

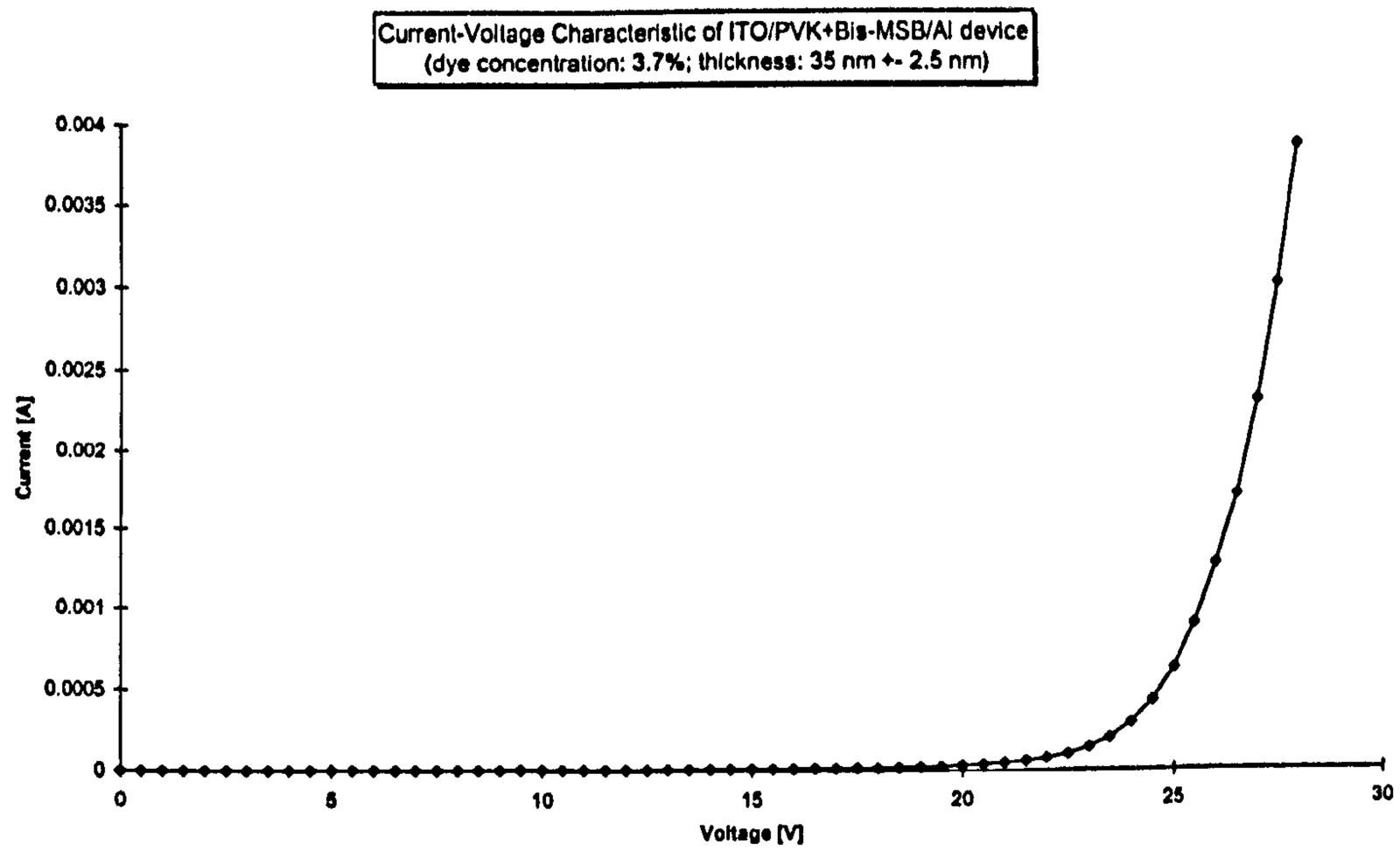

Fig. 5.30: I-V Characteristic of ITO/PVK+Bis-MSB/Al device (dye concentration: 3.7 ± 0.1%; thickness: 35 ± 2.5 nm; area: 0.071 cm^2)

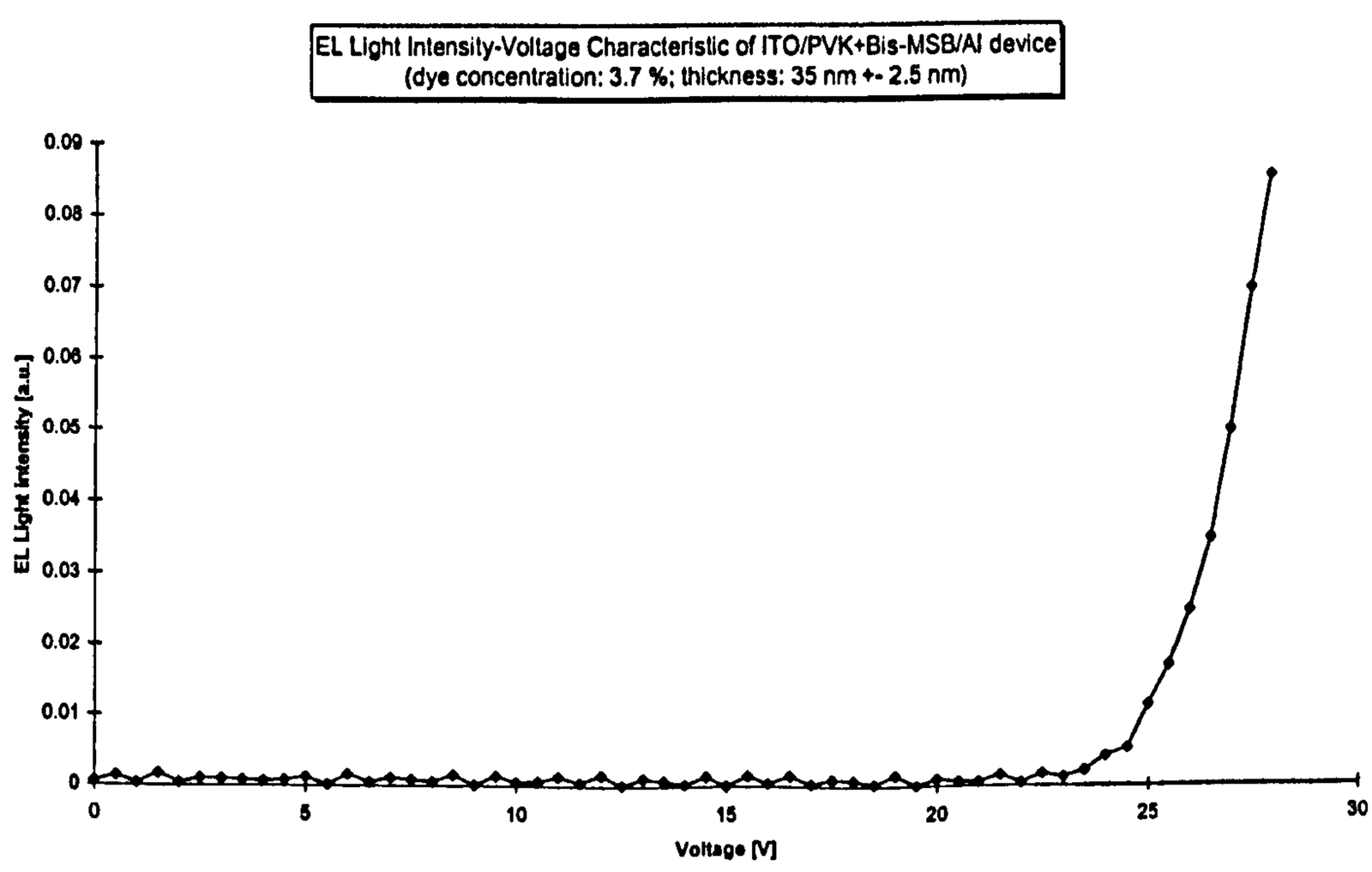

Fig. 5.31: L-V Characteristic of ITO/PVK+Bis-MSB/Al device (dye concentration: 3.7 ± 0.1%; thickness: 35 ± 2.5 nm; area: 0.071 cm^2)

[35] Any layer thickness has to be interpreted as an average thickness.

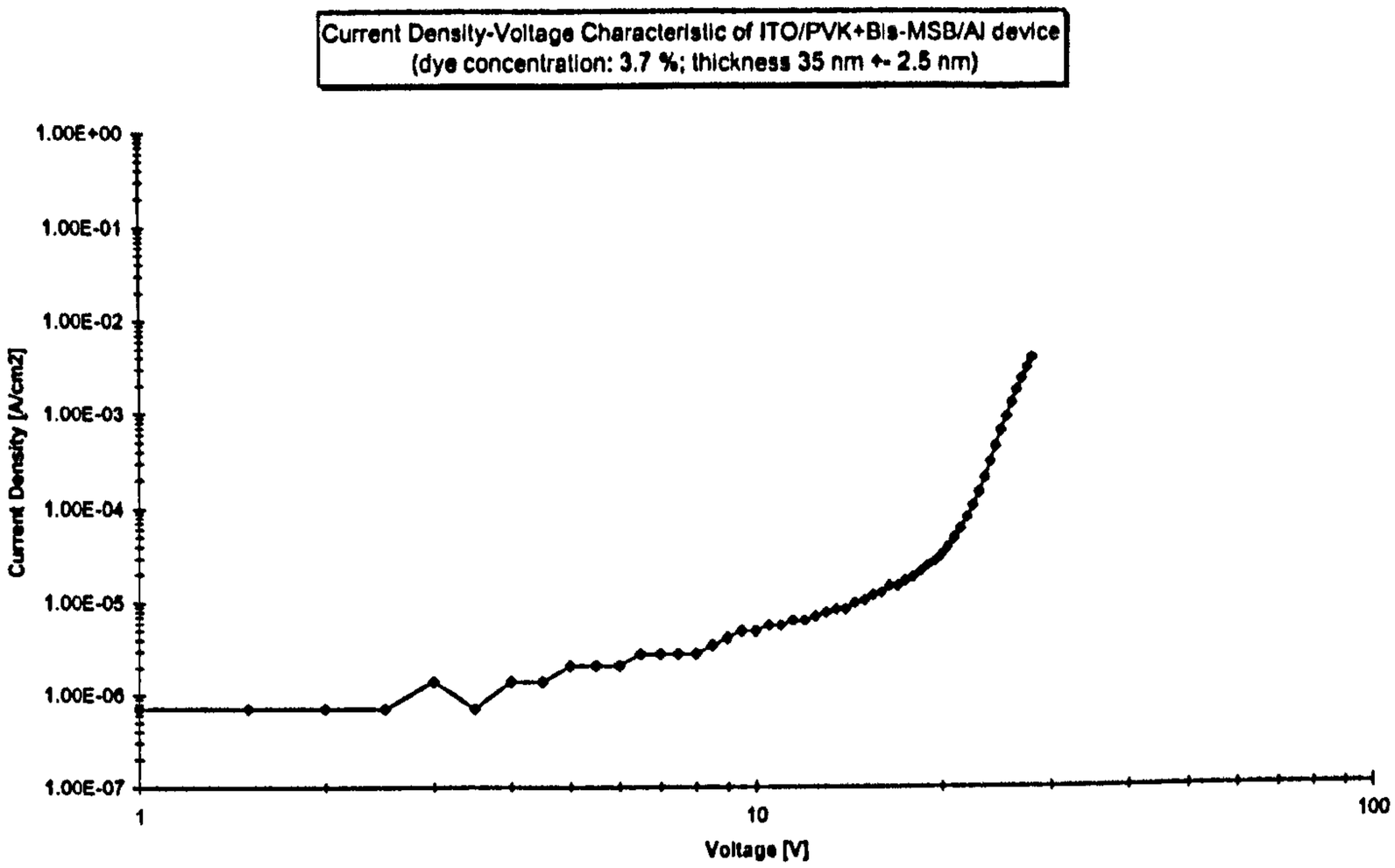

Fig. 5.32: J-V Characteristic of ITO/PVK+Bis-MSB/Al device in log-log scale (dye concentration: 3.7 ± 0.1%; thickness: 35 ± 2.5 nm; area: 0.071 cm^2)

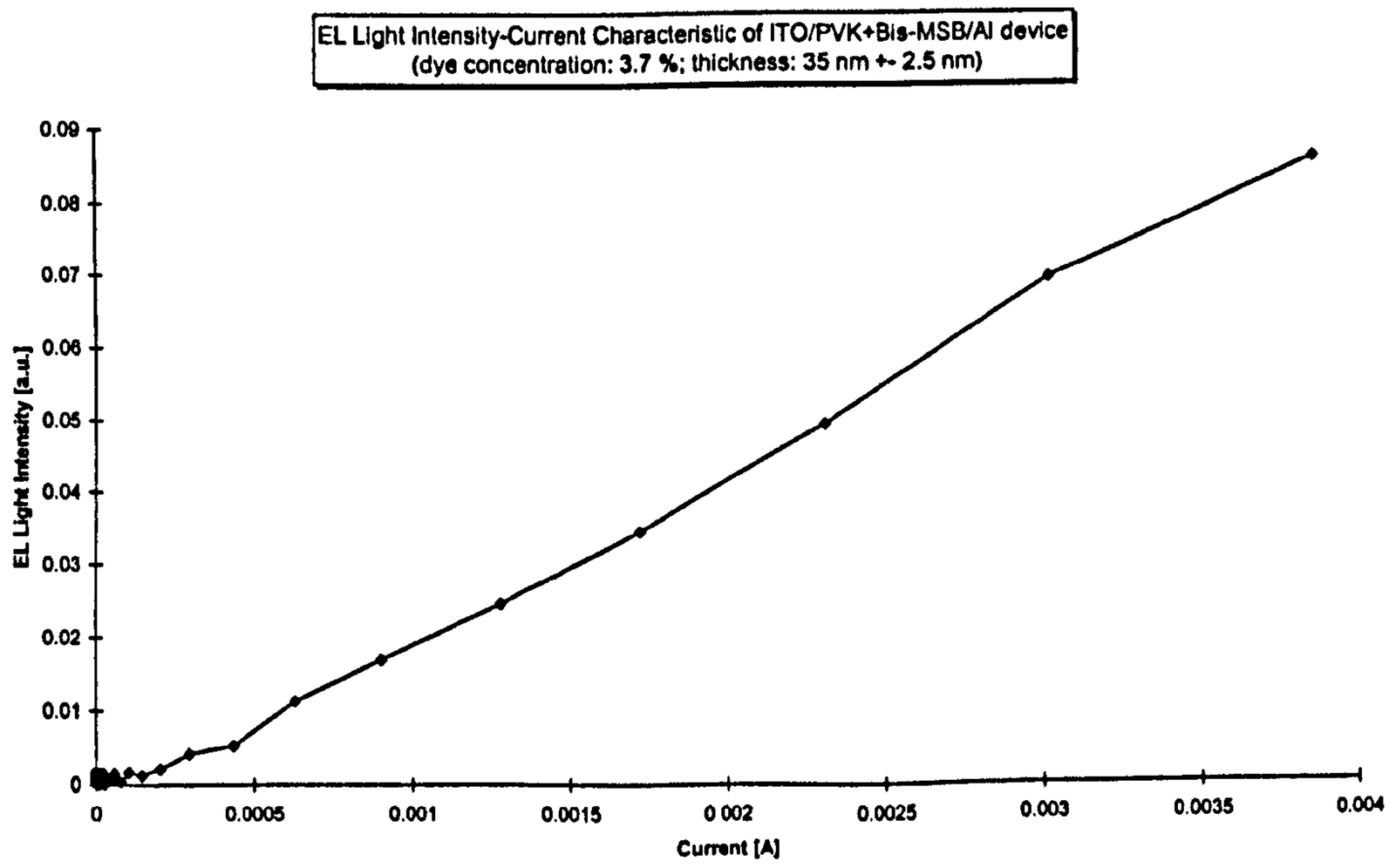

Fig. 5.33: L-I Characteristic of ITO/PVK+Bis-MSB/Al device (dye concentration: 3.7% ± 0.1%; thickness: 35 ± 2.5 nm; area: 0.071 cm^2)

The I-V characteristics of the ITO/PVK+Bis-MSB/Al device with a 3.7 wt % dye concentration and 35 nm thickness, Fig. 5.30, shows a clear exponential diode type behaviour with a turn-on voltage of about 22 V. The maximum value was taken at 28 V with a corresponding current of 3.9 mA.

The L-V characteristics, Fig. 5.31, follows the I-V characteristics. EL light emission starts at around 23 V (EL light intensity: 0.001 [a.u.]) and increases dramatically to a value of about 0.085 [a.u.] at 28 V.

The J-V characteristics plotted in a log-log scale, Fig. 5.32, reveals two linear regions[36]: 5 V to 19 V and from 22 V onwards with gradients of 0.2 and 2.5, respectively.

The L-I plot (Fig. 5.33) shows except at very low currents below 0.5 mA, an almost perfect linear increase of the EL emitted light with the current. An EL light intensity of about 0.08 [a.u.] at a current of about 35 mA is observed and a gradient of about 23.0 a.u./A..

5.3.2.2.Sample 2: Dye concentration: 5.0 %; emission-layer thickness: 37 nm; active area: 0.071 cm^2

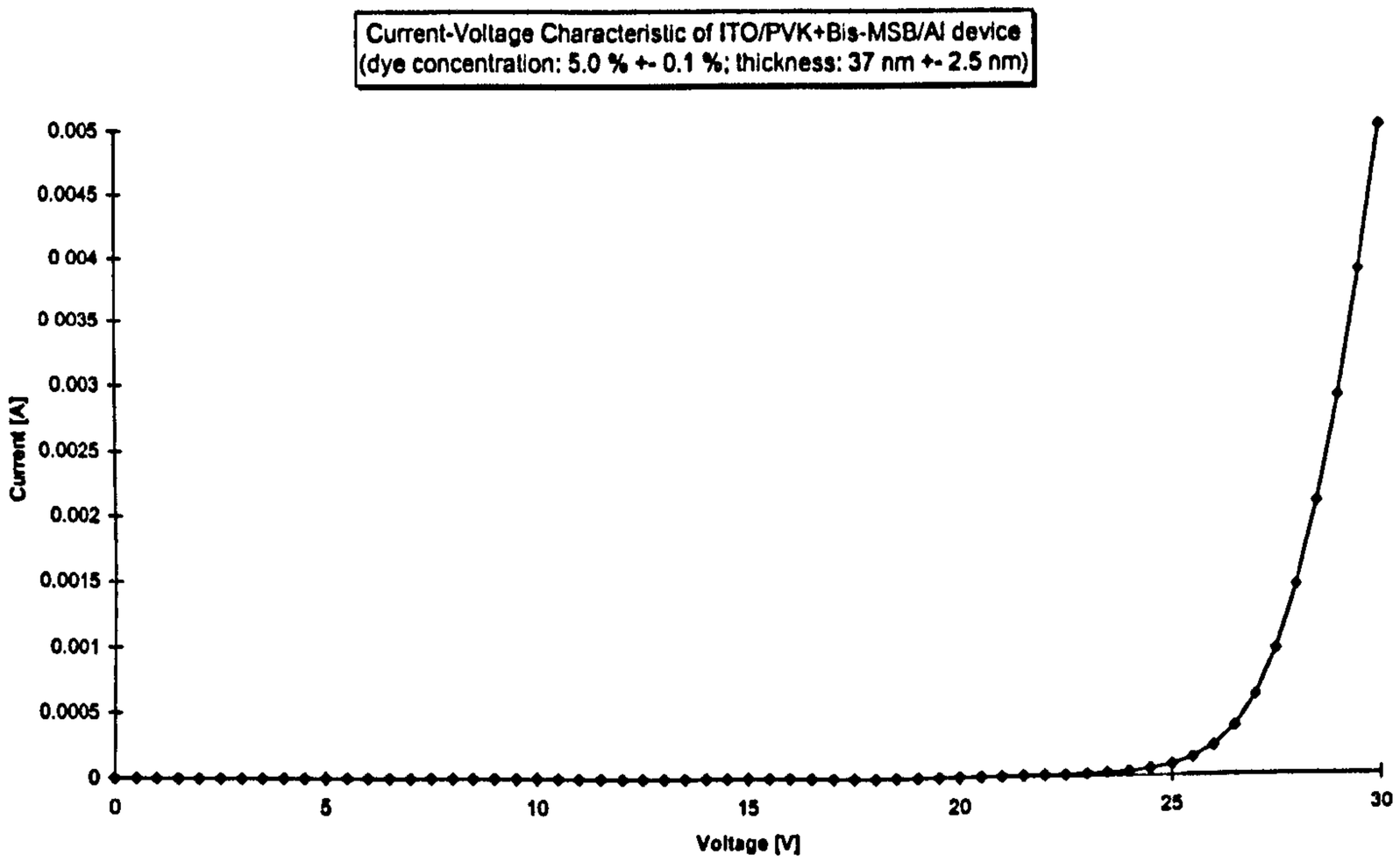

Fig. 5.34: I-V Characteristic of ITO/PVK+Bis-MSB/Al device (dye concentration: 5.0 % ± 0.1%; thickness: 37 ± 2.5 nm; area: 0.071 cm^2)

[36] It is technically not possible to implement trendlines of selected data points using the provided data analysis software EXCEL from Microsoft.

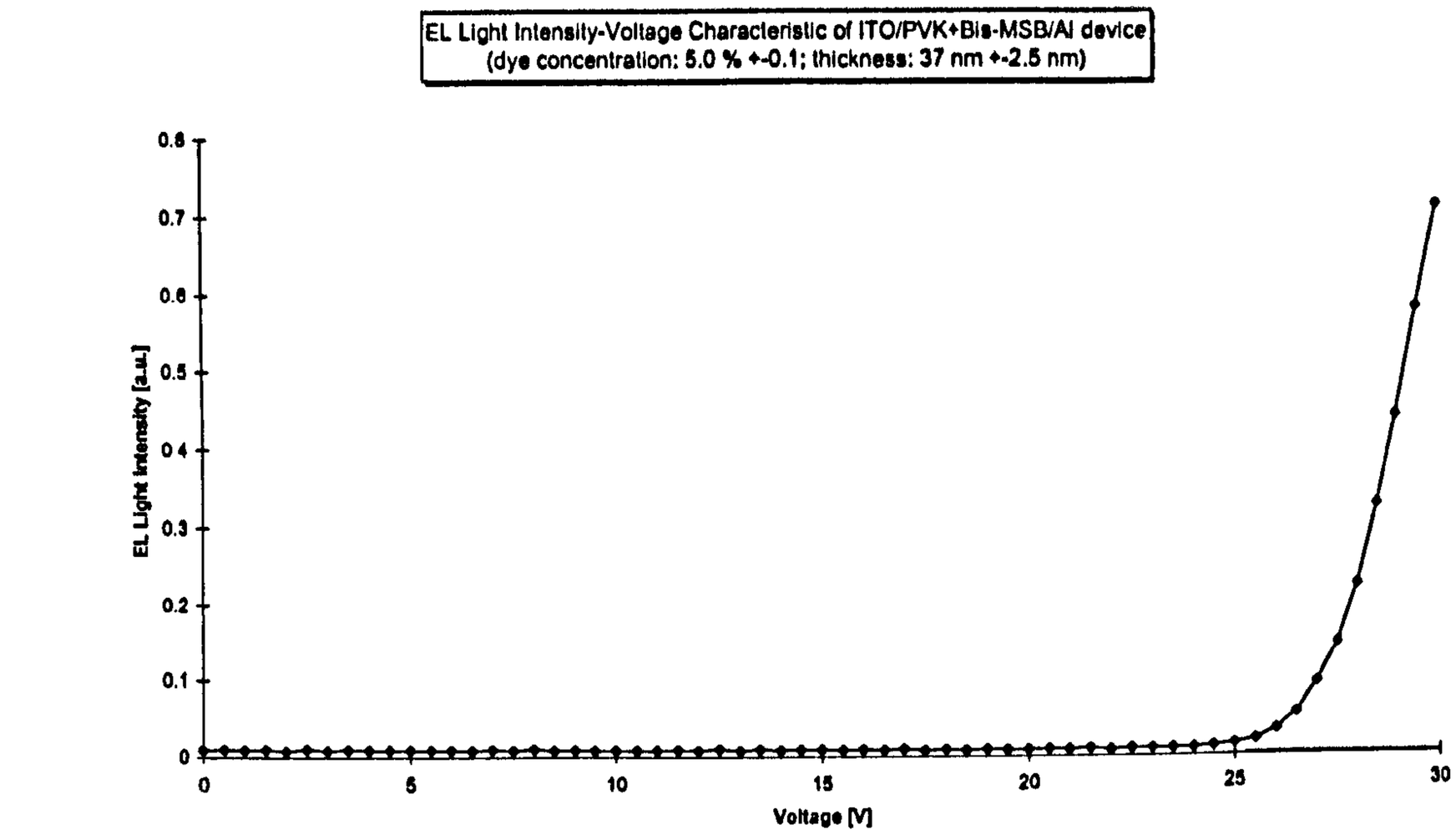

Fig. 5.35: L-V Characteristic of ITO/PVK+Bis-MSB/Al device (dye concentration: 5.0 % ± 0.1%; thickness: 37 ± 2.5 nm; area: 0.071 cm^2)

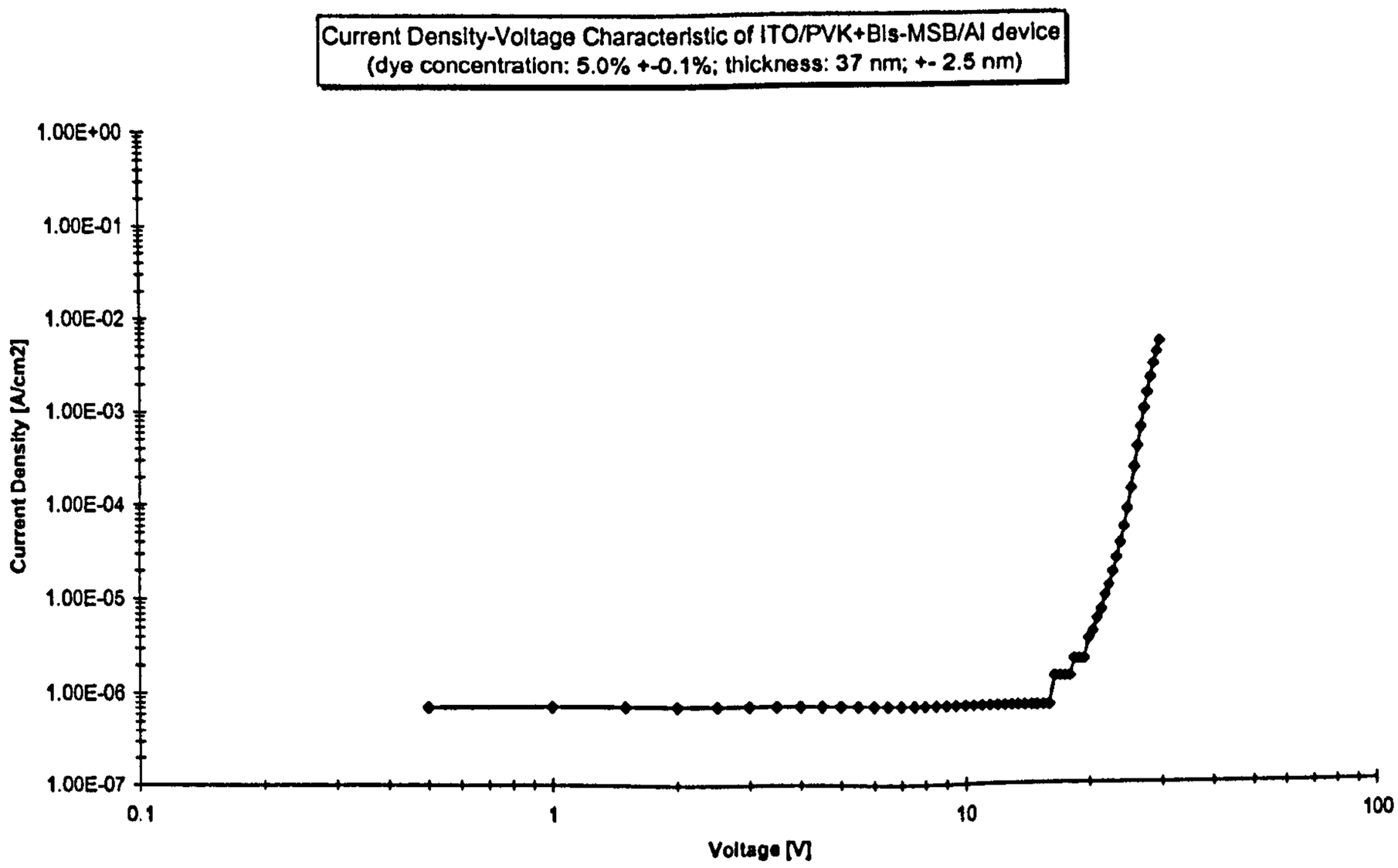

Fig. 5.36: J-V Characteristic of ITO/PVK+Bis-MSB/Al device in log-log scale (dye concentration: 5.0 % ± 0.1%; thickness: 37 ± 2.5 nm; area: 0.071 cm^2)

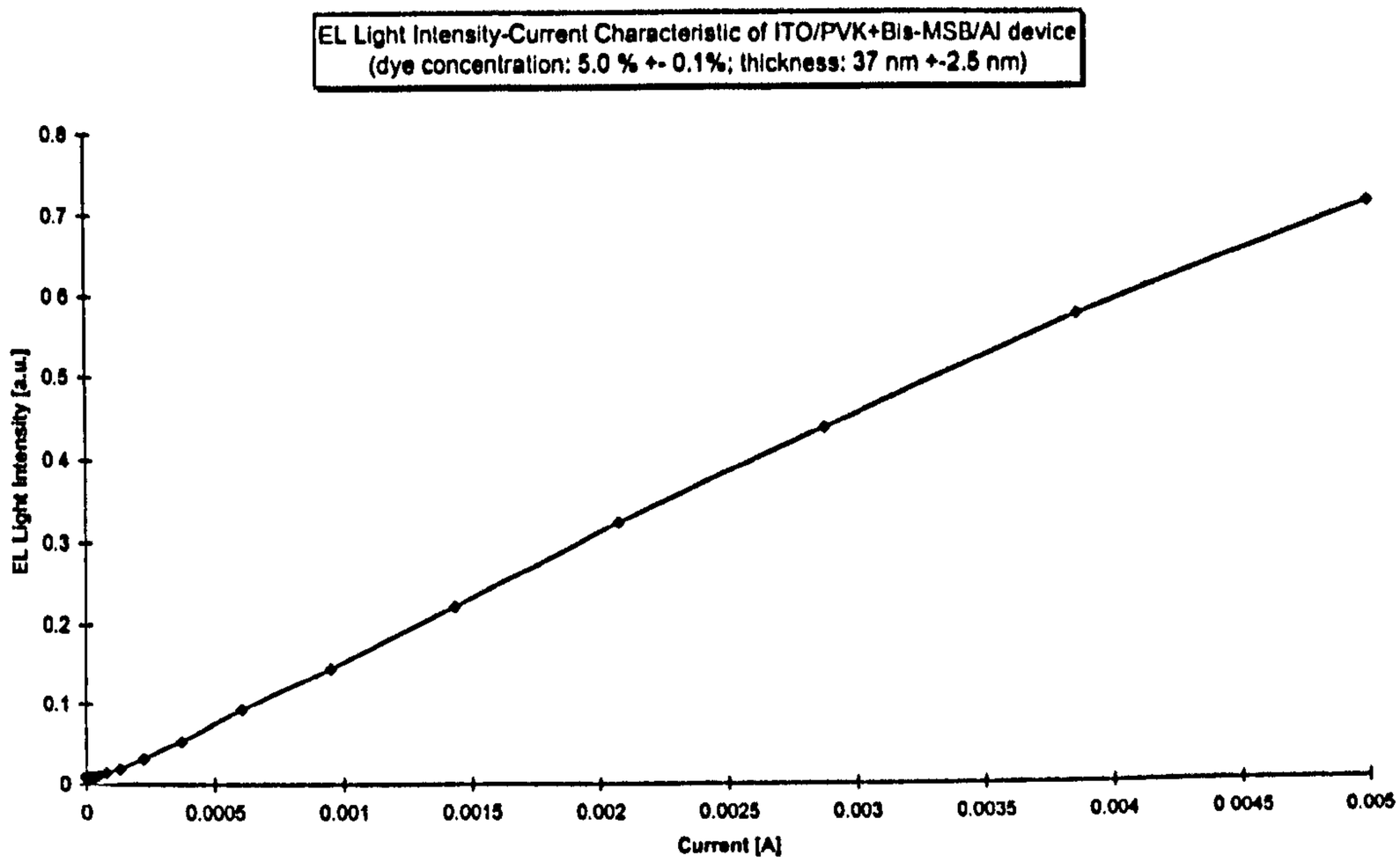

Fig. 5.37: L-I Characteristic of ITO/PVK+Bis-MSB/Al device (dye concentration: 5.0 % ± 0.1%; thickness: 37 ± 2.5 nm; area: 0.071 cm^2)

Fig. 5.34 shows the I-V characteristics of an ITO/PVK+Bis-MSB/Al device with 5.0 wt % dye concentration and 37 nm thickness. The current increases exponentially with the applied voltage with a turn-on voltage of about 25 V up to 5 mA at 30 V.

The EL light intensity, Fig. 5.35 follows the current with a high brightness of about 0.71 [a.u.] at 30 V.

Only one linear region in the J-V characteristics in log-log presentation, Fig. 5.36, can be identified. It starts at a voltage of about 23 V and has a slope of 4.7.

A linear relation between the current and the emitted EL light intensity is clearly visible in the L-I characteristics, Fig. 5.37. At 35 mA an EL light intensity of o.52 [a.u.] is measured with a gradient of 141.3 a.u./A.

5.3.2.3.Sample 3: Dye concentration: 2.8 %; emission-layer thickness: 122 nm; active area: 0.071 cm^2

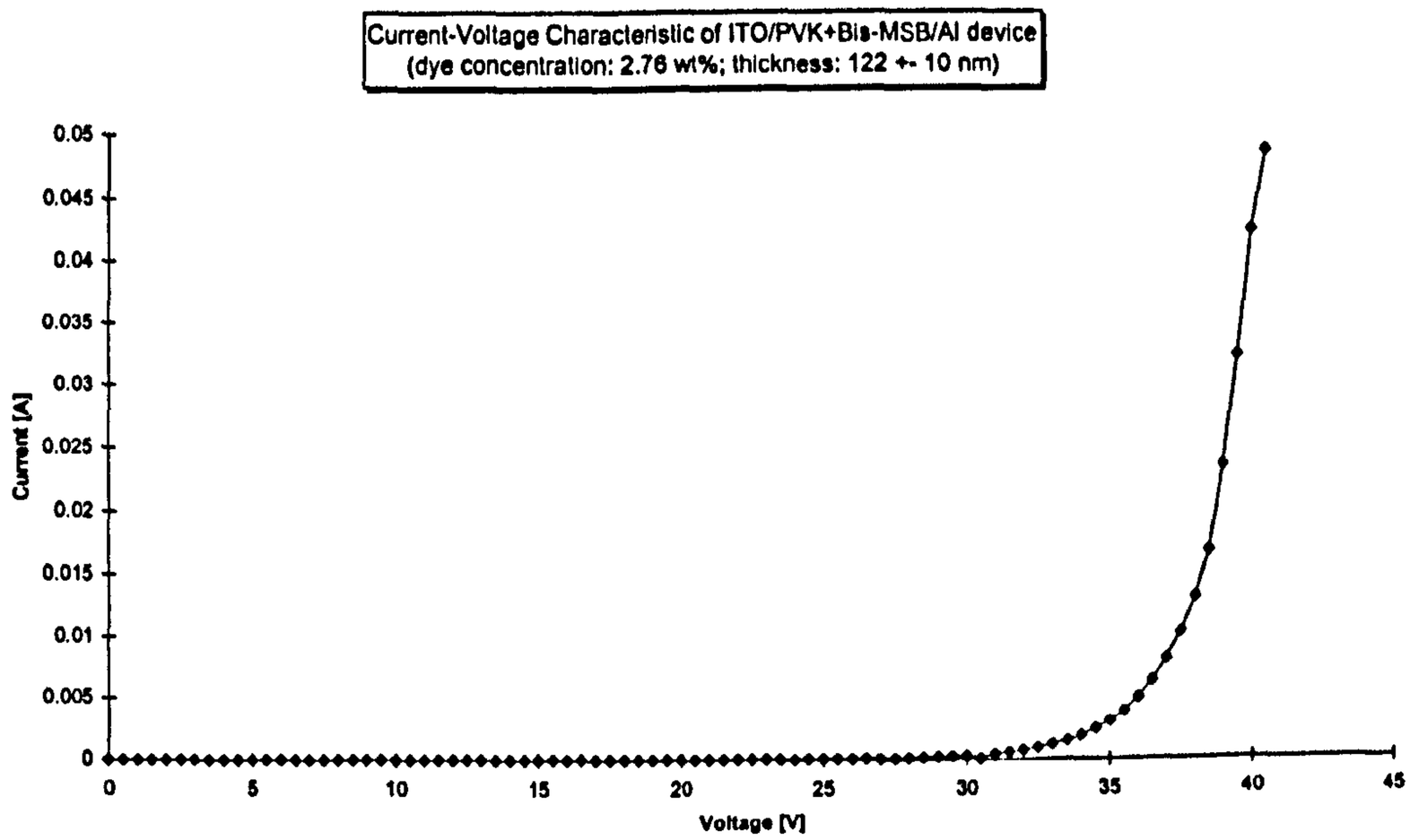

Fig. 5.38: I-V Characteristic of ITO/PVK+Bis-MSB/Al device (dye concentration: 2.76 % ± 0.1%; thickness: 122 ± 10 nm; area: 0.071 cm^2)

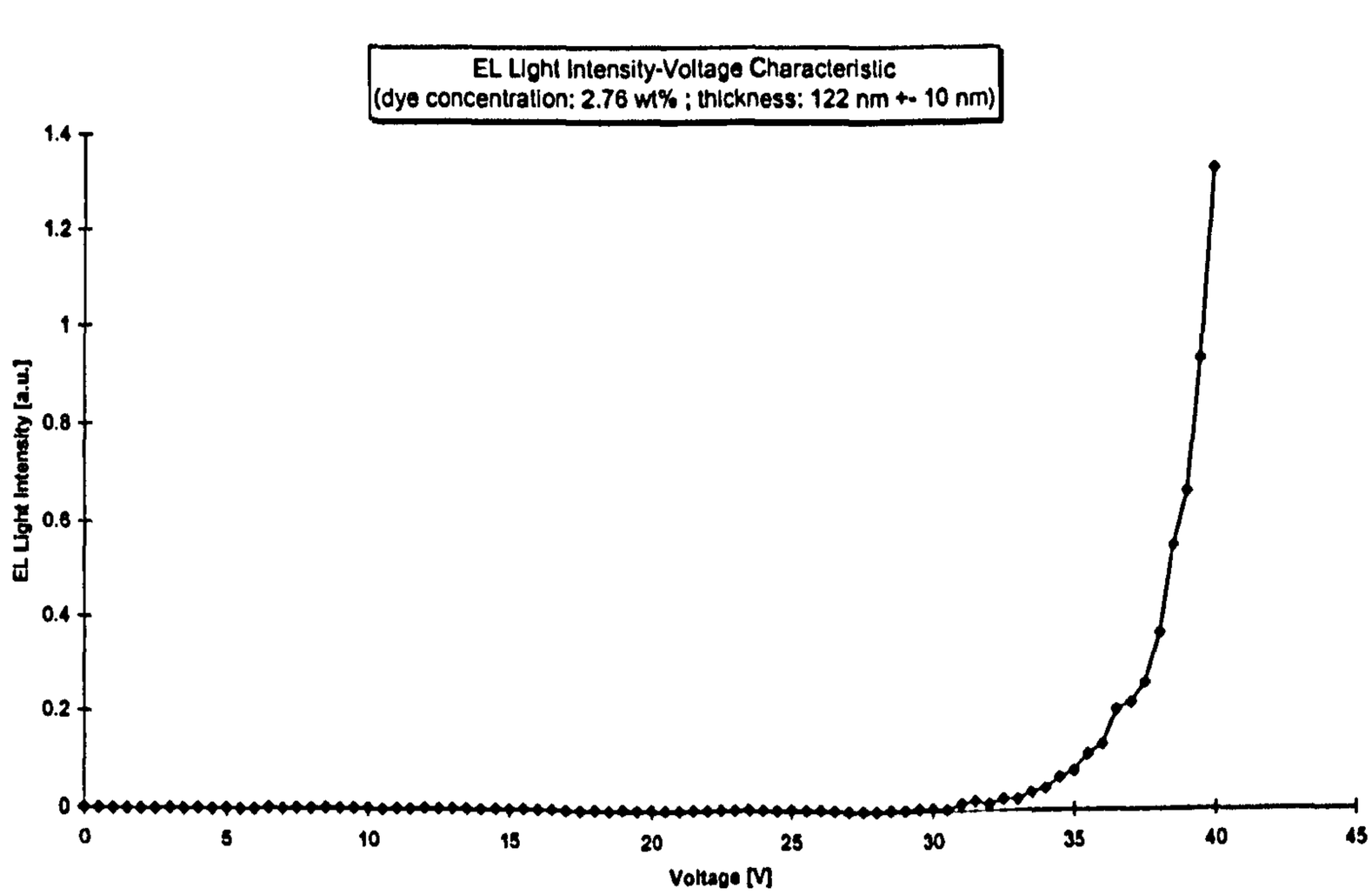

Fig. 5.39: L-V Characteristic of ITO/PVK+Bis-MSB/Al device (dye concentration: 2.76 % ± 0.1%; thickness: 122 ± 10 nm; area: 0.071 cm^2)

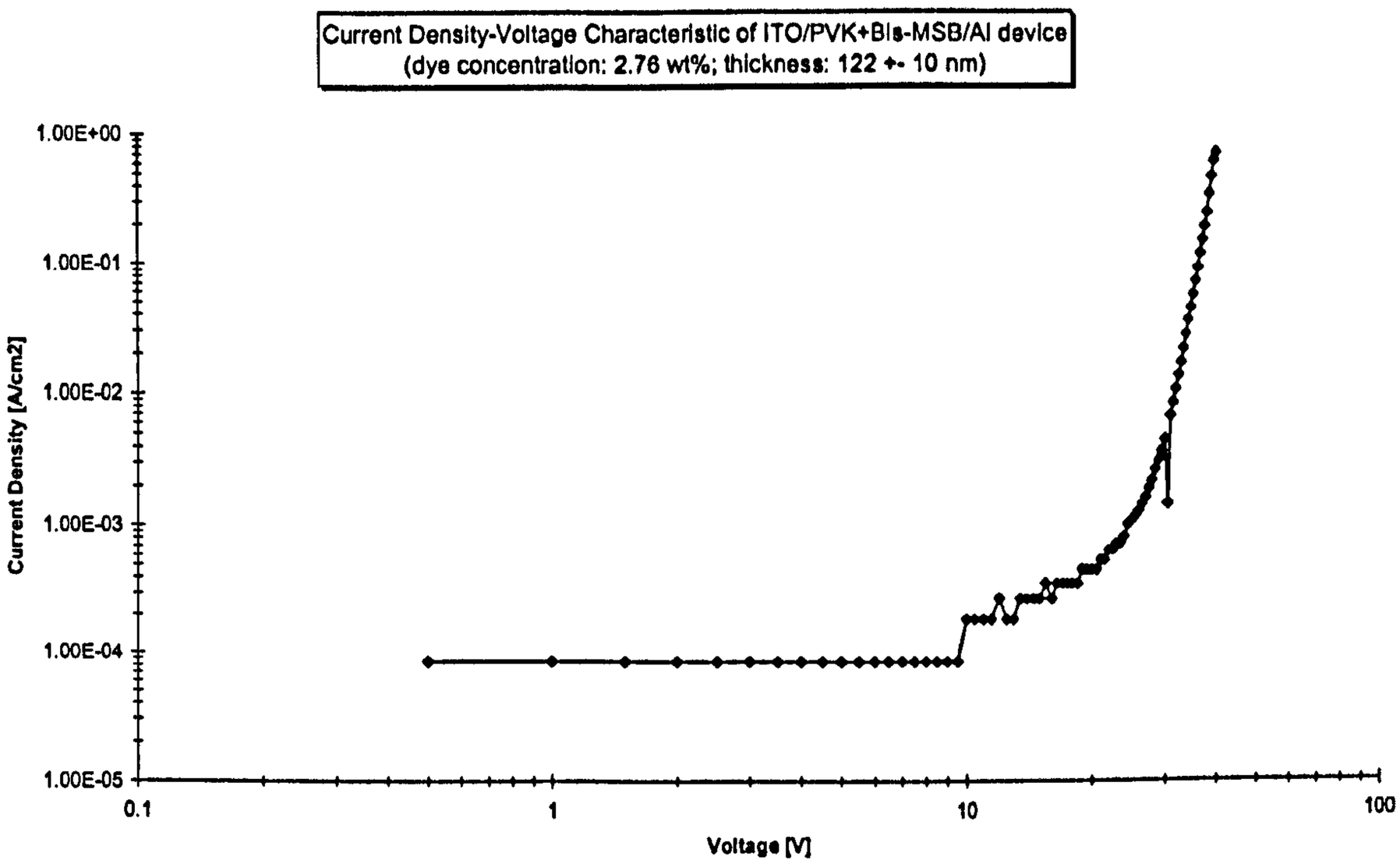

Fig. 5.40: J-V Characteristic of ITO/PVK+Bis-MSB/Al device in log-log scale (dye concentration: 2.76 % ± 0.1%; thickness: 122 ± 10 nm; area: 0.071 cm^2)

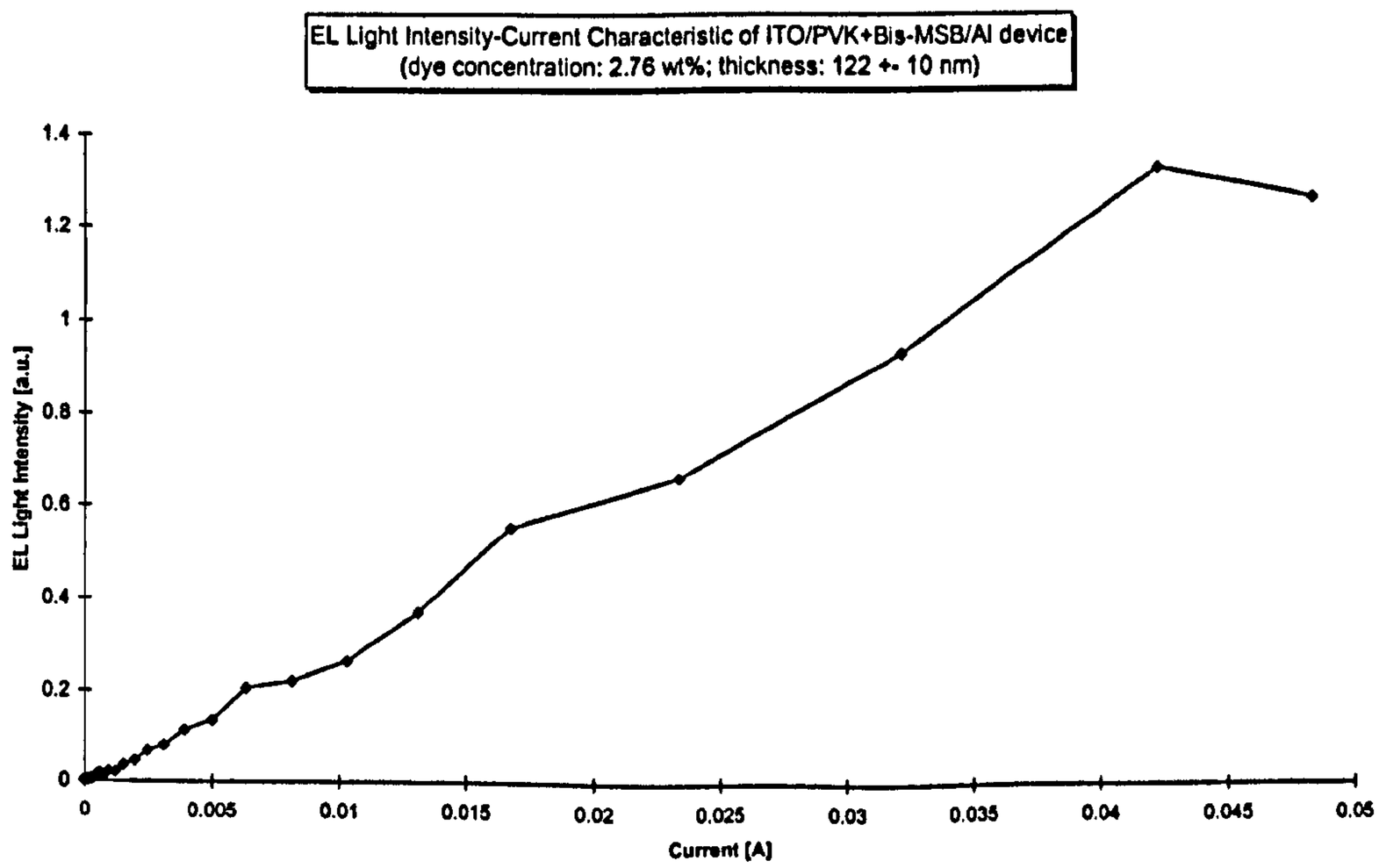

Fig. 5.41: L-I Characteristic of ITO/PVK+Bis-MSB/Al device (dye concentration: 2.76 % ± 0.1%; thickness: 122 ± 10 nm; area: 0.071 cm^2)

The I-V characteristics of an ITO/PVK+Bis-MSB/Al device with 2.76 wt % dye concentration and 122 nm thickness of the emission layer, Fig. 5.38, shows the expected diode type behaviour and a turn-on voltage of about 33 V and a value of 4.2 mA measured at the highest applied voltage of 40 V.

The emitted EL light intensity, Fig. 5.39, follows the I-V characteristics with a maximum light intensity of about 1.30 [a.u.] measured at 40 V.

A linear region in the J-V characteristics, Fig. 5.40, starting at 33 V with a slope of 5.7 can be identified. It would not be easy to justify the fit of another linear region in the voltage region between about 10 V to 18 V.

The L-I characteristics, Fig. 5.41, shows with exception of the last measurement at 48 mA a quite linear correlation between the current in the device and the emitted EL light intensity. An EL light intensity of about 1.34 [a.u.] was observed at 0.042 A.

The sample was destroyed by driving it with currents of about 52 mA. Omitting the last data point at 48 mA a gradient of 30.9 a.u./A is obtained.

5.3.2.4.Sample 4: Dye concentration: 3.6 %; emission-layer thickness: 100 nm (± 20 nm) (estimated); active area: 0.785 cm^2

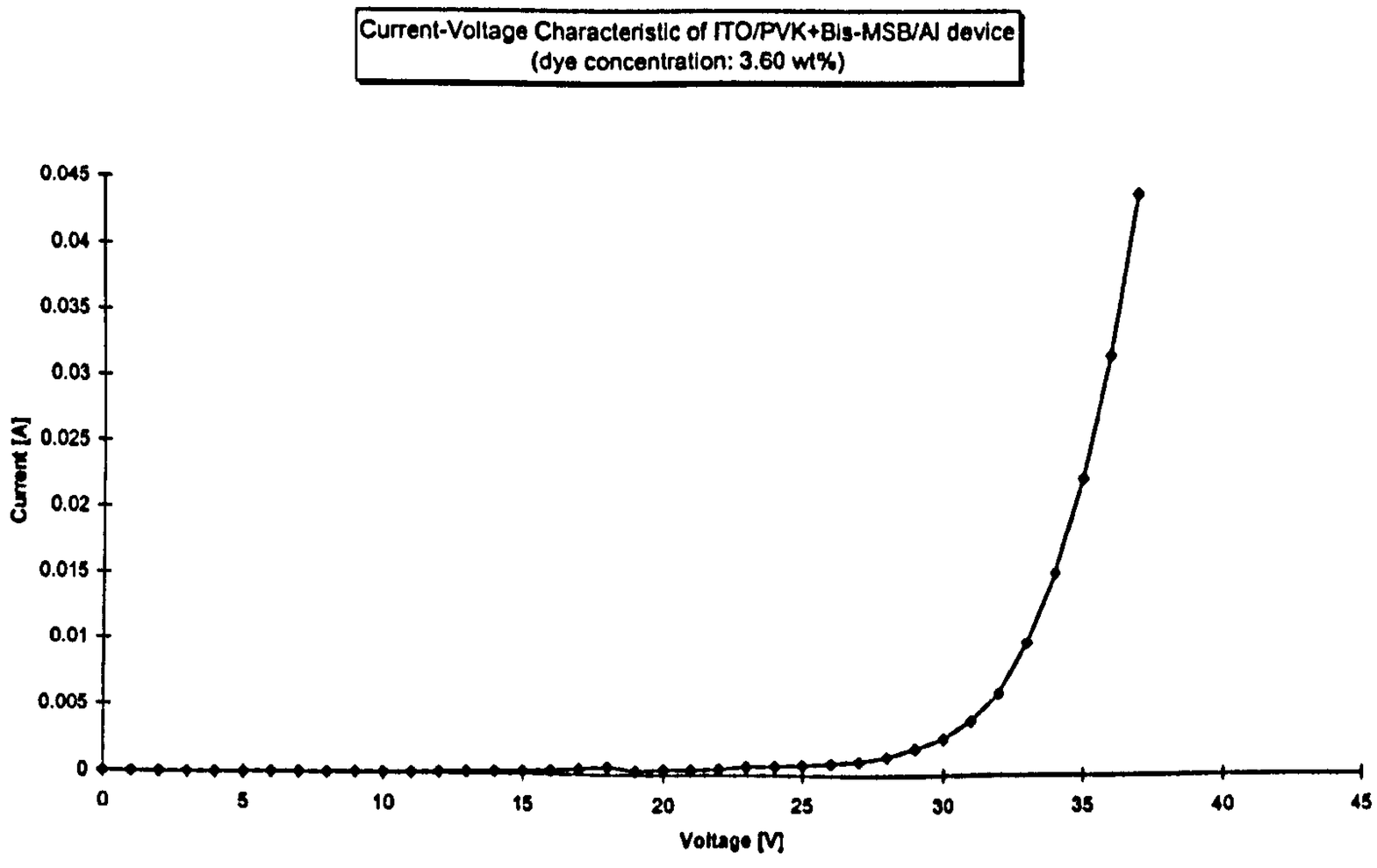

Fig. 5.42: I-V Characteristic of ITO/PVK+Bis-MSB/Al device (dye concentration: 3.60 %; area: 0.785 cm^2)

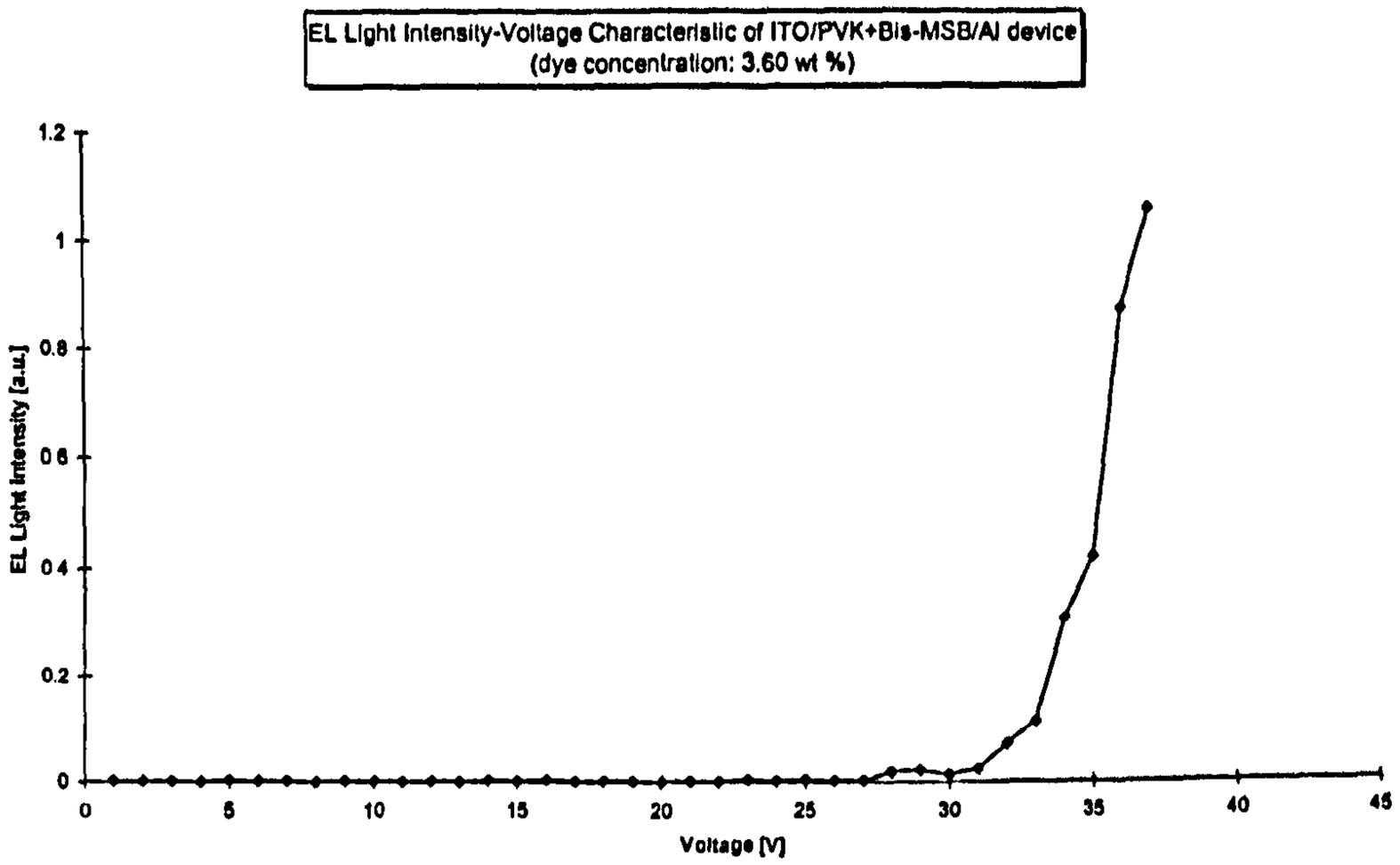

Fig. 5.43: L-V Characteristic of ITO/PVK+Bis-MSB/Al device (dye concentration: 3.60 %; 0.785 cm^2)

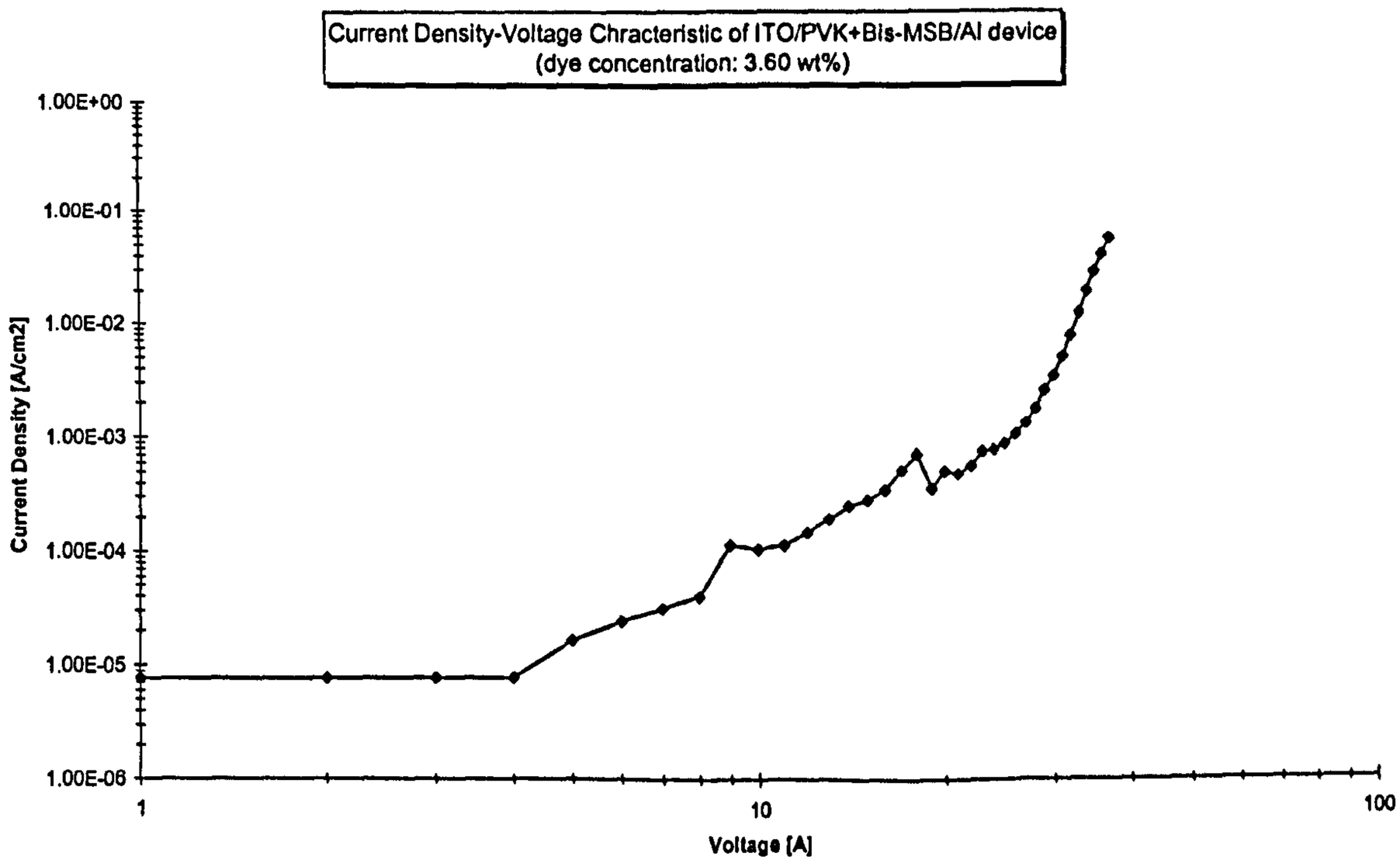

Fig. 5.44: J-V Characteristic of ITO/PVK+Bis-MSB/Al device in log-log scale (dye concentration: 3.60 %; area: 0.785 cm^2)

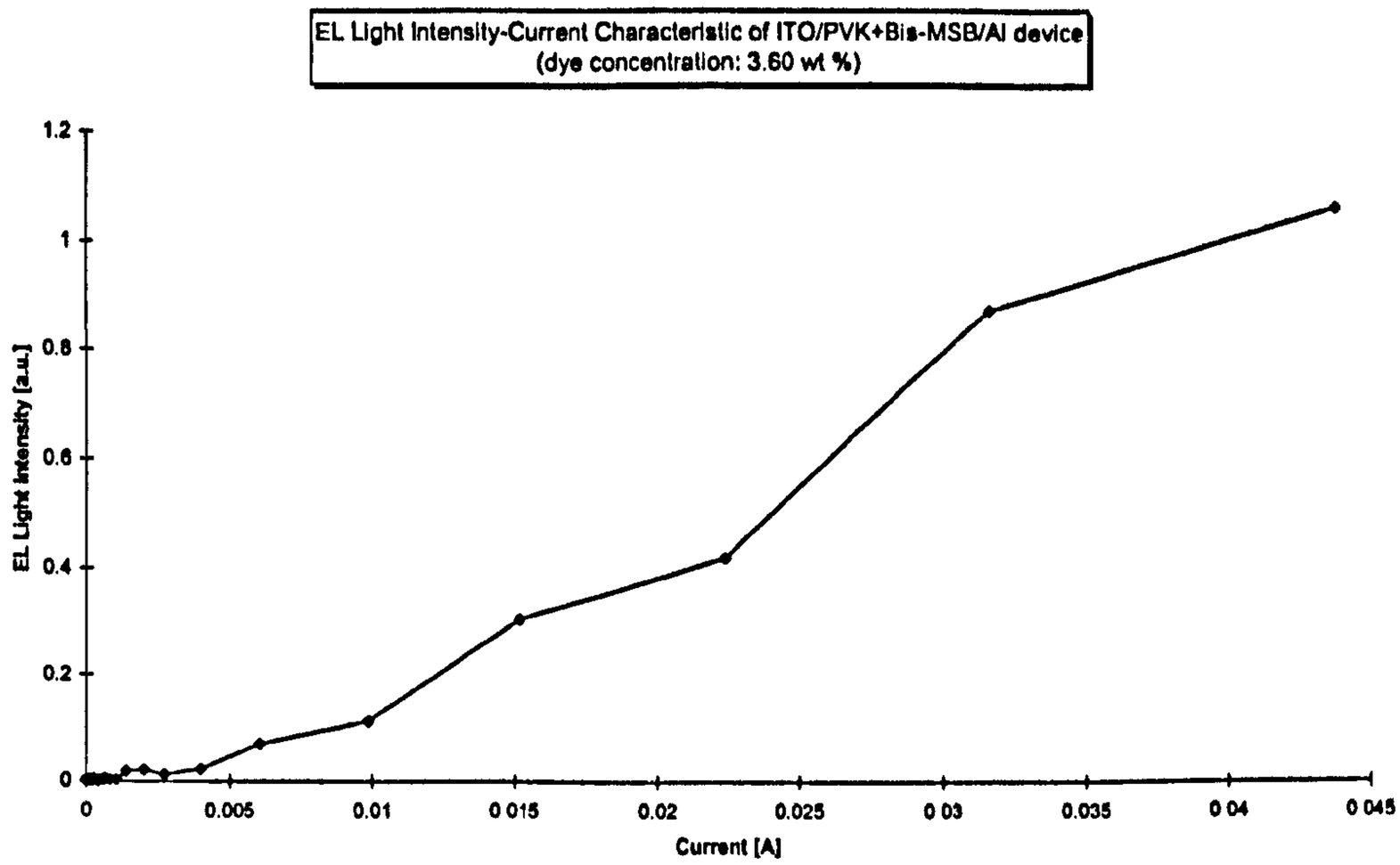

Fig. 5.45: L-I Characteristic of ITO/PVK+Bis-MSB/Al device (dye concentration: 3.60 %; 0.785 cm^2)

The thickness of the emission layer of the above characterised ITO/PVK+Bis-MSB/Al device with a dye concentration of 3.60 % was not measured explicitly, however, according to the viscosity of the PVK-monomer and Bis-MSB solution and the turn-on voltage of 28 V, Fig. 5.42, it is estimated to be in the order of about 100 ± 20 nm. The I-V characteristic in Fig. 5.42 shows the typical diode type behaviour with the above mentioned turn-on voltage of 28 V and a maximum value taken at 37 V with a corresponding current of 43.7 mA.

The L-V characteristic, Fig. 5.43, follows basically the I-V characteristic and has a maximum EL light intensity of 1.06 [a.u.] at 37 V applied voltage.

In Fig. 5.44, the presentation of the J-V characteristic in log-log scale, two linear regions could be identified: The first from about 5 V to 18 V with a gradient of 0.5 and the second form about 30 V onwards with a gradient of 2.5.

The EL Light Intensity vs. current curve in Fig. 5.45 shows some slight variations but overall there is a linear dependence of the light intensity from the current. The gradient of this graph lies in the order of 27.5 a.u./A with the highest EL value observed at 44 mA with an intensity of 1.06 [a.u.].

Discussion of Data Presented for Sample 1 (Chapter 5.3.2.1) to Sample 4 (Chapter 5.3.2.4)

The main results of the measurements described above are summarised in Table 5.2 for clarity of the discussion.

Parameter	Sample 1 (5.3.2.1)	Sample 2 (5.3.2.2)	Sample 3 (5.3.2.3)	Sample 4 (5.3.2.4)
Thickness [nm]	35	37	122	100 (estimated)
Dye concentration [wt %]	3.7	5.0	2.8	3.6
Active area [cm²]	0.071	0.071	0.071	0.785
$V_{turn-on}$ [V]	22	25	33	28
slope(s) log J-log V [-]	0.2 (*5 - 19 V*) 2.5 (*22 V+*)	- 4.7 (*23 V +*)	- 5.7 (*33 V+*)	0.5 (*5 - 18 V*) 2.5 (*30 V+*)
slope L-I [a.u./A]	23	141.3	30.9	27.7

Table 5.2: Parameters and characteristics for samples 1 to 4 under d.c. operation

1. Individual samples:

The exponential-like behaviour of all I-V characteristics indicates that tunnelling over a Schottky barrier according to equation 3.26 could be the dominating underlying process.

The J-V characteristics in log-log scale revealed gradients of 2.5 for set 1 and set 4 which indicates a SCL current according to Eq. 3.41 which would result in a gradient of 2. The higher gradients of 4.7 (set 2) and 5.7 (set 3) may be explained by the difference in the structure of the polymer PVK compared to a trap free insulator to which the theory relates. The turn-on voltages for sets 1 to 4 (22 V, 25V, 33V and 28V) almost coincide with the beginning of the linear regions in the fitted J-V data (22 V, 23 V, 33V and 30 V) which shows that at least a SCL current is needed to trigger the light emission process.

The fact that the EL light intensity in all sets is approximately proportional to the current indicates that the quantum efficiency is mainly constant over the range of currents used. The EL light intensity decreases for the last data point in set 3. This can be interpreted as a hint that the device has been driven close to it's breakdown current.

Numerical estimation of barrier height

The current density-voltage data for sample 1 has been plotted in the form of ln (J/F^2) against 1/F, where F is the electric field. This is because the quantum mechanical tunnelling for charge injection, Eq. 3.26 and Eq. 3.27 (chapter 3.6.4),

$$J = \frac{A_1^* T^2}{\phi_b}\left(\frac{qF}{\alpha kT}\right)^2 \exp\left[-\frac{2\alpha\phi_b^{3/2}}{3qF}\right], \qquad \text{Eq. 3.26}$$

with

$$\alpha = \frac{4\pi (2m^*)^{1/2}}{h} \qquad \text{Eq. 3.27}$$

allow an estimate of the barrier height, ϕ_b.

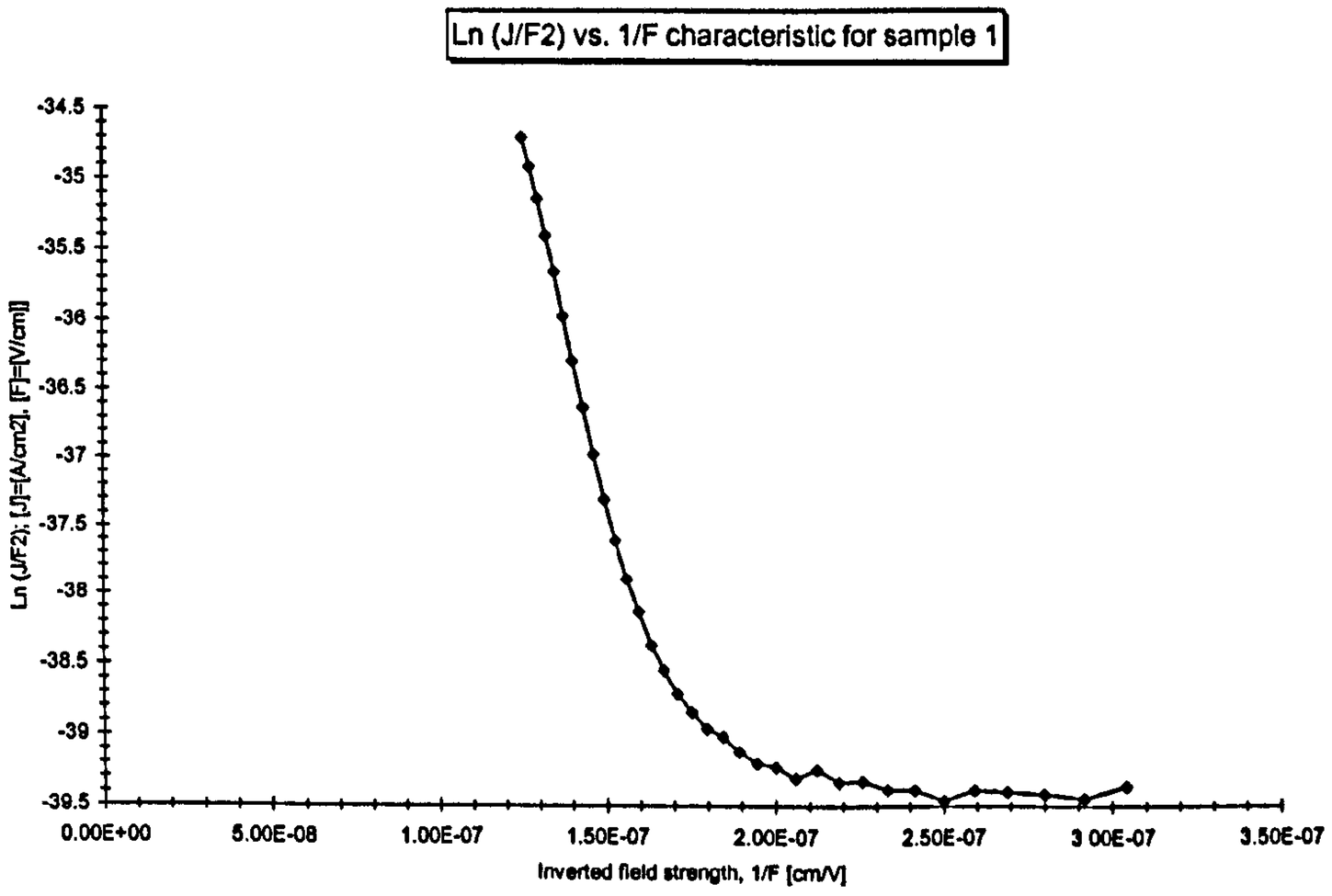

Fig. 5.46: Ln (J/F^2) vs. 1/F characteristic for sample 1

For low values of 1/F, i.e. voltages where the device is in operation, a slope, *s*, with a gradient of -1.31×10^8 Vm^{-1} was obtained, Fig. 5.46. Following from Eq. 3.26 and Eq. 3.27

$$s = -\frac{8\pi\sqrt{2}}{3}\frac{\sqrt{m^*}\phi_b^{3/2}}{qh}. \qquad \text{Eq. 5.2}$$

Using the electron rest mass, m_0, instead of the effective electron mass m* for a first order estimate gives a barrier height ϕ_b=0.072 eV. Considering that the effective electron mass in PVK is smaller than the free electron mass a somewhat higher value for the barrier height would result.

2. Relative comparison of samples 1 to 4:

Only the most significant results of the comparison between set 1 and set 2 is considered here: An additional doping of the pure PVK with the Bis-MSB dye of 1.3 wt% results in an 6.5 times higher EL light intensity (values are compared for both sets at 35 mA) and a

more than 6 times higher gradient of the EL light intensity per current flow on the cost of a higher turn-on voltage of only 3 V. In other words, the current injection is slightly affected by the higher dye concentration but at the same time significantly more excitons can be generated.

The observed higher turn-on voltage for light generation for higher film thicknesses, for instance set 1 (thickness: 35 nm and $V_{turn-on}$: 22 V) compared with set 3 (thickness: 122 nm and $V_{turn-on}$: 33 V), is due to the electrical field required for carrier injection which is a function of the film thickness. The electrical field for which sufficient injection takes place lies in the order of 10^8 V/m (set 1: 6.3 10^8 V/m; set 2: 2.7 10^8 V/m) for the investigated device.

The relatively high deviations from ideal linearity of the data in set 4 and also the higher scattering of the values of the J-V characteristic in set 3 compared to the other sets indicates that by increasing the active area or thickness, respectively, inhomogenities of surfaces in the device became apparent.

Further ideas for the data interpretation are outlined in chapter 7, Suggestions for Future Work.

5.3.3. Operational Lifetime

A fixed voltage of 2 V above the turn on voltage, see chapter 5.3.2, was applied to the device (sample 1) in air under room temperature and the EL light intensity measured for over three hours using a photodiode with an accuracy of more than 0.01 a.u.. The result is shown in Fig. 5.47.

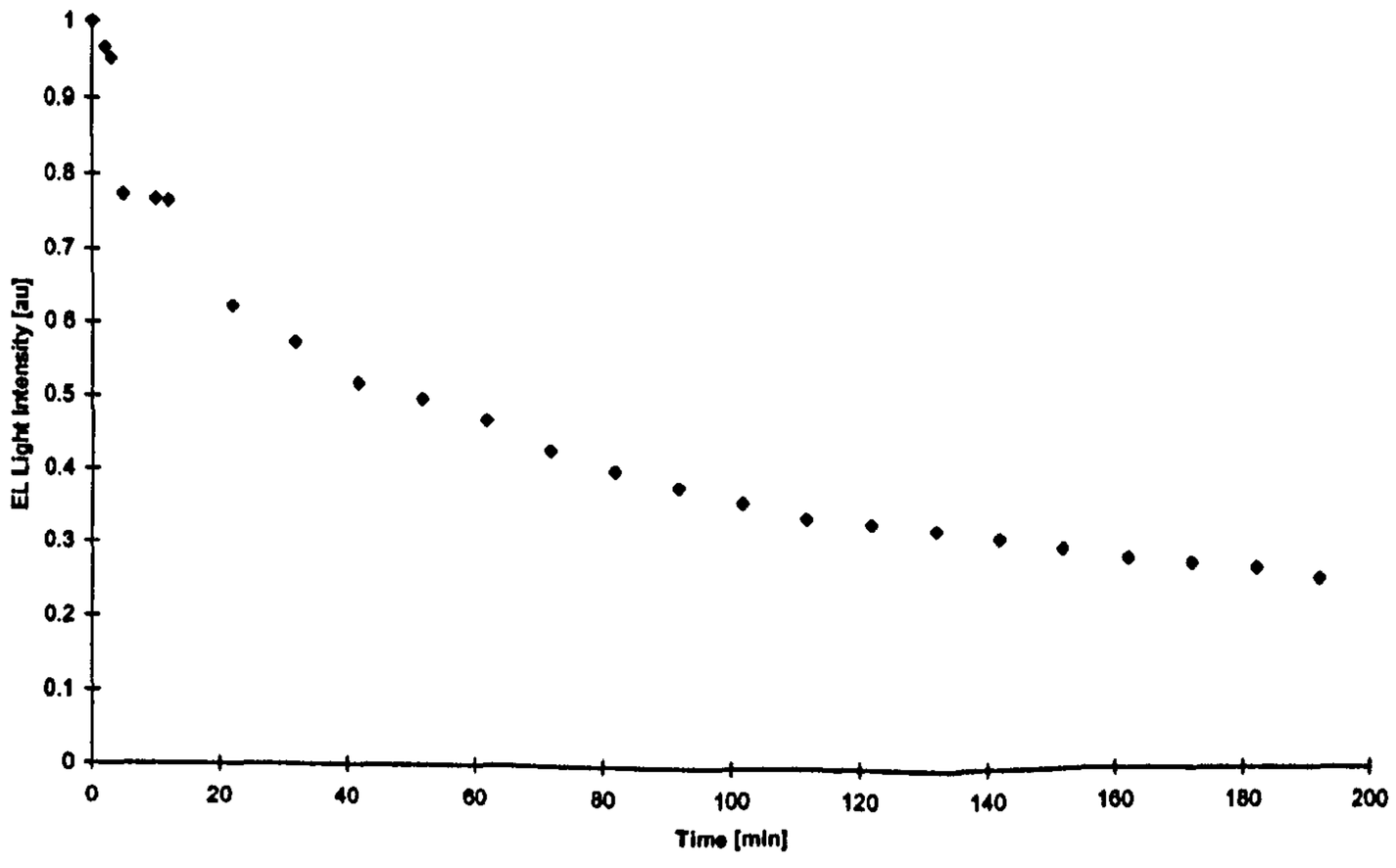

Fig. 5.47: D.C. operational life time of a typical device

The EL light intensity decreases rapidly to about one third of its original value after only three hours in a way which is reminiscent of an exponential decay.

The EL intensity drop of the device is probably caused by a superposition of several effects such as oxidation of the cathode and the polymer-dye film and thermal degradation of the dye and the polymer.

5.4. Unipolar Pulsed Electroluminescence Characterisation

In this sub-chapter the fabricated ITO/PVK+Bis-MSB/Al devices with an active sample area of 0.071 cm^2 were investigated using rectangular positive driving pulses with 50% time on and 50% time off (50% duty cycle)[37]. The findings, EL light intensity under the applied pulsed driving voltage (chapter 5.4.1) and the EL light intensity as a function of the pulse frequency (chapter 5.4.2) are presented and discussed including a.c. conductivity measurements of Bis-MSB doped PVK films (chapter 5.4.2.5).

[37] No EL was observed under reverse DC bias.

5.4.1. EL Response Time under Fixed Unipolar Pulsed Operation

5.4.1.1.Instrumentation and Experimental Set-Up

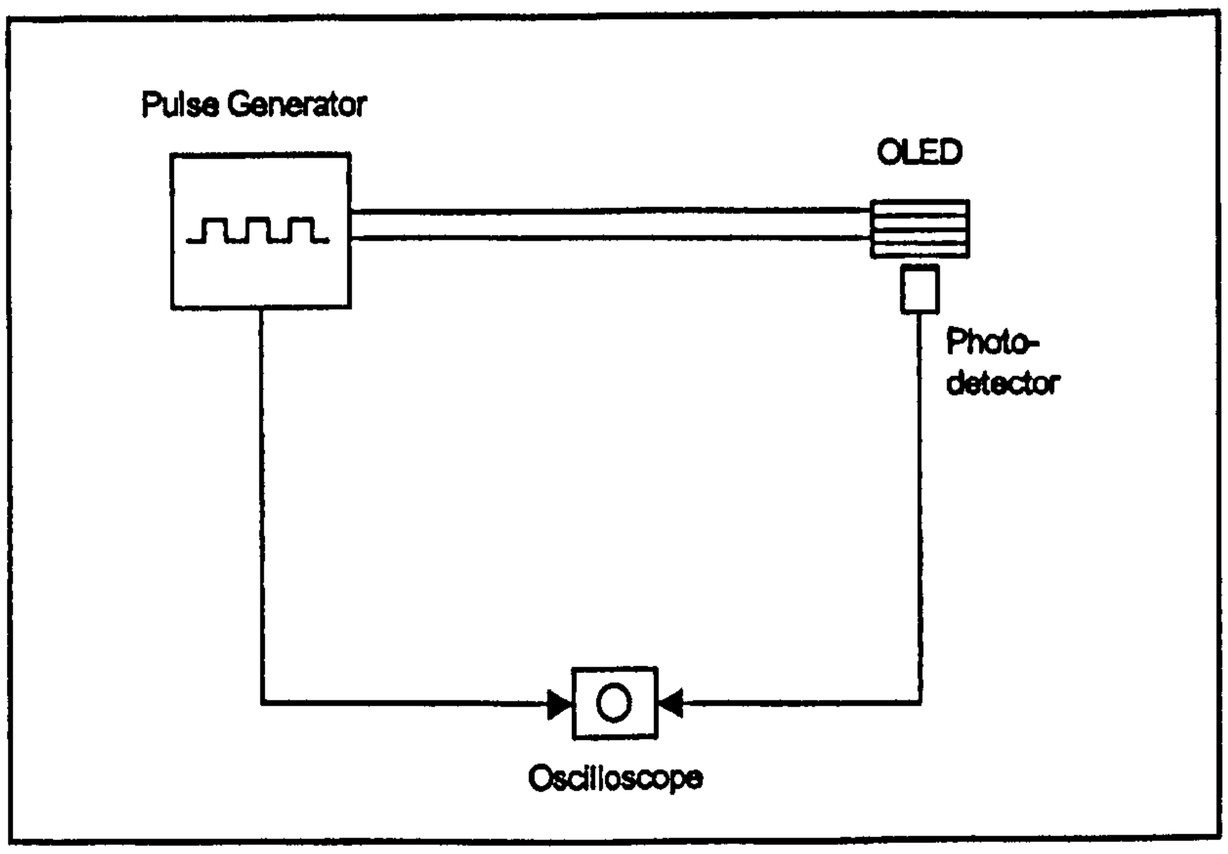

Fig. 5.48: Schematically experimental set-up to measure EL light intensity as a function of the applied unipolar pulsed driving frequency

The block diagram for measuring EL light intensity as a function of the driving pulse frequency is shown in Fig. 5.48. A Thurlby-Thandar Tg 1304 programmable function generator was used to provide rectangular voltage pulses in the positive segment only in the frequency range from 1 kHz to 500 kHz. The pulses were applied in such a way that the positive polarity was connected to the ITO side of the device (the same as for driving the device under d.c. forward bias). The light, emitted from the device, has been measured by using a RS 194-076 IZ1 silicon photodiode with a fast response time (τ = 12 ns ± 0.5 ns). Both the voltage across the device and the photovoltage across the photodiode (proportional to the EL light intensity) were displayed and measured using a Hewlett Packard storage oscilloscope.

5.4.1.2.Experimental Results

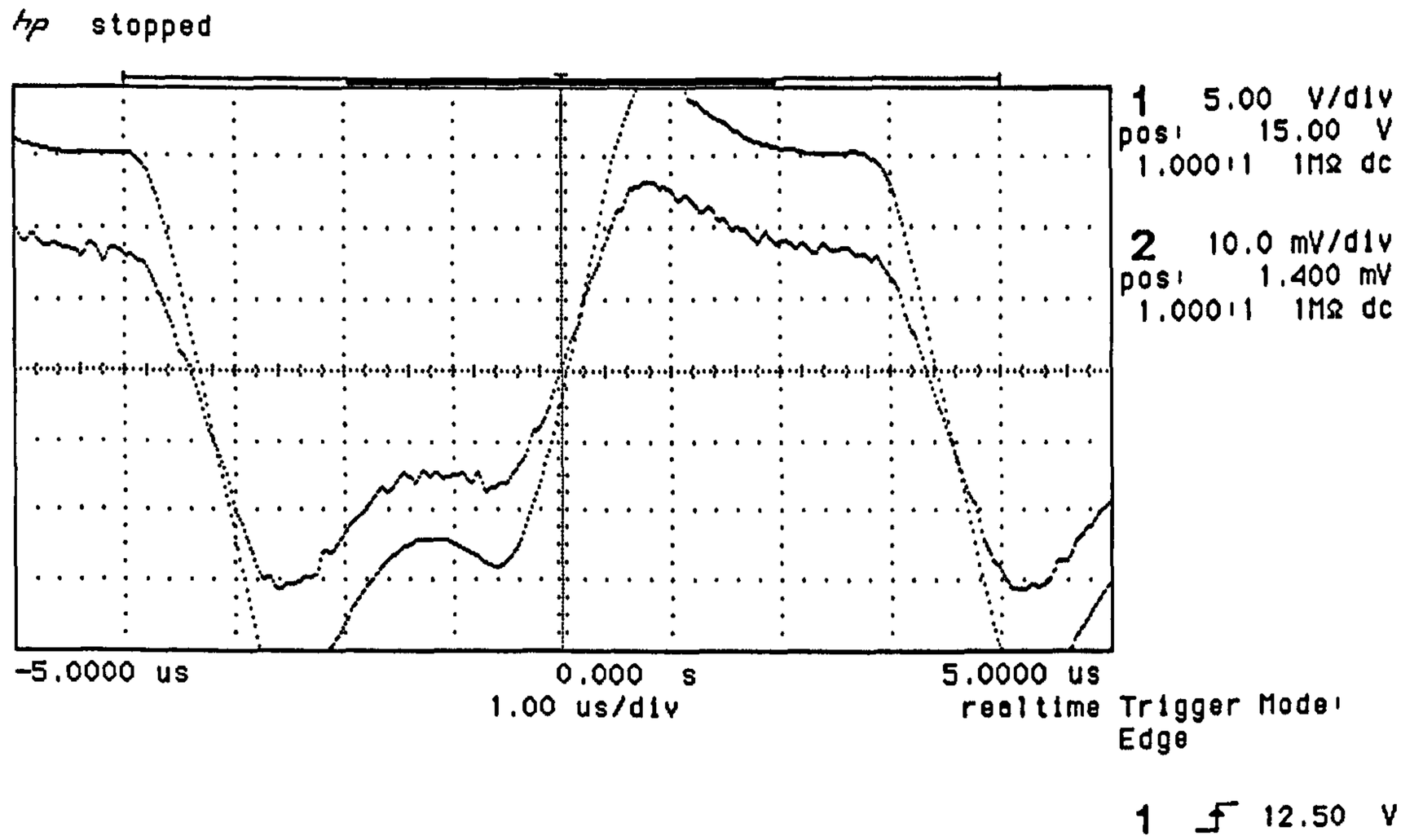

Fig. 5.49: Rectangular positive driving pulse (upper graph, channel 1) and EL light intensity (lower graph, channel 2) as a function of time. (0V around lowest horizontal dotted line.)

Fig. 5.49 shows a quasi-rectangular pulsed voltage across the device (upper curve, channel no. 1) and the voltage (lower curve, channel no. 2) at the photodetector which is proportional to the EL light intensity. The longer rise and fall time of curve 2 compared to curve 1 is due to the delay in response when the generated electroluminescent light follows the applied field. An EL response time[38] of about 0.75 μs can be taken from the data.

As the response time of the photodiode (τ = 12 ns) is much smaller than the measured response of 0.75 μs this is a real characteristic of the device.

5.4.2. EL Light Intensity vs. Pulse Frequency

Three samples (No. 5 - 7) were characterised. The data obtained for sample 7 includes also an analysis of the data in log-log scale. All data is discussed after the presentation of the measurements.

5.4.2.1.Instrumentation and Experimental Set-Up

The same experimental set-up as for the above analysis was used just measuring a mean EL light intensity at the photodiode.

[38] The response time is defined as the time passed for instance during sudden rise from 10% to 90% of a new maximum value.

5.4.2.2.Sample 5

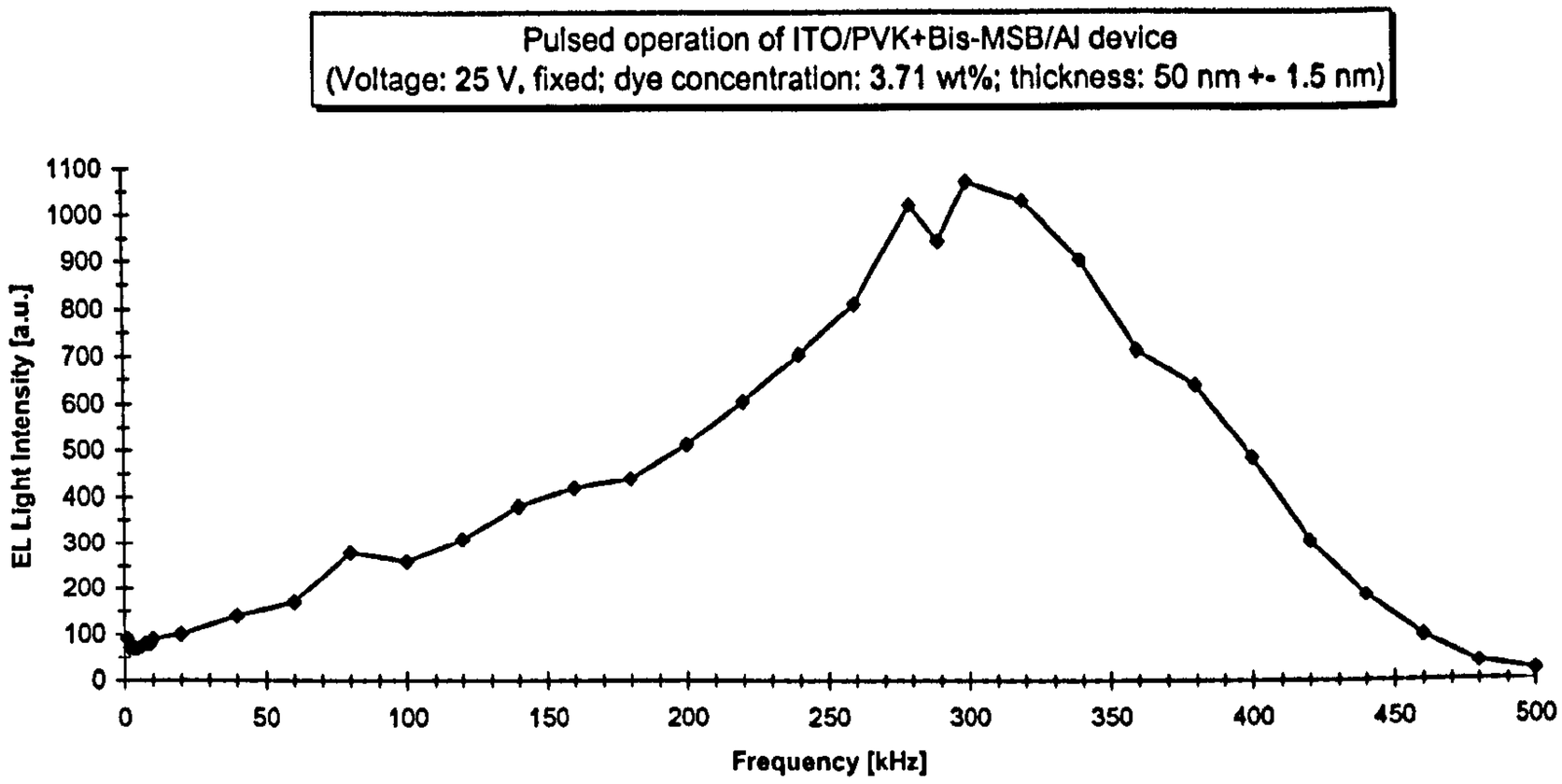

Fig. 5.50: EL vs. pulse frequency of ITO/PVK+Bis-MSB/Al device (Voltage: 25 V, fixed; dye concentration: 3.71 wt %; thickness: 50 ± 1.5 nm)

The EL light intensity vs. frequency plot of an ITO/PVK+Bis-MSB/Al device with 3.71 wt % dye concentration and a thickness of the emission layer of 50 ± 1.5 nm measured at a fixed voltage of 25 V is given in

Fig. 5.50. It is not symmetrical and shows starting at 1 kHz (light intensity: 90 in a.u.), with the exception of two obviously irregular points a steady but non-linear increase and reaches a maximum at a frequency of about 300 kHz with a corresponding light intensity of 1070 [a.u.]. At higher frequencies the light intensity drops off quite steeply and also in a non-linear way to values close to zero for frequencies of over 500 kHz.

5.4.2.3.Sample 6

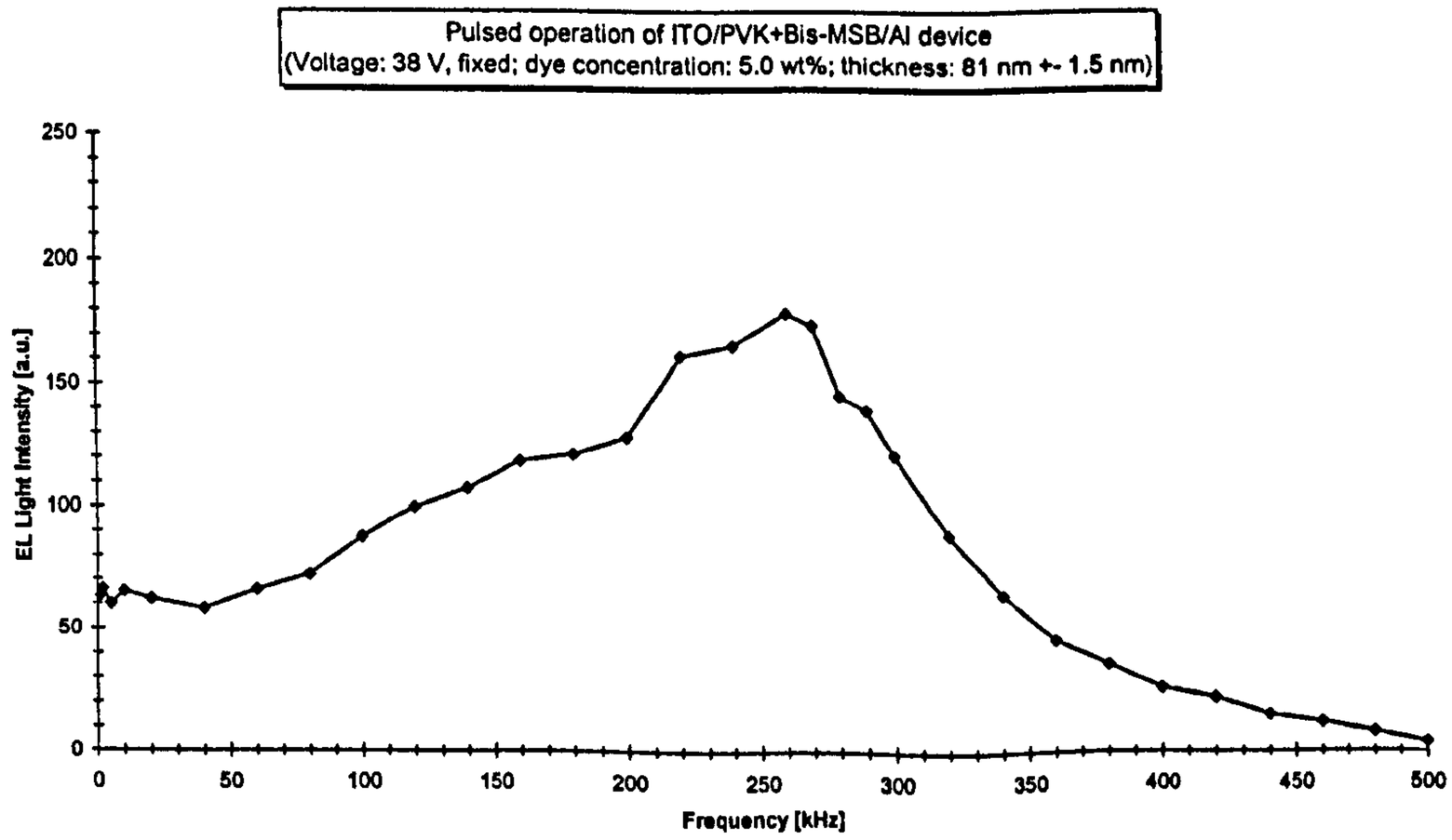

Fig. 5.51: EL vs. pulse frequency of ITO/PVK+Bis-MSB/Al device (Voltage: 38 V, fixed; dye concentration: 5.00 wt %; thickness: 81 ± 1.5 nm)

Fig. 5.51 shows the EL light intensity under A.C. operation of an investigated device of above mentioned structure, dye concentration: 5.00 wt %; thickness: 81 ± 1.5 nm, with a fixed applied voltage of 38 V. The graph has the same shape as the previous one (Fig. 5.50), however, with an EL light intensity of 63 in a.u. at 1 kHz and its maximum at a frequency of 260 kHz associated with an EL light intensity of 179 [a.u.].

5.4.2.4.Sample 7

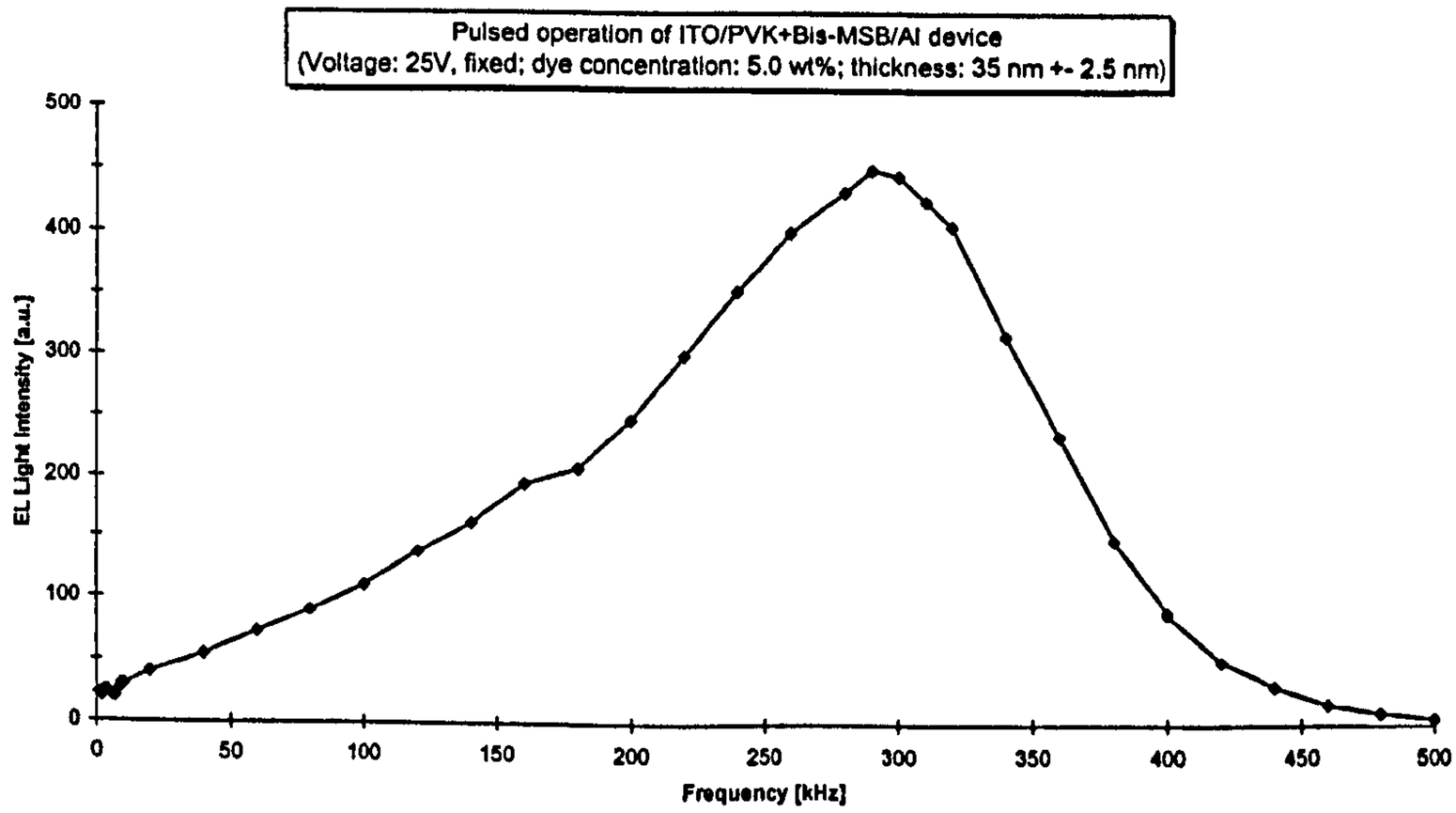

Fig. 5.52: EL vs. pulse frequency of ITO/PVK+Bis-MSB/Al device (Voltage: 25 V, fixed; dye concentration: 5.00 wt %; thickness: 35 ± 2.5 nm)

Fig. 5.52 (device with a dye concentration of 5.00 wt % and a thickness of the emissive layer of 35 nm ± 2.5 nm at a fixed applied voltage of 25 V) shows again the same underlying characteristics as observed in Fig. 5.51 and Fig. 5.52. In this case the light intensity scales between values of 23 [a.u.] at 1 kHz and 450 [a.u.] at its maximum at 290 kHz and decreases rapidly from about 320 kHz onwards.

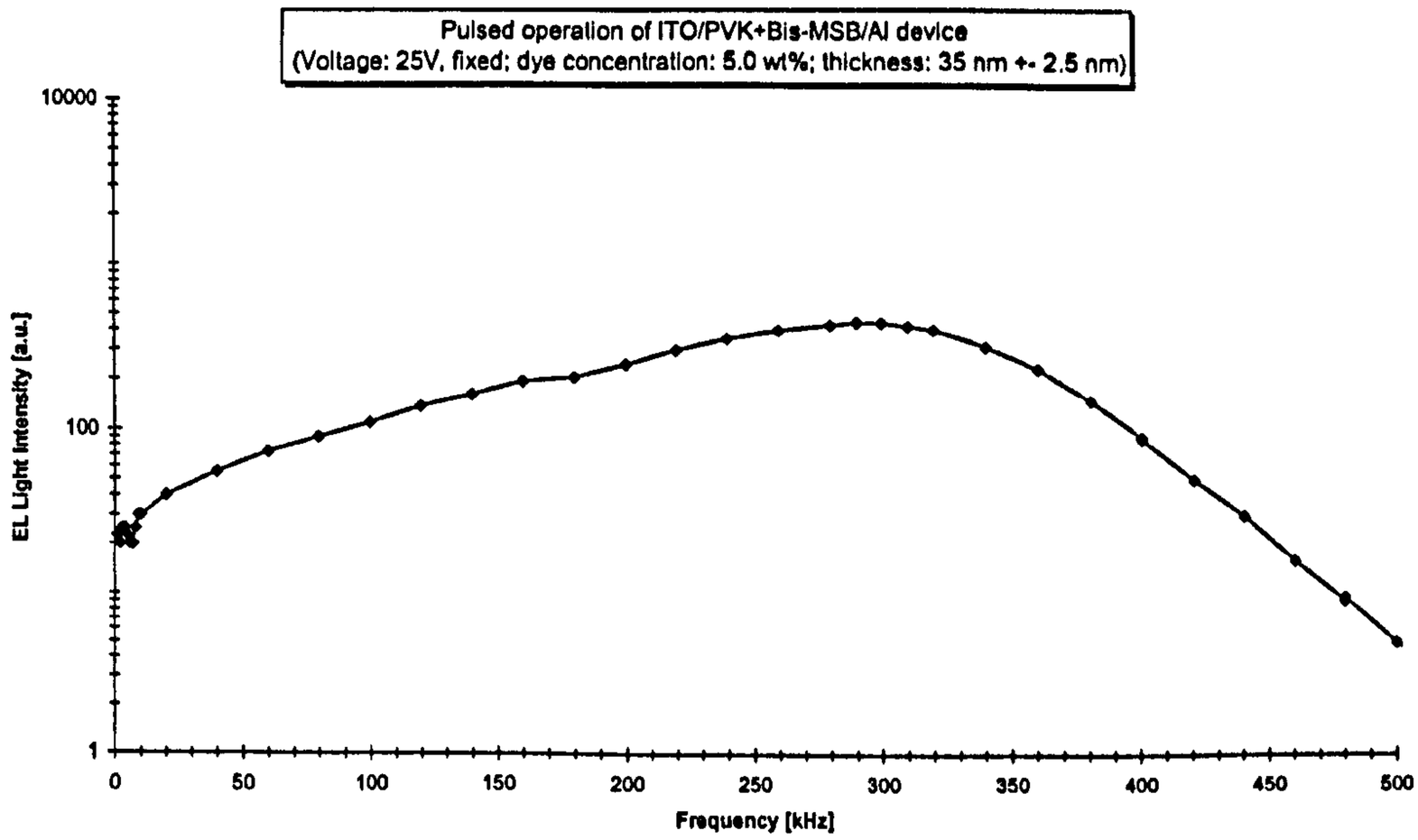

Fig. 5.53: EL vs. pulse frequency of ITO/PVK+Bis-MSB/Al device in log-lin scale (Voltage: 25 V, fixed; dye concentration: 5.00 wt %; thickness: 35 ± 2.5 nm)

Fig. 5.53 is the logarithmic-linear presentation of the same measurement of the device characterised in Fig. 5.52. For very low frequencies, below 10 kHz, the values obtained for the EL light intensity show considerable variation. In the region from about 10 kHz to 50 kHz there is a gradually decreasing gradient. Above this frequency two linear regions can clearly be identified: The first one from about 50 kHz to 250 kHz with a modest positive gradient of 1.5 [a.u./kHz], the second one from about 380 kHz to 420 kHz (500 kHz as the highest frequency measured) with a negative gradient of 4 [a.u./kHz]. There is a gradual transition between the two linear regions.

5.4.2.5.A.C. conductivity of PVK film doped with Bis-MSB

The a.c. conductivity of a PVK film doped with 5 wt% Bis-MSB has been measured using a Schlumberger a.c. parameter analyser.

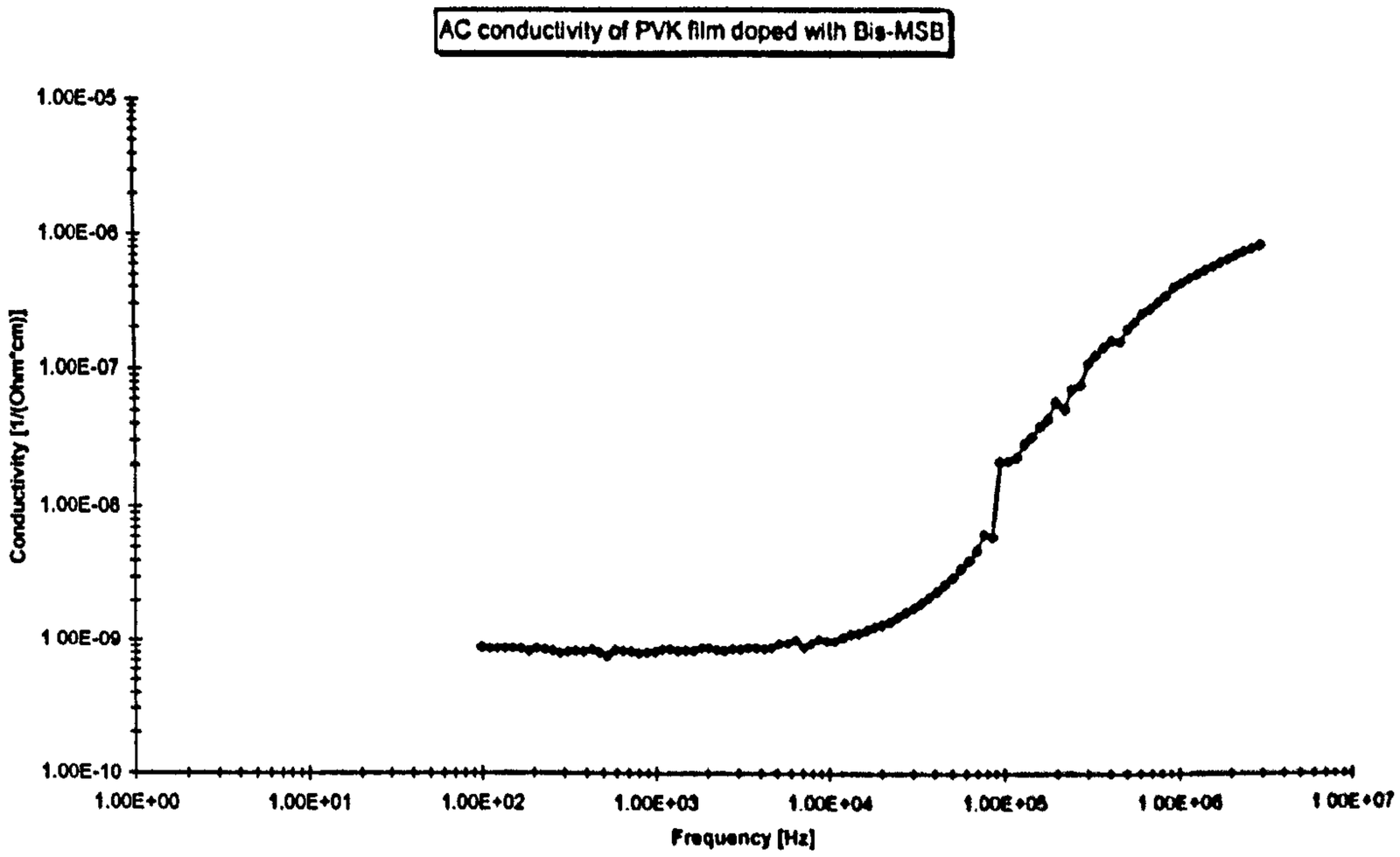

Fig. 5.54: A.C. conductivity of PVK doped with Bis-MSB

Fig. 5.54 shows that the conductivity does increase substantially in the frequency region from around 10 kHz (10^{-9} Ω^{-1} cm^{-1}) to 1000 kHz (4×10^{-7} Ω^{-1} cm^{-1}).

Discussion of A.C. conductivity of PVK film doped with Bis-MSB

There are two possible reasons for the observed increase of conductivity:

1) The a.c. conductivity of the polymer increases with increasing frequency, see chapter 3.7.3.
2) From the pure device point of view the capacitive reactance, X_c, ($X_c = 1/2\pi fC$ with frequency f and capacitance C) decreases as the applied frequency[39] increases.

Both processes cause a rise in the current (at a fixed voltage) when the applied frequency increases.

Discussion of Data Measured from Sample 5 (Chapter 5.4.2.2) to Sample 7 (Chapter 5.4.2.4)

To clarify the discussion, the main results are summarised in Table 5.3 and the measured EL intensity vs. pulse frequency for samples 5 to 7 are displayed in a single graph normalised to the individual intensity maxima (Fig. 5.55).

[39] The above theory refers to a sinusoidal applied voltage. The voltage used, however, has a square wave form for which Fourier analysis contains also overtones of the fundamental frequency. Increasing the fundamental frequency would still result in a lower capacitive resistance.

Parameter	Sample 5 (5.4.2.2)	Sample 6 (5.4.2.3)	Sample 7 (5.4.2.4)
Thickness [nm]	50	81	35
Dye concentration [wt %]	3.7	5.0	5.0
Active area [cm^2]	0.071	0.071	0.071
Max. pulse height [V]	25	38	25
Max. appl. field [V/cm]	5.0×10^8	4.7×10^8	7.1×10^8
Intensity maximum ([kHz];[a.u.])	300; 1070	260; 179	290; 450

Table 5.3: Parameters and characteristics for samples 5 to 7 under unipolar pulsed operation

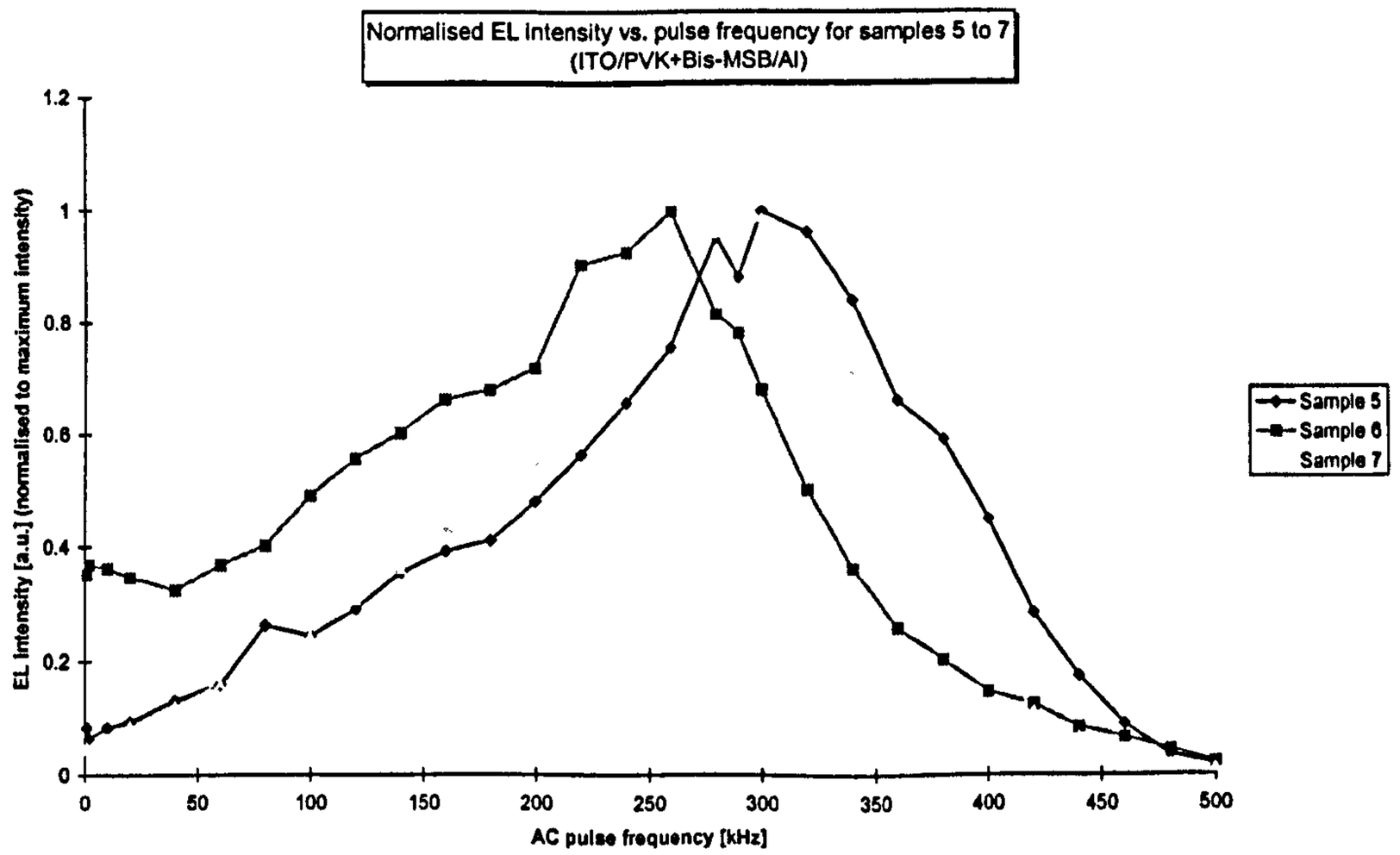

Fig. 5.55: Normalised EL vs. pulse frequency measurements of samples 5 to 7

General trend

All three devices show the same trend: The EL intensity in general rises from a positive value at 1 kHz in a non-linear way as the pulse frequency increases and saturates with a broad maximum in the range of 260 kHz to 310 kHz followed by a decrease to a value near to zero. The intensity peak is clearly asymmetric as also the rise at lower frequencies is less steep than the decrease of the intensity from higher frequencies.

In order to explain the general characteristics it is assumed that the light due to EL originates from radiative recombination of electrons and holes as in the case of d.c. operation, see chapter 3.2.

The observed EL intensity increase is *not* due to the effect of a different power fill factor as it is constant over the whole frequency range investigated.

A possible reason for the increase of the EL light intensity at the measured frequencies (up to about 260 kHz to 300 kHz) is because the conductivity of the Bis-MSB doped PVK film increases with the frequency (see chapter 5.4.2.5) this giving possible greater current flow and hence measured light output.

Without an additional effect the current and consequently the EL intensity would increase in a monotonic but not necessarily linear way with the pulse frequency. However, at higher frequencies another effect becomes dominant to reduce the EL intensity. At high frequencies the probability for electrons and holes to meet is significantly reduced within the time when the positive field is applied across the structure. Consequently the electrons and holes will recombine mostly in a non-radiative way.

Numerical validation

Based on the experimental data on the pulse frequency dependence of EL-light intensity, it is possible to obtain some quantitative data on the mobility of charge carriers. For a typical polymer layer thickness of about 100 nm (1 x 10^{-5} cm), the onset of EL light generation is at about 25 V (see Table 5.2). This corresponds to an electric field of $E \cong 2.5 \times 10^{6}$ V cm^{-1}, i.e. EL light is generated at a very large electric field across the polymer layer. The EL light intensity at a fixed maximum pulse voltage has its maximum at a frequency of around $f \cong 300$ kHz. Assuming that the injected electron-hole pairs have to travel to the centre of the sample to meet (i.e. the longest distance is 50 nm or 5 x 10^{-6} cm) and comparing this distance with a transit time of $1/f = 1/300$ kHz = 3.33 x 10^{-6} sec, it is possible to obtain an average drift velocity v = 1.5 cm sec^{-1} for the charge carriers. This gives a charge carrier mobility value of $\mu = v/E = (1.5 \text{ cm sec}^{-1}) / (2.5 \times 10^{6} \text{ V cm}^{-1}) = 6 \times 10^{-7} \text{ cm}^2 \text{ V}^{-1} \text{ sec}^{-1}$. This mobility value is in accord with that for a typical charge carrier mobility in PVK polymers, see chapter 4.2.1.

Relative comparison of samples 5 to 7

The sample with the greatest thickness of the light-emitting layer, sample 6, shows compared to samples 5 and 7 in the normalised presentation a significantly higher EL intensity at 1 kHz (normalised initial EL intensity: 0.38 a.u.) than sample 5 (normalised

initial EL intensity: 0.08 a.u.) and sample 7 (normalised initial EL intensity: 0.04 a.u.). Furthermore, the maximum frequency for sample 6 of about 260 kHz is noticeably below the maxima of sample 5 (300 kHz) and sample 7 (290 kHz). However, due to the limited amount of measurements it cannot be concluded that this result presents a real effect.
The EL intensity maximum of sample 7 (450 a.u. at 290 kHz) compared to the EL intensity maximum for sample 5 (1070 at 300 kHz) is significantly lower even though the dye concentration of sample 7 is 1.3% higher than for sample 5. This might indicate that for this operation there may be an optimum dye concentration between 3.7 and 5.0 wt% dye. Again, due to the limited amount of successfully carried out measurements this does not necessarily represent a real effect.

6. Concluding Remarks

Thin film OLEDs using the commercially readily available Polymer PVK and blue light-emitting laser dye Bis-MSB were successfully fabricated without further treatment of these materials. A technological need to synthesise new compounds for this application was not found being necessary.

Measurements of PL intensity vs. doped dye concentration (chapter 5.2.1.7) and EL intensity vs. unipolar pulsed voltage operation (chapter5.4.2) showed the influence of these two parameters for the device performance revealing optimum settings. It is recommended to take the influence of these two important parameters for any OLED optimisation into consideration.

A pulsed operation with the associated advantages of higher EL intensity and expected longer lifetime (due to a lower overall operation time) might be sufficient for applications involving human beings looking at a display as the human eye cannot recognise flickering of frequencies over 50 Hz and can therefore be recommended.

Problems associated with the quality of the devices fabricated became apparent when increasing the circular active area of 3 mm diameter to 10 mm diameter (chapter 5.3.2) and furthermore in measurements of the d.c. operational device lifetime (chapter 5.3.3). In order to overcome these problems improvements are suggested in the next chapter, Suggestions for Future Work.

7. Suggestions for Future Work

For future work the following points classified into those which can be achieved on the experimental side and those which can result from calculations are suggested:

7.1. Experimental

7.1.1 ITO Surface Treatment

The cleaning process for the ITO glasses could be improved for instance according to a standard procedure for silicon wafers: (1) 10 min acetone soak in an ultrasonic bath; (2) a 1 min rinse in deionized (>16 mΩ cm) water; (3) a 15 min soak at 60°C in freshly mixed 5:1 18-M sulphuric acid to 30% hydrogen peroxide; (4) a repeated 1-min rinse in deionized water; (5) a 20-sec dip in 10:1 water to 49% hydrofluoric acid; (6) a final 1-min rinse in deionized water (FLACK, 1984:1202).

Furthermore, a literature search for available procedures to achieve homogenous metal oxide surfaces, e.g. by applying chemical etching, could be carried out or simply the glass be purchased from another supplier who applies such a processes.

7.1.2 Optimal adjustment of the Spin Coating Procedure for the Used Materials

The surface texture of the spin coated PVK thin film could be thoroughly characterised and the coating process systematically optimised for the materials used in order to achieve pin-hole-free homogeneous layers with minimum possible thickness. The parameters to vary include solvent concentration, spinning speed, spinning acceleration rate, partial saturation of the overlying gas with the used solvent and use of a binary solvent-system containing solvents of both high and low volatility.

7.1.3 Materials

Other polymer matrixes such as polycarbonates, polymethylmethacylate, polystyrene, etc. and other laser dyes (coumarine, rhodamine, etc.) should be considered.

Also, instead of blending the polymer with the dye, chemical attachment of the dye to the polymer chain could be considered including economical aspects.

As quenching might occur due to impurities a further improvement would be to purify the PVK and Bis-MSB or to purchase the materials from a source which guarantees the highest possible level of purity, see chapter 3.3.

Toxicity tests of materials used where no safety data is provided and an evaluation of their potential for recycling are recommended to be taken into account for material selection.

7.1.4 Sample Encapsulation

The encapsulation of the devices on the side of the positive electrode and along the edges to reduce diffusion of oxygen and water considering standard epoxy resin is recommended. Encapsulation should also improve the mechanical stability.

7.1.5 Fluorescence Quantum Yield (Quantum Efficiency)

The fluorescence quantum yield (quantum efficiency) of the fabricated dye embedded polymer films, as referred to in chapter 3.2.2, could be determined.

7.1.6 Absolute Brightness

The calibration of the photodiode is recommended or the use of precalibrated equipment to measure absolute light intensity values so that different measurements carried out in different series can be compared and results be compared with the literature especially taking into account the different physical units used.

7.1.7 External Quantum Efficiency/EL Energy Conversion Efficiency

Measurements using an integrating sphere, a calibrated spherical light detector, for the emitted light intensity and, in parallel, measuring the applied field and resulting current through the device are recommended. The energy conversion efficiency, the ratio of optical and electrical power, can then be calculated.

7.1.8 Operational Lifetime under Pulsed Operation

It is recommended to carry out operational lifetime measurements under pulsed operation. Some processes which lead to device degradation such as oxidation or thermal degradation of the polymer can be expected to be reduced under such a driving mode. If this should be the case this might, on top of the observed increase in EL intensity, be a further supportive argument to consider pulsed operation for applications where possible.

7.1.9 Multilayer Devices

Difficulties listed in chapter 3.8.3 associated with single layer devices multilayer devices should be assessed.

Also device structures which allow A.C. operation, see introduction (chapter 2.2), could be constructed.

7.2. Theoretical

7.2.1 Device Simulation

To measure the current carrier density and electrical field strength inside an OLED is extremely difficult, if not impossible. Therefore simulation models should be developed to carry out numerical calculations on the different parameters affecting the current density voltage characteristic of an OLED, mainly charge injection, current transport and recombination.

As a possibility the Regional-Approximation-Model (LAMPERT and MARK, 1970:233ff) could be used to model a single layer OLED which consists of negative and positive space charged regions (according to electron and hole injection from opposite sides) which is separated by a recombination zone. However, differential equations for the electrical potential, field strength, and carrier density in each region as well as boundary conditions would have to be developed. In addition, equations for carrier trap distribution and recombination rate along with system parameters such as carrier mobility, relative permittivity value, film thickness, trap sites energy and trap sites density would have to be supplied for the model.

8. References

AMMERMANN, D: Organische Leuchtdioden. Reihe 9: Elekrtonik, Nr.: 253; Duesseldorf: VDI Verlag GmbH, 1997.

ANDERSON, M; PEI, Q; HJERTBERG, et. al.: "Synthesis of soluble poly(alkylthiophenes) which are thermally stable in the doped state". In: Synthetic Metals. 55 (2-3), 1993, pp. 1227 - 1231.

ANDREATTA, A; CAO, Y; CHIANG, JC; SMITH, P; HEEGER, AJ; "Electrically conductive fibres of polyaniline spun form solutions in concentrated sulphuric acid". In: Synthetic Metals. 26 (4); 1988, pp. 383 - 389.

ANGELOPOULOS, M; ASTURIAS, GE; ERMER, SP; et al.: "Polyaniline - solutions, films and oxidation-state". In: Molecular Crystals and Liqid Crystals. 160; 1988, pp. 151 - 163.

BÄSSLER, H; "Charge transport in molecularly doped polymers". In: Philosophical Magazome B-Physics of Condensed Matter Statistical Mechanics Electronic Optical and Magnetic Properties. 50 (3); 1984; pp. 347 - 362.

BORNSIDE, DE; MAKOSCO, CW; SCRIVEN, LE: "Spin coating - one dimensional model". In: Journal of Applied Physics. 66 (11); 1989; pp. 5185-5193.

BOWONDER, B; SARNOT, SL; RAO, MS: Electronic display technologies: state-of-the-art. New Delhi: Electronics Information & Planning. 21 (12) 1994, pp. 683-746.

BRADLEY, DDC: "Electroluminescence - A bright future for conjugated polymers". In: Advanced Materials. 4 (11), 1992; pp. 756 - 759.

BROSIUS, S; LANGE, G; PIESCHE, M; WIEGMANN, H-B: "Erzeugung ultraduenner Schichten durch Spin-Coating-Prozesse". In: Chemie Ingenieur Technik. 62; Nr. 2; D-Weinheim: VCH Verlagsgesellschaft mbH, 1990; pp. 142-143.

BURROUGHES, JH; BRADLEY, DDC; BROWN, AR et al.: "Light-emitting diodes based on conjugated polymers". In: Nature. 347; 1990, 539-541.

CAMBRIDGE DISPLAY TECHNOLOGY LTD. homepage: http://www.cdtltd.co.uk

CAO, Y; SMITH, P; HEEGER, AJ; "Counterion induced processibility of conducting polyaniline and of conducting polyblends of polyaniline in bulk polymers". In: Synthetic Metals. 48 (1), 1992; pp. 91 - 97.

CHATURVEDI, V; TANAKA, S; KAERIYAMA, K; "Preparation of poly(p-phenylene) via a new precursor route". In: Macromolecules; 26 (10), 1993, pp. 2607 - 2611.

CHILD, AD; REYNOLDS, JR. "Water-soluble rigid-rod polyelectrolytes - A new self-doped electroactive sulfonatoalkoxy-substituted poly(p-phenylene)" Macromolecules; 27 (7), 1994, pp. 1975 - 1977.

CONWELL, EM; "Transport in Transpolyacetylene" In: IEEE Transactions on Electrical Insulation EL-22 (5), 1987; pp. 591 - 627.

CONWELL, EM; MIZES, HA: Handbook on Semiconductors. (MOSS, T.S., ed.). Vol. 3. Amsterdam: North-Holland, 1992.

DESTRIAU, J: J. Chim. Phys.. 33; 1936, pp. 587 - ff.

DRESNER, J: "Double injection electroluminescence in anthracene". In: RCA Rev. 30; 1969, pp. 322-334.

DUGDALE, RH; MORFETT, JC: Mechanics of Fluids. London: George Godwin, 1983.

EDWARDS, JH; FEAST, WJ; BOTT, DC; "New routes to conjugated polymers - 1. A 2 step route to polyacetylene". In: Polymer. 25 (3), 1984, pp. 395 - 398.

FLACK, WW; SOONG, DS; BELL, AT, HESS, DW: "A mathematical model for spin coating of polymer resists". In: Journal of Applied Physics. 56 (4): 1984; pp. 1199-1206.

FRIEND, R; BURROUGHES, J; SHIMODA, T: "Polymer Diodes". In Physics World. June, 1999; pp. 35-40.

GALVIN, ME; WNEK, GE: "Electrically conductive polymer composites - polymerisation of acetylene in polyethylene". In: Polymer. 23 (6), 1982, pp. 795 - 797.

GALVIN, ME; "Electrically active polymers and their application". In: JOM-Journal of the Minerals Metals & Materials Society. Vol. 49; No. 3; 1997, pp. 52 - 55.

GILBERT, A; BAGGOTT, J: Essentials of molecular photochemistry. London, Edinburgh, Boston, Melbourne, Paris, Berlin, Vienna: Blackwell Scientific Publications, 1991.

GINSBERG, EJ; et al.: Conjugated Polymeric Materials. BREDAS, JL (ed.); CHANCE, RR (ed.). Dodrecht: Kluwer Academic, 1990.

GREENHAM, NC; FRIEND, RC: "Semiconductor Device Physics of Conjugated Polymers". In: Solid State Physics. Vol. 49; 1995, pp. 1-149.

HAN, CC; SHAKLETTE, LW; ELSENBAUMER, RL: Program of Symposium "Electrical, optical & magnetic properties of organic solid state materials". Boston; Materials Research Society, 1991.

HARRISON, RM; De MORA, SJ: Introductory chemistry for the environmental sciences. Second edition; Cambridge, New York, Melbourne: Cambridge University Press, 1996.

HE, Z; MILBURN, GHW; DANEL, A et al.: "Blue electroluminescence of novel pyrazoloquinoline and bispyrazolopyridine derivatives in doped polymer matrices". In: Journal of Material Chemistry. 7 (12); 1997, pp. 2323 - 2325.

HEEGER, AJ; KIVELSON, S; SCHRIEFFER, JR et al. "Solitons in conducting polymers". In: Reviews of Modern *Physics; 60 (3); 1988, pp. 781 - 850.*

HEEGER, AJ: "Self-assembled networks of conducting polyaniline: A new class of conducting polymer blends". In: Trends in Polymer Science. 3 (2); 1995, pp. 39 - 47.

HEEGER, AJ: "Light emission from semiconductiong polymers: light-emitting diodes, light-emitting electrochemical cells, lasers and white light for the future". In: Solid State Communications. Vol. 107, No. 11; 1998, pp. 673-679.

HELFRICH, W; SCHNEIDER, WG: "Recombination and radiation in anthracene crystals". In: Phys. Rev. Lett.. 14 (7); 1965, pp. 229-231.

HÖFLER, GE; VANDERWATER, DC; DeFEVERE, FA et al.: "Wafer bonding of 50-mm diameter GaP to AlGaInP-GaP light emitting diode wafers. In: Appl. Phys. Lett.; 69 (6); 1996, pp. 803-806.

HOLONYAK, N; BEVACQUA, SF: "Coherent (visible) light emission from $Ga(As_{1-x}P_x)$junctions". In: Appl. Phys. Lett. 1 (4): 1962, pp. 82-83.

HÖRHOLD, HH; RAABE, D: "Poly(arylen-phenylvinylene)". Patentschrift ("Deutsche Demokratische Republik"). Wirtschaftspatent WP C 08 G/2424 338; 12/08/1982; 25/04/1984.

IKENOUE, Y; CHIANG, J; PATIL, AO; WUDL, F; HEEGER, AJ: "Verification of the cation-popping doping mechanism of self-doped polymers". In: J. of the Am. Chemical Society. 110 (9); 1988, pp. 2983 - 2985.

INGANAS, O: "Conformational flexibility, electronic structure and chromism in conjugated polyalkylthiophenes". In: Trends in Polymer Science. 2 (6), 1994, pp. 189 - 196.

IRO, T; SHIRAKAWA, H; IKEDA, S: "Simultaneous polymerisation and formation of polyacetylene films on the surface of concentrated soluble Ziegler-type catalyst solution". In: J. Polymer Science: Polymer Chemistry.12 (1); 1974, pp. 11 - 20.

KAO, KC; HWANG, W. Electrical Transport in Solids. Oxford; Pergamon Press, 1981.

KASIM, RK; ELSENBAUMER, RL: "Forward/Reverse dc bias or ac electroluminescence in poly(p-phenylene vinyle) prepared via sulfonium-salt and xanthate routes". In: Synthetic Metals. 85, 1997, pp. 1291 - 1292.

KIDO, J; HONGAWA, K; OKUYAMA, K; KATSUTOSHI, N: "Bright blue electroluminescence from poly(*N*-vinylcarbazole)". In: Applied Physics Letters. 63 (19); 1993, pp. 2627-2629.

KIDO, J; SHIONOYA, H; NAGAI, K: "Single-layer white light-emitting organic electroluminescent devices based on dye dispersed poly(*N*-vinylcarbazole)". Appl. Physics Letters; 67 (16), 1995, pp. 2281 - 2283.

KOBAYASHI, M; CHEN, J; MOREAS, TC; HEEGER, AJ; WUDL, F: "Synthesis and properties of chemically coupled poly(thiophene)". In: Synthetic Metals. 9 (1), 1984, pp. 77 - 86.

LAMPERT, MA; MARK, P: Current injection in solids. New York, London; Academic Press, 1970.

LOAGAN, SR: Physical Chemistry for the Biomedical Sciences. London, Bristol (USA): Taylor & Francis Ltd./Inc., 1998.

MAL'TSEV, EI; BRUSENTSEVA, MA; KOLESNIKOV, VA; VANNIKOV, AV: "Electroluminescence of poly(hydroxyamino esters)-aluminium complexes" In: Chemical Physics Letters. Elsevier 238, 1995, pp.295-300.

MARKS, RN. "The optical and electronic response of poly(p-phenylene vinylene) thin film devices". Ph.D. thesis, University of Cambridge, 1993.

MARTENS, JHF; MARSEGLIA, EA; BRADLEY, DDC et al.; "The effect of side groups on the structure and ordering of poly(p-phenylene vinylene derivatives". In: Synthetic Metals. 55 (1); 1993, pp. 449 - 453.

METZGER, RA: "Turning blue to green". In: Compound Semiconductor Journal. 1 (1); 1995, pp. 26-28.

MIZES, HA; CONWELL, EM. "Stability of polarons in conducting polymers". In: Physical Review Letters; 70 (10); 1993, pp. 1505 - 1508.

MOON, RL; "Organic EL devices for displays". In: IS&T's 48th Annual Conference Proceedings; 1995, pp. 386-391.

MORITA, M; MIYAZAKI, S; ISHIKAWA, M. et al.: "Layered Polyaniline composites with cation-exchanging properties for positive electrodes of rechargeable lithium batteries". In: J. of the Electrochemical Society. 142 (1); 1995, pp. L3 - L5.

MORT, J; PFISTER, G (editors): Electronic Properties of Polymers. Canada: J. Wiley & Sons Inc., 1982.

MOTT, NF; DAVIS, EA. "Electronic Processes in Non-crystalline Materials". Oxford, Clarendon Press, 1971.

NAKAMURA, S; MUKAI, T; SENOH, M; "Candela-class high brightness InGaN/AlGaN double-heterostructure blue-light emitting diodes. In: Appl. Phys. Lett.; 64 (13); 1994, pp. 1687-1689.

NALWA, HS (Editor): Handbook of organic conductive Molecules and polymers.Vol. 4; Chichester, New York, Weinheim, Brisbane, Singapore, Toronto: John Wilcy & Sons, 1997.

NGUYEN, MT; LECLERC, M; DIAZ, AF: "Water-soluble conductive-electroactive polymers". Trends in Polymer Science. 3 (6), 1995, pp. 186 - 190.

OBRZUT, J; OBRZUT, MJ; KARASZ, FE: "Photoelectron-spectroscopy of poly(para-phenylene vinylene". In: Synthetic Metals. 29 (1); 1989; pp. E109 - E114.

PARAMENTER, RH; RUPPEL, W. In J. Appl. Phys. 30; 1959, pp. 1548 - ff.

PATIL, AO; IKENUE, Y; BASESCU, N et al.: "Self-doped conducting polymers". In: Synthetic Metals. 20 (2), 1987, pp. 151 - 159.

PEI, Q; INGANAS, O; GUSTAFSSON, G et al.: "The routes towards processible and stable conducting poly(thiophene)s". In: Synthetic Metals. 55 (2-2); 1993, pp. 1221 - 1226.

PENWELL, RC; PREST Jr. WM: Orientation in poly(N-vinyl carbazole) by melt extrusion". In: Polymer. Vol. 19; 1978; pp. 537-541.

POPE, M; KALLMANN, H; MAGNATE, P: "Electroluminescence in organic crystals". In: J. Chem. Phys.. 38; 1963, 2042-2043.

RAU, IV; REHAHN, M; "Rigid-rod polyelectrolytes-carboxylated poly(para-phenylene)s via a novel precursor route". In: Polymer. 34 (13); 1993, pp. 2889 - 2893.

RAY, A; ASTURIAS, GF; KERSHNER, DL et al.: "Polyaniline - Doping, structure, and derivatives". In: Synthetic Metals. 29 (1); 1988; pp. E141 - E150.

RENDELL, D: Fluorescence and Phosphorescence. Editor: MOWTHORPE, D..Chichester, New York, Brisbane, Toronto, Singapore: John Wiley & Sons, 1987.

RHODERICK, EH; WILLIAMS, RH: Metal-Semiconductor Contacts. Oxford, Clarendon Press, 1988.

RONCALI, J:"Conjugated poly(thiophenes) - Synthesis, functionalisation, and applications". In: Chemical Reviews. 92 (4); 1992, pp. 711 - 738.

ROUND, HJ: "A note on carborundum". In: Electron. World. 19; 1907; pp. 309-310.

SCHWOB, HP; ZSCHOKKE-GRÄNACHER, I: "Doppelinjektion und Elektrolumineszenz in dotierten Anthracenkristallen". In: Mol. Cryst. Liq. Cryst.; 13; 1971, pp. 115-136.

SHIMOJI, S: "A new analytical model for spin coating processes with solvent evaporation". In: Japanese Journal of Applied Physics. Vol. 26; No. 6; 1987; pp. L905-L907.

SHIMOJI, S: "Numerical analysis of the spin-coating process". In: Journal of Applied Physics. 66(6); 1989; pp. 2712-2718.

SZE: Physics of semiconductor devices. Wiley & Sons Inc.: New York, 1981.

TANG, CW; VanSLYKE, SA: "Organic electroluminescent diodes". In: Appl. Phys. Lett. 51 (12); 1987; 913-915.

VOGL, P; CAMPBELL, DK: "1st principles calculations of the 3-dimensional structure and intrinsic defects in trans-polyacetylene". In: Physics Review B; 41 (18); 1990; pp. 12797 - 12817.

WALLOW, TI; NOVAK, BM: "In aqua synthesis of water-soluble poly(para-phenylene) derivatives". In: J. of the Am. Chemical Society.113 (19); 1991, pp. 7411 - 7412.

WANG, YZ et. al.; WANG, HL; EPSTEIN, AJ: "Alternating-current light-emitting devices based on conjugated polymers". Appl. Phys. Lett.. 68 (7), 1996, pp. 894 - 896.

WILKINSON, WL: NON_Newtonian Fluids. Oxford: Pergamon Press, 1960.

YASSER, A; RONCALI, J; GARNIER, F: "Aqueous suspension of conducting material from polypyrole-coated submicronic latex-particles". In: Polymer Communications. 28 (4); 1987, pp. 103 - 104.

ZOLINA, KG; KUDRYASHOV, VE; TURKIN, AN et al.: "Luminescence spectra of superbright blue and green InGaN/AlGaN/GaN light emitting diodes." In: MRS Internet Journal Nitride Semiconductor Research. 1; 1996; p. 11.

ZOTTI, G; SCHIEVON, G: "Poly (2,5-thienylene)-coated electrodes formed by electroreduction of a nickel adduct with 2,5 dibromothiophene". In: J. of Electroanalytical Chemistry. 163 (1-2); 1984, pp. 385 - 388.

Appendices

Appendix A: Excitation and Emission Spectra of Indium Tin Oxide (ITO) Coated Glass

Excitation spectra of ITO coated glass

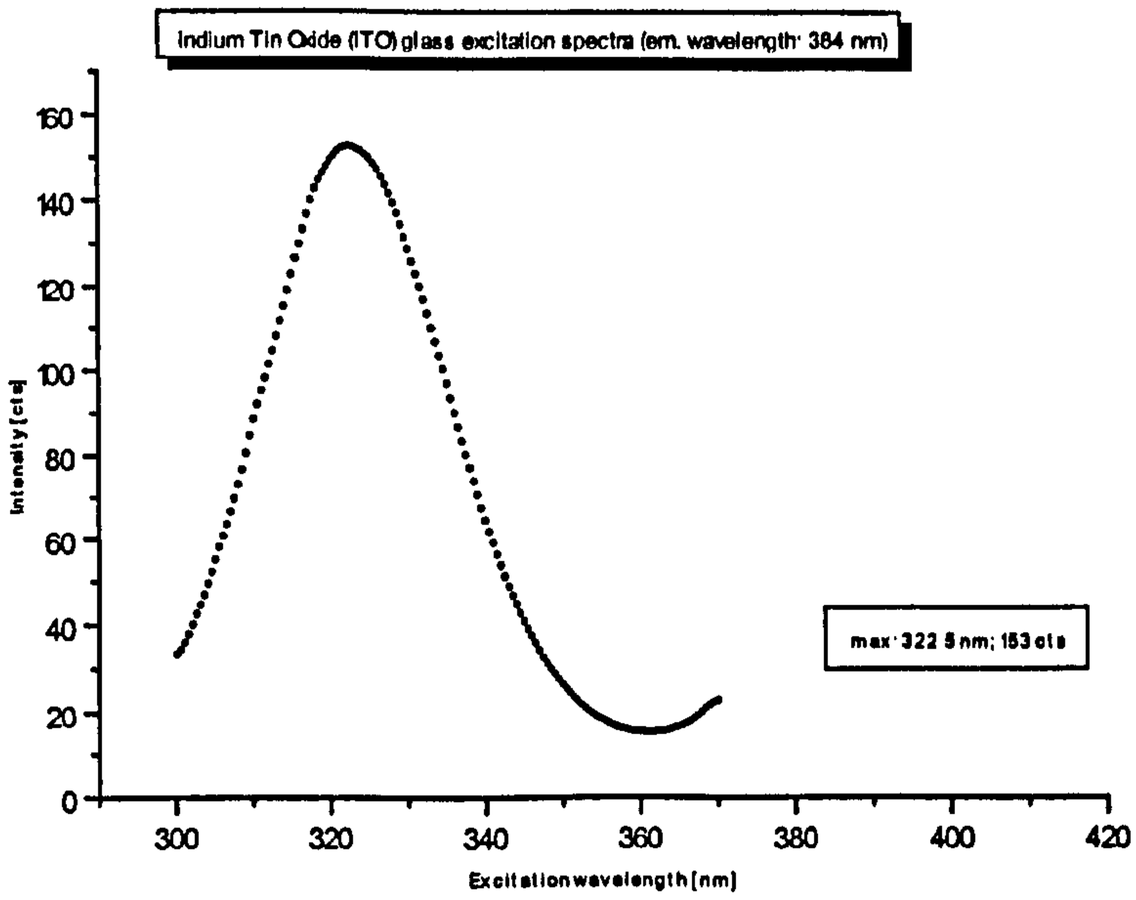

Fig. App. 1: Excitation spectra of indium tin oxide coated glass (PELS)

The spectra consists of a symmetrical single peak with its maximum at 322.5 nm, a corresponding light intensity of 153 counts and a full width at half maximum of 26 nm.

Compared to light emission in Bis-MSB dye doped PVK films, the light emission from ITO films is very small and therefore can be neglected.

Emission spectra of ITO coated glass

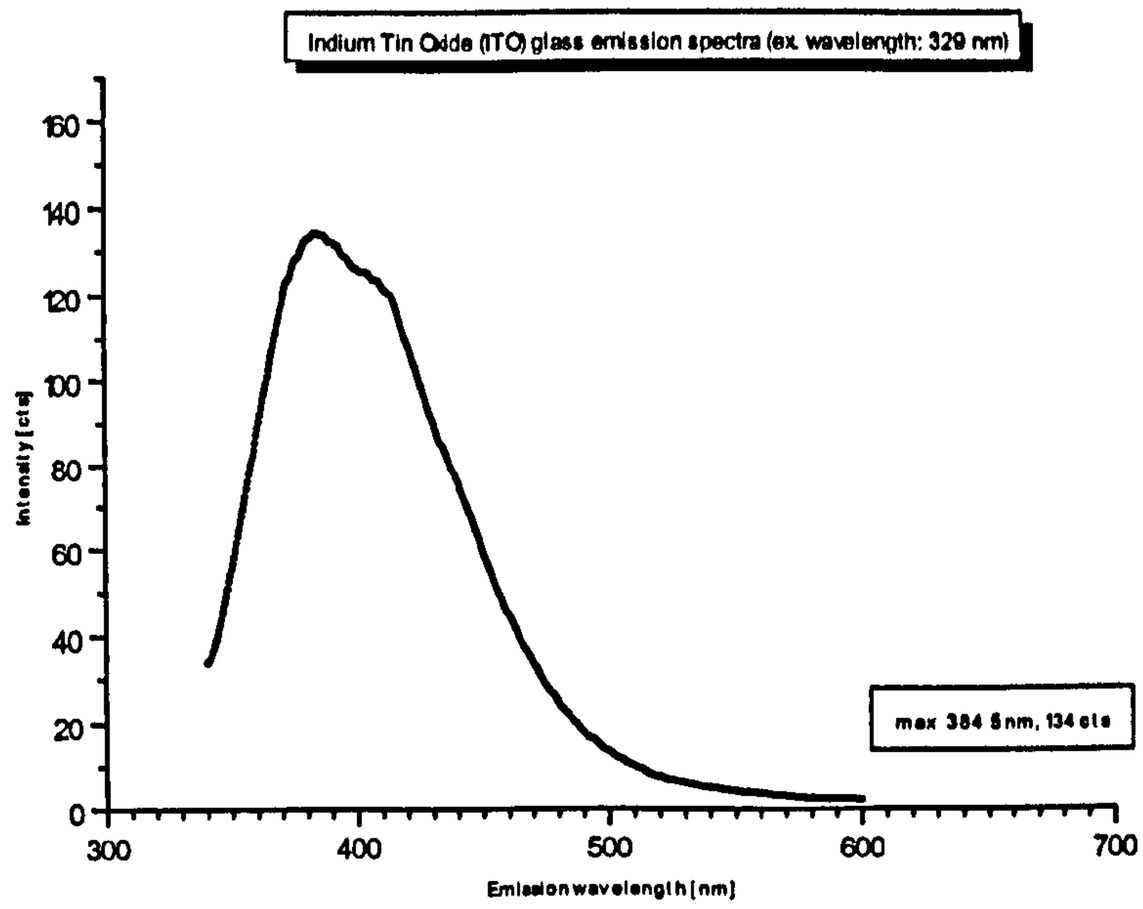

Fig. App. 2: Emission spectra of indium tin oxide coated glass (PELS)

The spectra consists of one main peak (FWHM: approx. 92 nm) which can be seen as split up into two sub peaks: one clearly identifiable at 384.5 nm (134 cts) and the second one not so characteristic at around 410 nm.

The very low peak intensity shows that potential contributory emission from the ITO underlying layer can be neglected compared to emission from Bis-MSB doped PVK films.

Appendix B: Calculation of the Average Distance of Dye Molecules Dispersed in a Thin Polymer Film

Assumptions:

- $m_{dye} << m_{repeat\_unit}$ with m_{dye} mass of dye and m_{repeat_unit} mass of repeated unit.
- The content of remaining solvent and monomer in the polymer after the casting process is negligible.
- The dye molecules are separated and equally distributed so as to form a simple cubic lattice structure within the polymer.

Definitions:

$$c_{mass\_ratio} \equiv \frac{m_{dye}}{m_{repeat\_unit}},$$

$\rho_{polymer\_thin\_film}$ Density of the thin polymerised film,

W_{molar_dye} Molecular weight of the dye.

Using the general definition of density gives the mass of the polymer in a virtual cube of the thin film, $m_{polymer\_in\_virtual\_cube}$,

$$m_{Polymer\_in\_virtual\_cube} = \rho_{polymer\_thin\_film} \cdot V_{virtual\_cube}.$$

The number of dye molecules in this virtual cube, $n_{dye\_molecules\_in\_virtual\_cube}$, can be calculated as:

$$n_{dye\_molecules\_in\_virtual\_cube} = \frac{c_{mass\_ratio} \cdot m_{polymer\_in\_virtual\_cube} \cdot N_A}{W_{molar\_dye}},$$

with N_A standing for Avogadro's constant.

The average distance between dye molecules $\bar{d}$ can be obtained as the ratio of the length of the virtual volume, $l_{virtual\_cube}$, and the cubic root of $n_{dye\_molecules\_in\_virtual\_cube}$:

$$\bar{d} = c_{mass\_ratio}^{-1/3} \cdot \sqrt[3]{\frac{W_{molar\_dye}}{\cdot \rho_{polymer\_thin\_film} \cdot N_A}} \cdot$$

(Note: Using the density in [g/cm^3] also gives the average distance in [cm].)

For the distance calculations a density of PVK in thin film form of 1.184 [g/cm3] had been used (PENWELL, 1978:537).

Appendix C: Standard Deviations for Fitted Time Resolved Emission Spectra of Bis-MSB as a Powder, Bis-MSB in Chloroform Solution, undoped PVK film and PVK Films doped with Bis-MSB in 10 Different Concentrations

Sample	Std. Dev. of τ_1 [s]	Std. Dev. of τ_2 [s]	Std. Dev. of τ_3 [s]	Std. Dev. of τ_4 [s]	Std. Dev. of B_1	Std. Dev. of B_2	Std. Dev. of B_3	Std. Dev. of B_4
5.2.2.2	3.45E-11	1.59E-10	-	-	0.0017	0.0019	-	-
5.2.2.3	5.12E-10	7.04E-12	-	-	1.79E-4	9.49E-4	-	-
5.2.2.4	7.28E-11	2.46E-10	6.23E-10	5.62E-10	0.0053	0.0022	0.0009	0.0011
5.2.2.5								
0.00006	4.76E-10	6.31E-11	2.25E-10	5.26E-10	0.0012	0.0073	0.0029	0.0003
0.0001	3.10E-10	4.67E-11	1.28E-09	1.01E-09	1.69E-03	2.84E-03	7.22E-04	1.42E-03
0.0006	7.39E-11	3.66E-10	7.60E-10	7.27E-10	0.0041	0.0026	0.0008	0.0017
0.0065	3.33E-10	4.66E-11	9.69E-10	1.43E-09	1.78E-03	2.73E-03	1.52E-03	7.09E-04
0.0117	3.62E-10	7.15E-11	1.16E-09	2.10E-09	2.14E-03	2.68E-03	1.33E-03	1.53E-03
0.27	5.86E-11	1.74E-10	fixed	fixed	9.06E-03	1.24E-02	2.91E-04	2.75E-05
2.14	1.14E-11	2.99E-09	4.14E-09	3.93E-10	4.47E-03	2.28E-04	9.11E-05	1.54E-03
4.93	2.52E-10	1.15E-11	5.71E-08	2.63E-09	7.04E-04	9.15E-03	2.75E-05	4.27E-05
10.09	1.63E-09	9.29E-12	5.49E-08	2.81E-10	9.88E-05	5.75E-03	1.99E-05	1.06E-03
17.65	1.76E-09	8.58E-12	1.76E-08	4.75E-10	2.17E-04	7.75E-03	2.72E-05	8.91E-04

Table App. 1: Standard deviations for fitted time resolved emission spectra of Bis-MSB as a powder (Sample: 5.2.2.2), Bis-MSB in Chloroform solution (Sample: 5.2.2.3), undoped PVK film (Sample: 5.2.2.4) and PVK film doped with dye Bis-MSB in 10 different concentrations [wt%] (Sample: 5.2.2.5)

The standard deviations are very small compared to the actual measurements. For example τ_1 is in the order of 1 to 10 ns (see Table 5.1) whereas the standard deviation of τ_1 is in the order of 10^{-10} seconds.